GE Energy Nuclear

26A6642AP
Revision 3
February 2007

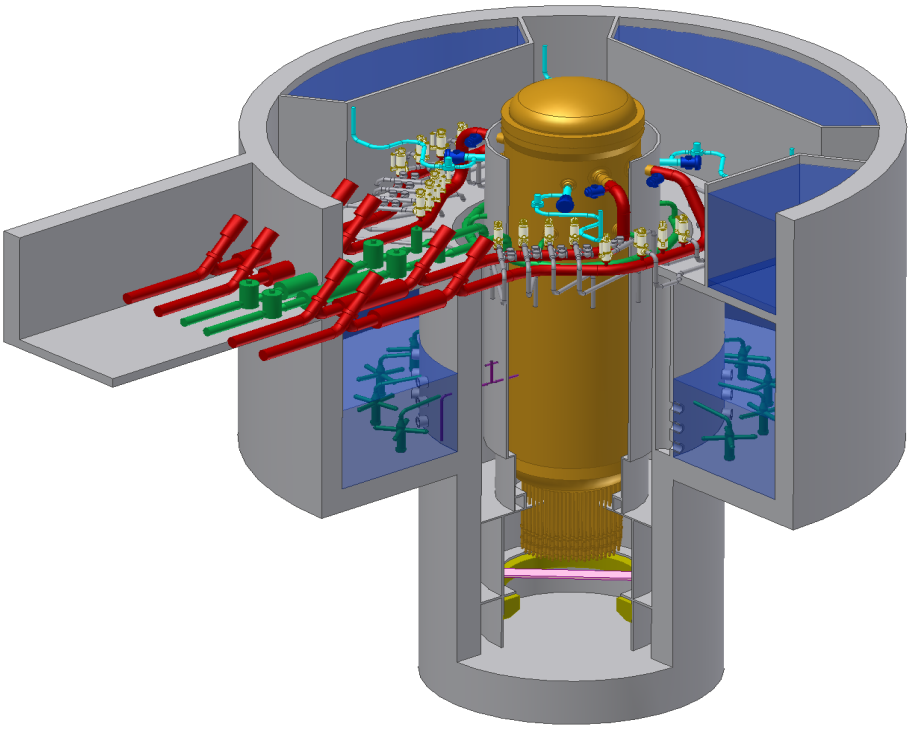

ESBWR Design Control Document

Tier 2

Chapter 4

Reactor

Contents

List of Tables

List of Illustrations

Abbreviations And Acronyms

Term	Definition
10 CFR	Title 10, Code of Federal Regulations
ABWR	Advanced Boiling Water Reactor
ANS	American Nuclear Society
AOO	Anticipated Operational Occurrence
APRM	Average Power Range Monitor
ARI	Alternate Rod Insertion
ASME	American Society of Mechanical Engineers
ASTM	American Society of Testing Methods
ATWS	Anticipated Transients Without Scram
AWS	American Welding Society
B&PV	Boiler and Pressure Vessel
BOC	Beginning of Cycle
BTU	British Thermal Unit
BWR	Boiling Water Reactor
C&FS	Condensate and Feedwater System
COL	Combined Operating License
CPR	Critical Power Ratio
CR	Control Rod
CRD	Control Rod Drive
CRDH	Control Rod Drive Housing
CRGT	Control Rod Guide Tube
CS&TS	Condensate Storage and Transfer System
CS / CST	Condensate Storage Tank
DPS	Diverse Protection System
ECCS	Emergency Core Cooling System
EQ	Environnemental Qualification
ESF	Engineered Safety Feature
FCISL	Fuel Cladding Integrity Safety Limit
FIV	Flow-Induced Vibration
FMCRD	Fine Motion Control Rod Drive
FW	Feedwater
GDC	General Design Criteria
GDCS	Gravity-Driven Cooling System
GE	General Electric Company
GEEN	General Electric Energy Nuclear
GE-NE	GE Nuclear Energy
GENE	General Electric Nuclear Energy
GETAB	General Electric Thermal Analysis Basis
GNF	Global Nuclear Fuel

Term	Definition
HCU	Hydraulic Control Unit
HP	High Pressure
HX	Heat Exchanger
I&C	Instrumentation and Control
ICPR	Initial Critical Power Ratio
LHGR	Linear Heat Generation Rate
LOCA	Loss-of-Coolant-Accident
LOFW	Loss-of-feedwater
LOOP	Loss of Offsite Power
LP	Low Pressure
LPRM	Local Power Range Monitor
MCPR	Minimum Critical Power Ratio
MPL	Master Parts List
MS	Main Steam
MSIV	Main Steam Isolation Valve
MT	Main Transformer
NBS	Nuclear Boiler System
NPSH	Net Positive Suction Head
NRC	Nuclear Regulatory Commission
OLMCPR	Operating Limit Minimum Critical Power Ratio
OOS	Out-of-service
PAS	Plant Automation System
PH	Pump House
PSS	Process Sampling System
RB	Reactor Building
RC&IS	Rod Control and Information System
RCPB	Reactor Coolant Pressure Boundary
RCS	Reactor Coolant System
RDA	Rod Drop Accident
RLP	Reference Loading Pattern
RMS	Root Mean Square
RPS	Reactor Protection System
RPV	Reactor Pressure Vessel
RWCU/SDC	Reactor Water Cleanup/Shutdown Cooling
RWE	Rod Withdrawal Error
S/C	Digital Gamma-Sensitive GM Detector
SBWR	Simplified Boiling Water Reactor
SCRRI	Selected Control Rod Run-in
SDC	Shutdown Cooling
SDM	Shutdown Margin

Term	Definition
SER	Safety Evaluation Report
SLC	Standby Liquid Control
SLCS	Standby Liquid Control System
SR	Surveillance Requirement
SRNM	Startup Range Neutron Monitor
SSE	Safe Shutdown Earthquake
TRAC	Transient Reactor Analysis Code
TS	Technical Specification(s)
USNRC	United States Nuclear Regulatory Commission
WH	Warehouse
WT	Water Treatment

4. REACTOR

4.1 SUMMARY DESCRIPTION

The reactor assembly consists of the reactor pressure vessel, pressure-containing appurtenances including control rod drive (CRD) housings and in-core instrumentation housings. The reactor internal components are described in Subsection 4.1.2, Reactor Internal Components. Figure 5.3-3 (Reactor Pressure Vessel System Key Features) shows the arrangement of the reactor assembly components. A summary of the important design and performance characteristics of the reactor and plant is given in Table 1.3-1. Loading conditions for reactor assembly components are specified within Subsection 3.9.5.

Section 4.3 presents the fuel and control rod design and core loading pattern that is adapted for the ESBWR as the basis for the system response studies in Section 5.2, Section 6.3 and Chapter 15.

4.1.1 Reactor Pressure Vessel

The reactor pressure vessel includes the shroud support brackets. Flow restrictors are included in the steam outlet nozzles and the GDCS/equalizing line nozzles. The reactor pressure vessel design and description are covered in Section 5.3.

4.1.2 Reactor Internal Components

The major reactor internal components described within Subsection 3.9.5 include:

- Core support structures (shroud, shroud support, top guide, core plate, control rod guide tubes and fuel supports),
- Chimney and partitions,
- Chimney head and steam separators assembly,
- Steam dryer assembly,
- Feedwater spargers,
- Standby liquid control header, sparger and piping assembly, and
- In-core guide tubes.

Except for the Zircaloy in the reactor core, these reactor internals are stress corrosion-resistant stainless steels or other high alloy steels. The fuel assemblies (including fuel rods and channels), control rods, chimney head and steam separator assembly, steam dryers and in-core instrumentation assemblies are removable when the reactor vessel is opened for refueling or maintenance.

4.1.2.1 Reactor Core

Important features of the reactor core are:

- The control rods are bottom-entry, cruciform shaped. Rods of this design were first introduced in the Dresden-1 reactor in April 1961 and have accumulated thousands of hours of service in BWRs around the world.

- Local power range monitors (LPRMs) are in-core fission chambers that are assembled and fixed inside enclosing tubes located in the core. These instrument assemblies provide signals for continuous local power range neutron flux monitoring. Fixed in-core gamma thermometer detectors, called automatic fixed in-core probe (AFIP) sensors, are also installed to provide axial local power information for LPRM calibration and core power calculation. The AFIP sensors are installed within the LPRM assembly with one sensor next to each LPRM detector. Startup range neutron monitors (SRNMs) are provided for monitoring core neutron flux at low power conditions. The SRNM sensors are fixed inside tubes that are located as shown in Figure 4.1-1. The LPRM cover tubes contain holes for the reactor coolant flow, whereas the SRNM tubes are pressure barrier dry tubes. All in-core instrument leads enter from the vessel bottom; this allows instrument assemblies to remain undisturbed in service through refueling. More information on in-core instrumentation is presented in Subsection 7.2.2. The instrument tubes are protected from water flow by in-core guide tubes in the bottom head plenum (Subsection 3.9.5).
- As shown by experience obtained at Dresden-1 and other BWR plants that utilize the in-core flux monitor system, the desired power distribution can be maintained within a large core by proper control rod scheduling.
- The fuel channels provide a flow path for the boiling coolant, serve as a guiding surface for the control rods, and protect the fuel during handling operations.
- The mechanical reactivity control permits criticality checks during refueling and provides maximum plant safety. The core is designed to be subcritical at any time in its operating history with any single control rod, or rod pair, fully withdrawn and the other control rods fully inserted.
- The selected control rod pitch represents a practical value of individual control rod reactivity worth, and allows adequate clearance below the pressure vessel between CRD mechanisms for ease of maintenance and removal.
- The reactor core is arranged as an upright circular cylinder containing a large number of fuel cells and is located within the core shroud inside the reactor vessel.

4.1.2.1.1 Fuel Assembly Description

The fuel assembly description is provided in Section 4.2.

4.1.2.1.2 Fuel Assembly Support and Control Rod Location

A few peripheral fuel assemblies that are not adjacent to a control rod are supported by the core plate via single-assembly fuel supports. Otherwise, individual fuel assemblies in groups of four rest on orificed fuel supports that are mounted on top of the control rod guide tubes. Each guide tube, with its orificed fuel support, bears the weight of four assemblies and is supported on a CRD penetration nozzle in the bottom head of the reactor vessel. The core plate provides lateral support and guidance at the top of each control rod guide tube and directs most of the reactor coolant flow into the fuel supports and the fuel assemblies. The top guide, mounted on top of the shroud, provides lateral support and guidance for the top of each fuel assembly.

The reactivity of the core is controlled by cruciform control rods and their associated electro-mechanical/hydraulic drive system (Section 4.6). The control rods occupy alternate spaces

between fuel assemblies. Each independent CRD inserts a control rod into the core from the bottom, and accurately positions its associated control rod during normal operation with an electric motor-driven ball screw. Hydraulic pressure is applied on the hollow cylinder of a CRD to exert several times the force of gravity on the control rod for insertion during the scram mode of CRD operation. Bottom entry allows optimum power shaping in the core, ease of refueling and convenient drive maintenance.

4.1.2.1.3 Other Internals

Information on other major reactor internal components identified in Subsection 4.1.2, Reactor Internal Components is presented in Subsection 3.9.5.

4.1.3 Reactivity Control Systems

4.1.3.1 Operation

The control rods perform dual functions of power distribution shaping and reactivity control. Power distribution in the core is controlled during operation of the reactor by manipulation of selected patterns of rods (Appendix 4A). These rods are positioned to counterbalance steam voids in the top of the core and effect significant power flattening. These groups of control elements, used for power flattening, experience a somewhat higher duty cycle and neutron exposure than the other rods in the control system.

The reactivity control function requires that all rods be available for either reactor "scram" (prompt shutdown) or reactivity control. Because of this, the control elements are mechanically designed to withstand the dynamic forces resulting from a scram. They are connected to bottom-mounted, electro-hydraulically actuated drive mechanisms that allow either electric motor controlled axial positioning for reactivity regulation or hydraulic scram insertion. The design of the rod-to-drive connection permits each rod to be attached or detached from its drive without disturbing the remainder of the control system. The bottom-mounted drives permit the entire control system to be left intact and remain operable for tests with the reactor vessel open.

4.1.3.2 Description of Control Rods

A description of the control rods is presented in Section 4.2 with a description of the CRD System in Section 4.6.

4.1.3.3 Supplementary Reactivity Control

The core control requirements are met by use of the combined effects of the movable control rods, supplementary burnable poison, and the reactor coolant natural flow. A description of the supplementary burnable poison is presented in Sections 4.2 and 4.3.

4.1.4 Analysis Techniques

4.1.4.1 Reactor Internal Components

Computer codes used for the analysis of the internal components are as follows:

- SAP4G07

- ANSYS
- SEISM03

4.1.4.1.1 SAP4G07

SAP4G07 is a general-purpose finite element computer program used to perform stress, dynamic, and seismic analyses of structural, mechanical and piping components. Dynamic analysis can be done using direct integration or mode superposition. Response spectrum analysis (a mode superposition method) can include multiple support excitation. SAP4G07 is a GENE in-house program based on similar programs developed by Professors E. L. Wilson and K. J. Bathe at UC Berkeley.

4.1.4.1.2 ANSYS

ANSYS is a general-purpose finite element computer program designed to solve a variety of problems in engineering analysis. The ANSYS program features the following capabilities:

- Structural analysis, including static elastic, plastic and creep, dynamic, seismic and dynamic plastic, and large deflection and stability analyses.
- One-dimensional fluid flow analysis.
- Transient heat transfer analyses, including conduction, convection, and radiation with direct input to thermal-stress analyses.
- An extensive finite element library, including gaps, friction interfaces, springs, cables (tension only), direct interfaces (compression only), curved elbows, etc. Many of the elements contain complete plastic, creep, and swelling capabilities.
- Plotting - Geometry plotting is available for all elements in the ANSYS library, including isometric and perspective views of three-dimensional structures.
- Restart Capability - The ANSYS program has restart capability for several analysis types. An option is also available for saving the stiffness matrix once it is calculated for the structure, and using it for other loading conditions.

ANSYS is used extensively in GENE for elastic and elastic-plastic analyses of the reactor pressure vessel, core support structures, reactor internals, fuel and fuel channel.

4.1.4.1.3 SEISM03

SEISM03 is a GENE proprietary computer program for non-linear dynamic analysis. It is based on the component element method developed by S. Levy and J.P. Wilkinson of GECR&D. The method uses basic mass, spring, damper, gap, and coupling elements in a direct integration approach to solve non-linear dynamic analysis. This dynamic analysis engineering computer program (ECP) is used in conjunction with the following:

- **SEPRE:** This ECP is a preprocessor for SEISM. It takes the output from CRTFI and phases the input time histories of all loads with the basic load time histories. SEPRE also converts all input loads to the format required for input to SEISM.
- **SEPST:** This ECP is the SEISM post-processor. SEPST condenses the SEISM output data into a form that is more practical to interpret. It determines and prints the initial

values, the maximum and minimum values for all components, and the times of their occurrence. In addition, it generates the response time history plots of selected components.

- **CRTFI:** This ECP uses, as input, the scaled or composite horizontal acceleration time histories at the mid-fuel and end-fuel positions to determine (1) the clamping forces to be applied to the analysis model friction elements, (2) the scram uplift forces on a bundle, (3) inertial forces of the fuel in order to obtain reaction forces on both ends of the fuel, and (4) fuel-center deflection and uplift forces due to scram.

4.1.4.2 Fuel Design Analysis

The fuel design analysis is discussed in Section 4.2.

4.1.4.3 Reactor Systems Dynamics

The analysis techniques and computer codes used in reactor systems dynamics are based on those approved or developed using NRC-approved criteria.

4.1.4.4 Nuclear Analysis

The analysis techniques are discussed in Section 4.3.

4.1.4.5 Neutron Fluence Calculations

Neutron vessel fluence calculations were carried out using a two-dimensional, discrete ordinates, Sn transport code with general anisotropic scattering.

This DORT code is the most widely used two-dimensional, discrete ordinates code that solves a wide variety of radiation transport problems. The program solves both fixed source and multiplication problems. Rectangular (X, Y), cylindrical (R, Z), or polar (R, θ) geometry is allowed with various boundary conditions. The fluence calculations incorporate, as an initial starting point, neutron fission distributions prepared from core physics data as a distributed source. Anisotropic scattering is considered for all regions. The cross sections are prepared with 1/E flux weighting using polynominal expansion matrices for anisotropic scattering but do not include the resonance self-shielding factors (Section 12.3).

4.1.4.6 Thermal-Hydraulic Calculations

The thermal-hydraulic models are discussed in Section 4.4.

4.1.5 COL Unit-Specific Information

None.

4.1.6 References

None.

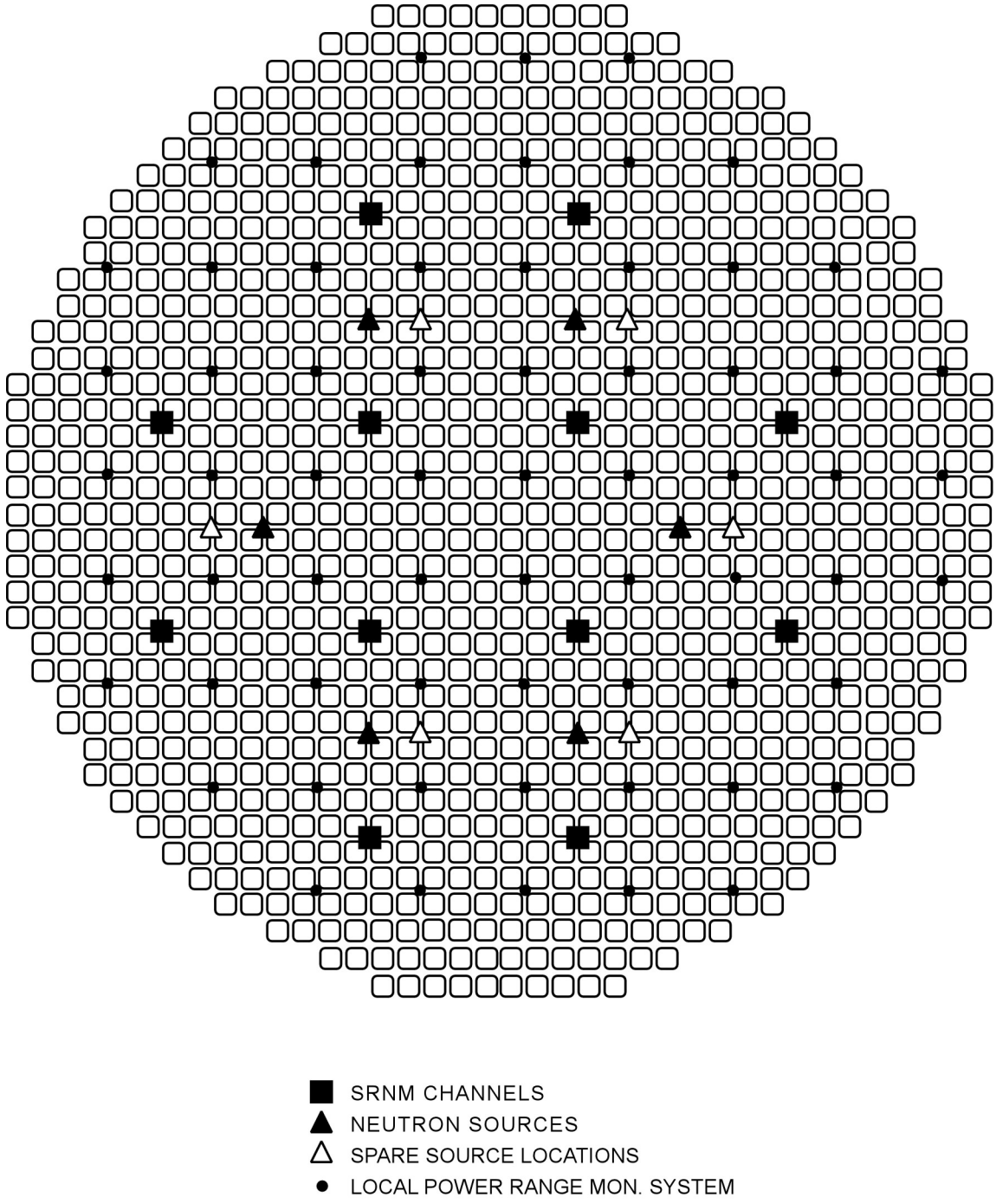

Figure 4.1-1. Core Configuration with Location of Instrumentation

4.2 FUEL SYSTEM DESIGN

The fuel system is defined as consisting of the fuel assembly and the reactivity control assembly. The fuel assembly is comprised of the fuel bundle, channel and channel fastener. The fuel bundle is comprised of fuel rods (some of which may contain burnable neutron absorbers), water rods, spacers, springs and assembly fittings. Appendix 4B contains a set of design criteria to be satisfied by new fuel designs to be loaded into an ESBWR reactor.

A reference core, based upon a current NRC-approved GE14 fuel design and modified to account for the shorter active fuel length, is used to demonstrate the ESBWR system response. The latest GE14 information is provided in the most recent revision of the GE Fuel Bundle Designs Report and its supplements (Reference 4.2-1).

This section also addresses the reactivity control elements that extend from the coupling interface of the control rod drive mechanism (per Regulatory Guide 1.70). The functional design of the reactivity control system is detailed in Section 4.6. Any control rod design to be used in an ESBWR reactor shall meet the criteria documented in Appendix 4C.

The following subsection provides the fuel system design bases and design limits. It is consistent with the criteria of the NRC Standard Review Plan, Section 4.2.

4.2.1 Design Bases

4.2.1.1 Fuel Assembly

The fuel assembly (comprised of the fuel bundle, channel and channel fastener) is designed in compliance with requirements of 10 CFR 20, 10 CFR 50 and 10 CFR 100 to ensure that possible fuel damage will not result in the release of radioactive materials in excess of prescribed limits, and that fuel assembly coolability is maintained during postulated accidents. The core nuclear and hydraulic characteristics, plant equipment characteristics, and instrumentation and protection systems are evaluated to assure that this requirement is met.

The thermal-mechanical design process emphasizes that:

- The fuel assembly provides substantial fission products retention capability during all potential operational modes.
- The fuel assembly provides sufficient structural integrity to prevent operational impairment of any reactor safety equipment.

The fuel assembly and its components are designed to withstand:

- The predicted thermal, pressure and mechanical interaction loadings occurring during startup testing, normal operation, and anticipated operational occurrences, infrequent incidents and accidents.
- Loading predicted to occur during handling.

Steady-state operating limits are established to ensure that actual fuel operation, including anticipated operational occurrences (AOOs), is maintained within the fuel rod thermal-mechanical design bases. These operating limits define the maximum allowable fuel operating power level as a function of fuel exposure in terms of Maximum Linear Heat Generation Rate

(MLHGR). Lattice local power and exposure distributions are applied in the determination of the MLHGR limits.

The detailed design bases for each of the fuel assembly damage, fuel rod failure and fuel assembly cooling criteria, as defined in Section II.A of NRC Standard Review Plan 4.2 (except control rod reactivity; see Subsection 4.2.1.2) are provided in Section 4B.2 of Appendix 4B.

4.2.1.1.1 Fuel Temperature

The fuel rod centerline temperature is limited to ensure with high probability that fuel melting will not occur during normal operation, including AOOs.

4.2.1.1.2 Fuel Rod Internal Pressure

During fabrication, the fuel rod is filled with helium to a specified pressure. With the initial rise to power, this fuel rod internal pressure increases due to the corresponding increase in the gas average temperature and the reduction in the fuel rod void volume due to fuel pellet expansion and inward cladding elastic deflection due to the higher reactor coolant pressure. With continued irradiation, the fuel rod internal pressure will progressively increase further due to the release of gaseous fission products from the fuel pellets to the fuel rod void volume. With sufficient irradiation, a potential adverse thermal feedback condition may arise due to excessive fuel rod internal pressure.

When the internal pressure exceeds the reactor coolant pressure, the cladding will deform outward (cladding creepout). If the rate of this cladding outward deformation exceeds the rate at which the fuel pellet expands due to irradiation (fission product) swelling (fuel swelling rate), the pellet-cladding gap will begin to open (or increase if the gap is already open). An increase in the pellet-cladding gap will reduce the pellet-cladding thermal conductance thereby increasing fuel temperatures. The increased fuel temperatures will result in further fuel pellet fission gas release, greater fuel rod internal pressure, and correspondingly a faster rate of cladding outward deformation and gap opening.

This potential thermal feedback condition is avoided by limiting the cladding creepout rate, due to fuel rod internal pressure, to less than or equal to the fuel pellet irradiation swelling rate.

4.2.1.1.3 Cladding Strain

The fuel rod cladding strain is limited to ensure that fuel rod failure due to pellet-clad mechanical interaction will not occur. To achieve this objective the calculated cladding circumferential plastic strain is limited as described in Reference 4.2-5 during anticipated operational occurrences.

4.2.1.1.4 Cladding Corrosion and Corrosion Product Buildup

Zircaloy cladding tubes undergo oxidation at slow rates during normal reactor operation and reactor water corrosion products (crud) are deposited on the cladding outside surface (see Reference 4.2-10). The cladding oxidation causes thinning of the cladding tube wall and introduces a resistance to the fuel rod-to-coolant heat transfer. Crud buildup can also introduce a resistance to heat transfer. The expected extent of the oxidation and the buildup of the corrosion products is specifically considered in the fuel rod design analyses. Thus the impacts of the temperature increase, the correspondingly altered material properties and the thinning of the

cladding wall resulting from cladding corrosion on fuel rod behavior relative to impacted design criteria (such as fuel temperature and cladding strain) are explicitly addressed. The oxide thickness itself is not separately limiting and no direct design limit on cladding oxide thickness is therefore specified.

4.2.1.1.5 Fuel Rod Hydrogen Absorption

There are two considerations relative to fuel rod hydrogen absorption. The first consideration involves the potential for hydrogenous impurity evolution, historically from the fuel pellets, resulting in primary hydriding and fuel rod failure. This consideration is addressed by the application of a specification limit on the as-fabricated fuel pellets. The absence of primary-hydriding induced fuel rod failures demonstrates the effectiveness of this limit since its first application in 1972. The second consideration is the partial absorption by the fuel rod cladding of hydrogen liberated by the cladding waterside corrosion reaction. Mechanical properties testing demonstrates that the cladding mechanical properties are negligibly affected for hydrogen contents far in excess of that experienced during normal operation. On this basis, there is no specific design criterion applied to the cladding hydrogen content.

4.2.1.1.6 Cladding Creep Collapse

The fuel rod is evaluated to ensure that fuel rod failure due to cladding collapse into a fuel column axial gap will not occur. This criterion is discussed in detail in Reference 4.2-3.

4.2.1.1.7 Fuel Rod Stresses

Based upon the limits specified in ANSI/ANS 57.5-1981, the fuel rod is evaluated to ensure that the fuel will not fail due to cladding stresses or strains exceeding the cladding ultimate stress or strain capability. The figure of merit employed is termed the Design Ratio, where:

$$\text{Design Ratio} = \frac{\text{Effective Stress}}{\text{Stress Limit}} \text{ or } \frac{\text{Effective Strain}}{\text{Strain Limit}}$$

The effective stress or strain is determined by applying the distortion energy theory. The limit is the material ultimate stress or strain. To be within the limit, the Design Ratio must be less than or equal to 1.0.

4.2.1.1.8 Dynamic Loads / Cladding Fatigue

The fuel rod is evaluated to ensure that cladding strains due to cyclic loadings will not exceed the cladding material fatigue capability. The design limit for fatigue cycling is determined from Zircaloy fatigue experiments and is conservatively specified to ensure with high confidence that failure by cladding fatigue will not occur. Based on the LWR cyclic design basis presented in Reference 4.2-5, the cladding fatigue life usage is calculated and maintained below the cladding material fatigue limit.

As noted in Subsection 4.2.1.1, for each fuel design, steady-state operating limits are established to ensure that actual fuel operation, including AOOs, complies with the fuel rod thermal–mechanical design and safety analysis bases above. These operating limits define the maximum allowable fuel operating power level as a function of fuel exposure. Lattice local power and exposure peaking factors may be applied to transform the maximum allowable fuel power level into Maximum Linear Heat Generation Rate (MLHGR) limits for individual fuel bundle designs.

4.2.1.2 Control Rods

The control rod is designed to have:

- Sufficient mechanical strength to prevent displacement of its reactivity control material
- Sufficient mechanical strength to prevent deformation that could inhibit its motion

The detailed design bases for the control rod are provided in Appendix 4C.

The control rod patterns and associated power distribution for an ESBWR are provided in Appendix 4A.

4.2.2 Description and Design Drawings

4.2.2.1 Fuel Assembly

The components of the reference fuel assembly (GE14E) are shown in Figure 4.2-2, and consist of a fuel bundle, a channel that surrounds the fuel bundle, and a channel fastener that attaches the bundle to the channel. The fuel and water rods are spaced and supported by upper and lower tieplates and intermediate spacers. The lower tieplate has a nosepiece that has the function of supporting the fuel assembly in the reactor. The upper tieplate has a handle for transferring the fuel bundle from one location to another. The identifying fuel assembly serial number is engraved on the top of the handle; no two assemblies bear the same serial number. A boss projects from one side of the handle to ensure proper orientation of the assembly in the core. Finger springs are located between the lower tieplate and channel and are utilized to control the bypass flow through that flow path. The differences between GE14E and GE14C are shown in Reference 4.2-4.

4.2.2.1.1 Fuel Rods

Each fuel rod consists of high–density ceramic uranium dioxide fuel pellets stacked within Zircaloy cladding that is evacuated, backfilled with helium and sealed with Zircaloy end plugs welded on each end. A thin zirconium barrier liner is metallurgically bonded to the innermost part of the Zircaloy cladding during cladding fabrication. Three types of fuel rods are used in a fuel bundle; tie rods, standard rods, and partial length rods. The tie rods in each fuel bundle have lower end plugs that thread into the lower tieplate and threaded upper end plugs that extend through the upper tieplate. A nut and locking tab are installed on the upper end plug to hold the fuel bundle together. The tie rods support the weight of the assembly only during fuel handling operations. During normal operation, the assembly is supported by the lower tieplate.

The end plugs of the standard rods have shanks that fit into holes in the tieplates. An expansion spring is located over the upper end plug shank of each rod in the bundle to support the weight of the upper tieplate, channel and channel fastener and to provide the necessary expansion space to accommodate the maximum expected fuel rod growth.

The partial length rods reduce the bundle pressure drop and have lower end plugs that thread into the lower tieplate, similar to the tie rods. The upper endplugs do not extend to the upper tieplate and are only used to seal the top end of the partial length rods.

U-235 enrichments may vary axially within a fuel rod and from fuel rod to fuel rod within a bundle to reduce local peak-to-average fuel rod power ratios. Selected fuel rods within each bundle may include small amounts of gadolinium as a burnable poison.

Adequate free volume to accommodate gaseous fission products released from the fuel pellets during normal operation is provided within each fuel rod in the form of a pellet-to-cladding gap and a plenum region at the top of each fuel rod. A plenum spring, or retainer, is provided in the plenum space to minimize the movement of the column of fuel pellets inside the fuel rod during shipping and handling.

4.2.2.1.2 Water Rods

Water rods are hollow Zircaloy tubes with several holes around the circumference near each end to allow coolant to flow through the rod. One water rod in each bundle axially positions the spacers. This spacer–positioning water rod is designed with spacer positioning tabs that are welded to the tube exterior above and below each spacer location. An expansion spring is located between the water rod shoulder and upper tieplate to allow for differential axial expansion similar to the full–length fuel rods.

4.2.2.1.3 Fuel Spacer

The primary function of the spacer is to provide lateral support and maintain lateral spacing of the fuel rods, with consideration of thermal-hydraulic performance, fretting wear, strength, and neutron economy.

4.2.2.1.4 Upper and Lower Tieplates

Stainless steel upper and lower tieplates carry the weight of the fuel and position the rod ends laterally during operation and handling.

4.2.2.1.5 Finger Springs

Finger springs may be employed to control the bypass flow through the channel-to-lower tieplate flow path for some fuel assemblies.

4.2.2.1.6 Channels

The fuel channel is composed of a zirconium based material or equivalent, and performs the following functions:

- Forms the fuel bundle flow path outer periphery for bundle coolant flow
- Provides surfaces for control rod guidance in the reactor core
- Provides structural stiffness to the fuel bundle sufficient to support lateral loadings applied from fuel rods through the fuel spacers
- Minimizes, in conjunction with the finger springs (if present) and bundle lower tieplate, coolant bypass flow at the channel/lower tieplate interface
- Transmits fuel assembly seismic loadings to the core internal structure (fuel top guide and fuel support)
- Provides a heat sink during loss-of-coolant accident (LOCA)

- Provides a stagnation envelope for fuel sipping

The channel is open at the bottom and makes a sliding seal fit on the lower tieplate surface. The upper ends of the fuel assemblies in a four-bundle cell are positioned in the corners of the cell against the top guide beams by the channel fastener springs. At the top of the channel, two diagonally opposite corners have welded tabs which support the weight of the channel on the two raised posts of the upper tieplate. One of these raised posts has a threaded hole. The channel is attached to the fuel bundle by threading the channel fastener screw into the upper tieplate post thread. The channel fastener assembly also includes the fuel assembly positioning spring. Proper bundle alignment in the core is aided by the fuel bundle spacer buttons located on the upper portion of the channel above the control rod passage area.

4.2.2.2 Control Rods

The control rod assemblies (Figure 4.2-3) perform the functions of power shaping, reactivity control, and scram reactivity insertion for safety shutdown response. Power distribution in the core is controlled during operation of the reactor by manipulating selected patterns of control rods to counterbalance steam void effects at the top of the core.

The control rod main structure consists of a top handle, an absorber section, and a bottom connector assembled into a cruciform shape. The top handle contains a grapple opening for handling. The absorber section is an array of stainless steel tubes filled with boron carbide powder or a combination of boron carbide powder and hafnium rods. The connector is positioned on the bottom of the control rod for attachment to the control rod drive. While being inserted into the core, the control rod is restricted to the cruciform envelope created by the fuel bundles. Handle pads guide the control rod along the channels and connector rollers guide the control rod within the guide tube as the control rod is inserted and withdrawn from the core. Configuration of the control rod is shown in Figure 4.2-4.

4.2.3 Fuel Assembly Design Evaluations

4.2.3.1 Evaluation Methods

Most of the fuel rod thermal-mechanical design analyses are performed using GSTRM (Reference 4.2-2). GSTRM analyses are performed for the following conditions:

1. For each analysis, fuel rod input parameters are based on either the most unfavorable manufacturing tolerances (‘worst case’ analyses) or statistical distributions of the input values. Calculations are then performed to provide either a ‘worst case’ or statistically bounding tolerance limit for the resulting output parameter(s).
2. Operating conditions are postulated which cover the conditions anticipated during normal steady-state operation and anticipated operational occurrences.

The first step in the fuel rod design evaluations is to establish an upper bound power history envelope for the different fuel rod types, e.g., limiting power histories as a function of the peak exposure in the fuel rod. These power histories are then used for all fuel rod thermal-mechanical design analyses to evaluate the fuel rod design features and demonstrate conformance to the design criteria. These power histories are also applied as a design constraint to the reference core loading nuclear design analyses.

In the GSTRM analyses it is assumed that during the fuel rod operating lifetime that the fuel rod (axial) node with the highest power operates on the limiting power-exposure envelope during its entire operating lifetime. The axial power distribution is changed three times during each operating cycle (BOC, MOC and EOC), to assure conservative prediction of the release of gaseous fission products from the fuel pellets to the rod free volume. The relative axial power distributions used for a standard fuel rod are shown in Figure 4.2-1.

4.2.3.1.1 Worst Tolerance Analyses

The analyses performed to evaluate the cladding circumferential plastic strain during an anticipated operational occurrence applies worst tolerance assumptions. In this case, the GSTRM inputs important to this analysis are all biased to the fabrication tolerance extreme in the direction that produces the most severe result. The biases are discussed in detail in Reference 4.2-5.

4.2.3.1.2 Statistical Analyses

The remaining GSTRM analyses are performed using standard error propagation statistical methods. The statistical analysis procedure is presented in Reference 4.2-5.

4.2.3.2 Cladding Plastic Strain

The cladding plastic strain analysis is performed using the GSTRM code and the worst-tolerance methodology noted above. For each fuel rod type the cladding plastic strain is calculated at different exposure points, whereby an overpower is assumed relative to the limiting power history. At the most limiting exposure point, the magnitude of the overpower event is further increased until the cladding plastic strain approaches limits described in Reference 4.2-5. The result from this analysis is used to establish the Mechanical Overpower (MOP) discussed below.

4.2.3.3 Fuel Rod Internal Pressure

The fuel rod internal pressure analysis is performed using the GSTRM code and the statistical methodology noted above. Values for the fuel rod internal pressure average value and standard deviation are determined at different fuel rod exposure points. At each of these exposure points, the fuel rod internal pressure required to cause the cladding to creep outward at a rate equal to the fuel pellet irradiation swelling rate is also determined using the same method. Based on the two calculated distributions a design ratio defined as the ratio of 'cladding creepout rate – to – fuel swelling rate' is determined such that, with at least 95% confidence, the fuel rod cladding will not creep out at a rate greater than the fuel pellet irradiation swelling rate.

4.2.3.4 Fuel Pellet Temperature

The fuel pellet temperature analysis is performed statistically using the GSTRM code. For each fuel rod type the fuel pellet center temperature is statistically calculated at different exposure points, whereby an overpower is assumed relative to the limiting power history. At the most limiting exposure point, the magnitude of the overpower event is further increased until incipient fuel center-melting occurs. The result from this analysis establishes the Thermal Overpower (TOP) discussed below.

4.2.3.5 Cladding Fatigue Analysis

The cladding fatigue analysis is performed statistically using the GSTRM code. For calculating the cladding fatigue, variations in power and coolant pressure, as well as coolant temperature, are superimposed on the limiting power history.

The fuel duty cycles shown in Reference 4.2-5 represent conservative assumptions regarding power changes anticipated during normal reactor operation including anticipated operational occurrences, planned surveillance testing, normal control blade maneuvers, shutdowns, and special operating modes such as daily load following. Based on these assumptions, the cladding strain cycles are analyzed as shown in Reference 4.2-5.

4.2.3.6 Cladding Creep Collapse

The cladding creep collapse analysis consists of a detailed finite element mechanics analysis of the cladding. This evaluation is described in detail in References 4.2-3 and 4.2-5.

4.2.3.7 Fuel Rod Stress Analysis

The fuel rod stress analysis is performed using the Monte Carlo statistical methodology and addresses local fuel rod stress concerns, such as the stresses at spacer contact points, that are not addressed by the GSTRM code. Results from GSTRM analyses are used to generate inputs for the stress analysis. The cladding stress analysis is described in detail in Reference 4.2-5.

4.2.3.8 Thermal and Mechanical Overpowers

As discussed above, analyses are performed to determine the values of the maximum overpower magnitudes that do not result in violation of the cladding circumferential plastic strain criterion (MOP-Mechanical Overpower) and the incipient fuel center-melting criterion (TOP-Thermal Overpower). Conformance to these criteria is demonstrated as a part of the normal core design and transient analysis process by comparison of the calculated core transient mechanical and thermal overpowers, as defined in Reference 4.2-5, to the mechanical and thermal overpower limits determined by the GSTRM analyses.

4.2.3.9 Fretting Wear

Testing is performed to assure that the mechanical features of the design, particularly those related to spacers and tie plates, do not result in significant vibration and consequent fretting wear, particularly at spacer –fuel rod contact points. The vibration response of the new design is compared to a design that has demonstrated satisfactory performance through discharge exposure.

4.2.3.10 Water Rods

Calculations are performed to determine component stresses at the bounding load conditions and compared to applicable criteria, such as yield and ultimate stresses. The load conditions take into account shipping and handling loads, seismic induced bending moment, and the pressure differential across the water rod. The design is also evaluated using finite element analysis to determine the critical buckling load and insure adequacy relative to axial loads resulting from differential growth of water rods and other fuel assembly components.

4.2.3.11 Tie Plates

Adequacy of tie plate designs is demonstrated by detailed finite element analysis and/or mechanical testing for bounding fuel handling and seismic load conditions.

4.2.3.12 Spacers

Fuel spacer acceptability is proven by testing in accordance with NRC approved methods. The bounding load condition is seismic loading. Tests are conducted to demonstrate spacer fatigue capability and compliance with load limits and to demonstrate that a coolable geometry is maintained by showing minimal deformation at the combined load condition. Fretting wear is addressed by performing FIV tests and evaluating the results relative to spacer designs that have demonstrated acceptable performance.

4.2.3.13 Channel

Channel adequacy relative to applicable design criteria is confirmed by performing the following evaluations:

- Calculation of elastic stress and deflection due to channel wall ΔP
- Calculation of thermal stresses due to the various temperature gradients to which the channel is subjected during normal operation and handling
- Calculations of fatigue and stress rupture that consider the combined effect of pressure-temperature cycling and hold time
- Elastic-plastic and creep calculations of channel wall permanent deflection
- Calculation of channel stress due to control rod contact
- Channel/lower tie plate differential thermal expansion analysis

4.2.3.14 Conclusions

The results for the analyses described above are presented in detail in References 4.2-4 and 4.2-5. In summary, the GE14 design for ESBWR operation meets all the criteria noted above, plus those that address accidents discussed in References 4.2-4 and 4.2-5.

4.2.4 Control Rod Design Evaluations

The control rod evaluation methods described in Section 4C.2 use established methodology for control rods. The evaluation methodology history demonstrates that the criteria of Appendix 4C are satisfactory for the ESBWR Marathon control rod. The Marathon control rod for ESBWR is based on the Marathon control rod design for BWR/2 through BWR/6, which has been licensed and applied to actual plants (Reference 4.2-7). Where the BWR/2 through BWR/6 was not adequate to apply to ESBWR, the ABWR design and evaluations are used.

4.2.4.1 SCRAM

The dynamic loads on the control rods are bounded by the fine motion control rod drive (FMCRD) imposed loads (scram loads) in the vertical direction. The ESBWR inoperative buffer loads are the highest vertical loads experienced by the control rod due to the high terminal

velocity. The control rod is evaluated using a dynamic analysis in Reference 4.2-8. A model of mass, springs and gap elements is used to simulate a detailed representation of all the load bearing components of the assembly during a scram event. The computer program runs the model at cold temperature speeds and properties as well as elevated temperature speeds and properties. The resultant loads are evaluated using the material properties and geometry for the area subject to the load. The effective stress is determined using distortion energy theory. The limit is the material ultimate stress or strain.

4.2.4.2 Seismic

Fuel channel deflections which result from seismic and LOCA events impose lateral loads on the control rods. The Marathon control rod is analyzed for Safe Shutdown Earthquake (SSE) events, Reference 4.2-8. The BWR/2 through 6 and the ABWR have similar channel lengths and deflections. Due to the shorter length of the ESBWR channel with the same relative cross section, the expected deflection is less.

The SSE analysis is performed by evaluating the strain in the Marathon absorber section when deflected approximately 6 mm. During a seismic event, it is assumed the seismic deflections could be added to any preexisting channel bow. The absorber section strain has been analyzed for channel deflections due to seismic and channel bow deflections when deflected approximately 10 mm and found to be acceptable, Reference 4.2-8.

The SSE analysis could be performed through testing to show full insertion during fuel channel deflections. For example, testing was performed on the ABWR Marathon to confirm seismic scramability. The ABWR Marathon was tested at amplitudes of 10, 20, 30 and 40mm. The scram times were found to be acceptable and the control rod was not damaged. The ESBWR channels will be shorter making the fuel assembly stiffer and the fuel channel lateral deflections less. The increase in system stiffness and the decrease in lateral deflection makes the ABWR Marathon seismic scramability test bounding for the ESBWR conditions.

4.2.4.3 Stuck Rod

Compression due to a stuck rod at the time of scram is controlled by the FMCRD. Assuming the FMCRD will exert the same compression loads, the shorter ESBWR control rod buckling is acceptable, even for one wing, Reference 4.2-8.

4.2.4.4 Absorber Burn-Up Related Loads

The absorber containment licensed in Reference 4.2-7 is applicable to the ESBWR Marathon. The same methodology is used for ESBWR Marathon in Reference 4.2-8. The square tube design accommodates loads created by the neutron irradiation of the absorber material. In the case of B4C powder; tube wall stresses due to helium gas generation, B4C swelling, and moisture vapor heat-up are considered. The stress due to helium pressure and strain due to B4C swelling are adequate for the nuclear design life of the control rod.

4.2.4.5 Load Combinations and Fatigue

The ESBWR Marathon is designed to withstand load combinations including anticipated operational occurrences (AOOs) and fatigue loads associated with those combinations. Absorber tube loads are evaluated during a SCRAM, in a cell with severe channel bow near end of control

rod life when absorber burn-up helium gas generation is highest. Absorber tube loads are evaluated during a seismic event near the end of control rod life when absorber burn-up helium gas generation is highest. Absorber section to connector welds and absorber section to handle loads are evaluated during a SCRAM when the absorber helium gas build-up is highest. Per Reference 4.2-8, the ESBWR Marathon does not exceed the ultimate stress or strain limit of the material. Based on the reactor cycles, the combined loads are then evaluated for the cumulative effect of the cyclic loadings in Reference 4.2-8. The fatigue usage is evaluated against a limit of 1.0.

4.2.4.6 Handling Loads

The ESBWR Marathon is designed to accommodate three times the weight of the control rod, Reference 4.2-8.

4.2.4.7 Hydraulics

Inspection experience over 15 years has shown the Marathon control rod is not damaged by the vibrations or cavitations set up by coolant velocities and velocity distributions in the bypass region between fuel channels.

4.2.4.8 Materials

Materials selected for use in the Marathon control rod components are chosen to minimize the component end-of-life radioactivity in order to reduce personnel exposure during handling on-site, and for final off-site shipping and burial. All Marathon control rod materials are less than 0.03 weight percent cobalt. The average niobium content for the handle and absorber section, less boron carbide and hafnium, is less than 0.1 weight percent.

4.2.4.9 Nuclear Performance

The nuclear lifetime of the initial ESBWR Marathon control rod type will be established as 10 percent reduction in reactivity worth ($\Delta k/k$) in any quarter axial segment, Reference 4.2-9.

4.2.4.10 Mechanical Compatibility

Similar to the control rods supplied to ABWR and BWR/2 through BWR/6, the ESBWR Marathon control rod is designed to be compatible with core and reactor internal interfaces.

The ESBWR Marathon is designed to be compatible with the control rod guide tube (CRGT) cylindrical boundary, to provide a seat with the guide tube base during Fine Motion Control Rod Drive (FMCRD) removal, to provide lower guide rollers for smooth transitions, and to have clearance with the orificed fuel support for insertion and withdrawal from the core.

The control rod coupling socket provides a compatible interface with the FMCRD. The coupling engages the FMCRD by rotating one-eighth turn (45°). With the FMCRD, control rod drive housing, and CRGT positively assembled, any orientation of the cruciform control rod between the fuel assemblies shall be a coupled position, and rotation to an uncoupled position shall not be possible during reactor operation. The four lobes of the FMCRD coupling spud are in line with the four wings of the control rod in the coupled position.

The control rod is designed to permit coupling and uncoupling of the control rod drive from below the vessel for FMCRD servicing without necessitating the removal of the reactor vessel head. The control rod is also designed to allow uncoupling and coupling from above the vessel using control rod handling tools.

The control rod is positively coupled to the FMCRD and shall be designed to remain coupled during all scrams and loading conditions, including inoperative buffer scram loads. The control rod withstands the loads induced by the FMCRD without exceeding the structural design criteria as stated in Subsections 4.2.4.1 and 4.2.4.2 above.

The control rod is dimensionally compatible with the fuel assemblies (unirradiated and irradiated). The control rod is guided, rotationally restrained and laterally supported by the adjacent fuel assemblies. The control rod is designed and constructed to establish and maintain the alignment of the control rod drive line (i.e., the control rod, drive housing, CRGT, and fuel assemblies) so that control rod insertion and withdrawal is predictable. The top of the active absorber of a fully withdrawn control rod is below the Bottom of the Active Fuel (BAF). Absorber gap requirements are placed on the control rod in the operating condition to be compatible with the core nuclear design requirements.

4.2.5 Testing, Inspection, and Surveillance Plans

GE has an active program for the surveillance of both production and developmental fuel. The NRC has reviewed the GE program and approved it in Reference 4.2-6.

4.2.6 COL Unit-Specific Information

This section contains no requirement for additional information to be provided in support of the combined license. Combined License applicants referencing the ESBWR certified design will address changes to the reference design of the fuel assembly or control rods from that presented in the DCD.

4.2.7 References

4.2-1 GE Nuclear Energy, “GE Fuel Bundle Designs,” NEDE-31152P, Revision 8, April 2001.

4.2-2 GE Nuclear Energy, “Fuel Rod Thermal Analysis Methodology (GSTRM)”, NEDC-31959P, April 1991.

4.2-3 GE Nuclear Energy, “Cladding Creep Collapse”, NEDC-33139P-A, July 2005.

4.2-4 GE Nuclear Energy, “GE14 for ESBWR Fuel Assembly Mechanical Design Report”, NEDC-33240P, Class III (proprietary), January 2006.

4.2-5 GE Nuclear Energy, “GE14 for ESBWR Fuel Rod Thermal-Mechanical Design Report”, NEDC-33242P, Class III (proprietary), Revision 1, February 2007.

4.2-6 USNRC Letter, L. S. Rubenstein (NRC) to R. L. Gridley (GE), "Acceptance of GE Proposed Fuel Surveillance Program", June 27, 1984.

4.2-7 GE Nuclear Energy, “GE Marathon Control Rod Assembly,” NEDE-31758P-A, October 1991.

4.2-8 GE Nuclear Energy, "ESBWR Marathon Control Rod Mechanical Design Report", NEDC-33244P, Class III (proprietary), June 2006.

4.2-9 GE Nuclear Energy, "ESBWR Marathon Control Rod Nuclear Design Report", NEDE-33243P, Class III (proprietary), May 2006.

4.2-10 GE Nuclear Energy, "GESTR-LOCA – A model for Prediction of Fuel Rod Thermal Performance", NEDE-23785-1-PA (Volume 1), June 1984.

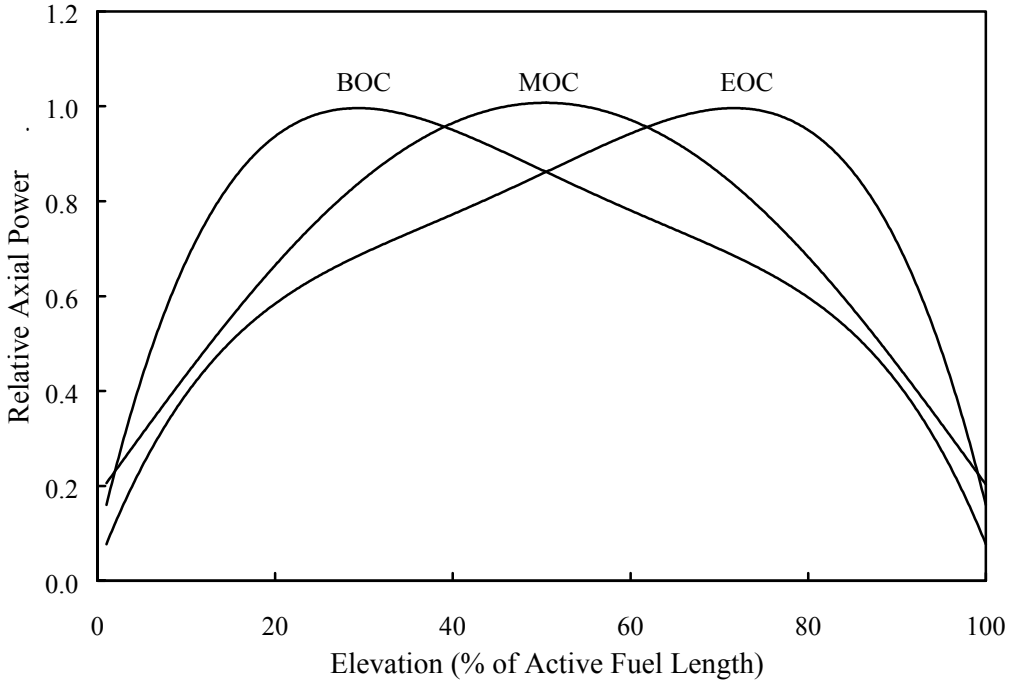

Figure 4.2-1. Axial Power Distributions (Full Length Fuel Rod)

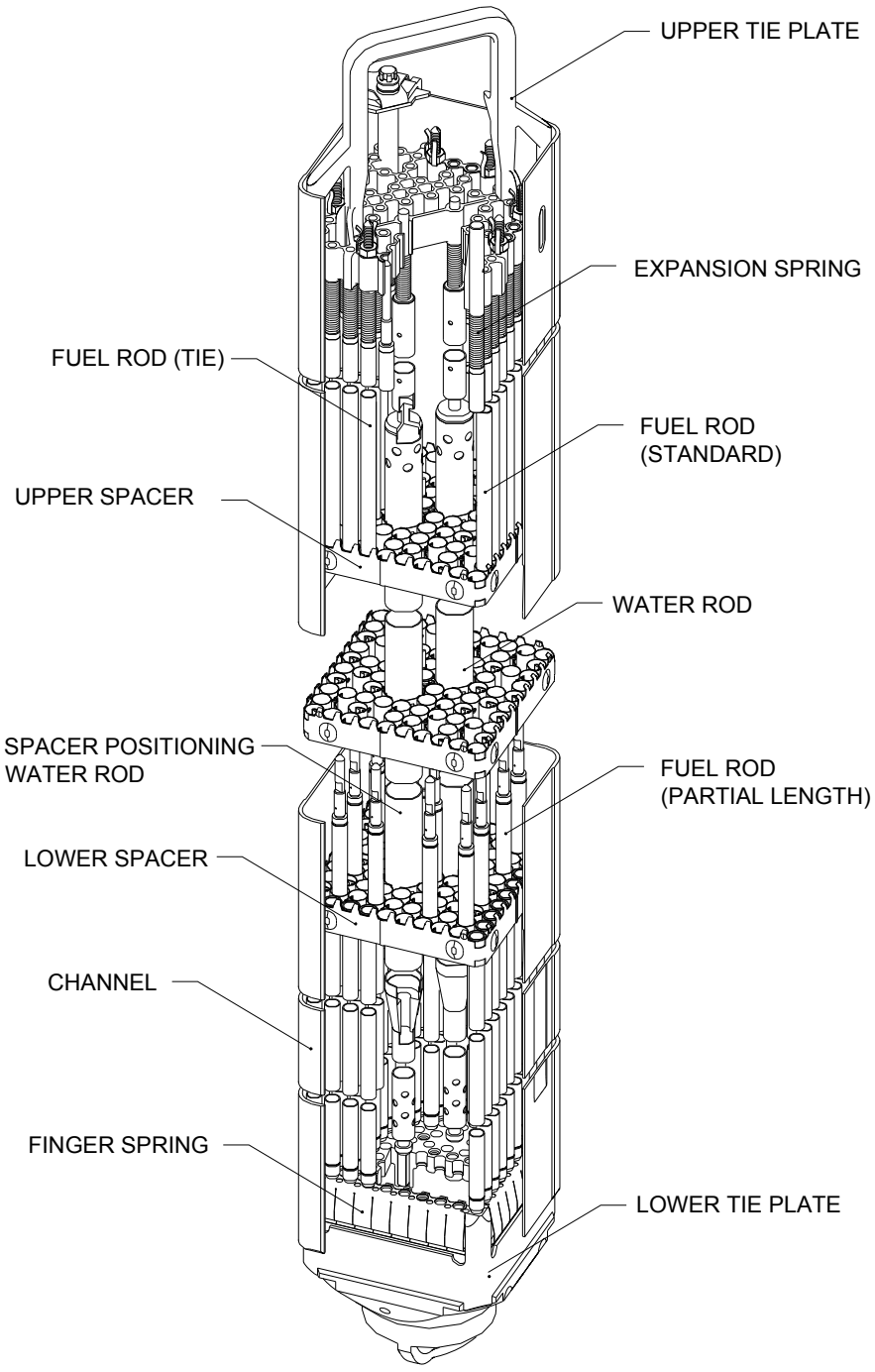

Figure 4.2-2. Fuel Assembly

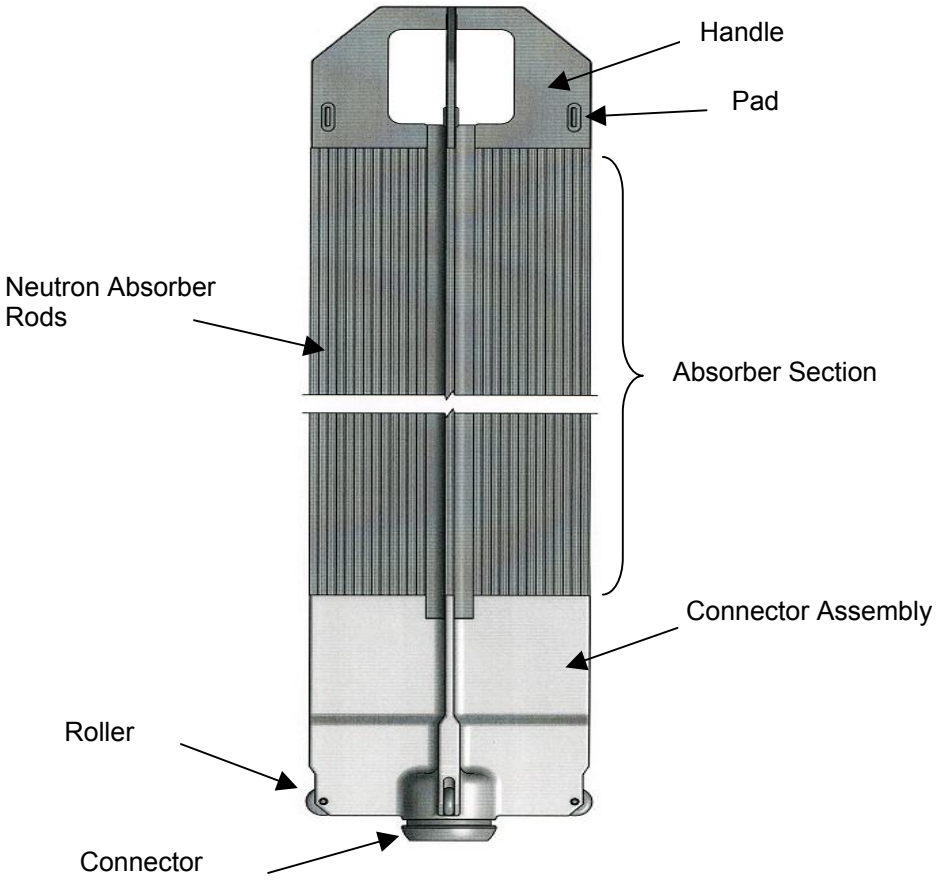

Figure 4.2-3. Typical Control Rod Assembly

Span (except at lower rollers)	= 247.7 +/- 2.3 mm
Maximum Wing Thickness	= 9.14 mm
Nominal Absorber Column Length	= 2896 mm

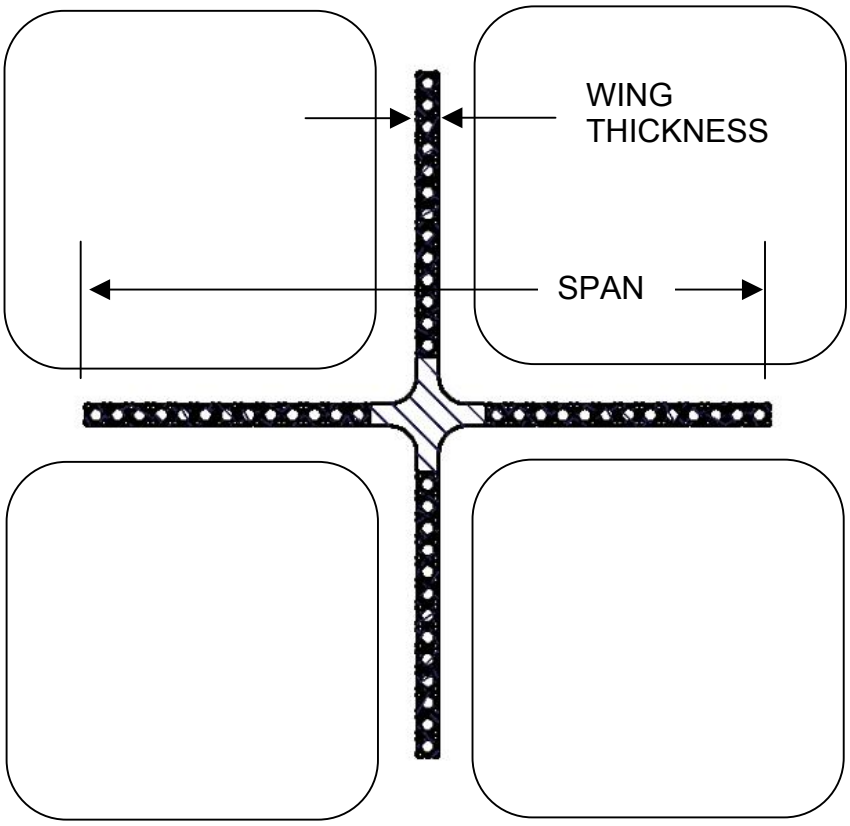

ALL VALUES NOMINAL

Absorber Rods per Wing	= 13 to 14
B_4C Density	= 1.76 grams/cm^3
Absorber Tube – Square	= 7.92 mm
Absorber Tube Material	= Stainless Steel
Control Rod Structural Material	= Stainless Steel

Figure 4.2-4. Typical ESBWR Control Rod Configuration

4.3 NUCLEAR DESIGN

This section describes the design bases and functional requirements used in the nuclear design of the fuel, core and reactivity control system and relates these design bases to the General Design Criteria (GDC) from 10 CFR Part 50, Appendix A (Reference 4.3-9).

4.3.1 Design Basis

The design bases are those that are required for the plant to operate, meeting all safety requirements. The safety design bases that are required fall into two categories:

- The reactivity basis, which prevents an uncontrolled positive reactivity excursion, and
- The overpower bases for the control of power distribution, which prevent the core from operating beyond the fuel integrity limits.

4.3.1.1 Negative Reactivity Feedback Bases

Reactivity coefficients, the differential changes in reactivity produced by differential changes in core conditions, are useful in calculating stability and evaluating the response of the core to external disturbances. The base initial condition of the system and the postulated initiating event determine which of the several defined coefficients are significant in evaluating the response of the reactor. The coefficients of interest are the Doppler coefficient, the moderator void reactivity coefficient and the moderator temperature coefficient. Also associated with the BWR is a power reactivity coefficient. The power coefficient is a combination of the Doppler and void reactivity coefficients in the power operating range; this is not explicitly evaluated. The Doppler coefficient, the moderator void reactivity coefficient and the moderator temperature coefficient of reactivity shall be negative for power operating conditions, thereby providing negative reactivity feedback characteristics.

The above design basis meets General Design Criterion 11.

4.3.1.2 Control Requirements (Shutdown Margins)

The core must be capable of being made subcritical, with margin, in the most reactive condition throughout the operating cycle with the highest worth control rod, or rod pair, stuck in the full-out position and all other rods fully inserted. This satisfies General Design Criterion 26.

4.3.1.3 Control Requirements (Overpower Bases)

The nuclear design basis for control requirements is that Maximum Linear Heat Generation Rate (MLHGR) and Minimum Critical Power Ratio (MCPR) constraints shall be met during operation. The MCPR and MLHGR are determined such that, with 95% confidence, the fuel does not exceed required licensing limits during abnormal operational occurrences.

These parameters are defined as follows:

Maximum Linear Heat Generation Rate: The MLHGR is the maximum linear heat generation for the fuel rod with the highest surface heat flux at a given nodal plane in the bundle. The MLHGR operating limit is bundle type dependent. The MLHGR can be monitored to assure that all mechanical design requirements are met. The fuel will not be operated at MLHGR values greater than those found to be acceptable within the body of the safety analysis under

normal operating conditions. Under abnormal conditions, including the maximum overpower condition, the MLHGR will not cause fuel melting or cause the stress and strain limits to be exceeded, as discussed in Section 4.2.

Minimum Critical Power Ratio: The MCPR is the minimum CPR allowed for a given bundle type to avoid boiling transition. The CPR is a function of several parameters; the most important are bundle power, bundle flow, the local power distribution and the details of the bundle mechanical design. The plant Operating Limit MCPR (OLMCPR) is established by considering the limiting anticipated operational occurrences (AOOs) for each operating cycle. The OLMCPR is determined such that 99.9% of the rods avoid boiling transition during the transient of the limiting analyzed AOO, as discussed in Section 4.4.

The above basis satisfies General Design Criterion 10.

4.3.1.4 Control Requirements (Standby Liquid Control System)

GDC 27 requires that the reactivity control systems have a combined capability, in conjunction with poison addition by the emergency core cooling system, of reliably controlling reactivity changes under postulated accident conditions, with appropriate margin for stuck rods. The nuclear design basis is that, assuming a stuck rod, or rod pair, the SLCS provide sufficient liquid poison into the system so that sufficient shutdown margin is achieved.

4.3.1.5 Stability Bases

The General Design Criteria related to stability are Criteria 10 and 12.

The reactor core and associated coolant, control, and protection systems are designed with appropriate margin to assure that specified acceptable fuel design limits are not exceeded during any condition of normal operation, including the effects of anticipated operational occurrences.

The reactor core and associated coolant, control, and protection systems are designed to assure that power oscillations which can result in conditions exceeding specified acceptable fuel design limits are not possible or can be reliably and readily detected and suppressed.

4.3.2 Nuclear Design Analytical Methods

4.3.2.1 Steady-state nuclear methods

The principal tool used in the steady-state nuclear core analysis is the three-dimensional BWR simulator code, which computes core reactivity, power distributions, exposure, and reactor thermal-hydraulic characteristics, with spatially varying voids, control rods, burnable poisons and other variables. It is used to calculate reactivity variations through the cycle, shutdown margins and thermal limits (MLHGR and MCPR).

The steady-state nuclear evaluations of the reference core design are performed using the analytical tools and methods approved in Reference 4.3-2. The applicability of these methods to the nuclear analysis of ESBWR is given in Reference 4.3-8. Changes may be made to these techniques provided that NRC-approved methods, models, and application methodologies are used.

Neutronic parameters used by the core simulator are obtained from the 2-D lattice physics code and parametrically fitted as a function of moderator density, exposure, control and moderator density history for a given fuel type. Lattice physics calculations are performed using a two-dimensional, fine mesh, few group diffusion theory computer program (TGBLA) that determines the nodal flux and power distributions in a fuel bundle (Reference 4.3-2). The lattice analyses are performed during the bundle design process. The results of these single bundle calculations are reduced to "libraries" of lattice reactivities, relative rod powers, and few group cross-sections as a function of instantaneous void, exposure, exposure-void history, control state and history, and fuel and moderator temperature. The lattice analyses depend only on fuel lattice parameters and are valid for all plants and cycles for a specific bundle design. The ESBWR core is of the N-lattice type, which is identical to the ABWR, and the lattice physics methods have been qualified for this geometry, including core tracking of operating ABWRs.

The lattice physics code calculates lattice average nuclear constants, rod-by-rod distribution of power and lattice average isotopic data for an infinite array of identical lattices. These are all calculated as a function of exposure, voids, control state, and temperature. Specific applications of the lattice physics program include fuel lattice design, fuel bundle design and fuel bundle reconstitution physics analysis.

The solution technique begins with the generation of thermal broad-group neutron cross sections for all homogenized fuel rod cells and external regions in a bundle. In the thermal energy range, the rod-by-rod thermal spectra are calculated by a collision probability method similar to the THERMOS formulation. The major difference is that neutron leakage from rod to rod is taken into account. The leakage is determined by diffusion theory and is fed into the thermal spectrum calculation. Iterations between diffusion theory and thermal spectrum calculations are carried out to determine accurate, spatially dependent, thermal cross sections. In the epithermal and fast energy range, the level-wise resonance integrals are calculated by an improved intermediate resonance (IR) approximation in which the IR parameters are fuel-rod-temperature dependent. The fast and epi-thermal regional flux is determined by a multi-group collision probability process.

A two-dimensional, coarse-mesh, broad-group, diffusion-theory calculation is used to determine the nodal flux distributions in the bundle. By combining the two-dimensional, coarse-mesh, broad-group flux and the intra-nodal collision probability flux profiles, the lattice intra-nodal flux and power distributions are obtained. In the depletion calculation, 100 nuclides are treated, including 25 fissile and fertile nuclides and up to 48 fission products, one pseudo fission product and one gadolinia tail pseudo product. A Runge-Kutta-Gill burnup integration scheme is employed to determine the isotopic inventory for fuel material depletion. The TGBLA program includes a sub-channel void distribution model to capture the impact of non-uniform voids on local pin powers.

The BWR core simulator (PANACEA) is a static, three-dimensional coupled nuclear-thermal-hydraulic computer program representing the BWR core exclusive of any external flow loops. Provisions are made for fuel cycle and thermal limits calculations. The program is used for detailed three-dimensional design and operational calculations of BWR neutron flux and power distributions and thermal performance as a function of control rod position, refueling pattern, coolant flow, reactor pressure, and other operational and design variables. A power-exposure iteration option is available for target exposure distribution and cycle length predictions.

The nuclear model is based on coarse-mesh nodal, static diffusion theory. Eigenvalue iteration yields the fundamental mode solution. This is coupled to static parallel channel thermal-hydraulics containing a modified Zuber-Findlay void-quality correlation. Pressure drop balancing yields the flow distribution among the channels.

These methods (TGBLA06/PANAC11) include a 1½ energy group neutron diffusion model with non-linearly coupled spatially asymptotic thermal flux model, spectral history reactivity model, control blade history reactivity and local peaking models, explicit temperature (density) dependence for cold critical data, pin power reconstruction, and internal cross section library generation. The control blade history model uses TGBLA cross section data from a controlled depletion with uncontrolled restarts for each specific fuel type. The impacts on reactivity and local peaking are included using an exponentially weighted scheme.

PANACEA is used in core design and operational calculations to produce reactivity, power distribution, and thermal performance information as functions of design and operational variables such as fuel loading pattern, control rod position, coolant flow, and reactor pressure. Specific applications include fuel loading, fuel cycles, core design configuration, core management and on site core monitoring.

TRACG is iteratively used with the simulator code to establish the total core flow for a given core power in order to account for the flow loop external to the core. This iteration is described in Section 4.4. The application of TRACG to the ESBWR core is described in Reference 4.3-7. The ESBWR core is not substantially different from operating BWRs from the viewpoint of steady-state nuclear simulations of core parameters.

4.3.2.2 Reactivity Coefficient Methods

The Doppler reactivity coefficient is determined by using an NRC-approved lattice physics code. The Doppler coefficient is determined using the theory and methods for steady-state nuclear calculations, described above.

The lattice physics code is used to calculate k_∞ for any lattice at two temperatures. The first temperature is the standard hot operating temperature. The second temperature is set at 1773 K. The calculations are made at as a function of void fraction and at every standard hot uncontrolled exposure depletion point.

The Doppler Reactivity Coefficient (DRC) is characterized as follows:

$$DRC = \frac{1000(k_{T_1} - k_{T_0})}{k_{T_0}\left(\sqrt{T_1} - \sqrt{T_0}\right)}$$

where:

T_0 = normal hot operating temperature (Kelvin).

T_1= elevated temperature (Kelvin).

k_{T1} = eigenvalue at elevated temperature.

k_{T0}= eigenvalue at normal operating temperature.

While the reactivity change caused by the Doppler effect is small compared to the moderator void reactivity changes during normal operation, it becomes very important during postulated rapid power excursions in which large fuel temperature changes occur (see Chapter 15).

The 3D core simulator is used in determining the void coefficient of reactivity. A detailed discussion of the methods used to calculate moderator void reactivity coefficients, the accuracy and application to plant transient analyses, is presented in Reference 4.3-4. The In-Channel Void Coefficient (VODCOF) is the ratio of the change in k-effective to the change in (percent) void fraction because of a perturbation in some particular parameter:

$$VODCOF = \frac{1}{k}\frac{\partial k}{\partial(\%VOID)}$$

The calculation of the void reactivity coefficient is accomplished through perturbation of the inlet enthalpy to the core, although perturbation of pressure or core flow are also possible to effect a change in voids and reactivity. The derivative in the above equation is determined by a higher-order numerical scheme, which requires two points above and two points below the base point in addition to the base point itself. After evaluating four perturbations to the original system, one obtains a better estimate than any of the original four approximate derivatives. This type of evaluation is subsequently less sensitive to the type and size of the perturbation for evaluation of a particular derivative.

The moderator temperature coefficient (MODCOF) is calculated using a combination of the lattice physics code and core simulator. The lattice physics code is used to evaluate infinite lattice properties of each of the various lattices in the fuel bundle as a function of exposure, void history and temperature. Introducing the temperature specific nuclear libraries from the lattice physics code into the core simulator and performing a standard cold eigenvalue calculation then simulates a core temperature change. From the differential in core eigenvalue, the moderator temperature coefficient of reactivity may be obtained as:

$$MODCOF = \frac{1}{k}\frac{\partial k}{\partial(^{\circ}K)}$$

4.3.2.3 Stability Methods

A detailed discussion of the methods used to analyze ESBWR thermal hydraulic stability is presented in Reference 4.3-7.

4.3.3 Nuclear Design Evaluation

The core design consists of a light-water moderated reactor, fueled with slightly enriched uranium-dioxide. The use of water as a moderator produces a neutron energy spectrum in which fissions are caused principally by thermal neutrons. At normal operating conditions, the moderator boils, producing a spatially variable distribution of steam voids in the core. The void reactivity feedback effect is an inherent safety feature of the ESBWR system. Any system

change which increases reactor power, either in a local or core-wide sense, produces additional steam voids and thus reduces the power.

4.3.3.1 Nuclear Design Description

The reference core design is examined in detail in Reference 4.3-8. The reference core design is characterized by the loading pattern given in Figure 4.3-1. This core design is the basis for the system analyses in other sections of this Design Control Document. For cores other than the reference core design or the initial core, the Reference Loading Pattern (RLP) is the nuclear design basis for fuel licensing. The RLP core is designed to represent, as closely as possible, the actual core loading pattern. However, there may be occurrences where the number and/or types of bundles in the reference design and the actual core loading do not exactly agree. Any differences between the reference loading pattern and the actual loading pattern are evaluated to ensure that there is no adverse impact to key parameters that may affect the licensing calculations.

4.3.3.2 Negative Reactivity Feedback Evaluation

Reactivity coefficients are a measure of the differential changes in reactivity produced by differential changes in core conditions. These coefficients are useful in understanding the response of the core to external disturbances. The Doppler reactivity coefficient and the moderator void reactivity coefficient are the two primary reactivity coefficients that characterize the dynamic behavior of boiling water reactors.

The safety analysis methods (described in Chapter 15) are based on system and core models that include an explicit representation of the core space-time kinetics. Therefore, the reactivity coefficients are not directly used in the safety analysis methods, but are useful in the general understanding and discussion of the core response to perturbations.

4.3.3.2.1 Doppler Reactivity Coefficient Evaluation

The Doppler coefficient is a measure of the reactivity change associated with an increase in the absorption of resonance-energy neutrons caused by a change in the temperature of the material in question. The Doppler reactivity coefficient provides instantaneous negative reactivity feedback to any rise in fuel temperature, on either a gross or local basis. The magnitude of the Doppler coefficient is inherent in the fuel design and does not vary significantly among BWR designs. For most structural and moderator materials, resonance absorption is not significant, but in U-238 and Pu-240 an increase in temperature produces a comparatively large increase in the effective absorption cross-section. The resulting parasitic absorption of neutrons causes an immediate loss in reactivity.

Analyses were performed using the analytical models described above, as described in Reference 4.3-8. The values are identical to the analysis supporting compliance for GE14 found in Reference 4.3-3, which consists of examination of the lattice level Doppler coefficients for several lattice configurations. Evaluating the Doppler coefficient at the 2D lattice level obviates the need for more detailed calculations involving the 3D core simulator. For all cases evaluated, the calculated Doppler coefficient was found to be negative. A typical value calculated is -1.10 $\Delta k/°K^{0.5}$ (at zero exposure, 0.4 void fraction).

4.3.3.2.2 Moderator Void Coefficient Evaluation

The moderator void coefficient should be large enough to prevent power oscillation due to spatial xenon changes yet small enough that pressurization transients do not unduly limit plant operation. In addition, the void coefficient has the ability to flatten the radial power distribution and to provide ease of reactor control due to the void feedback mechanism. The overall void coefficient is always negative over the complete operating range.

Analyses of the moderator void coefficient of the reference core design were performed, as described in Reference 4.3-8. The results of these analyses show that boiling of the moderator in the active channel flow area results in negative reactivity feedback for all expected modes of operation. The operating mode selected to represent the most limiting condition (the least negative value of moderator void coefficient) was the cold critical state at the middle of an equilibrium cycle. The value of moderator void coefficient for this condition was calculated to be -0.0052 $\Delta k/\%$ void at zero void, for a moderator temperature of 100°C at the middle of the reference design fuel cycle. The variation of the void coefficient as a function of temperature is shown in Figure 4.3-2 for several exposure points in the reference fuel cycle.

4.3.3.2.3 Moderator Temperature Coefficient Evaluation

The moderator temperature coefficient is an aspect of the BWR core that is routinely evaluated as part of core and fuel design. The moderator temperature coefficient is associated with the change in the water moderating capability. A negative moderator temperature coefficient during power operation provides inherent protection against power excursions. Hot standby is the condition under which the BWR core coolant has reached rated pressure and temperature and is the state point at which a negative moderator temperature coefficient is required. Once boiling begins, the core dynamic response is dominated by the void coefficient.

The BWR core can exhibit a positive moderator temperature coefficient; although, fleet operation experience has shown it is uncommon or otherwise manageable. The primary parameters that lead to a positive moderator temperature coefficient are the critical control rod density, the gadolinia content present, the lattice geometry and the enrichment. The two most important parameters are the control rod density and the gadolinia content. As insertion of the control rod displaces water in the intra-assembly gap, controlled nodes tend to contribute to a negative moderator temperature coefficient. Similarly, both gadolinia and control rods are strong local absorbers and as neutron migration area increases with moderator temperature both absorbers become more effective leading to a negative moderator temperature coefficient. As the core is depleted through power operation both the critical control rod density and the gadolinia content reduces which can lead to positive temperature coefficients at low temperature for late cycle startups. It is noted that most, if not all, modern BWR fuel designs can be evaluated as having a positive moderator temperature coefficient under certain conditions at moderator temperatures below hot standby; however, as the transient response of the core to a positive moderator temperature coefficient during startup is slow due to the time required to increase the coolant temperature, and reduce the fuel temperature after an initial power increase, a positive moderator temperature coefficient does not pose a problem for reactivity control.

Analyses of the moderator temperature coefficient of the reference core design were performed, as described in Reference 4.3-8. The variation of the moderator temperature coefficient as a

function of temperature is shown in Figure 4.3-3 for several exposure points in the reference fuel cycle.

The most limiting state condition was determined to be at the end of the reference fuel cycle for a critical core configuration. The results of the analyses at these conditions were that the moderator temperature coefficient is negative for all moderator temperatures above approximately 130°C.

The results of these analyses at these conditions indicate that the moderator temperature coefficient is negative for all moderator temperatures in the operating temperature range. Therefore, the moderator temperature coefficient criteria are met.

4.3.3.3 Control Requirements Evaluation

The ESBWR control rod system is designed to provide adequate shutdown margin and control of the maximum excess reactivity anticipated during the plant operation.

There are 135 Hydraulic Control Units (HCUs) that move all 269 control rods. Thus, there are 134 HCUs associated with two control rods while the center control rod is powered by one HCU. Figure 4.3-5 shows the HCU to FMCRD assignments.

4.3.3.3.1 Shutdown Margin Evaluation

The shutdown margin is evaluated by calculating the core neutron multiplication with the core simulator at selected exposure points, assuming the highest worth control rod, or rod pair, is stuck out in the fully withdrawn position.

As exposure accumulates and burnable poison depletes in the lower exposure fuel bundles, an increase in core reactivity may occur. The nature of the increase depends on the specifics of the fuel loading and control state. For fuel cycles beyond the initial core, the shutdown margin is calculated based on the carryover of the expected exposure at the end of the previous cycle. The core is assumed to be in the cold, xenon-free condition in order to ensure that the calculated values are conservative. Further discussion of the uncertainty of these calculations is given in Reference 4.3-5.

The cold k_{eff} is calculated with the highest worth control rod, or rod pair, out at various exposures through the cycle. A value R is defined as the difference between the highest worth rod out k_{eff} at beginning of cycle (BOC) and the maximum calculated highest worth rod out k_{eff} at any exposure point.

The strongest rod, or rod pair, out k_{eff} at any exposure point in the cycle is equal to or less than

$$k_{eff} = k_{eff}(\textit{Strongest rod withdrawn @ BOC}) + R$$

where R is conservatively determined to be greater than or equal to 0. The value of R includes equilibrium samarium.

The calculated k_{eff} with the highest worth rod pair withdrawn at BOC are reported in Table 4.3-1. The uncontrolled and fully controlled k_{eff} values are also reported in Table 4.3-1. The minimum required shutdown margin is given in the technical specifications. Details of the calculation of shutdown margin are given in Reference 4.3-8.

4.3.3.3.2 Reactivity Variation Evaluation

The excess reactivity designed into the core is controlled by the control rod system supplemented by gadolinia-urania fuel rods. These integral fuel burnable absorber rods may be used to provide partial control of the excess reactivity available during the fuel cycle. The burnable absorber loading controls local peaking factors and lowers the reactivity of the fuel bundle. The burnable absorber performs this function by reducing the requirement for control rod inventory in the core at the beginning of the fuel cycle, as described previously. Control rods are used during the cycle to compensate for reactivity changes due to burnup and also to control the power distribution.

The nuclear design of the fuel assemblies comprising the equilibrium cycle reference core design, including enrichment and burnable absorber distributions within the assembly, is given in Reference 4.3-8, as is information relating to the reactivity variation through the cycle (i.e., hot excess reactivity). The control rod patterns through the cycle of the reference core design are given in Appendix 4A using a quarter core (mirror reflected) representation.

4.3.3.3.3 Standby Liquid Control System Evaluation

The Standby Liquid Control System (SLCS) is designed to provide the capability of bringing the reactor, at any time in a cycle, from full power with a minimum control rod inventory (which is defined to be at the peak of the xenon transient) to a subcritical condition with the reactor in the most reactive xenon-free state. The SLCS is described in detail in Subsection 9.3.5.

The requirements of this system are dependent primarily on the reactor power level and on the reactivity effects of voids and temperature between full-power and cold, xenon-free conditions. The shutdown capability of the SLCS for the reference ESBWR core is discussed in detail in Reference 4.3-8. The shutdown margin is calculated for a uniformly mixed equivalent concentration of natural boron, which is required in the reactor core to provide adequate cold shutdown margin after operation of the SLCS. Calculations are performed throughout the cycle including the most reactive critical, xenon-free condition. Calculations are performed with all control rods withdrawn. Figure 4.3-4 demonstrates the adequate SLCS shutdown margin for the ESBWR core compared to a limit of 1%.

4.3.3.4 Criticality of Reactor During Refueling Evaluation

The basis for maintaining the reactor subcritical during refueling is presented in Subsection 4.3.1.2, and a discussion of how control requirements are met is given in Subsection 4.3.3.3.1. The minimum required shutdown margin is given in the technical specifications.

4.3.3.5 Power Distribution Evaluation

The core power distribution is a function of fuel bundle design, core loading, control rod pattern, core exposure distributions and core coolant flow rate. The thermal performance parameters, MLHGR and MCPR, limit the core power distribution. The analysis of the performance of the reference core design in terms of power distribution, and the associated MLHGR and MCPR distributions within the core throughout the cycle exposure, is given in detail in Reference 4.3-8.

4.3.3.5.1 Power Distribution Measurements

The techniques for measurement of the power distribution within the reactor core, together with instrumentation correlations and operation limits, are discussed in Subsections 7.2.2 and 7.7.6.

4.3.3.5.2 Power Distribution Accuracy

The accuracy of the calculated power distribution is discussed in Reference 4.3-1.

4.3.3.5.3 Power Distribution Anomalies

Stringent inspection procedures are utilized to ensure the correct arrangement of the core following fuel loading. A fuel loading error (a mislocated or a misoriented fuel bundle in the core) is a very improbable event, but calculations have been performed to determine the effects of such events. The fuel loading error is discussed further in Chapter 15.

The inherent design characteristics of the ESBWR are well suited to limit gross power tilting. The stabilizing nature of the large moderator void coefficient effectively reduces the effect of perturbations on the power distribution. In addition, the in-core instrumentation system, together with the online computer, provides the operator with prompt information on the power distribution so that control rods or other means to limit the undesirable effects of power tilting can readily be used. Because of these design characteristics, it is not necessary to allocate a specific margin in the peaking factor to account for power tilt. If, for some reason, the power distribution cannot be maintained within normal limits using control rods, then the total core power can be reduced.

4.3.3.6 Stability Evaluation

4.3.3.6.1 Xenon Transients

Boiling water reactors do not have instability problems due to xenon. This has been demonstrated by:

- Never having observed xenon instabilities in operating BWRs;
- Special tests which have been conducted on operating BWRs in an attempt to force the reactor into xenon instability; and
- Calculations.

All of these indicators have proven that xenon transients are highly damped in a BWR due to the large negative moderator void feedback. Xenon stability analysis and experiments are reported in Reference 4.3-6. Specific evaluations demonstrating the damping of xenon transients (oscillations) in the ESBWR core are carried out in Reference 4.3-8.

4.3.3.6.2 Thermal Hydraulic Stability

The most limiting stability condition in the ESBWR normal operating region is at the rated power/flow condition. Therefore, the ESBWR is designed so that the core remains stable throughout the whole operating region, including plant startup. In order to establish a high degree of confidence that oscillations will not occur, conservative design criteria were imposed on the channel, core wide and regional decay ratios under all conditions of normal operation and

anticipated transients. The ESBWR licensing basis for stability is satisfied by determining a stability criteria map of core decay ratio vs. channel decay ratio to establish margins to stability.

Because oscillations in power and flow are precluded by design, the requirements of GDC 10 are met through the analysis for AOOs, and are automatically satisfied with respect to stability.

In addition, the ESBWR will implement a Detect and Suppress solution as a defense-in-depth system. The thermal hydraulic stability is discussed in detail in Appendix 4D.

4.3.4 Changes

Not applicable.

4.3.5 COL Unit-Specific Information

Combined Operating License applicants referencing the ESBWR certified design will address changes to the reference design of the fuel or core design from that presented in the DCD.

4.3.6 References

4.3-1 Letter from R. J. Reda (GE) to R. C. Jones (NRC), MFN-098-96, "Implementation of Improved GE Steady-State Methods", July 2, 1996.

4.3-2 Letter from Stuart A. Richards to Glen A. Watford, “Amendment 26 to GE Licensing Topical Report NEDE–24011–P–A, GESTAR II – Implementing Improved GE Steady–State Methods (TAC No. MA6481),” November 10, 1999.

4.3-3 Global Nuclear Fuel, “GE14 Compliance With Amendment 22 of NEDE-24011-P-A (GESTAR II),” NEDC-32868P, Rev. 1, September 2000.

4.3-4 R. C. Stirn, “Generation of Void and Doppler Reactivity Feedback for Application to BWR Design,” NEDO–20964, December 1975.

4.3-5 General Electric Company, “BWR/4,5,6 Standard Safety Analysis Report,” Revision 2, Chapter 4, June 1977.

4.3-6 R. L. Crowther, “Xenon Considerations in Design of Boiling Water Reactors,” APED–5640, June 1968.

4.3-7 General Electric Company, “TRACG Application for ESBWR Stability Analysis,” NEDE-33083, Supplement 1, B. S. Shiralkar, et al., December 2004.

4.3-8 Global Nuclear Fuel, “GE14 for ESBWR Nuclear Design Report”, NEDC-33239-P, February 2007.

4.3-9 Title 10, Part 50 Appendix A (10 CFR 50 Appendix A) of the Federal Code of Regulations, “General Design Criteria for Nuclear Power Plants.”

Table 4.3-1

Calculated Core Effective Multiplication and Control System Worth - No Voids, 20°C

Control Rod Pattern *	K-effective
Uncontrolled	1.1112
Fully Controlled	0.9508
Strongest Control Rod Pair Out **	0.9843

* For the Reference Core Loading Pattern at the limiting exposure of 0 GWd/MT.

** The rod pair are shown in Figure 4.3-5.

	1	2	3	4	5	6	7	8	9	10	11	12	13	14	15	16	17	18	19
1															36.86	35.60	38.91	35.94	37.24
2													43.03	37.56	36.70	19.13	17.65	16.90	0.00
3											39.40	36.77	19.76	0.00	21.57	22.59	19.88	0.00	33.57
4									39.21	37.16	17.70	0.00	0.00	0.00	22.56	20.50	0.00	0.00	14.76
5								41.07	14.88	0.00	0.00	0.00	18.69	0.00	0.00	0.00	32.42	0.00	22.59
6							38.26	16.34	0.00	0.00	0.00	21.39	0.00	22.80	0.00	23.28	0.00	22.99	0.00
7						38.26	38.90	0.00	18.39	0.00	32.15	20.06	0.00	0.00	27.24	20.84	21.99	0.00	23.61
8					41.08	16.34	0.00	0.00	0.00	22.12	17.29	31.50	0.00	13.40	15.39	16.11	0.00	21.89	23.07
9				39.21	14.88	0.00	18.39	0.00	18.59	0.00	0.00	0.00	21.10	0.00	21.96	0.00	22.04	0.00	21.94
10				37.17	0.00	0.00	0.00	22.12	0.00	23.11	0.00	21.88	0.00	22.55	0.00	0.00	0.00	22.08	0.00
11			39.41	17.69	0.00	0.00	32.15	17.28	0.00	0.00	30.65	21.94	21.72	0.00	30.82	21.97	22.36	0.00	23.35
12			36.78	0.00	0.00	21.39	20.05	31.51	0.00	21.87	21.94	22.98	0.00	0.00	21.79	22.39	0.00	0.00	22.15
13		43.00	19.76	0.00	18.68	0.00	0.00	0.00	21.09	0.00	21.72	0.00	23.10	0.00	22.20	0.00	22.59	0.00	22.44
14		37.56	0.00	0.00	0.00	22.80	0.00	13.41	0.00	22.54	0.00	0.00	0.00	22.98	0.00	22.21	0.00	22.06	0.00
15	36.86	36.72	21.57	22.55	0.00	0.00	27.25	15.38	21.96	0.00	30.83	21.79	22.20	0.00	30.65	22.77	0.00	0.00	29.09
16	35.60	19.13	22.58	20.50	0.00	23.27	20.84	16.11	0.00	0.00	21.97	22.39	0.00	22.20	22.76	22.98	0.00	21.48	22.69
17	38.91	17.65	19.88	0.00	32.43	0.00	21.99	0.00	22.04	0.00	22.36	0.00	22.58	0.00	0.00	0.00	22.98	0.00	22.60
18	35.95	16.90	0.00	0.00	0.00	22.98	0.00	21.89	0.00	22.07	0.00	0.00	0.00	22.06	0.00	21.48	0.00	23.11	0.00
19	37.24	0.00	33.58	14.76	22.58	0.00	23.60	23.06	21.94	0.00	23.34	22.15	22.44	0.00	29.09	22.69	22.60	0.00	23.11

Figure 4.3-1. Core Loading Map – Reference Loading Pattern Exposures (GWD/MT)

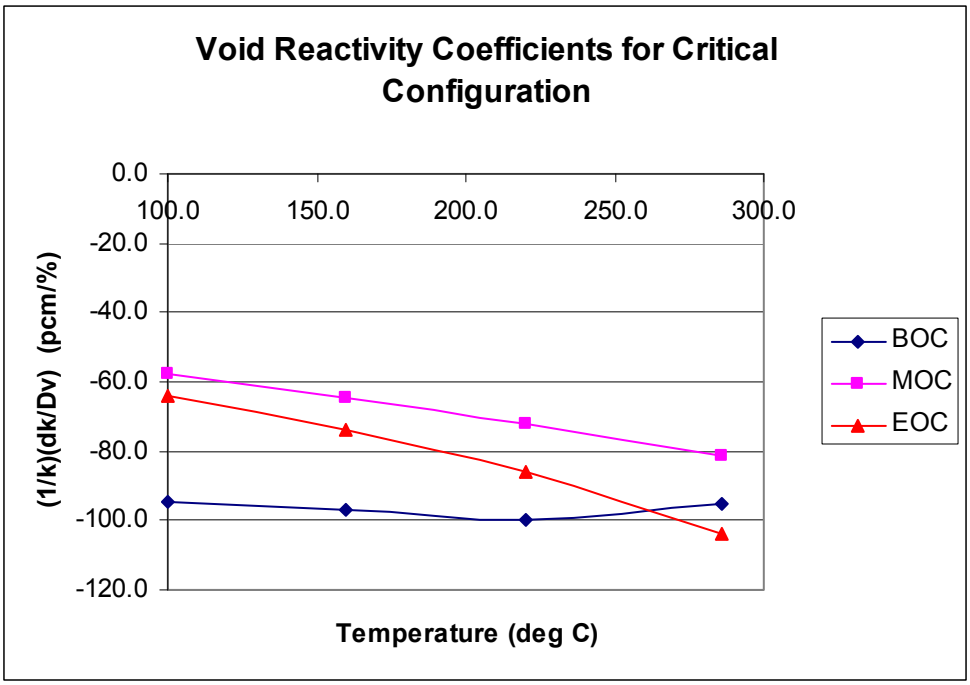

Figure 4.3-2. Moderator Void Coefficient for Reference Core Design

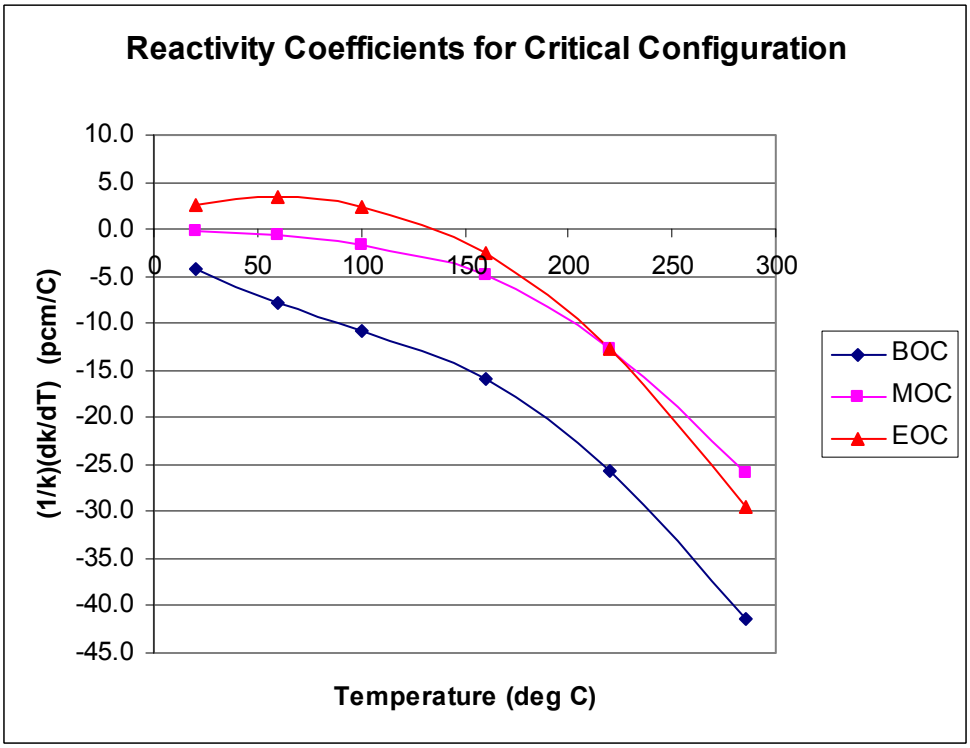

Figure 4.3-3. Moderator Temperature Coefficient for Reference Core Design

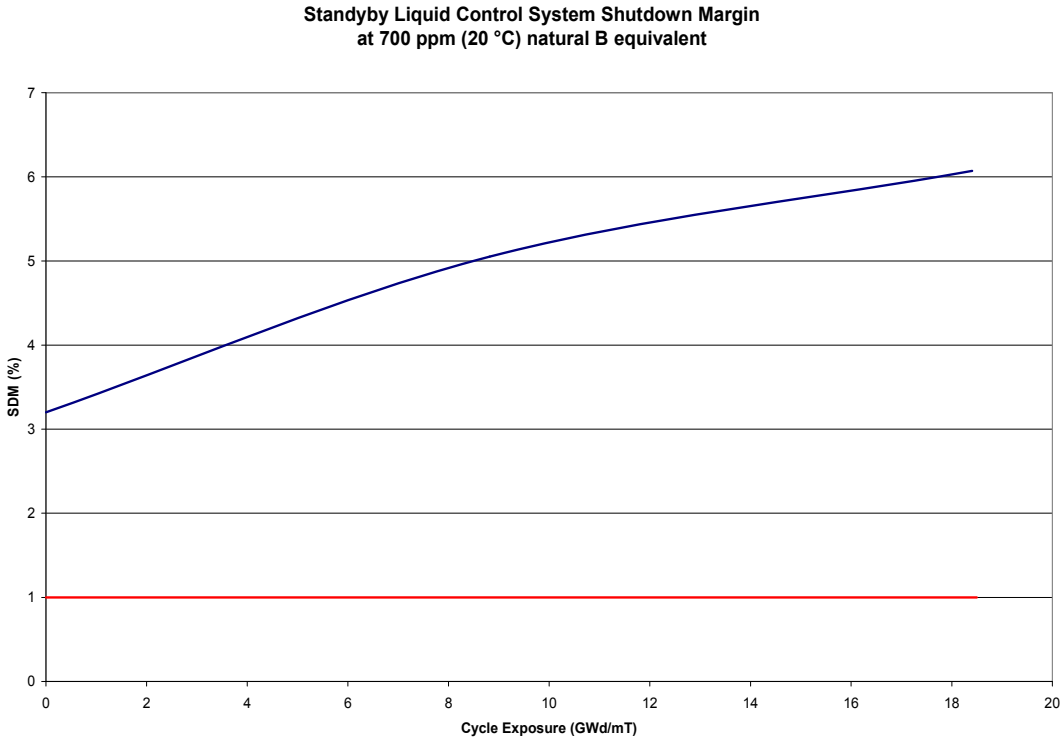

Figure 4.3-4. SLCS Shutdown Margin for Reference Core Design

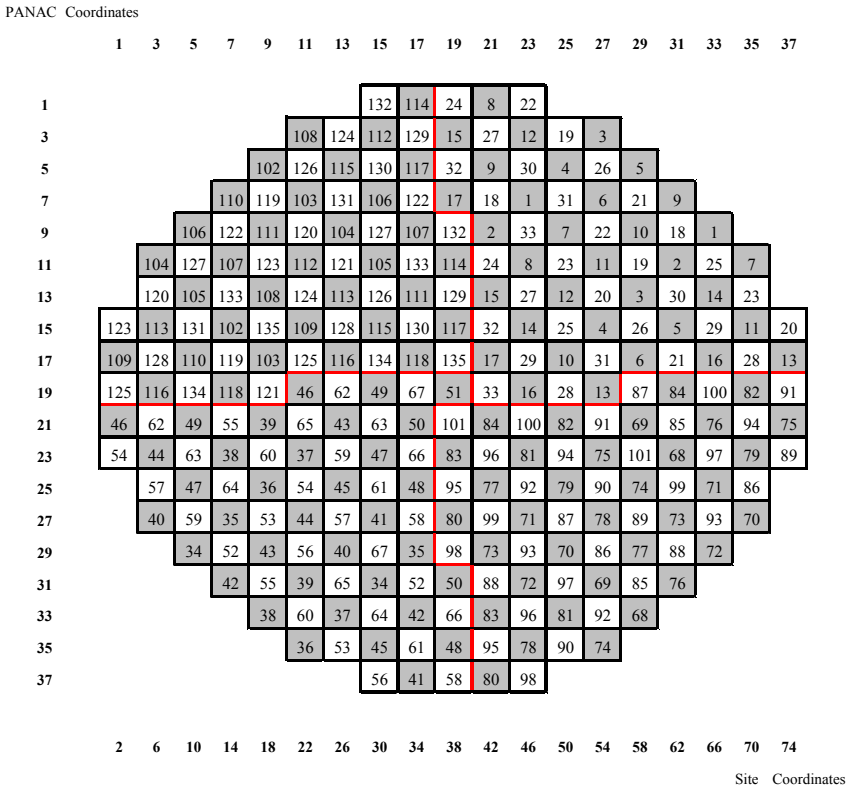

Figure 4.3-5. Hydraulic Control Unit Assignments

4.4 THERMAL AND HYDRAULIC DESIGN

This section describes the design bases and functional requirements used in the thermal and hydraulic design of the fuel, core and reactivity control system and relates these design bases to the General Design Criteria (GDC). Subsections 4.4.1, 4.4.2 and 4.4.3 describe the Design Basis, Methods and Evaluations of Reactor Core Thermal Hydraulics, respectively. Within each of these subsections, several topics, e.g., critical power, void fraction, pressure drop, etc., are discussed sequentially, A reader may, therefore, go through subsections, 4.4.1.n, 4.4.2.n and 4.4.3.n to obtain the complete information on a particular topic, n.

4.4.1 Reactor Core Thermal and Hydraulic Design Basis

Thermal-hydraulic design of the core shall establish the thermal-hydraulic safety limits for use in evaluating the safety margin in accordance with GDC 10. The thermal hydraulic stability performance of the core addressing GDC 12 is covered in Section 4.3 and Appendix 4D.

Margin to specified acceptable fuel design limits is maintained during normal steady-state operation when the minimum critical power ratio (MCPR) is greater than the required MCPR operating limit (OLMCPR) and the linear heat generation rate (LHGR) is maintained below the maximum LHGR (MLHGR) limit(s). The steady-state OLMCPR and MLHGR limits are determined by analysis of the most severe anticipated operational occurrences (AOOs) to accommodate uncertainties and provide reasonable assurance that no fuel damage results during AOOs. These limits are required by the Technical Specifications.

4.4.1.1 Critical Power Bases

The objective for normal operation and AOOs is to maintain nucleate boiling and thus avoid a transition to film boiling. Limits are specified to maintain adequate margin to the onset of the boiling transition. The figure of merit utilized for plant operation is the critical power ratio (CPR). The CPR is the ratio of the bundle power at which some point within the assembly experiences onset of boiling transition to the operating bundle power. Thermal margin is stated in terms of the minimum value of the critical power ratio (MCPR) that corresponds to the most limiting fuel assembly in the core. The design requirement is based on a statistical analysis such that for AOOs at least 99.9% of the fuel rods would be expected to avoid boiling transition (Reference 4.4-8 and 4.4-9).

4.4.1.1.1 Fuel Cladding Integrity Safety Limit Bases

GDC 10 requires, and safety limits ensure, that specified acceptable fuel design limits are not exceeded during steady-state operation, normal operational transients, and anticipated operational occurrences (AOOs). Since the parameters that result in fuel damage are not directly observable during reactor operation, the thermal and hydraulic conditions that result in the onset of boiling transition have been used to mark the beginning of the region in which fuel damage could occur. The Fuel Cladding Integrity Safety Limit (FCISL) is set such that no significant fuel damage is calculated to occur during normal operation and AOOs. Although it is recognized that the onset of boiling transition would not result in damage to BWR fuel rods, a calculated fraction of rods expected to avoid boiling transition has been adopted as a convenient limit. The FCISL is defined as the fraction (%) of total fueled rods that are expected to avoid boiling

transition during normal operation and AOOs. A value of 99.9% provides assurance that specified acceptable fuel design limits are met.

4.4.1.1.2 MCPR Operating Limit Calculation Bases

A plant-unique MCPR operating limit (OLMCPR) is established to provide adequate assurance that the FCISL for that plant is not exceeded during normal operation and any AOO. By operating with the MCPR at or above the OLMCPR, the FCISL for that plant is not exceeded during normal operation and AOOs. This operating requirement is obtained by statistically combining the maximum ΔCPR/ICPR (the change in CPR through the transient divided by the initial CPR) value for the most limiting AOO from conditions postulated to occur at the plant with the uncertainties associated with plant initial conditions and modeling of the transient ΔCPR.

4.4.1.2 Void Fraction Distribution Bases

The void fraction in a boiling water reactor (BWR) fuel bundle has a strong effect on the nuclear flux and power distribution. Therefore accurate prediction of the void fraction is important for evaluation of the performance of the BWR reactor and fuel. In design and licensing calculations the void fraction is evaluated using empirical correlations based on the characteristic dimensions of the fuel bundle and hydraulic properties of the two-phase flow in the fuel bundle.

4.4.1.3 Core Pressure Drop and Hydraulic Loads Bases

The accuracy on the prediction of core pressure drop is essential to the modeling of fuel and core inlet flow and hydraulic loads. Further details are given in Subsection 4.4.2.3.

4.4.1.4 Core Coolant Flow Distribution Bases

Based on the prediction of core pressure drop, the distribution of flow into the fuel channels and the core bypass regions are calculated. The core coolant flow distribution forms the basis of the prediction of steady-state and transient critical power and void fraction.

4.4.1.5 Fuel Heat Transfer Bases

The model must accurately predict heat transfer between the coolant, fuel rod surface, cladding, gap, and fuel pellet in the evaluation of core and fuel safety criteria. Standard and well-accepted heat transfer correlations between the coolant and the rod surfaces are used. Further details are given in Subsection 4.4.2.5.

4.4.1.6 Maximum Linear Heat Generation Rate Bases

The Maximum Linear Heat Generation Rate (MLHGR) bases are described in Section 4.2. The adequacy of MLHGR limits are evaluated for the most severe anticipated operational occurrences (AOOs) to provide reasonable assurance that no fuel damage results during AOOs.

4.4.1.7 Summary of Design Bases

The steady-state operating limits have been established to assure that the design bases are satisfied for the most severe AOO, discussed in Section 15.2. The effects of the limiting AOO do not result in any violation of the acceptance criteria set forth in Subsection 15.0.3.1, for which

the fuel, the reactor pressure vessel or the containment are designed. Therefore, these barriers maintain their integrity and function as designed.

4.4.2 Reactor Core Thermal and Hydraulic Methods

This section contains a description of the application of NRC-approved methods to the ESBWR. Changes may be made to these techniques provided that NRC-approved (including applicability to ESBWR) methods, models, and application methodologies are used.

4.4.2.1 Critical Power Methods

The qualification of the critical power methods for ESBWR is discussed in Subsection 4.4.3.

4.4.2.1.1 Bundle Critical Power Performance Method

The bundle critical power performance methodology is described in References 4.4-8 and 4.4-16. These references describe the form of the GEXL correlation and the experimental qualification that demonstrates the GEXL correlation adequately predicts the bundle critical power over a wide range of fluid parameters, axial power shapes and heated lengths. Each fuel bundle design has a specific set of correlation coefficients developed from full-scale test data. The specific GEXL correlation applied in the analysis of GE14E for ESBWR is designated GEXL14. The applicability of GEXL14 to GE14E is addressed in Reference 4.4-12.

4.4.2.1.2 Fuel Cladding Integrity Safety Limit Statistical Method

The statistical analysis utilizes a model of the core that simulates the core monitoring system. The model produces a critical power ratio (CPR) map of the core based on steady-state uncertainties defined in Table 5-1 of Reference 4.4-12. This is coupled with the TRACG ΔCPR/ICPR results to develop the OLMCPR. Details of the procedure are documented in Section 5.13 of Reference 4.4-12 and Subsection 4.6.3 of Reference 4.4-9. Random Monte Carlo selections of all operating parameters based on the uncertainty ranges of manufacturing tolerances, uncertainties in measurement of core operating parameters, calculation uncertainties, the uncertainty in the calculation of the transient ΔCPR/ICPR and statistical uncertainty associated with the critical power correlations are imposed on the analytical representation of the core and the resulting bundle critical power ratios are calculated.

The number of rods expected to avoid boiling transition is determined for each random Monte Carlo trial. The initial MCPR during normal operation corresponds to the OLMCPR when the FCISL (99.9% of the rods are expected to avoid boiling transition) is met for a statistical combination of the trials. Reference 4.4-9 defines the statistical combination method.

4.4.2.1.3 MCPR Operating Limit Calculation Method

All ESBWR AOO events are analyzed using the TRACG model described in Reference 4.4-10. The core thermal hydraulic models have been qualified in Reference 4.4-11. Uncertainties have been developed for all High and Medium ranked model parameters. The model uncertainties are documented in Reference 4.4-9. The ΔCPR/ICPR is calculated in accordance with Reference 4.4-9.

4.4.2.2 Void Fraction Distribution Methods

The empirical correlations used for the calculation of the void fraction are the GE void fraction correlation that is used in the 3D core simulator and steady state thermal hydraulic calculations and the correlations for the interfacial shear that is used in TRACG. The GE void fraction model is described in Reference 4.4-15, and details on the qualification are contained in Attachment A to Reference 4.4-13. The TRACG void fraction model is described in Reference 4.4-10 and details on the qualification are contained in Reference 4.4-11.

4.4.2.3 Core Pressure Drop and Hydraulic Loads Methods

The total bundle pressure drop is defined as the sum of four components: friction, elevation, acceleration, and local losses. In these models, the bundle is also divided into control volumes over which the four components of total pressure drop are evaluated separately, thus allowing to capture the effects on pressure drop of axially variable geometry parameters such as flow area, hydraulic diameter, wetted/heated perimeters, heat flux, and spacer elevations. The TRACG methods for core pressure drop modeling are described in Reference 4.4-10. The TRACG hydraulic formulation for core pressure drop is identical to the model utilized in the core design analysis with the exception of the acceleration pressure drop component. The models utilized in the core design analysis are as follows:

4.4.2.3.1 Friction Pressure Drop

Friction pressure drop is calculated with a basic model as follows:

$$\Delta P_f = \frac{w^2}{2 g_c \rho} \frac{fL}{D_H A_{ch}^2} \phi_{TPF}^2$$

where

ΔP_f = friction pressure drop, psi

w = mass flow rate

g_c = conversion factor

ρ = average nodal liquid density

D_H = channel hydraulic diameter

A_{ch} = channel flow area

L = incremental length

f = friction factor

ϕ_{TPF} = two–phase friction multiplier

The formulation for the two-phase multiplier is similar to that presented in References 4.4-4 and 4.4-5. The single-phase friction factor and two-phase friction multiplier in the above equation were validated by extensive comparisons to full-scale rod bundle pressure drop data provided in Reference 4.4-14.

4.4.2.3.2 Local Pressure Drop

The local pressure drop is defined as the irreversible pressure loss associated with an area change, such as the orifice, lower tie plate, and spacers of a fuel assembly.

The general local pressure drop model is similar to the friction pressure drop and is

$$\Delta P_L = \frac{w^2}{2 g_c \rho} \frac{K}{A_{ch}^2} \phi_{TPL}^2$$

where

ΔP_L = local pressure drop, psi

K = local pressure drop loss coefficient

A = reference area for local loss coefficient

ϕ_{TPL} = two–phase local multiplier

and w, g_c, and ρ are as previously defined. The formulation for the two-phase multiplier is similar to that reported in Reference 4.4-5. The local loss component of the total pressure drop across a region inside the fuel assembly is deduced from the measured total pressure drop by subtracting the frictional and acceleration components. The corresponding local loss coefficient is then determined using the above local pressure drop formula. The pressure drop data taken for the specific designs of the BWR fuel assembly, discussed in Reference 4.4-14, were obtained from tests performed in single-phase water to calibrate the orifice, the lower tie plate, and the holes in the lower tie plate, and in both single and two-phase flow, to derive the best fit design values for spacer and upper tie plate pressure drop. The range of test variables was specified to include the range of interest for boiling water reactors. New test data are obtained whenever there is a significant design change to ensure the most applicable methods are used. However, the ESBWR reference fuel assembly (GE14E) utilizes the same hardware currently used in the GE14 fuel assembly, i.e. the same upper-tie plate, spacers, water rods, and the same bundle inlet design. Therefore, its pressure drop characteristics at the upper-tie plate region, spacers, water rods, and the bundle inlet region remains unchanged and no new test data is required. The applicability of the data to ESBWR is discussed in Subsection 4.4.2.3.5.

4.4.2.3.3 Elevation Pressure Drop

The elevation pressure drop is based on the relation:

$$\Delta P_E = \bar{\rho} \Delta L \frac{g}{g_c}$$

$$\bar{\rho} = \rho_f (1 - \alpha) + \rho_g \alpha$$

where

ΔP_E = elevation pressure drop

ΔL = incremental length

$\bar{\rho}$ = average mixture density

g = acceleration of gravity

α = nodal average void fraction

ρ_f, ρ_g = saturated water and vapor density, respectively

Other terms are as previously defined. The TRACG void fraction model is described in Reference 4.4-10. The void fraction model utilized in the core design analysis is described in References 4.4-6 and 4.4-15.

4.4.2.3.4 Acceleration Pressure Drop

A reversible pressure change occurs when an area change is encountered, and an irreversible loss occurs when the fluid is accelerated through the boiling process. The basic formulation for the reversible pressure change resulting from a flow area change in the case of single–phase flow is given by:

$$\Delta P_{ACC} = \left(1 - \sigma_A^2\right) \frac{w^2}{2 g_c \rho_f A_2^2}$$

$$\sigma_A = \frac{A_2}{A_1} = \frac{final\ \ flow\ area}{initial\ \ flow\ area}$$

where:

ΔP_{ACC} = acceleration pressure drop

A_2 = final flow area

A_1 = initial flow area

In the case of two–phase flow, the liquid density is replaced by a density ratio so that the reversible pressure change is given by:

$$\Delta P_{ACC} = \left(1 - \sigma_A^2\right) \frac{w^2 \rho_H}{2 g_c \rho_{KE}^2 A_2^2}$$

where:

$\frac{1}{\rho_H} = \frac{x}{\rho_g} + \frac{1-x}{\rho_f}$, homogeneous density,

$\frac{1}{\rho_{KE}^2} = \frac{x^3}{\rho_g^2 \alpha^2} + \frac{(1-x)^3}{\rho_f^2 (1-\alpha)^2}$, kinetic energy density,

α = void fraction at A_2

x = steam quality at A_2

Other terms are as previously defined. The basic formulation for the acceleration pressure change due to density change is:

$$\Delta P_{ACC} = \frac{w^2}{g_c A_{ch}^2}\left[\frac{1}{\rho_{OUT}} - \frac{1}{\rho_{IN}}\right]$$

where ρ is either the homogeneous density, ρ_H, or the momentum density, ρ_M

$$\frac{1}{\rho_M} = \frac{x^2}{\rho_g \alpha} + \frac{(1-x)^2}{\rho_f (1-\alpha)}$$

ρ is evaluated at the inlet and outlet of each axial node. Other terms are as previously defined. The total acceleration pressure drop in boiling water reactors is on the order of a few percent of the total pressure drop. Note that the TRACG model is different for the acceleration pressure drop modeling (see Reference 4.4-10).

4.4.2.3.5 Total Pressure Drop Qualification

The GE14 pressure drop is characterized in Reference 4.4-14. The loss coefficients are qualified against pressure drop test data. The test range includes the operating conditions for the ESBWR. The ESBWR reference fuel assembly (GE14E) utilizes the same hardware currently used in the GE14 fuel assembly, i.e. the same upper-tie plate, spacers, water rods, and the same bundle inlet design. Therefore, its pressure drop characteristics at the upper-tie plate region, spacers, water rods, and the bundle inlet region remains unchanged. Moreover, the differences in active fuel length, spacer separation, and part-length rod height between the GE14 and GE14E fuel design are accounted for in determining the local loss coefficients from the experimental data as explained in Subsection 4.4.2.3.2. Because operating conditions and geometry are compatible, the loss coefficients can be applied to the ESBWR. The uncertainty in the core pressure drop is defined by Reference 4.4-9 Subsection 4.4.1 item C23.

4.4.2.3.6 Hydraulic Loads

Hydraulic loads are determined based on the reactor internal pressure differences (RIPDs) discussed in Subsection 3.9.5.3. The TRACG computer code is used to analyze the transient conditions within the reactor vessel following AOOs, infrequent events and accidents (e.g., LOCA).

4.4.2.4 Core Coolant Flow Distribution Methods

The core coolant flow distribution methods used in TRACG are described in Reference 4.4-10 Chapters 6 and 7. TRACG treats all fuel channels as one-dimensional (axial) components, but the vessel is modeled as a three-dimensional component. Hence, the pressure drop across two planes in the vessel is the same at all radial and azimuth locations if the geometry of the components in the vicinity of these planes has radial and azimuthal symmetry. Otherwise, this pressure differential displays some (locally) radial and azimuth non-uniformity.

The flow distribution to the fuel assemblies and bypass flow paths in the core simulator model is calculated on the assumption that the pressure drop across all fuel assemblies and bypass flow paths is the same. The bundle pressure drop evaluation includes frictional, local, elevation, and acceleration losses (Subsections 4.4.2.3.1 - 4.4.2.3.4). The pressure drop methodology has been qualified to the whole range of test data discussed in Reference 4.4-14. The core inlet flow is an input to the core simulator model. The value used in the core design analysis is determined

based on the TRACG prediction of the natural circulation core inlet flow. In operation, the core monitoring system will determine core inlet flow based on plant instrumentation (see Chapter 7).

The bypass flow methodology is described in Reference 4.4-10 Subsection 7.5.1. The same methodology supports the core simulator model.

4.4.2.5 Fuel Heat Transfer Methods

The Jens-Lottes (Reference 4.4-7) heat transfer correlation is used in fuel design to determine the cladding-to-coolant heat transfer coefficients for nucleate boiling. For the single-phase convection or liquid region, the well-established Dittus-Boelter correlation is used. The methodology for fuel cladding, gap and pellet heat transfer is described in Section 4.2.

4.4.2.6 Maximum Linear Heat Generation Rate Methods

The Maximum Linear Heat Generation Rate (MLHGR) methods are described in Section 4.2. Margin to design limits for circumferential cladding strain and centerline fuel temperature is evaluated for AOOs in accordance with Reference 4.4-9 Subsection 4.6.2.1.

4.4.3 Reactor Core Thermal and Hydraulic Evaluations

Typical thermal-hydraulic parameters for the ESBWR are compared to those for a typical BWR/6 plant and the ABWR in Table 4.4-1.

4.4.3.1 Critical Power Evaluations

4.4.3.1.1 Bundle Critical Power Performance Evaluation

The bundle critical power performance results are described in Reference 4.4-12. This reference utilizes full-scale test data to support the development of the critical power correlation for ESBWR. Compliance to steady-state MCPR operating limits is demonstrated for a typical simulation of an equilibrium cycle in Appendix 4A.

4.4.3.1.2 Fuel Cladding Integrity Safety Limit Evaluation

The Fuel Cladding Integrity Safety Limit (FCISL) is defined as 99.9% of the total fueled rods are expected to avoid boiling transition during normal operation and AOOs. Section 6 of Reference 4.4-12 provides a summary of the basis for the representative operating limit MCPR used for the ESBWR to protect the FCISL. Section 5 of Reference 4.4-12 provides the basis for the uncertainties specific to the ESBWR used in this evaluation.

4.4.3.1.3 MCPR Operating Limit Evaluation

The MCPR Operating Limit ΔCPR/ICPR results are described in Section 15.2. The MCPR Operating Limit development including incorporation of the Fuel Cladding Integrity Safety Limit uncertainties is described in Reference 4.4-12.

4.4.3.2 Void Fraction Distribution Evaluations

The axial distribution of void fractions for the radially average channel and a conservative hot channel as predicted by TRACG are given in Table 4.4-2. The core average and maximum exit values are also provided. Similar distributions for steam quality are given in Table 4.4-3. The

axial power distribution used to produce these tables is given in Table 4.4-4. The axial void and power distributions for the channel with the highest exit void fraction for the core reference loading pattern (Figure 4.3-1 and Appendix 4A) are given in Table 4.4-5.

The expected operating void fraction for the ESBWR is within the qualification basis of the void fraction methods. The void fractions in Table 4.4-2a and 4.4-2b are based on TRACG. The hot channel in Table 4.4-2b is a hypothetical channel with a bundle power (radial power) set so as to result in a CPR of 1.20. This hot channel has a maximum void fraction of 0.92. This is conservative compared to the assumed OLMCPR for ESBWR. The void fraction qualification database (References 4.4-11 and 4.4-15) contains void fractions in excess of 0.92 and covers the void fraction range expected for normal steady-state operation as well as AOOs. The core simulator maximum exit void fraction, for the steady-state simulation in Appendix 4A, is 0.90 as shown in Table 4.4-5.

The TRACG AOO calculations in Chapter 15 include the consideration of uncertainty in the void fraction.

4.4.3.3 Core Pressure Drop and Hydraulic Loads Evaluations

The expected operating pressure for the ESBWR is within the qualification basis of the pressure drop methods. The TRACG AOO calculations in Chapter 15 include the consideration of uncertainty in the channel pressure drop. The statistical OLMCPR method also assumes pressure drop uncertainty. The impact of uncertainty in core pressure drop is included in the results provided in Reference 4.4-12. Evaluations of hydraulic loads for the reactor internals and the fuel assembly are discussed in Subsection 3.9.5.4 and 4.2.3, respectively.

4.4.3.4 Core Coolant Flow Distribution Evaluations

The impact of uncertainty in core flow distribution is included in the results provided in Reference 4.4-12.

4.4.3.5 Fuel Heat Transfer Evaluations

The fuel heat transfer models are included in evaluations described in Section 4.2 and Chapter 15.

4.4.3.6 Maximum Linear Heat Generation Rate Evaluations

The AOO results are described in Chapter 15 Section 15.2. Compliance to steady-state MLHGR limits is demonstrated for a typical simulation of an equilibrium cycle in Appendix 4A.

4.4.4 Description of the Thermal–Hydraulic Design of the Reactor Coolant System

4.4.4.1 Plant Configuration Data

4.4.4.1.1 Reactor Coolant System Configuration

The Reactor Coolant System is described in Chapter 5. The ESBWR reactor coolant system is shown in Figure 5.1-1. The ESBWR design is similar to that of the operating BWRs, except that the recirculation pumps and associated piping are eliminated. Circulation of the reactor coolant through the ESBWR core is accomplished via natural circulation. The natural circulation flow

rate depends on the difference in water density between the down comer region and the core region. The core flow varies according to the power level, as the density difference changes with changes in power levels. Therefore, a core power-flow map is only a single line and there is no active control of the core flow at any given power level.

4.4.4.1.2 Reactor Coolant System Thermal–Hydraulic Data

The steady-state distribution of temperature, pressure and flow rate for each flow path in the Reactor Coolant System is shown in Figure 1.1-3.

4.4.4.1.3 Reactor Coolant System Geometric Data

Volumes of regions and components within the reactor vessel are shown in Figure 5.1-1. Table 4.4-6 provides the flow path length, height, liquid level, minimum elevations, and flow areas for each major flow path volume within the reactor vessel.

4.4.4.2 Operating Restrictions on Pumps

Not Applicable to the ESBWR. The ESBWR is a natural circulation design.

4.4.4.3 Power/Flow Operating Map

The core power-flow map is only a single line and there is no active control of the core flow at a given power level. To provide additional operational flexibility, a core power – feedwater temperature operating map is being envisioned. The system hardware required to develop and implement such an operating map is discussed in Subsection 10.4.7.2.2.3. As mentioned in Subsection 10.4.7.2.3, the maximum feedwater temperature is limited to less than or equal to 215.6°C (420°F) at all power levels by use of administrative controls, equipment design, or a combination of both.

4.4.4.4 Temperature-Power Operating Map

Not Applicable to the ESBWR.

4.4.4.5 Load Following Characteristics

Load following is implemented through the Plant Automation System (PAS). This is described in Chapter 7 Subsection 7.7.4.

4.4.4.6 Thermal-Hydraulic Characteristics Summary Tables

The thermal-hydraulic characteristics are provided in Table 4.4-1 and Table 4.4-6. The axial power distributions for the average and hot channels are shown in Table 4.4-4. The axial distribution of void fractions for the average power channel and the hot channel are given in Table 4.4-2. The core average and core maximum exit void fractions are also provided. Similar distributions for coolant flow quality are provided in Table 4.4-3.

4.4.4.7 Inadequate Core Cooling (ICC) Monitoring System

The issue of Inadequate Core Cooling (ICC) monitoring system has been discussed in Appendix 1A (Response to TMI Related Matters) of this ESBWR DCD, Tier 2 Specifically, the TMI Item II.F.2 in Table 1A-1 (TMI Action Plan Items) addresses this issue related to the ESBWR.

4.4.5 Loose-Parts Monitoring System

This system has been deleted.

4.4.6 Testing and Verification

The testing and verification techniques to be used to assure that the planned thermal and hydraulic design characteristics of the core have been provided, and remain within required limits throughout core lifetime, are discussed in Chapter 14.

4.4.7 COL Unit-Specific Information

4.4.7.1 Reactor Core Thermal and Hydraulic Design

This section contains no requirement for additional information to be provided in support of the combined license. Combined Operating License applicants referencing the ESBWR certified design would address changes to the thermal-hydraulic design of the reactor coolant system, if different from that presented in the DCD.

4.4.8 References

4.4-1 General Electric Company, "Core Flow Distribution in a Modern Boiling Water Reactor as Measured in Monticello," NEDO-10299A, October 1976.

4.4-2 General Electric Company, "Core Flow Distribution in a General Electric Boiling Water Reactor as Measured in Quad Cities Unit 1," NEDO-10722A, August 1976.

4.4-3 General Electric Company, "Brunswick Steam Electric Plant Unit 1 Safety Analysis Report for Plant Modifications to Eliminate Significant In-Core Vibrations," NEDO-21215, March 1976.

4.4-4 R. C. Martinelli and D.E. Nelson, "Prediction of Pressure Drops During Forced Convection Boiling of Water," ASME Trans., 70, 695-702, 1948.

4.4-5 C. J. Baroczy, "A Systematic Correlation for Two-Phase Pressure Drop," Heat Transfer Conference (Los Angeles), AIChE, reprint No. 37, 1965.

4.4-6 N. Zuber and J. A. Findlay, "Average Volumetric Concentration in Two-Phase Flow Systems," Transactions of the ASME Journal of Heat Transfer, November 1965.

4.4-7 W. H. Jens and P. A. Lottes, "Analysis of Heat Transfer, Burnout, Pressure Drop and Density Data for High Pressure Water," USAEC Report ANL-4627, 1951.

4.4-8 General Electric Company, "General Electric BWR Thermal Analysis Basis (GETAB): Data Correlation and Design Application," NEDO-10958-A, January 1977.

4.4-9 GE Nuclear Energy, "TRACG Application for ESBWR," NEDE-33083P-A Revision 0, Class III (proprietary), March 2005.

4.4-10 GE Nuclear Energy, "Licensing Topical Report TRACG Model Description", NEDE-32176P, Revision 3, Class III (proprietary), April 2006.

4.4-11 GE Nuclear Energy, "Licensing Topical Report TRACG Qualification," NEDE-32177P Revision 2, Class III (proprietary), January 2000.

4.4-12 GE Nuclear Energy, "GE14 for ESBWR-Critical Power Correlation, Uncertainty, and OLMCPR Development", NEDC-33237P, Revision 1, Class III (proprietary), December 2006.

4.4-13 GE Nuclear Energy, "Methodology and Uncertainties for Safety Limit MCPR Evaluations", NEDC–32601P-A, Class III (proprietary), August 1999.

4.4-14 GE Nuclear Energy, "GE14 Pressure Drop Characteristics", NEDC-33238P, Class III (proprietary), December 2005.

4.4-15 "TASC-03A, A Computer Program for Transient Analysis of a Single Channel", NEDC-32084P-A, Revision 2, Class III (proprietary), July 2002.

4.4-16 Letter, J.S. Charnley (GE) to C. O. Thomas (NRC), Amendment 15 to General Electric Licensing Topical Report NEDE-24011-P-A, January 25, 1986.

Table 4.4-1a

Typical Thermal–Hydraulic Design Characteristics of the Reactor Core (SI Units)

General Operating Conditions	BWR/6	ABWR	ESBWR
Reference design thermal output (MWt)	3579	3926	4500
Power level for engineered safety features (MWt)	3730	4005	4590
Steam flow rate, at 420°F final feedwater temperature (kg/s)	1940	2122	2433
Core coolant flow rate (kg/s)	13104	14502	9034-10584
Feedwater flow rate (kg/s)	1936	2118	2451
System pressure, nominal in steam dome (kPa)	7171	7171	7171
System pressure, nominal core design (kPa)	7274	7274	7240
Coolant saturation temperature at core design pressure (°C)	288	288	288
Average power density (kW/L)	54.1	50.6	54.3
Core total heat transfer area (m^2)	6810	7727	9976
Core inlet enthalpy (kJ/kg)	1227	1227	1183-1197
Core inlet temperature (°C)	278	278	270-272
Core maximum exit voids within assemblies (%)	79.0	75.1	90.0
Core average void fraction, active coolant	0.414	0.408	0.530
Active coolant flow area per assembly (m^2)	0.0098	0.0101	0.0093
Core average inlet velocity (m/s)	2.13	1.96	1.12
Maximum inlet velocity (m/s)	2.60	2.29	1.15
Total core pressure drop (kPa)	182.0	168.2	70.0
Core support plate pressure drop (kPa)	151.7	137.9	41.3
Average orifice pressure drop, central region (kPa)	39.4	60.3	20.3
Average orifice pressure drop, peripheral region (kPa)	129	122	37.1
Maximum channel pressure loading (kPa)	106	75.2	24.4
Average-power assembly channel pressure loading (bottom) (kPa)	97.2	65.5	21.5
Shroud support ring and lower shroud pressure loading (kPa)	177	165	7.4
Upper shroud pressure loading (kPa)	25.5	24.1	17.4

Table 4.4-1b

Typical Thermal–Hydraulic Design Characteristics of the Reactor Core (English Units)

General Operating Conditions	BWR/6	ABWR	ESBWR
Reference design thermal output (MWt)	3579	3926	4500
Power level for engineered safety features (MWt)	3730	4005	4590
Steam flow rate, at 420°F final feedwater temperature (Mlb/hr)	15.40	16.84	19.31
Core coolant flow rate (Mlb/hr)	104.0	115.1	71.7-84.0
Feedwater flow rate (Mlb/hr)	15.4	16.8	19.5
System pressure, nominal in steam dome (psia)	1040	1040	1040
System pressure, nominal core design (psia)	1055	1055	1050
Coolant saturation temperature at core design pressure (°F)	551	551	550.6
Average power density (kW/L)	54.1	50.6	54.3
Core total heat transfer area (ft^2)	73,303	83,176	107,376
Core inlet enthalpy (Btu/lb)	527.7	527.6	508.7-514.7
Core inlet temperature (°F)	533	533	517.5-522.4
Core maximum exit voids within assemblies (%)	79.0	75.1	90.0
Core average void fraction, active coolant	0.41	0.41	0.53
Active coolant flow area per assembly ($in.^2$)	15.2	15.7	14.4
Core average inlet velocity (ft/sec)	7.0	6.4	3.7
Maximum inlet velocity (ft/sec)	8.5	7.5	3.8
Total core pressure drop (psi)	26.4	24.4	10.2
Core support plate pressure drop (psi)	22	20	6.0
Average orifice pressure drop, central region (psi)	5.7	8.8	2.9
Average orifice pressure drop, peripheral region (psi)	18.7	17.7	5.4
Maximum channel pressure loading (psi)	15.40	10.9	3.5
Average-power assembly channel pressure loading (bottom) (psi)	14.1	9.5	3.1
Shroud support ring and lower shroud pressure loading	25.7	23.9	1.1
Upper shroud pressure loading (psi)	3.7	3.5	2.5

Table 4.4-2a

Void Distribution for Analyzed Core - TRACG Average Channel

Channel Power = 4.427 MW, CPR = 1.67
Active Fuel Length = 3.048 m / 120.00 inches

Node (m above BAF)	Average Node Value	Node (m above BAF)	Average Node Value
1 (BAF+0.02)	0.00	17 (BAF+0.69)	0.35
2 (BAF+0.06)	0.00	18 (BAF+0.84)	0.45
3 (BAF+0.10)	0.00	19 (BAF+0.99)	0.53
4 (BAF+0.13)	0.00	20 (BAF+1.14)	0.60
5 (BAF+0.17)	0.01	21 (BAF+1.30)	0.65
6 (BAF+0.21)	0.01	22 (BAF+1.45)	0.69
7 (BAF+0.25)	0.02	23 (BAF+1.60)	0.72
8 (BAF+0.29)	0.05	24 (BAF+1.75)	0.73
9 (BAF+0.32)	0.07	25 (BAF+1.91)	0.74
10 (BAF+0.36)	0.09	26 (BAF+2.06)	0.75
11 (BAF+0.40)	0.12	27 (BAF+2.21)	0.77
12 (BAF+0.44)	0.14	28 (BAF+2.36)	0.79
13 (BAF+0.48)	0.17	29 (BAF+2.51)	0.81
14 (BAF+0.51)	0.19	30 (BAF+2.67)	0.82
15 (BAF+0.55)	0.22	31 (BAF+2.82)	0.82
16 (BAF+0.59)	0.24	32 (BAF+2.97)	0.82

Table 4.4-2b

Void Distribution for Analyzed Core - TRACG Hot Channel

Channel Power = 5.817 MW, CPR = 1.20
Active Fuel Length = 3.048 m / 120.00 inches

Node (m above BAF)	Average Node Value	Node (m above BAF)	Average Node Value
1 (BAF+0.02)	0.00	17 (BAF+0.69)	0.59
2 (BAF+0.06)	0.00	18 (BAF+0.84)	0.67
3 (BAF+0.10)	0.00	19 (BAF+0.99)	0.72
4 (BAF+0.13)	0.02	20 (BAF+1.14)	0.74
5 (BAF+0.17)	0.04	21 (BAF+1.30)	0.75
6 (BAF+0.21)	0.07	22 (BAF+1.45)	0.78
7 (BAF+0.25)	0.11	23 (BAF+1.60)	0.81
8 (BAF+0.29)	0.15	24 (BAF+1.75)	0.84
9 (BAF+0.32)	0.19	25 (BAF+1.91)	0.86
10 (BAF+0.36)	0.23	26 (BAF+2.06)	0.88
11 (BAF+0.40)	0.27	27 (BAF+2.21)	0.89
12 (BAF+0.44)	0.31	28 (BAF+2.36)	0.90
13 (BAF+0.48)	0.35	29 (BAF+2.51)	0.91
14 (BAF+0.51)	0.39	30 (BAF+2.67)	0.92
15 (BAF+0.55)	0.43	31 (BAF+2.82)	0.91
16 (BAF+0.59)	0.46	32 (BAF+2.97)	0.92

Table 4.4-3a

Flow Quality Distribution for Analyzed Core - TRACG Average Channel

Channel Power = 4.427 MW, CPR = 1.67
Active Fuel Length = 3.048 m / 120.00 inches

Node (m above BAF)	Average Node Value	Node (m above BAF)	Average Node Value
1 (BAF+0.02)	0.00	17 (BAF+0.69)	0.04
2 (BAF+0.06)	0.00	18 (BAF+0.84)	0.06
3 (BAF+0.10)	0.00	19 (BAF+0.99)	0.08
4 (BAF+0.13)	0.00	20 (BAF+1.14)	0.10
5 (BAF+0.17)	0.00	21 (BAF+1.30)	0.12
6 (BAF+0.21)	0.00	22 (BAF+1.45)	0.14
7 (BAF+0.25)	0.00	23 (BAF+1.60)	0.16
8 (BAF+0.29)	0.00	24 (BAF+1.75)	0.18
9 (BAF+0.32)	0.00	25 (BAF+1.91)	0.20
10 (BAF+0.36)	0.00	26 (BAF+2.06)	0.22
11 (BAF+0.40)	0.01	27 (BAF+2.21)	0.24
12 (BAF+0.44)	0.01	28 (BAF+2.36)	0.26
13 (BAF+0.48)	0.01	29 (BAF+2.51)	0.27
14 (BAF+0.51)	0.01	30 (BAF+2.67)	0.28
15 (BAF+0.55)	0.02	31 (BAF+2.82)	0.28
16 (BAF+0.59)	0.02	32 (BAF+2.97)	0.29

Table 4.4-3b

Flow Quality Distribution for Analyzed Core - Hot Channel

Channel Power = 5.817 MW, CPR = 1.20
Active Fuel Length = 3.048 m / 120.00 inches

Node (m above BAF)	Average Node Value	Node (m above BAF)	Average Node Value
1 (BAF+0.02)	0.00	17 (BAF+0.69)	0.10
2 (BAF+0.06)	0.00	18 (BAF+0.84)	0.13
3 (BAF+0.10)	0.00	19 (BAF+0.99)	0.16
4 (BAF+0.13)	0.00	20 (BAF+1.14)	0.20
5 (BAF+0.17)	0.00	21 (BAF+1.30)	0.23
6 (BAF+0.21)	0.00	22 (BAF+1.45)	0.26
7 (BAF+0.25)	0.01	23 (BAF+1.60)	0.29
8 (BAF+0.29)	0.01	24 (BAF+1.75)	0.32
9 (BAF+0.32)	0.01	25 (BAF+1.91)	0.35
10 (BAF+0.36)	0.02	26 (BAF+2.06)	0.37
11 (BAF+0.40)	0.02	27 (BAF+2.21)	0.40
12 (BAF+0.44)	0.03	28 (BAF+2.36)	0.42
13 (BAF+0.48)	0.04	29 (BAF+2.51)	0.44
14 (BAF+0.51)	0.05	30 (BAF+2.67)	0.45
15 (BAF+0.55)	0.05	31 (BAF+2.82)	0.44
16 (BAF+0.59)	0.06	32 (BAF+2.97)	0.44

Table 4.4-4a

Axial Power Distribution Used to Generate Void and Quality for Analyzed Core - TRACG Average Channel

Channel Power = 4.427 MW, CPR = 1.67
Active Fuel Length = 3.048 m / 120.00 inches

Node (m above BAF)	Average Node Value	Node (m above BAF)	Average Node Value
1 (BAF+0.02)	0.63	17 (BAF+0.69)	1.39
2 (BAF+0.06)	0.63	18 (BAF+0.84)	1.37
3 (BAF+0.10)	0.63	19 (BAF+0.99)	1.35
4 (BAF+0.13)	1.11	20 (BAF+1.14)	1.33
5 (BAF+0.17)	1.23	21 (BAF+1.30)	1.30
6 (BAF+0.21)	1.23	22 (BAF+1.45)	1.26
7 (BAF+0.25)	1.34	23 (BAF+1.60)	1.20
8 (BAF+0.29)	1.41	24 (BAF+1.75)	1.12
9 (BAF+0.32)	1.41	25 (BAF+1.91)	0.95
10 (BAF+0.36)	1.43	26 (BAF+2.06)	0.87
11 (BAF+0.40)	1.44	27 (BAF+2.21)	0.80
12 (BAF+0.44)	1.44	28 (BAF+2.36)	0.71
13 (BAF+0.48)	1.44	29 (BAF+2.51)	0.58
14 (BAF+0.51)	1.42	30 (BAF+2.67)	0.43
15 (BAF+0.55)	1.42	31 (BAF+2.82)	0.28
16 (BAF+0.59)	1.42	32 (BAF+2.97)	0.15

Note: Nodes 1 through 16 have a height of 0.0381 m and nodes 17 through 32 have a height of 0.1524 m. The power in a node is the height divided by the total height times the axial value above times the channel power.

Table 4.4-4b

Axial Power Distribution Used to Generate Void and Quality for Analyzed Core - TRACG Hot Channel

Channel Power = 5.817 MW, CPR = 1.20
Active Fuel Length = 3.048 m / 120.00 inches

Node (m above BAF)	Average Node Value	Node (m above BAF)	Average Node Value
1 (BAF+0.02)	0.63	17 (BAF+0.69)	1.39
2 (BAF+0.06)	0.63	18 (BAF+0.84)	1.37
3 (BAF+0.10)	0.63	19 (BAF+0.99)	1.35
4 (BAF+0.13)	1.11	20 (BAF+1.14)	1.33
5 (BAF+0.17)	1.23	21 (BAF+1.30)	1.30
6 (BAF+0.21)	1.23	22 (BAF+1.45)	1.26
7 (BAF+0.25)	1.34	23 (BAF+1.60)	1.20
8 (BAF+0.29)	1.41	24 (BAF+1.75)	1.12
9 (BAF+0.32)	1.41	25 (BAF+1.91)	0.95
10 (BAF+0.36)	1.43	26 (BAF+2.06)	0.87
11 (BAF+0.40)	1.44	27 (BAF+2.21)	0.80
12 (BAF+0.44)	1.44	28 (BAF+2.36)	0.71
13 (BAF+0.48)	1.44	29 (BAF+2.51)	0.58
14 (BAF+0.51)	1.42	30 (BAF+2.67)	0.43
15 (BAF+0.55)	1.42	31 (BAF+2.82)	0.28
16 (BAF+0.59)	1.42	32 (BAF+2.97)	0.15

Note: Nodes 1 through 16 have a height of 0.0381 m and nodes 17 through 32 have a height of 0.1524 m. The power in a node is the height divided by the total height times the axial value above times the channel power.

Table 4.4-5

Axial Distribution for Typical Core – Core Simulator Hot Channel

Channel Power = 5.32 MW, CPR = 1.49
Active Fuel Length = 3.048 m / 120.00 inches

Node (m above BAF)	Axial Power Factor	Void Fraction
1 (BAF+0.06)	0.63	0.00
2 (BAF+0.18)	1.22	0.02
3 (BAF+0.30)	1.49	0.13
4 (BAF+0.43)	1.53	0.30
5 (BAF+0.55)	1.49	0.43
6 (BAF+0.67)	1.42	0.52
7 (BAF+0.79)	1.35	0.59
8 (BAF+0.91)	1.30	0.65
9 (BAF+1.04)	1.25	0.69
10 (BAF+1.16)	1.22	0.72
11 (BAF+1.28)	1.18	0.74
12 (BAF+1.40)	1.15	0.76
13 (BAF+1.52)	1.12	0.78
14 (BAF+1.65)	1.09	0.80
15 (BAF+1.77)	1.06	0.82
16 (BAF+1.89)	1.00	0.83
17 (BAF+2.01)	0.95	0.84
18 (BAF+2.13)	0.90	0.86
19 (BAF+2.26)	0.83	0.87
20 (BAF+2.38)	0.75	0.87
21 (BAF+2.50)	0.65	0.88
22 (BAF+2.62)	0.54	0.89
23 (BAF+2.74)	0.42	0.89
24 (BAF+2.87)	0.29	0.89
25 (BAF+2.99)	0.16	0.90

Table 4.4-6

ESBWR Reactor Coolant System Geometric Data

	Flow Path Length (m)	Height and Liquid Level (m)	Elevation of Bottom of Volume (m)	Average Flow Area (m^2)
Lower Plenum	4.13 (Axial)) 1.78 (Radial)	4.13/4.13	0.000	16.83
Core	3.79	3.77/2-Phase	4.13	20.22
Chimney	6.61	6.61/2-Phase	7.90	29.27
Upper Plenum	2.75	2.75/2-Phase	14.51	29.53
Dome	1.78 (Radial) 2.79 (Axial)	2.79/Steam	24.77	28.67
Downcomer	14.53	14.53/14.53	2.74	8.40

4.5 REACTOR MATERIALS

4.5.1 Control Rod Drive System Structural Materials

4.5.1.1 Material Specifications

Materials

The metallic structural components of the control rod drive (CRD) mechanism are made from four types of materials: 300 series stainless steel, Nickel-Chrome-Iron alloy X-750, XM-19 and 17-4 PH materials. The only primary pressure boundary components are the lower housing of the spool piece assembly, and flange of the Outer tube assembly. These components are made with 300 series stainless steel materials in accordance with the ASME Code, Section III.

The properties of the non-primary pressure retaining materials selected for the CRD mechanism are equivalent to those given in Parts A, B and D of Section II of the ASME Code, or are included in Regulatory Guide 1.84. Cold worked 300 series austenitic stainless steels are not used except that minor forming and straightening are controlled by limiting the material hardness, bend radius, or the amount of strain induced by a process.

Special Materials

The bayonet coupling, latch and latch spring, and separation spring are fabricated from Alloy X-750 in the annealed condition, and aged 20 hours at 704 degrees Celsius (1300 degrees Fahrenheit). The ball spindle and ball nut are 17-4 PH in condition H-1075 [aged 4 hours at 580 degrees Celsius (1075 degrees Fahrenheit)]. These are widely used materials, whose properties are well known. The parts are readily accessible for inspection and replaceable if necessary.

All materials for use in this system are selected for their compatibility with the reactor coolant as described in Articles NB-2160 and NB-3120 of the ASME Code.

XM-19 is used for the bayonet coupling on the buffer assembly, the hollow piston tube, and the outer tube. This material has been successfully used for many years in similar drive mechanisms. Extensive laboratory tests have demonstrated that XM-19 is a suitable material and that it is resistant to stress corrosion in a BWR environment.

No austenitic stainless steels strengthened by cold working are employed in the CRD system. For incidental cold working introduced during fabrication and installation, special controls are used to limit the induced strain and hardness, and the bend radii are kept above a minimum value.

4.5.1.2 Austenitic Stainless Steel Components

4.5.1.2.1 Processes, Inspections and Tests

All austenitic stainless steels are used in the solution heat-treated condition. In all welded components that are exposed to service temperature exceeding 93°C, the carbon content is limited not to exceed 0.020%. On qualification, there is a special process employed which subjects selected 300 Series stainless steel components to temperatures in the sensitization range. The drive shaft and buffer sleeve are examples of hard surfaced parts with Colmonoy and Stellite (or their equivalent). Colmonoy and Stellite (or its equivalent) hard surfaced components have

performed successfully for many years in drive mechanisms. It is normal practice to remove some CRDs at each refueling outage and disassemble them for routine inspection. At this time, all drive parts, including the CRD bolting and hard-surfaced parts are accessible for visual examination in accordance with the manufacturer's CRD maintenance procedures. This inspection program is adequate to detect any incipient defects before they could become serious enough to cause operating problems. The CRD penetration and bolting are included in the reactor coolant pressure boundary inservice inspection program (Subsection 5.2.4). The degree of conformance to Regulatory Guide 1.44 is presented in Subsection 4.5.2.4.

4.5.1.2.2 Control of Delta Ferrite Content

Discussion of this subject and the degree of conformance to Regulatory Guide 1.31 is presented in Subsection 4.5.2.4.

4.5.1.3 Other Materials

Stellite 3/Haynes 25 are used for rollers/pins at latch (outside), and Haynes 25 for the latch joint pin. A Stellite 6 equivalent is used in the guide shaft at the top of the ball spindle. Stellite 12 is used for the bushing at the top of the ball spindle and the bushing on the drive shaft. Stellite Star J-metal is used for the ball check valve.

Non-cobalt hard alloys are used in guide rollers and guide pins. These components are located above and below the labyrinth seal, on the stop piston, ball screw stationary guide, piston head and ball nut.

4.5.1.4 Cleaning and Cleanliness Control

All the CRD parts are fabricated under a process specification that limits contaminants in cutting, grinding and tapping coolants and lubricants. It also restricts all other processing materials (marking inks, tape, etc.) to those that are completely removable by the applied cleaning process. All contaminants are then required to be removed by the appropriate cleaning process prior to any of the following:

- Any processing which increases part temperature above 93°C
- Assembly which results in decrease of accessibility for cleaning
- Release of parts for shipment

The specification for packaging and shipping the control rod drive provides the following:

The CRD is rinsed in hot de-ionized water and dried in preparation for shipment. The ends of the drive are then covered with a vapor-tight barrier with desiccant. Packaging is designed to protect the drive and prevent damage to the vapor barrier. Audits have indicated satisfactory protection.

Semiannual examination of 10% of the units humidity indicators is performed to verify that the units are dry and in satisfactory condition. The position indicator probes are not subject to this inspection.

Site or warehouse storage specifications require inside heated storage comparable to Level B of NQA-2-1983, Part 2.2.

The degree of surface cleanliness obtained by these procedures meets the requirements of Regulatory Guide 1.37.

4.5.2 Reactor Internal Materials

4.5.2.1 Material Specifications

Reactor internal material specifications are provided in Table 4.5-1. All core support structures are fabricated from ASME specified materials, and designed in accordance with requirements of ASME Code Section III, Subsection NG. The other reactor internals are non-coded, and they may be fabricated from ASTM or ASME specification materials or other equivalent specifications.

4.5.2.2 Controls on Welding

Core support structures are fabricated in accordance with requirements of ASME Code Section III, Subsection NG-4000, and the examination and acceptance criteria shown in NG-5000. The internals, other than the core support structures meet the requirements of the industry standards, e.g., ASME or AWS, as applicable. ASME B&PV Code Section IX qualification requirements are followed in fabrication of core support structures. All welds are made with controlled weld heat input.

4.5.2.3 Non-Destructive Examination

Materials for core support structures will fully conform and be certified to ASME Section III, Subsection NG. Examination of materials (examination methods and acceptance criteria) is specified in NG-2500. Examination methods and acceptance criteria for core support structure weld edge preparations and welds are provided in NG-5000. Tubular products that are pressure boundary components (CRD and in-core housings) will be examined according to ASME Section III, NB-2500, and associated pressure retaining welds will be examined according to NB-5000. For non-ASME Code reactor internal structures and associated welds, examinations are established based on relevant design and analysis information, and take guidance from NG-2500 and NG-5000 respectively.

4.5.2.4 Fabrication and Processing of Austenitic Stainless Steel—Regulatory Guide Conformance

Significantly cold-worked stainless steels are not used in the reactor internals except for vanes in the steam dryers. Applying limits on hardness controls cold work, bend radii and surface finish on ground surfaces. Furnace sensitized material are not allowed. Electroslag welding is not applied for structural welds. ESBWR will comply fully with Regulatory Guide 1.31, “Control of Ferrite Content in Stainless Steel Weld Metal”, including application of the following provisions to all stainless steel weld filler metal applied to reactor internal components: The delta ferrite content for weld materials used in welding austenitic stainless steel assemblies is verified on undiluted weld deposits for each heat or lot of filler metal and electrodes. The delta ferrite content is defined for weld materials as 5.0 Ferrite Number (FN) minimum, 8.0FN average and 20FN maximum. Ferrite content will be determined by use of magnetic instruments calibrated according to AWS A4.2. This ferrite content is considered adequate to prevent any micro-

fissuring (Hot Cracking) in austenitic stainless steel welds. This procedure complies with the requirements of Regulatory Guide 1.31.

The limitation placed upon the delta ferrite in austenitic stainless steel castings is 8% minimum and a maximum value of 20%. The maximum limit is used for those castings designed for a 60-year life such as the fuel support pieces, in order to limit the effects of thermal aging degradation.

Proper solution annealing of the 300 series austenitic stainless steel is verified by testing per ASTM-A262, "Recommended Practices for Detecting Susceptibility to Intergranular Attack in Stainless Steels." Welding of austenitic stainless steel parts is performed in accordance with Section IX (Welding and Brazing Qualification) and Section II Part C (Welding Rod Electrode and Filler Metals) of the ASME B&PV Code. Welded austenitic stainless steel assemblies require solution annealing to minimize the possibility of the sensitizing. However, welded assemblies are dispensed from this requirement when the assemblies are of material of low carbon content (less than 0.020%). These controls are employed in order to comply with the intent of Regulatory Guide 1.44.

Careful control of all cleaning materials and process materials that contact stainless steel during manufacture and construction prevent exposure to contaminants. Any inadvertent surface contamination is removed to avoid potential detrimental effects.

Special care is exercised to insure removal of surface contaminants prior to any heating operation. Water quality for rinsing, flushing, and testing is controlled and monitored.

The degree of cleanliness obtained by these procedures meets the requirements of Regulatory Guide 1.37.

4.5.2.5 Other Materials

Hardenable martensitic stainless steel and precipitation hardening stainless steels are not used in the reactor internals.

Materials, other than Type-300 stainless steel, employed in reactor internals are:

- Type or Grade XM-19 stainless steel
- Niobium modified Alloy 600 per ASME Code Case No. N-580-1
- N07750 (Alloy X-750) or equivalent

All Niobium modified Alloy 600 material is used in the solution annealed condition.

Alloy X-750 components are fabricated in the annealed and aged condition. Where maximum resistance to stress corrosion is required, the material is used in the high temperature (1093°C) annealed plus single aged condition.

Hard chromium plating surface is applied to austenitic stainless steel couplings.

All materials used for reactor internals shall be selected for their compatibility with the reactor coolant as shown in ASME Code Section III, NG-2160 and NG-3120. The fabrication and cleaning controls preclude contamination of nickel-based alloys by chloride ions, fluoride ions, sulfur, or lead.

All materials referenced in this subsection have been successfully used for many years in BWR applications.

Use of Alloy 182 is prohibited in contact with reactor water.

4.5.3 COL Unit-Specific Information

None.

4.5.4 References

None

Table 4.5-1

Reactor Internals Material Specifications

Component	Form	Material	ASME Specification
Materials Used for the Core Support Structure:			
Shroud Support	Plate or Forging	Columbium[1)] modified Ni-Cr-Fe Alloy	Modified Nickel Alloy 600 per ASME Code Case N-580-1
Shroud	Plate	Stainless Steel[2)]	SA-240, Type 304 / 304L / 316 / 316L
Core Plate	Plate and Forging	Stainless Steel[2)]	SA-240 and SA-182/SA-182M, Type or Grade 304 / 304L / 316 / 316L
Top Guide	Plate and Forging	Stainless Steel[2)]	SA-240 and SA-182/SA-182M, Type or Grade 304 / 304L / 316 / 316L
Peripheral Fuel Supports	Forging	Stainless Steel[2)]	SA-182/SA-182M, Grade 304 / 304L / 316 / 316L
Orificed Fuel Support	Casting	Stainless Steel	SA-351/SA-351M, Grade CF3
Core Plate and Top Guide Studs, Nuts, and Sleeves	Bar	Stainless Steel[2)]	SA-479/SA-479M, Type 304 / 304L / 316 / 316L and XM-19
Control Rod Drive Housing	Forging	Stainless Steel[2)]	SA-336/SA-336M or SA-182/SA-182M Grade 304 or 316
Control Rod Guide Tube	Pipe, Bar and Forging	Stainless Steel[2)]	SA-312/SA-312M and SA-479/SA-479M, Type 304 / 304L / 316 / 316L and XM-19
Control Rod Drive Penetration Stub Tubes	Forging	Columbium[1)] modified Ni-Cr-Fe Alloy	Modified Nickel Alloy 600 per ASME Code Case N-580-1
Materials Used for the Internal Structures:			
Chimney, Chimney Partitions and Chimney Restraints	Plate and Bar	Stainless Steel[2)]	SA-240 and SA-479/SA-479M, Type 304 / 304L / 316 / 316L. The equivalent ASTM specification “A-“ acceptable
Chimney Head and Steam Separator Assembly	Plate and Bar	Stainless Steel[2)]	SA-240 and SA-479/SA-479M, Type 304 / 304L / 316 / 316L. The equivalent ASTM specification “A-“ acceptable

Table 4.5-1

Reactor Internals Material Specifications

Component	Form	Material	ASME Specification
Steam Separator	Pipe, Plate and Casting	Stainless Steel[2)]	SA-312/SA-312M and SA-240, Grade or Type 304 / 304L / 316 / 316L; SA-351/SA-351M, Grade CF3. The equivalent ASTM specification "A-" acceptable
Chimney Head Bolts	Tube, Bar, Spring	Stainless Steel[2)] and Ni-Cr-Fe Alloy	SA-213/SA-213M and SA-479/SA-479M, Type 304 / 304L / 316 / 316L; SA-479/SA-479M, Type XM-19; SB-637, N07750 (Alloy X-750). The equivalent ASTM specification "A- or B-" acceptable. Modified Nickel Alloy 600 per ASME Code Case N-580-1
Steam Dryer	Plate, Bar and Pipe	Stainless Steel[2)]	SA-240, SA-479/SA-479M and SA-312/SA-312M, Type 304 / 304L / 316 / 316L; SB-637, N07750 (Alloy X-750). The equivalent ASTM specification "A- or B-" acceptable
Steam Dryer Seismic Blocks	Forging or Bar	Stainless Steel[2)]	SA-182/SA-182M or SA-479/SA-479M, Grade XM-19. The equivalent ASTM specification "A-" acceptable
Feedwater Spargers	Pipe, Bar, Fitting and Casting	Stainless Steel[2)]	SA-312/SA-312M and SA-479/479M and SA-403, Type, Grade or Class 304 / 304L / 316 / 316L; SA351/351M, Grade CF3. The equivalent ASTM specification "A-" acceptable
Standby Liquid Control (SLC) Piping and Distribution Headers	Pipe, Bar or Plate	Stainless Steel[2)]	SA-312/SA-312M and SA-479/SA-479M or SA-240, Type or Grade 304 / 304L / 316 / 316L. The equivalent ASTM specification "A-" acceptable
In-Core Guide Tubes	Pipe	Stainless Steel[2)]	SA-312/SA-312M, Grade 304 / 304L / 316 / 316L. The equivalent ASTM specification "A-" acceptable
In-core Guide Tube restraints	Plate, Strip and Bar	Stainless Steel[2)] and Columbium[1)] modified Ni-Cr-Fe Alloy	SA-240 and SA-479/SA-479M, Type 304 / 304L / 316 / 316L. The equivalent ASTM specification "A-" acceptable. Modified Alloy 600 per ASME Code Case N-580-1

Table 4.5-1

Reactor Internals Material Specifications

Component	Form	Material	ASME Specification
Guide Rod	Bar and Pipe	Stainless Steel[2)] and Columbium[1)] modified Ni-Cr-Fe Alloy	SA-479/SA-479M, SA-312/SA-312M, Type or Grade 304 / 304L / 316 / 316L. The equivalent ASTM specification "A-" acceptable. Modified Nickel Alloy 600M per ASME Code Case N-580-1
Drain Line	Pipe, Bar or Plate	Stainless Steel[2)]	SA-312/SA-312M and SA-479/SA-479M or SA-240, Type or Grade 304 / 304L / 316 /316L. The equivalent ASTM specification "A-" acceptable

[1)] Also called Niobium in countries outside the U.S.

[2)] Maximum carbon content limited to 0.02% except for castings

4.6 FUNCTIONAL DESIGN OF REACTIVITY CONTROL SYSTEM

The Reactivity Control System consists of:

- Control rods and Control Rod Drive (CRD) system;
- Supplementary reactivity control in the form of gadolinia-urania fuel rods (Section 4.2); and
- The Standby Liquid Control System (Subsection 9.3.5).

Conformance of these reactivity control systems to General Design Criteria (GDC) 4, 23, 25, 26, 27, 28 and 29 is addressed in Section 3.1.

4.6.1 Information for Control Rod Drive System

4.6.1.1 Design Bases

4.6.1.1.1 Safety (10 CFR 50.2) Design Bases

The CRD system meets the following safety design bases:

- The design shall provide for rapid control rod insertion (scram) so that no fuel damage results from any Anticipated Operational Occurrence (Chapter 15).
- The design shall include positioning devices, each of which individually supports and positions a control rod.
- Each positioning device shall be capable of holding the control rod in position and preventing it from inadvertently withdrawing outward during any non-accident, accident, post-accident and seismic condition.
- Each positioning device shall be capable of detecting the separation of the control rod from the drive mechanism to prevent a rod drop accident.
- Each positioning device shall provide a means to prevent or limit the rate of control rod ejection from the core due to a break in the drive mechanism pressure boundary. This is to prevent fuel damage resulting from rapid insertion of reactivity.

4.6.1.1.2 Power Generation (Non-safety) Design Basis

The CRD system design meets the following power generation design bases:

- The design shall provide for controlling changes in core reactivity by positioning neutron-absorbing control rods within the core.
- The design shall provide for movement and positioning of control rods in increments to enable optimized power control and core power shaping.
- The design shall provide for the supply of high-pressure makeup water to the reactor when the normal makeup supply system (feedwater) is unable to maintain water level.

4.6.1.2 Description

The CRD system is composed of three major elements:

- Electro-hydraulic fine motion control rod drive (FMCRD) mechanisms;
- Hydraulic control units (HCU); and
- Control rod drive hydraulic subsystem (CRDHS).

The FMCRDs provide electric-motor-driven positioning for normal insertion and withdrawal of the control rods and hydraulic-powered rapid insertion (scram) of control rods during abnormal operating conditions.

The hydraulic power required for scram is provided by high-pressure water stored in the individual HCUs. Each HCU contains a nitrogen-water accumulator charged to high pressure and the necessary valves and components to scram two FMCRDs. Additionally, during normal operation, the HCUs provide a flow path for purge water to the associated FMCRDs.

The CRDHS supplies clean, demineralized water that is regulated and distributed to provide charging of the HCU scram accumulators and purge water flow to the FMCRDs during normal operation. The CRDHS is also the source of pressurized water for purging the Reactor Water Cleanup/Shutdown Cooling (RWCU/SDC) system pumps and the Nuclear Boiler System (NBS) reactor water level reference leg instrument lines. Additionally, the CRDHS provides high pressure makeup water to the reactor during events in which the feedwater system is unable to maintain reactor water level. This makeup water is supplied to the reactor via a bypass line off the CRD pump discharge header that connects to the feedwater inlet piping via the RWCU/SDC return piping.

The CRD system performs the following functions:

- Controls changes in core reactivity by positioning neutron-absorbing control rods within the core in response to control signals from the Rod Control and Information System (RC&IS).
- Provides movement and positioning of control rods in increments to enable optimized power control and core power shape in response to control signals from the RC&IS.
- Provides the ability to position large groups of rods simultaneously in response to control signals from the RC&IS.
- Provides rapid control rod insertion (scram) in response to manual or automatic signals from the Reactor Protection System (RPS) so that no fuel damage results from any plant anticipated operational occurrence (AOO).
- In conjunction with the RC&IS, provides automatic electric motor-driven insertion of the control rods simultaneously with hydraulic scram initiation. This provides an additional, diverse means of fully inserting a control rod.
- Supplies rod status and rod position data for rod pattern control, performance monitoring, operator display and scram time testing by the RC&IS.
- In conjunction with the RC&IS, prevents undesirable rod pattern or rod motions by imposing rod motion blocks in order to protect the fuel.

- In conjunction with the RC&IS, prevents the rod drop accident by detecting rod separation and imposing rod motion block.
- Provides rapid control rod insertion (scram) in response to signals from the Diverse Protection System (DPS). Also in response to signals from the DPS, provides alternate rod insertion (ARI), an alternate means of actuating hydraulic scram, should an anticipated transient without scram (ATWS) occur.
- In conjunction with the RC&IS, provides for selected control rod run-in (SCRRI).
- Prevents rod ejection from the core due to a break in the drive mechanism pressure boundary or a failure of the attached scram line by means of a passive brake mechanism for the FMCRD motor and a scram line inlet check valve.
- Supplies high-pressure makeup water to the reactor when the normal makeup supply system (feedwater) is unable to prevent reactor water level from falling below the normal water level range.
- Supplies purge water for the RWCU/SDC System pumps.
- Provides a continuous flow of water to the NBS to keep the reactor water level reference leg instrument lines filled.

The design bases and further discussion of both the RC&IS and RPS, and their control interfaces with the CRD system, are presented in Chapter 7.

The CRD System is arranged in a manner that separates the safety-related equipment from the nonsafety-related portions of the system. The FMCRDs are mounted to the reactor vessel bottom head inside primary containment. The HCUs are housed in four dedicated rooms located directly outside of the primary containment at the basemat elevation of the reactor building. These rooms are arranged around the periphery of the primary containment wall. Each HCU room serves the FMCRDs associated with one quadrant of the reactor core. The HCUs are connected to the FMCRDs by the scram insert piping that penetrates the primary containment wall.

The balance of the nonsafety-related hydraulic system equipment (pumps, valves, filters, etc.) is physically separated from the HCUs and housed in a separate room in the reactor building. It is connected to the HCUs by the nonsafety-related FMCRD purge water header, HCU charging water header and scram air header. These headers are classified as Seismic Category II so that they will maintain structural integrity during a seismic event and not degrade the functioning of the HCUs.

4.6.1.2.1 Fine Motion Control Rod Drive Mechanism

The FMCRD used for positioning the control rod in the reactor core is a mechanical/hydraulic actuated mechanism (Figures 4.6-1 and 4.6-2). An electric motor-driven ball-nut and ball screw assembly is capable of positioning the drive at both a minimum of 36.5 mm (1.44 in.) increments and continuously over its entire range at a speed of 28 ± 5 mm/sec. Hydraulic pressure is used for scrams. The FMCRD penetrates the bottom head of the reactor pressure vessel. The FMCRD does not interfere with refueling and is operative even when the head is removed from the reactor vessel.

The fine motion capability is achieved with a ball-nut and ball screw arrangement driven by an electric motor. The ball-nut is keyed to the guide tube (roller key) to prevent its rotation and traverses axially as the ball screw rotates. A hollow piston rests on the ball-nut, and upward motion of the ball-nut drives this piston and the control rod into the core. The weight of the control rod keeps the hollow piston and ball-nut in contact during withdrawal.

A single HCU powers the scram action of two FMCRDs. Upon scram valve initiation, high pressure nitrogen from the HCU raises the piston within the accumulator forcing water through the scram piping. This water is directed to each FMCRD connected to the HCU. Inside each FMCRD, high-pressure water lifts the hollow piston off the ball-nut and drives the control rod into the core. A spring washer buffer assembly stops the hollow piston at the end of its stroke. Departure from the ball-nut releases spring-loaded latches in the hollow piston that engage slots in the guide tube. These latches support the control rod and hollow piston in the inserted position. The control rod cannot be withdrawn until the ball-nut is driven up and engaged with the hollow piston. Stationary fingers on the ball-nut then cam the latches out of the slots and hold them in the retracted position. A scram action is complete when every FMCRD has reached its fully inserted position.

The use of the FMCRD mechanisms in the CRD system provides several features that enhance both the system reliability and plant operations. Some of these features are listed and discussed briefly as follows:

Diverse Means of Rod Insertion — The FMCRDs can be inserted either hydraulically or electrically. In response to a scram signal, the FMCRD is inserted hydraulically via the stored energy in the scram accumulators. A signal is also given simultaneously to insert the FMCRD electrically via its motor drive. This diversity provides a high degree of assurance of rod insertion on demand.

Absence of FMCRD Piston Seals — The FMCRD pistons have no seals and, thus, do not require maintenance.

FMCRD Discharge — The water that scrams the control rod discharges into the reactor vessel and does not require a scram discharge volume, thus eliminating a potential source for common mode scram failure.

Plant Maneuverability — The fine motion capability of the FMCRD allows rod pattern optimization in response to fuel burnup or load-following demands.

Plant Automation — The relatively simple logic of the FMCRD permits plant automation. This feature is utilized for automatic reactor startup and shutdown and for automatic load following.

Reactor Startup Time — The FMCRDs can be moved in large groups. Movements of large groups of control rods (called gangs) are utilized to reduce the time for reactor startup.

Rod Drop Accident Prevention — The control rod separation detection feature of the FMCRD virtually eliminates the possibility of a rod drop accident by preventing rod withdrawal when control rod separation is detected. Additionally, movement of rods in large groups during reactor startup greatly reduces the maximum relative rod worth to levels lower than current rod pattern controls. Rod pattern controls provide verification of proper automatic rod movements and to mitigate the consequences of a rod withdrawal error.

The drives are readily accessible for inspection and servicing. The bottom location makes maximum utilization of the water in the reactor as a neutron shield and gives the least possible neutron exposure to the drive components. Using water from the condensate treatment system, and/or condensate storage tanks as the operating fluid eliminates the need for special hydraulic fluid.

4.6.1.2.2 FMCRD Components

Figure 4.6-1 provides a simplified schematic of the FMCRD operating principles. Figure 4.6-2 illustrates the drive in more detail.

The basic elements of the FMCRD are as follows:

- Components of the FMCRD required for electrical rod positioning or fine motion control (including the motor, brake release, associated connector, ball screw shaft, ball-nut and hollow piston).
- Components of the FMCRD required for hydraulic scram (including hollow piston and buffer).
- Components of the FMCRD required for pressure integrity (including the outer tube, middle flange, installation bolts and spool piece).
- Rod position indication (position signal detectors).
- Reed position switches for scram surveillance.
- Control rod separation detection devices (dual Class 1E CRD separation switches).
- Bayonet coupling between the hollow piston and control rod.
- Brake mechanism to prevent rod ejection in the event of a break in the FMCRD primary pressure boundary and ball check valve to prevent rod ejection in the event of a failure of the scram insert line.
- Integral internal blowout support (to prevent CRD blowout).
- Magnetic coupling.

These features and functions of the FMCRD are described below.

Components for Fine Motion Control

The fine motion capability is achieved with a ball-nut and ball screw arrangement driven by an electric motor. The ball-nut is keyed to the guide tube (roller key) to prevent its rotation as it traverses axially as the ball screw rotates. A hollow piston rests on the ball-nut and upward motion of the ball-nut drives the control rod into the core. The weight of the control rod keeps the hollow piston and ball-nut in contact during withdrawal.

The drive motor, located outside the pressure boundary, is magnetically coupled to the drive shaft located inside the pressure boundary. A splined coupling connects the drive shaft to the ball screw. The lower half of the splined coupling is keyed to the drive shaft and the upper half keyed to the ball screw. The tapered end of the drive shaft fits into a conical seat on the end of the ball screw to keep the two axially aligned. A drive shaft thrust bearing carries the entire weight of the control rod and drive internals.

The axially moving parts are centered and guided by radial rollers. The ball-nut and bottom of the hollow piston include radial rollers bearing against the guide tube. Radially adjustable rollers at both ends of the labyrinth seal keep the hollow piston precisely centered in this region.

A stationary guide supports the top of the ball screw against the inside of the hollow piston. A hardened bushing provides the circumferential bearing between the rotating ball screw and stationary guide. Rollers of the guide run in axial grooves in the hollow piston to prevent the guide from rotating with the ball screw.

Components for Scram

The scram action is initiated by the HCU. High pressure water lifts the hollow piston off the ball-nut and drives the control rod into the core. A spring washer buffer assembly stops the hollow piston at the end of its stroke. Departure from the ball-nut releases spring-loaded latches in the hollow piston that engage slots in the guide tube. These latches support the control rod in the inserted position.

The control rod cannot be withdrawn until the ball-nut is driven up and engaged with the hollow piston. Stationary fingers on the ball-nut cam the latches in the hollow piston out of the slots in the guide tube and hold them in the retracted position when the ball-nut and hollow piston are re-engaged.

Re-engagement of the ball-nut with the hollow piston following scram is automatic. Simultaneous with the initiation of the hydraulic scram each FMCRD motor is signaled to start in order to cause movement of the ball-nut upward until it is in contact with the hollow piston. This action completes the rod full-in insertion and leaves the drives in a condition ready for restarting the reactor. With the latches in the hollow piston retracted, and the motor and brake de-energized, the control rods are kept fully inserted by the passive holding torque from the brake and the magnetic coupling between the motor and drive shaft.

The automatic run-in of the ball-nut using the electric motor drive following the hydraulic scram provides a diverse means of rod insertion as a backup to the accumulator scram.

FMCRD Pressure Boundary

The CRD housing (attached to the RPV) and the CRD middle flange and lower housing (spool piece) which enclose the lower part of the drive are a part of the reactor pressure boundary (Figure 4.6-1). The middle housing is attached to the CRD housing by four threaded bolts. The lower housing (spool piece) is, in turn, held to the middle housing and secured to the CRD housing by a separate set of eight main mounting bolts that become a part of the reactor pressure boundary. This arrangement permits removing the lower housing, drive shaft and seal assembly without disturbing the rest of the drive. Removing the lower housing transfers the weight of the driveline from the drive shaft to the seat in the middle housing. Both the ball screw and drive shaft are locked to prevent rotation while the two are separated.

The part of the drive inserted into the CRD housing is contained within the outer tube. The outer tube is the drive hydraulic scram pressure boundary, eliminating the need for designing the CRD housing for the scram pressure. The outer tube is welded to the middle flange at the bottom and is attached at the top with the CRD blowout support, which bears against the CRD housing. The blowout support and outer tube are attached by a slip type connection that accounts for any slight variation in length between the drive and the drive housing.

Purge water continually flows through the drive. The water enters through the ball check valve in the middle housing and flows around the hollow piston into the reactor. O-rings seal the lower housing. A labyrinth seal near the top of the drive restricts the flow into the reactor. During a scram, the labyrinth seals the high-pressure scram water from the reactor vessel without adversely affecting the movement of the hollow piston.

Rod Position Indication

Control rod position indication is provided by the FMCRDs to the control system by a position detection system, which consists of position detectors and position signal converters.

Each FMCRD provides two position detectors, one for each control system channel, in the form of signal detectors directly coupled to the motor shaft through gearing. The output signals from these detectors are analog. The analog signals are converted to digital signals by position signal converters. This configuration provides continuous detection of rod position during normal operation.

Scram Position Indication

Scram position indication is provided by a series of magnetic reed switches to allow for measurement of adequate drive performance during scram. The magnetic switches are located at intermediate intervals over 60% of the drive stroke. They are mounted in a position indicator probe exterior to the drive housing. A magnet in the hollow piston trips each reed switch, in turn, as it passes by.

As the bottom of the hollow piston contacts and enters the buffer, a magnet is lifted that operates a reed switch, indicating scram completion. This continuous full-in indicating switch is shown conceptually in Figure 4.6-3. It provides indication whenever the drive is at the full-in latched position or above.

Control Rod Separation Detection

Two redundant and separate Class 1E switches are provided to detect the separation of the hollow piston from the ball-nut. This means two sets of reed switches physically separated from one another with their cabling run through separate conduits. The separation switch is classified Class 1E, because its function detects a detached control rod and causes a rod block, thereby preventing a rod drop accident. Actuation of either switch also initiates an alarm in the control room.

The principle of operation of the control rod separation mechanism is illustrated in Figure 4.6-4. During normal operation, the weight of the control rod and hollow piston resting on the ball-nut causes the ball screw assembly to compress a spring on which the lower half of the splined coupling between the drive shaft and ball screw assembly rests (the lower half of the splined coupling is also known as the “weighing table”). When the hollow piston separates from the ball-nut, or when the control rod separates from the hollow piston, the spring is unloaded and pushes the weighing table and ball screw assembly upward. This action causes a magnet in the weighing table to operate the Class 1E reed switches located in probes outside the lower housing.

Bayonet Couplings

There are two bayonet couplings associated with the FMCRD. The first is at the FMCRD/control rod guide tube/housing interface as illustrated in Figure 4.6-1. This bayonet

locks the FMCRD and the base of the control rod guide tube to the CRD housing and functions to retain the control rod guide tube during normal operation and dynamic loading events. The bayonet also holds the FMCRD against ejection in the event of a hypothetical failure of the CRD housing weld. The locating pin on the core plate that engages the flange of the control rod guide tube and the bolt pattern on the FMCRD/housing flange assure proper orientation between the control rod guide tube and the FMCRD to assure that the bayonet is properly engaged.

The second bayonet is located between the control rod and FMCRD as shown on Figure 4.6-5. The coupling spud at the top end of the FMCRD hollow piston engages and locks into a mating socket at the base of the control rod. The coupling requires a 45° rotation for engaging or disengaging. Once locked, the drive and rod form an integral unit that can only be unlocked manually by specific procedures before the components can be separated.

The FMCRD design allows the coupling integrity of this second bayonet to be checked by driving the ball nut down into an overtravel-out position. After the weighing spring has raised the ball screw assembly to the limit of its travel, further rotation of the ball screw in the withdraw direction drives the ball-nut down away from the hollow piston (assuming the coupling is engaged). If the hollow piston is not properly coupled to the control rod, the hollow piston will remain in contact with the ball nut and move with it to the overtravel position. A reed switch at the overtravel position will detect this movement of the hollow piston.

FMCRD Brake and Ball Check Valve

The FMCRD design incorporates an electro-mechanical brake (Figure 4.6-6) keyed to the motor shaft. The brake is normally engaged by passive spring force when the FMCRD is stationary. It is disengaged for normal rod movements by signals from the RC&IS. Disengagement is caused by the energized magnetic force overcoming the spring load force. The braking torque of 49 N·m (minimum) and the magnetic coupling torque between the motor and the drive shaft are sufficient to prevent control rod ejection in the event of failure in the pressure retaining parts of the drive mechanism. The brake is designed so that its failure does not prevent the control rod from rapid insertion (scram).

The electromechanical brake is located between the motor and the position signal detectors. The stationary spring-loaded disk and coil assembly is contained within the brake mounting bolted to the bottom of the motor. The rotating disk is keyed to the motor shaft and synchro shaft.

The brake is classified as passive safety-related because it performs its holding function when it is in its normally de-energized condition.

A ball check valve is located in the middle flange of the drive at the scram inlet port. The check valve is classified as safety-related because it actuates to close the scram inlet port by reverse flow under system pressure, fluid flow and temperature conditions caused by a break of the scram line. This prevents the loss of pressure to the underside of the hollow piston and the generation of loads on the drive that could cause a rod ejection.

Integral Internal Blowout Support

An internal CRD blowout support replaces the support structure of beams, hanger rods, grids and support bars used in BWR/6 and product lines before that. The internal support concept is illustrated schematically in Figure 4.6-7. This system utilizes the CRD outer tube integral with the internal support to provide the anti-ejection support. The outer tube is locked at top via the

internal support to the control rod guide tube (CRGT) base by a bayonet coupling, which is described above. The outer tube is bolted to the CRD housing flange via the middle flange welded to it at the bottom, as described above in a discussion on FMCRD pressure boundary.

The CRD blowout support is designed to prevent ejection of the CRD and the attached control rod considering failures of two types at the weld (Point A in Figure 4.6-7) between the CRD housing and the stub tube penetration of the RPV bottom head: (1) a failure through the housing along the fusion line just below the weld with the weld and the housing extension inside the vessel remaining intact, or (2) a failure of the weld itself with the entire housing remaining intact but without support at the penetration.

With a housing failure, the weight plus pressure load acting on the drive and housing would tend to eject the drive. In this event, the CRGT base remains supported by the intact housing extension inside the vessel and the CRD remains supported in turn by its positive lock to the CRGT base. Coolant leakage is restricted to the small annular area between the CRD outer tube and the inside of the CRD housing. In the event of total failure of the weld itself, with the entire housing intact, the housing would tend to be driven downward by the total weight plus vessel pressure. However, after the interconnected assembly of the housing, CRD and CRGT moves down a short distance, the flange at the top of the CRGT contacts the core plate, stopping further movement of the assembly. Because the CRD is positively locked to the CRGT base, it cannot eject. In this case, the housing, which bears on top of the blowout support, is also prevented from leaving the penetration. Coolant leakage for this condition is restricted to the small annular area between the outside of CRD housing and the inside of the penetration stub tube.

An orderly shutdown would result if any of the two failures were to occur, because the restricted coolant leakage would be less than the supply from the normal make up systems. The components that provide the anti-ejection function are:

- internal CRD blowout support,
- CRD outer tube,
- entire CRD housing,
- CRGT, and
- core plate.

The materials of these components are specified to meet quality requirements consistent with that function.

If a total failure of all the flange bolts attaching the spool piece flange and also the middle flange with the CRD housing flange (Point B on Figure 4.6-7) were to occur, the drive would be prevented from moving downward by the middle flange seat provided for the ball screw adapter as part of the anti-rotation gear (see Subsection 4.6.2.1.3).

Magnetic Coupling

The magnetic coupling is located in the spool piece. It is employed to achieve seal-less, leak-free operation of the control rod drive mechanism. The magnetic coupling consists of an inner and an outer rotor. The inner rotor is located inside the spool piece pressure boundary. The outer rotor is located outside the spool piece pressure boundary. Each rotor has permanent

magnets mounted on it. As a result, the inner and outer rotors are locked together by the magnetic forces acting through the pressure boundary and work as a synchronous coupling. The outer rotor is coupled with the motor unit and driven by the motor and the inner rotor follows the rotation of the outer rotor.

The magnetic coupling is designed so that its maximum coupling torque exceeds the maximum torque of the motor unit to prevent decoupling or slippage due to motor torque.

Materials of Construction

The materials of construction for the FMCRD are discussed in Subsection 4.5.1.

4.6.1.2.3 Hydraulic Control Units

Each hydraulic control unit (HCU) furnishes pressurized water for hydraulic scram, on signal from the RPS, to two drive units. Additionally, each HCU provides the capability to adjust purge flow to the two drives. A test port is provided on the HCU for connection to a portable test station to allow controlled venting of the scram insert line to test the FMCRD ball check valve during plant shutdown. Operation of the electrical system that supplies scram signals to the HCU is described in Chapter 7.

The basic components of each HCU are described in the following paragraphs. The HCU configuration is shown on Figure 4.6-8.

The check valves shown inside the HCU boundary on Figure 4.6-8 have an active safety-related function to close under system pressure, fluid flow and temperature conditions during scram. This ensures that the water stored in the HCU accumulator is delivered to the FMCRDs to accomplish the scram function.

Scram Pilot Valve Assembly

The scram pilot valve assembly is operated from the RPS. The scram pilot valve assembly, with two solenoids, controls the scram inlet valve. The scram pilot valve assembly is solenoid-operated and is normally energized. Upon loss of electrical signal (such as the loss of external AC power) to the solenoids, the inlet port closes and the exhaust port opens. The pilot valve assembly (Figure 4.6-8) is designed so that the trip system signal must be removed from both solenoids before air pressure can be discharged from the scram valve operators. This prevents the inadvertent scram of both drives associated with a given HCU in the event of a failure of one of the pilot valve solenoids.

Scram Inlet Valve

The scram inlet valve opens to supply pressurized water to the bottom of the drive piston. This quick opening globe valve is operated by an internal spring and system pressure. It is closed by air pressure applied to the top of its diaphragm operator. A position indicator switch on this valve energizes a light in the control room as soon as the valve starts to open.

Scram Accumulator

The scram accumulator stores sufficient energy to fully insert two control rods at any reactor pressure. The accumulator is a hydraulic cylinder with a free-floating piston. The piston separates the water on top from the nitrogen below. A check valve in the accumulator charging line prevents loss of water pressure in the event that supply pressure is lost.

During normal plant operation, the accumulator piston is seated at the bottom of its cylinder. Loss of nitrogen decreases the nitrogen pressure, which actuates a pressure switch and sounds an alarm in the control room.

To ensure that the accumulator is always able to produce a scram, it is continuously monitored for water leakage. A float type level switch actuates an alarm if water leaks past the piston barrier and collects in the accumulator instrumentation block.

Purge Water Orifice and Makeup Valve

Each HCU has a restricting orifice in the purge water line to control the purge flow rate to the two associated FMCRDs. This orifice maintains the flow at a constant value while the drives are stationary. A bypass line containing a solenoid-operated valve is provided around this orifice. The valve is signaled to open and increase the purge water flow whenever either of the two associated FMCRDs is commanded to insert by the Rod Control and Information System (RC&IS). During FMCRD insertion cycles, the hollow piston moves upward, leaving an increased volume for water within the drive. Opening of the purge water makeup valve increases the purge flow to offset this volumetric increase and precludes the backflow of reactor water into the drive, thereby preventing long-term drive contamination.

Test Connection for FMCRD Ball Check Valve Testing and Friction Testing

Contained within the HCU is a test port to allow connection of temporary test equipment for the conduct of FMCRD ball check valve testing and drive friction testing. This test port, which has a quick-connect type coupling, is located downstream of the restricting orifice and check valve in the purge water line.

Performance of FMCRD ball check valve testing is accomplished by attaching the check valve test fixture to the HCU test port. The test fixture exercises the check valve by generating a controlled backflow through the check valve housing, causing the valve to backseat. The backflow is contained within a controlled volume inside the test fixture.

During plant shutdown, the friction of each control rod and its drive mechanism is measured to confirm that there is no abnormal driveline resistance that would adversely affect drive operation. Friction testing is performed after FMCRD maintenance or fuel reshuffling. Connecting a portable friction test cart between the CRD hydraulic system and the HCU test port using flexible hoses performs this test. The test cart contains all the necessary hydraulic, electrical and pneumatic equipment, controls and instrumentation to apply hydraulic pressure to the bottom surface of the FMCRD hollow piston that is resting on the ball nut. When the pressure under the hollow piston is high enough to overcome both the combined hollow piston and control rod weight and the driveline friction, the hollow piston will separate from the ball nut and drift the control rod into the core. The pressure acting on the bottom surface of the hollow piston is a direct indication of the driveline friction and is measured and recorded while the piston is being inserted. The recorded pressure trace for each rod is then compared against a reference trace. Any fluctuation in the peak-to-peak reading that exceeds acceptable limits is considered abnormal and indicates further maintenance is required. Only one rod is tested at a time. Since one HCU drives two rods, the rod not under test is isolated. Discharge water during testing is directed back to the RPV via the FMCRD labyrinth seal.

4.6.1.2.4 Control Rod Drive Hydraulic Subsystem

The CRDHS supplies water under high pressure to charge the accumulators, purge the FMCRDs and Reactor Water Cleanup/Shutdown Cooling (RWCU/SDC) system pumps, provide makeup water to the Nuclear Boiler System (NBS) reactor water level reference leg instrument lines and provide makeup water to the reactor vessel following the loss of the normal makeup supply (feedwater). The CRDHS provides the required functions with the pumps, valves, filters, piping, instrumentation and controls shown on Figure 4.6-8. Duplicate components are included where necessary to assure continuous system operation if an inservice component should require maintenance. For system and component classification, see Section 3.2.

The CRDHS hydraulic requirements and components are described in the following paragraphs.

Hydraulic Requirements

The CRDHS process conditions are shown in Figure 4.6-9. The hydraulic requirements, identified by the function they perform, are:

- The required purge water to the drives is shown in Table 4.6-1.
- The approximate purge flow provided to the RWCU/SDC a pump is shown in Table 4.6-1. This flow is provided at approximately CRD pump discharge pressure. The RWCU/SDC system provides its own pressure breakdown equipment to satisfy its individual hydraulic requirements.
- The approximate purge flow provided to the NBS reference leg instrument lines are shown in Table 4.6-1. The purge flow maintains the RPV water level reference leg instrument lines filled to address the effects of noncondensible gases in the instrument lines to prevent erroneous reference information after a rapid RPV depressurization event.
- The approximate flow provided to the Process Sampling System (PSS) is shown in Table 4.6-1. The PSS monitors this flow for CRD water conductivity and dissolved oxygen level.
- The minimum flow supplied to the reactor in the high-pressure makeup mode of operation is shown in Table 4.6-1. This flow is based on a reactor gauge pressure less than or equal to the reference pressure shown in Table 4.6-1.

CRD Supply Pump

One supply pump pressurizes the system with water from the condensate treatment system and/or condensate storage tanks. One spare pump is provided for standby. A discharge check valve prevents backflow through the non-operating pump. A portion of the pump discharge flow is diverted through a minimum flow bypass line to the condensate storage tank. This flow is controlled by an orifice and is sufficient to prevent pump damage if the pump discharge is inadvertently closed.

Redundant filters in both the pump suction and discharge lines process the system water. A differential pressure indicator and control room alarm monitor each filter element as they collect foreign materials.

For the high-pressure makeup mode of operation, the CRDHS operates with both pumps running simultaneously. The standby pump is initiated automatically by low reactor water level so that the combined flow from both pumps can provide the required high-pressure makeup flow to the reactor vessel. The standby pump also starts automatically if loss of discharge header pressure is sensed during normal operation, indicating a failure of the operating pump. This prevents a scram due to low charging water header pressure from occurring as result of an inadvertent pump trip.

The pump suction filters are bypassed automatically during two-pump operation to assure that adequate NPSH is available for the pumps. Two bypass lines are provided around the suction filters, each line containing a normally closed motor-operated valve. These valves are signaled to open when the high-pressure makeup mode of operation is initiated.

Accumulator Charging Water Header

Accumulator charging pressure is established by pre-charging the nitrogen accumulator to a precisely controlled pressure at known temperature. During scram, the scram valves open and permit the stored energy in the accumulators to discharge into the drives. The resulting pressure decrease in the charging water header allows the CRD supply pump to "run out" (i.e., flow rate to increase substantially) into the control rod drives via the charging water header. The flow element upstream of the charging water header senses high flow and provides a signal to the manual/auto flow control station which in turn closes the system flow control valve. This action effectively blocks the flow to the purge water header so that the runout flow is confined to the charging water header.

Pressure instrumentation is provided in the charging water header to monitor header performance. The pressure signal from this instrumentation is provided to both the RC&IS and RPS. If charging water header pressure degrades, the RC&IS initiates a rod block and alarm at a predetermined low-pressure setpoint. If pressure degrades even further, the RPS initiates a scram at a predetermined low-low pressure setpoint. This ensures the capability to scram and reactor shutdown before the HCU accumulator pressure can degrade to the level where scram performance is adversely affected following the loss of charging header pressure.

The charging water header contains a check valve and a bladder type accumulator. The accumulator is located downstream of the check valve in the vicinity of the low header pressure instrumentation. It is sized to maintain the header pressure downstream of the check valve above the scram setpoint until the standby CRD pump starts automatically, following a trip or failure of the operating CRD pump. Pressure instrumentation installed on the pump discharge header downstream of the CRD pump drive water filters monitors system pressure and generates the actuation signals for startup of the standby pump if the pressure drops below a predetermined value that indicates a failure of the operating pump.

An air-operated isolation valve is also provided in the charging water header. It closes automatically when the system is initiated into the high-pressure makeup mode of operation. It blocks the flow through the header to allow all CRDHS flow in this mode to be directed to the reactor via the feedwater system. The valve is designed to preferentially fail closed upon loss of control power or instrument air.

Purge Water Header

The purge water header is located downstream from the flow control valve. The flow control valve adjusts automatically to maintain constant flow to the FMCRDs as reactor vessel pressure changes. Because flow is constant, the differential pressure between the reactor vessel and CRDHS is maintained constant independent of reactor vessel pressure. A flow indicator in the control room monitors system flow. A differential pressure indicator is provided at a local panel to indicate the difference between reactor vessel pressure and purge water pressure.

An air-operated isolation valve is also provided in the purge water header. It closes automatically when the system is initiated into the high-pressure makeup mode of operation. It blocks the flow through the header to allow all CRDHS flow in this mode to be directed to the reactor via the feedwater system. The valve is designed to preferentially fail closed upon loss of control power or instrument air.

High Pressure Makeup Line

The CRDHS supplies high-pressure makeup water to the reactor vessel through piping connecting the discharge lines of the CRD pumps to the RWCU/SDC. The flow is then routed through RWCU/SDC piping to the feedwater system for delivery to the reactor via the feedwater sparger.

Each pump provides half the flow capacity for the high-pressure makeup mode of operation. Located downstream of each pump is a flow control station containing the flow instrumentation and control valve for regulating the pump flow during high-pressure makeup. The piping from the two flow control stations is then combined together into a single line to deliver the combined pump flow to the RWCU/SDC. This line contains a check valve and a normally open motor-operated isolation valve. The check valve is provided to prevent backflow from the RWCU/SDC system. The isolation valve is provided for system testing. During testing, it isolates the line and diverts the flow to the system test line.

System Test Line

A system test line is provided to allow testing of the high-pressure makeup mode during normal plant operation without injecting the relatively cold CRDHS water into the reactor. It connects with the high pressure makeup line at a point downstream of the two pump flow control stations and is routed back to the condensate storage tank (CST). The line contains a variable position valve, which is used to throttle the test flow so that the upstream pressure in the line can be varied to simulate operation over the full range of reactor pressure.

4.6.1.2.5 Control Rod Drive System Operation

The operating modes of the CRD system are described in this subsection.

Normal Operation

Normal operation is defined as those periods of time when no control rod drives are in motion. Under this condition, the CRD system provides charging pressure to the HCUs and supplies purge water to the control rod drives, the RWCU/SDC pumps and reactor water level reference leg instrument lines.

One of the two multi-stage centrifugal pumps supplies the system with water from the condensate and feedwater system and/or CST. The other pump is shutdown and on standby. A constant portion of the pump discharge is continuously bypassed back to the CST in order to maintain a minimum flow through the pump. This prevents overheating of the pump if the discharge line is blocked. The total pump flow during normal operation is the sum of the bypass flow, the FMCRD purge water flow through the flow control valve, the RWCU/SDC pump purge flow, the flow to the reactor water level reference leg instrument lines and the CRDHS water sample flow. The standby pump provides a full capacity backup capability to the operating pump. It starts automatically if failure of the operating pump is detected by pressure instrumentation located in the common discharge piping downstream of the drive water filters.

Redundant filters in both the pump suction and discharge lines process the system water. One suction filter and one drive water filter are normally in operation, while the backup filters are on standby and valved out of service. Differential pressure instrumentation and control room alarms monitor the filter elements as they collect foreign material.

The purge water header provides the purge water for each drive. The purge water flow control valve automatically regulates the purge water flow to the drive mechanisms. The purge water flow rate is indicated in the control room.

In order to maintain the ability to scram, the charging water header maintains the accumulators at a high pressure. The scram valves remain closed except during and after scram, so during normal operation no flow passes through the charging water header. Pressure in the charging water header is monitored continuously. A significant degradation in the charging header pressure causes a low-pressure warning alarm and rod withdrawal block by the RC&IS. Further degradation, if occurring, causes a reactor scram by the RPS.

Pressure in the pump discharge header downstream of the drive water filters is also monitored continuously. Low pressure in this line is used to indicate that the operating pump has failed or tripped. If it should occur, automatic startup of the standby pump is initiated and the system is quickly re-pressurized. A bladder-type accumulator located in the charging water header maintains the pressure in the header above the scram setpoint during the time delay associated with startup of the standby pump. These features protect against a loss of charging water header pressure which may occur as a result of a malfunction of the operating pump, and which could cause the reactor to scram due to a low charging water header pressure.

Control Rod Insertion and Withdrawal

The FMCRD design provides the capability to move a control rod in fine steps. Normal control rod movement is under the control of the RC&IS. The RC&IS controls the input of actuation power to the FMCRD motor from the electrical power supply in order to complete a rod motion command. The FMCRD motor rotates a ball screw that, in turn, causes the vertical translation of a ball-nut on the ball screw. This motion is transferred to the control rod via a hollow piston that rests on the ball-nut. Thus, the piston with the control rod is raised or lowered, depending on the direction of rotation of the FMCRD motor and ball screw.

During a control rod insertion, opening the solenoid-operated purge water makeup valve within the associated HCU increases the purge water flow to the drive. The increased flow offsets the volumetric displacement within the drive as the hollow piston is inserted into the core and prevents reactor water from being drawn back into the drive.

Scram

Upon loss of electric power to both scram solenoid pilot valve (SSPV) coils, the scram valve in the associated HCU opens to apply the hydraulic insert forces to its respective FMCRDs using high pressure water stored within the precharged accumulator (the nitrogen-water accumulator having previously been pressurized with charging water from the CRDHS). Once the hydraulic force is applied, the hollow piston disengages from the ball-nut and inserts the control rod rapidly. The water displaced from the FMCRD is discharged into the reactor vessel. Indication that the scram has been successfully completed (all rods full-in position) is displayed to the operator.

Table 4.6-2 shows the scram performance provided by the CRD system at full power operation, in terms of the maximum elapsed time for each control rod to attain the listed scram position (percent insertion) after loss of signal to the scram solenoid pilot valves (time zero).

The start of motion is the time delay between loss of signal to the scram solenoid pilot valve and actuation of the 0% reed switch.

Simultaneous with the hydraulic scram, each FMCRD motor is started in order to cause electric-driven run-up of the ball-nut until it reengages with the hollow piston at the full-in position. This action is known as the scram follow function. It completes the rod full-in insertion and prepares the drives for subsequent withdrawal to restart the reactor.

After reset of the RPS logic, each scram valve re-closes and allows the CRDHS to recharge the accumulators.

Alternate Rod Insertion

The alternate rod insertion (ARI) function of the CRD system provides an alternate means for actuating hydraulic scram that is diverse and independent from the RPS. The ARI is initiated by any of the following signals: persistent high power with a SCRRI command issued; persistent high power following an RPS scram demand; high reactor dome pressure; low reactor vessel water Level 2; or manual operator action.. Following receipt of any of these signals, solenoid-operated valves on the scram air header actuate to depressurize the header, allowing the HCU scram valves to open. The FMCRDs then insert the control rods hydraulically in the same manner as the RPS initiated scram. The same signals that initiate ARI simultaneously actuate the FMCRD motors to insert the control rods electrically.

The FMCRDs are capable of inserting the control rods hydraulically during ATWS pressure transients with peak reactor pressures of 10.34 MPaG (1500 psig) or less.

High Pressure Makeup

The high-pressure makeup mode of operation initiates on receipt of a low reactor water Level 2 signal. When this occurs, the following actions take place automatically:

- The CRD pump suction filter bypass valves open.
- The standby CRD pump is actuated. Both CRD pumps are operated in parallel in order to deliver the required makeup flow capacity to the reactor.
- The flow control valves in the high-pressure makeup lines open to regulate the makeup water flow rate to the reactor. The test valve in the high pressure makeup line to the

RWCU/SDC System opens, if it is closed at the start of the event, and the test valve in the return line to the CST closes, if it is open at the start of the event. The pump minimum flow bypass isolation valve closes.

- The isolation valves in the purge water header and charging water header close so that all makeup flow is delivered to the reactor through the high-pressure makeup lines.

At high reactor water Level 8, the high-pressure makeup flow control valves close to stop flow to the reactor in order to prevent flooding of the main steam lines. The pump minimum flow bypass valve reopens and both pumps continue to operate in a low flow condition by directing their flow back to the CST through the pump minimum flow lines. Alternately, the operator may choose at this time to manually realign the system into its normal operation mode by shutting down one pump and reopening the charging water header and purge water header isolation valves so that HCU accumulator charging and FMCRD purge water flow can be reestablished. In either case, the system is reset for an automatic restart of high-pressure makeup if a subsequent Level 2 should occur.

During testing of this mode of operation, the high-pressure makeup line isolation valve is closed and pump flow is directed back to the CST through the test line. The backpressure in the line is varied by positioning of the throttle valve in the test line to simulate system operation over the full range of reactor pressure.

4.6.1.2.6 Instrumentation and Control

Instrumentation

The instrumentation for the CRD system includes the following:

- Differential pressure sensors monitor pressure drop across the pump suction filters and drive water filters. High filter differential pressure is alarmed in the control room.
- A pressure sensor is located in the inlet piping to each CRD pump to monitor the suction pressure. A low-pressure condition trips the associated pump and is alarmed in the control room.
- Two pressure sensors are located in the common pump discharge line downstream of the drive water filters to monitor system pressure. A low-pressure condition indicates a failure of the operating pump. A low-pressure signal from either sensor actuates the standby pump.
- Four safety-related pressure sensors are located in the HCU accumulator charging water header. The output signals from these sensors are provided to the RC&IS logic and RPS logic. A low-pressure condition from two-out-of-four sensors causes the RC&IS to generate an all-rod-withdrawal block. A low-low pressure condition causes the RPS to generate a reactor scram.
- A flow sensor is provided in the common pump discharge line downstream of the drive water filters and upstream of the charging water and purge water headers. The flow signal from this sensor provides the control input signal to the purge water flow control valves.

- Each of the two high-pressure makeup lines downstream of the CRD pumps contains a flow sensor. The flow control signal from these sensors provides the control input signals to the high-pressure makeup flow control valves.
- A pressure sensor is provided in the scram air header piping at a location downstream of the air header dump valves and ARI valves and upstream of the scram valves. Both high and low-pressure conditions in the header are alarmed in the control room.
- Status indication for the scram valve position is provided in the control room.

Controls and Interlocks

The controls and interlocks for the CRD system include the following:

- The high-pressure makeup mode of operation is initiated by a low reactor water Level 2 signal. On receipt of this signal, the following automatic actions occur:
  - The standby CRD pump is started. Both pumps operate in parallel to deliver the required makeup flow capacity to the reactor.
  - The two pump suction filter bypass valves are opened.
  - The charging water header isolation valve and purge water header isolation valve are closed.
  - The pump minimum flow bypass line isolation valve closes.
  - The flow control valves in the high pressure makeup lines open to regulate the makeup water flow rate to the reactor.
  - The test valve in the high-pressure makeup line to the RWCU/SDC system opens if it is closed at the start of the event and the test valve in the return line to the CST closes if it is open at the start of the event.
  - The high-pressure makeup flow control valves close to stop flow to the reactor at high reactor water Level 8. The pump minimum flow bypass line isolation valve opens and both pumps continue to operate in a low flow condition by directing their flow back to the CST through the pump minimum flow lines. The control valves reopen and the pump minimum flow bypass isolation valve closes to restart high-pressure makeup flow if a subsequent Level 2 signal should occur.
- The standby CRD pump is started if a low system pressure condition occurs.
- The CRD pump trips upon receipt of a low suction pressure condition. An adjustable time delay is provided in the pump trip logic to protect against transient conditions.
- The CRD pumps are prevented from being started, or are tripped if running, if the pump lube oil pressure is low.
- The RC&IS and the RPS sense the CRD charging header pressure. The following actions occur based on the level of pressure degradation. The actions are based on 2-out-of-4 logic. A time delay is provided in the RPS to avoid spurious or inadvertent trips.
  - Alarm and all rod withdrawal block due to low charging header pressure.
  - Reactor trip due to low low charging header pressure.

- Control rod separation detection for any FMCRD causes both annunciation in the control room and a rod withdrawal block.
- The following signals in the CRD system initiate a rod withdrawal block by the RC&IS:
  - Rod separation detection (individual rod block).
  - Scram charging header pressure low (all rods block).
  - Rod gang misalignment (all rods in gang block).
- The high-pressure makeup flow control valves are prevented from opening when the inboard feedwater maintenance valve on the feedwater line through which the CRD system delivers flow to the reactor is closed.
- When in the high-pressure makeup mode of operation, the CRD pumps are tripped to terminate CRD system flow on receipt of low water level signals from two of the three Gravity Driven Cooling System (GDCS) pools.

4.6.1.2.7 Power Supplies

Each of the four divisional HCU charging header pressure sensors is powered from their respective divisional Class 1E power supply. Independence is provided between the Class 1E divisions for these sensors and between the Class 1E and non-Class 1E equipment.

For the FMCRD separation switches, independence is provided between the Class 1E divisions and between the Class 1E divisions and the non-Class 1E equipment.

The Medium Voltage Distribution System (MVD) provides the normal and standby electrical power to the nonsafety-related FMCRD motors.

4.6.1.2.8 Environmental Qualification

The following CRD system safety-related electrical equipment are located in either the Reactor Building or primary containment and are qualified for harsh environment: the HCU charging header pressure instrumentation, the scram solenoid pilot valves, and the FMCRD separation switches.

4.6.2 Evaluations of the CRD System

4.6.2.1 Safety Evaluation

The safety evaluation of the control rod drives is given below.

4.6.2.1.1 Evaluation of Scram Time

The rod scram function of the CRD system provides the negative reactivity insertion required by the Safety Design Bases in subsection 4.6.1.1.1. The scram time shown in the description is reflected in Chapter 15 safety analyses.

4.6.2.1.2 Scram Reliability

High scram reliability is the result of a number of features of the CRD system. For example:

- Each accumulator provides sufficient stored energy to scram two CRDs at any reactor pressure.
- Each pair of drive mechanisms has its own scram valve and dual solenoid scram pilot valve; therefore, only a single scram valve needs to open for scram to be initiated. Both pilot valve solenoids must be de-energized to initiate a scram.
- The RPS and the HCUs are designed so that the scram signal and mode of operation override all others.
- The FMCRD hollow piston and guide tube are designed so they do not restrain or prevent control rod insertion during scram.
- Each FMCRD mechanism initiates electric motor-driven insertion of its control rod simultaneous with the initiation of hydraulic scram. This provides a diverse means to assure control rod insertion.

4.6.2.1.3 Precluding Excessive Rate of Reactivity Addition

Excessive rates of reactivity addition are precluded in the design of the FMCRD. Prevention of rod ejection due to FMCRD pressure boundary failure and prevention of control rod drop are described below.

Control Rod Ejection Prevention

A failure of the CRD system pressure boundary generates differential pressure forces across the drive, which tends to eject the CRD and its attached control rod. The design of the FMCRD includes features that preclude rod ejection from occurring in these hypothetical circumstances. The following subsections describe how these features function for pressure boundary failures at various locations.

Failures at Drive Housing Weld - The bottom head of the reactor vessel has a penetration for each CRD location. A drive housing is raised into position inside each penetration and fastened by welding. The drive is raised into the drive housing and bolted to a flange at the bottom of the housing. In the event of a failure of the housing just below the housing-to-penetration weld, or a failure of weld itself with housing remaining intact, ejection of the CRD and attached control rod is prevented by the integral internal CRD blowout support. The details of this internal blowout support are contained in Subsection 4.6.1.2.2.

Rupture of Hydraulic Line to Drive Housing Flange

For the case of a scram insert line break, a partial or complete circumferential opening is postulated at or near the point where the line enters the housing flange. This failure, if not mitigated by special design features, could result in rod ejection at speeds exceeding maximum allowable limits. Failure of the scram insert line would cause loss of pressure to the underside of the hollow piston. The force resulting from full reactor pressure acting on the cross-sectional area of the hollow piston, plus the weights of the control rod and hollow piston, is imposed on the ball-nut. The ball-nut, in turn, translates this resultant force into a torque acting on the ball screw. When this torque exceeds the motor residual torque and seal friction, reverse rotation of the ball screw occurs permitting rod withdrawal.

The FMCRD design provides two diverse means of protection against the results of a postulated scram insert line failure. The first means of protection is a ball check valve located in the middle flange of the drive at the scram port. Reverse flow during a line break causes the ball to move to the closed position. This prevents loss of pressure to the underside of the hollow piston, which, in turn, prevents the generation of loads on the drive that could cause rod ejection.

The second means of protection is the FMCRD brake described in Subsection 4.6.1.2.2. In the event of the failure of the check valve, the passive brake prevents the ball screw rotation and rod ejection.

Total Failure of All Drive Flange Bolts - The FMCRD design provides an anti-rotation device which engages when the lower housing (spool piece) is removed for maintenance. This device prevents rotation of the ball screw and hence control rod motion when the spool piece is removed. The two components of the anti-rotation device are (1) the upper half of the coupling between the lower housing drive shaft and ball screw, and (2) the back seat of the middle flange (Figure 4.6-1). The coupling of the lower housing drive shaft to the ball screw is splined to permit removal of the lower housing. The underside of the upper coupling piece has a circumferentially splined surface that engages with a mating surface on the middle flange back seat when the ball screw is lowered during spool piece removal. When engaged, ball screw rotation is prevented. In addition to preventing rotation, this device also provides sealing of leakage from the drive while the spool piece is removed.

In the unlikely event of total failure of all the drive flange bolts attaching the spool piece flange and the middle flange of the drive to the housing flange, the anti-rotation device is engaged when the spool piece falls and the middle flange/outer tube/CRD blowout support is restrained by the control rod guide tube base bayonet coupling, thus preventing rod ejection (see Subsection 4.6.1.2.2).

Control Rod Drop Prevention

The following features prevent control rod drop:

- Two redundant Class 1E switches in the FMCRD sense separation of the hollow piston, which positions the control rod, from the ball-nut. These switches sense either separation of the piston from the nut or separation of the control rod from the piston, and block further lowering of the nut thereby preventing drop of either the control rod or the control rod and hollow piston as an assembly (see Subsection 4.6.1.2.2 for further details).
- Two redundant spring-loaded latches on the hollow piston open to engage in openings in the guide tube within the FMCRD to support the hollow piston if separation from the nut were to occur. These latches open to support the hollow piston (and control rod) following every scram until the ball-nut is run in to provide the normal support for the hollow piston (and control rod).
- The control rod to hollow piston coupling is a bayonet type coupling. Coupling is verified by pull test for the control rod upon initial coupling at refueling and again each time an attempt is made to drive beyond the “full out” position during reactor operation. The control rod can only be uncoupled from the FMCRD by relative rotation that is not possible during operation. The control rod cannot rotate, because it is always constrained between four fuel assemblies, and the hollow piston/CRD spud coupling cannot rotate,

because the hollow piston has rollers that operate in a track within the FMCRD. Only structural failure would permit or result in control rod to FMCRD uncoupling, which, in turn, could only result in rod drop if the redundant switches failed to sense separation. In such failure scenarios, the rate of rod drop may exceed acceptable reactivity addition rates; however, the sequence of failures assumed involve so numerous a failure that the probability of occurrence would be low enough for the event to be categorized as an incredible event.

4.6.2.1.4 CRD Maintenance

The procedure for removal of the FMCRD for maintenance or replacement is similar to previous BWR product lines. The control rod is first withdrawn to the full-out position. During removal of the lower housing (spool piece) following removal of the position indicator probes and motor unit, the control rod backseats onto the control rod guide tube. This metal-to-metal contact provides the seal that prevents draining of reactor water when the FMCRD is subsequently lowered out of the CRD housing. The control rod normally remains in this backseated condition at all times with the FMCRD out; however, in the unlikely event it also has to be removed, a temporary blind flange is first installed on the end of the CRD housing to prevent draining of reactor water.

If the operator inadvertently removes the control rod after FMCRD is out without first installing the temporary blind flange, or conversely, inadvertently removes the FMCRD after first removing the control rod, an un-isolable opening in the bottom of the reactor is created, resulting in drainage of reactor water. The possibility of inadvertent reactor drain-down by this means is considered remote for the following reasons:

- Procedural controls similar to those of current BWRs provide the primary means for prevention. Current BWR operating experience demonstrates this to be an acceptable approach. There has been no instance of an inadvertent drain-down of reactor water due to simultaneous CRD and control rod removal.
- During drive removal operations, personnel are required to monitor under the RPV for water leakage out of the CRD housing. Abnormal or excessive leakage occurring after only a partial lowering of the FMCRD within its housing indicates the absence of the full metal-to-metal seal between the control rod and control rod guide tube required for full drive removal. In this event, the FMCRD can then be raised back into its installed position to stop the leakage and allow corrective action.

The COL applicant shall develop maintenance procedures with provisions to prohibit coincident removal of the control rod and CRD of the same assembly. In addition, the COL applicant shall develop contingency procedures to provide core and spent fuel cooling capability and mitigative actions during CRD replacement with fuel in the vessel.

The FMCRD design also allows for separate removal of the motor unit, position indicator probe (PIP), separation indicator probe (SIP) and spool piece for maintenance during plant outages without disturbing the upper assembly of the drive. While these FMCRD components are removed for servicing, the associated control rod is maintained in the fully inserted position by one of two mechanical locking devices that prevent rotation of the ball screw and drive shaft.

The first anti-rotation device (Detail A in Figure 4.6-10) is engaged when the motor unit consisting of the induction motor, reduction gear, brake and position signal detector is removed. It is a spring-actuated locking cam located on the bottom of the spool piece. When the motor unit is lowered away from the spool piece, the locking cam is released from its normally retracted position and engaged by spring force with gear teeth on the bottom of the magnetic coupling outer rotor, thereby locking the shaft in place.

With the motor unit removed, the locking cam can be visually checked from below the drive to verify that it is properly engaged. When the vessel head is removed, another means of verification of proper locking is for the operator to view the top of the control rod from over the reactor vessel. If the top of the control rod is visible at its normal full in position, it provides both direct indication that the control rod remains fully inserted and additional assurance that the ball screw is restrained from reverse rotation. The drive shaft remains locked in this manner until the motor unit is reattached to the spool piece. During motor installation, a release pin on the motor unit pushes up a plunger linked to the locking cam as the motor unit is raised into contact with the spool piece. The release pin forces the locking cam away from the teeth on the bottom of the magnetic coupling outer rotor and into the normally retracted, unlocked position.

The second anti-rotation device (Detail B in Figure 4.6-10) is engaged when the spool piece is removed from the FMCRD. As described in Subsection 4.6.2.1.3, this device is a spline arrangement between the ball screw lower coupling and the middle flange backseat. When removing and lowering the spool piece, the weight of the ball screw, hollow piston and control rod provides a vertical force in the downward direction that brings the two splines together. This locks the ball screw into the backseat and prevents reverse rotation. As with the first anti-rotation device, proper engagement of this device can be visually checked from below the drive. If the splines do not completely lock together, there is indication of this because the ball screw does not seat against the backseat and there is a small gap for leakage of water. If this should occur, removal of the spool piece can be discontinued and corrective action taken. If there is no leakage, it confirms that the splines are properly locked together. Also as in the case of the first anti-rotation device, visual observation of the top of the control rod from over the reactor vessel provides another means for verifying proper locking of the ball screw. The ball screw remains locked in this position until the spool piece is reattached to the FMCRD. During spool piece installation, the end of the drive shaft fits into a seat on the end of the ball screw. As the ball screw piece is raised off the middle flange backseat, the anti-rotation splines disengage and the weight of the ball screw, hollow piston and control rod is transferred to the spool piece assembly.

4.6.3 Testing and Verification of the CRDs

4.6.3.1 Factory Quality Control Tests

The quality control specifications and procedures follow the general pattern established for such specifications and procedures in BWRs presently in operation.

Quality control of welding, heat treatment, dimensional tolerances, material verification and similar factors are maintained throughout the manufacturing process to assure reliable performance of the mechanical reactivity control components.

Some of the quality control tests performed on the CRD mechanisms and HCUs are listed below:

- CRD Mechanism Tests
  - Pressure welds on the drives are hydrostatically tested in accordance with ASME codes.
  - Electrical components are checked for electrical continuity and resistance to ground.
  - Drive parts that cannot be visually inspected for dirt are flushed with filtered water at high velocity. No significant foreign material is permitted in effluent water.
  - Each drive is tested for shim (drive-in and -out) motion and control rod position indication.
  - Each drive is subjected to cold scram tests at various reactor pressures to verify correct scram performance.
- HCU Tests
  - Hydraulic systems are hydrostatically tested in accordance with the applicable code.
  - Electrical components and systems are tested for electrical continuity and resistance to ground.
  - Correct operation of the accumulator pressure and level switches is verified.
  - Each HCU's ability to perform as part of a scram is demonstrated.

4.6.3.2 Functional Tests

These tests evaluate drive performance under conditions of crud/contamination, seismic misalignment, channel bulge, failed buffer, rod drop (to test hollow piston latch functionality), and rod ejection (to test FMCRD brake functionality).

4.6.3.3 Operational Tests

After installation, all rods and drive mechanisms can be tested through their full stroke for operability.

The switches that detect separation provide indication and automatic rod withdrawal block should a control rod separate from the drive mechanism during rod withdrawal. Additionally, the operator can observe the incore monitor indications to verify that the control rod is following the drive mechanism. All control rods that are partially withdrawn from the core can be tested for rod-following by inserting or withdrawing the rod one or two steps and returning it to its original position, while the operator observes the incore monitor indications.

To make a positive test of control rod to CRD coupling integrity, the operator can withdraw a control rod to the end of its travel and then attempt to withdraw the drive to the overtravel position. Failure of the hollow piston to overtravel-out demonstrates the integrity of the rod-to-drive coupling.

CRDHS pressures can be observed from instrumentation in the control room. Scram accumulator pressures can be observed on the nitrogen pressure gauges.

4.6.3.4 Acceptance Tests

Criteria for acceptance of the individual CRD mechanisms and the associated control and protection systems is incorporated in specifications and test procedures covering three distinct phases:

- Pre-installation
- After installation prior to startup
- During startup testing

The pre-installation specification defines criteria and acceptable ranges of such characteristics as seal leakage, friction and scram performance under fixed test conditions that must be met before the component can be shipped.

The after-installation, preoperational tests (Chapter 14) include normal and scram motion and are primarily intended to verify that piping, valves, electrical components and instrumentation are properly installed. The test specifications include criteria and acceptable ranges for drive speed, scram valve response times, and control pressures. These are tests intended more to document system condition rather than tests of performance.

As fuel is placed in the reactor, the startup test procedure (Chapter 14) is followed. The tests in this procedure are intended to demonstrate that the initial operational characteristics meet the limits of the specifications over the range of primary coolant temperatures and pressures from ambient to operating. The detailed specifications and procedures are similar to those in BWRs presently in operation.

4.6.3.5 Surveillance Tests

The surveillance requirements for the CRD system are described as follows:

- Sufficient control rods shall be withdrawn, following a refueling outage when core alterations are performed, to demonstrate with adequate shutdown margin that the core can be made subcritical at any time in the subsequent fuel cycle with the maximum worth control rod pair having the same HCU or the single rod attached to the unpaired HCU, if of greater worth, withdrawn and all other operable rods fully inserted.
- Each fully withdrawn control rod is exercised at least once each week. Each partially withdrawn control rod is exercised at least once each month.
- The coupling integrity shall be verified for each withdrawn control rod as follows:
  - When the rod is first withdrawn, observe the control rod separation switch response and discernible response of the nuclear instrumentation.
  - When the rod is fully withdrawn the first time, observe that the drive does not go to the overtravel-out position. Observation of the separation switches provides direct indication that the control rod is following the drive during withdrawal, but does not provide a direct check on coupling integrity. Additionally, observation of a response from the nuclear instrumentation during an attempt to withdraw a control rod provides another indirect indication that the rod and drive are coupled. The

overtravel-out position feature provides a positive check on the coupling integrity, for only an uncoupled drive can reach the overtravel-out position.

- During operation, accumulator pressure and level at the normal operating value are verified. Experience with CRD systems of the same type indicates that weekly verification of accumulator pressure and level is sufficient to assure operability of the accumulator portion of the CRD system.
- At the time of each major refueling outage, each operable control rod is subjected to scram time tests from the fully withdrawn position. Experience indicates that the scram times of the control rods do not significantly change over the time interval between refueling outages. A test of the scram times at each refueling outage is sufficient to identify any significant lengthening of the scram times. However, an additional test of a representative sample of the control rods, as defined in the plant Technical Specifications, is performed every 200 days of cumulative operation in Mode 1.
- Each affected control rod is subjected to scram tests from the fully withdrawn position following work on the control rod or CRD system that could affect scram time, and after fuel movement has occurred within the affected cell.
- The high-pressure makeup mode of operation is tested every refueling outage to verify the automatic response of the system to a simulated or actual initiation signal. Every quarter each CRD pump is tested to verify that it can develop the required flow rate for high-pressure makeup against a system head corresponding to the required reactor pressure. This test uses the system test return line to the CST.

4.6.4 Information for Combined Performance of Reactivity Control Systems

4.6.4.1 Vulnerability to Common Mode Failures

The Reactivity Control System is located such that it is protected from common mode failures due to missiles, failures of moderate and high energy piping, and fire. Sections 3.5, 3.6 and 3.7, and Subsection 9.5.1 discuss protection of safety-related systems against missiles, pipe breaks, seismic and fire, respectively.

4.6.4.2 Accidents Taking Credit for Multiple Reactivity Systems

There are no postulated accidents documented in Chapter 15 that take credit for two or more reactivity control systems preventing or mitigating an accident.

4.6.5 Evaluation of Combined Performance

As indicated in Subsection 4.6.4.2, credit is not taken for multiple reactivity control systems for any postulated accidents documented in Chapter 15.

4.6.6 COL Unit-Specific Information

4.6.6.1 CRD and FMCRD Maintenance Procedures

The COL applicant shall develop CRD and control rod removal maintenance procedures that include the provisions specified in Subsection 4.6.2.1.4.

4.6.7 References

None

Table 4.6-1

Hydraulic Requirements

Parameter	Value
Required purge water flow to control rod drives, l/min (gpm)	1.3 (0.34)
Approximate purge water flow to RWCU/SDC pumps, l/min (gpm)	20 (5.3)
Approximate makeup flow to NBS instrument lines, l/min (gpm)	4 (1)
Approximate makeup flow to PSS monitors, l/min (gpm)	1 (0.3)
Minimum flow to reactor in high pressure makeup mode with both pumps running, l/min (gpm)	3920 (1036)
Minimum flow to reactor in high pressure makeup mode with one pump running, l/min (gpm)	1960 (518)
Reference pressure for high pressure makeup mode, MPa (psig)	8.62 (1250)
Design pressure for the piping and components of the CRD pump suction supply, which extends from the CRD system interfaces with the Condensate and Feedwater System (C&FS) and Condensate Storage and Transfer System (CS&TS) to the inlet connections of the CRD pumps, MPa (psig)	2.82 (409)

Table 4.6-2

CRD System Scram Performance

Insertion	Time (sec)
Start of Motion	≤ 0.20
10%	≤ 0.34
40%	≤ 0.80
60%	≤ 1.15
100%	≤ 2.23

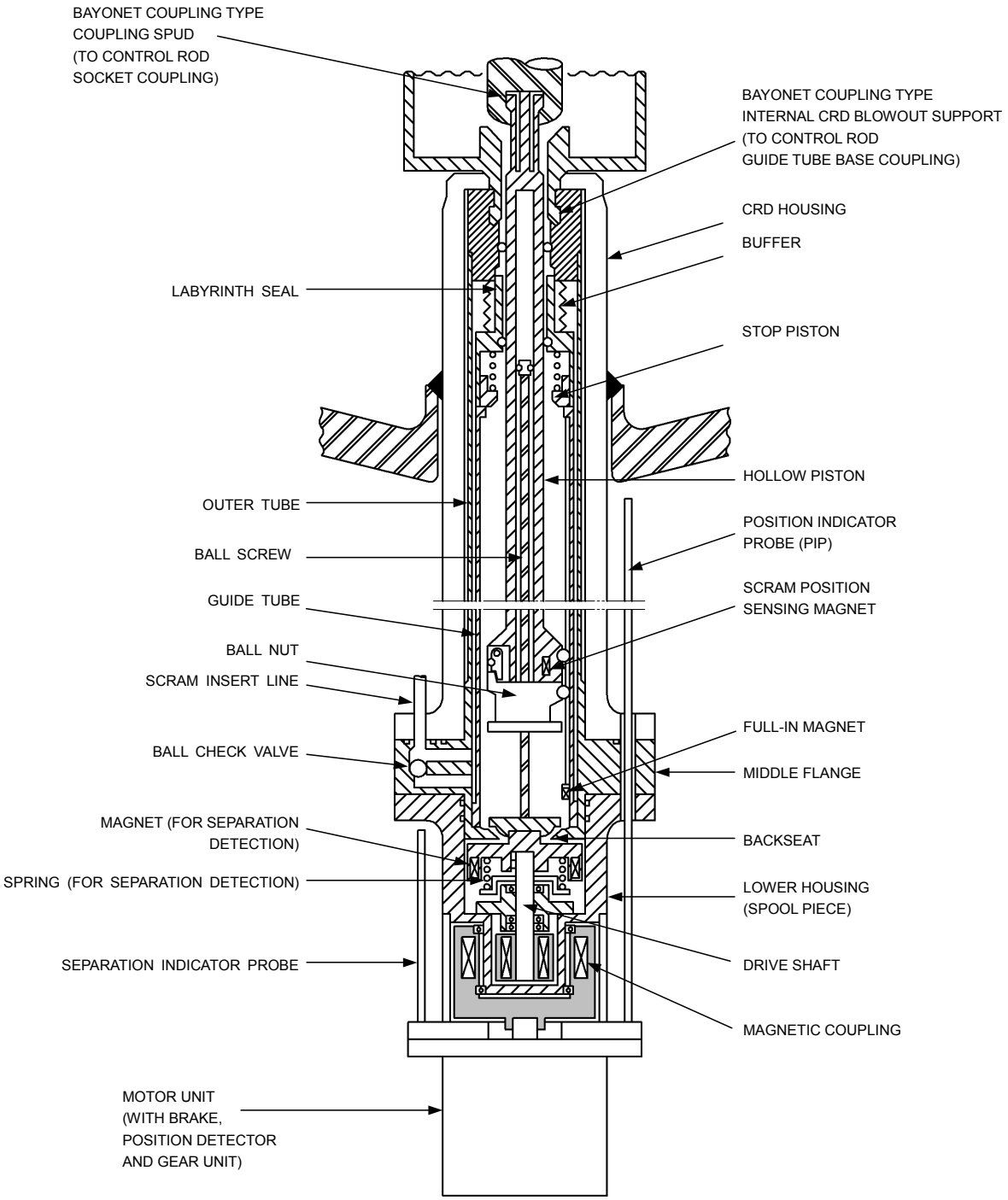

Figure 4.6-1. Fine Motion Control Rod Drive Schematic

No.	MAIN PART NAME
1	DRAIVE SHAFT
2	BEARING
3	MAGNET (INNER ROTOR)
4	MAGNET (OUTER ROTOR)
5	LOWER HOUSING (SPOOL PIECE)
6	BALL SCREW
7	BALL NUT AND BALL
8	GUIDE ROLLER AND PIN (FOR NUT)
9	GUIDE SHAFT
10	BUSHING (STATIONARY GUIDE)
11	SPRING (FOR SEPARATION DETECTION)
12	MAGNET (FOR SEPARATION DETECTION)
13	BUFFER SPRING
14	BUFFER SLEEVE (LABYRINTH SEAL)
15	GUIDE ROLLER, PIN
16	STOP PISTON
17	HOLLOW PISTON
18	DRIVE PISTON
19	LATCH
20	LATCH SPRING
21	SPUD (BAYONET COUPLING)
22	COMPRESSION ROD
23	GUIDE TUBE
24	OUTER TUBE
25	MIDDLE FLANGE
26	BALL CHECK VALVE
27	O RING SEAL (BETWEEN CRD HOUSING AND CRD)
28	CRD MOUNTING BOLT
29	BLOWOUT SUPPORT
30	FULL IN MAGNET

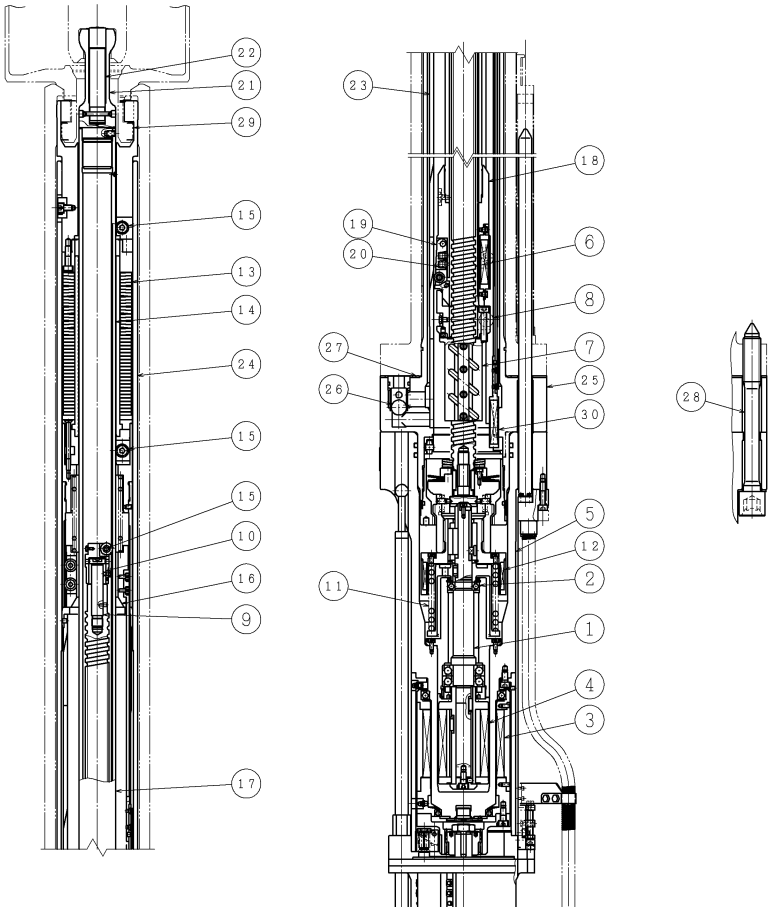

Figure 4.6-2. Fine Motion Control Rod Drive Unit (Cutaway)

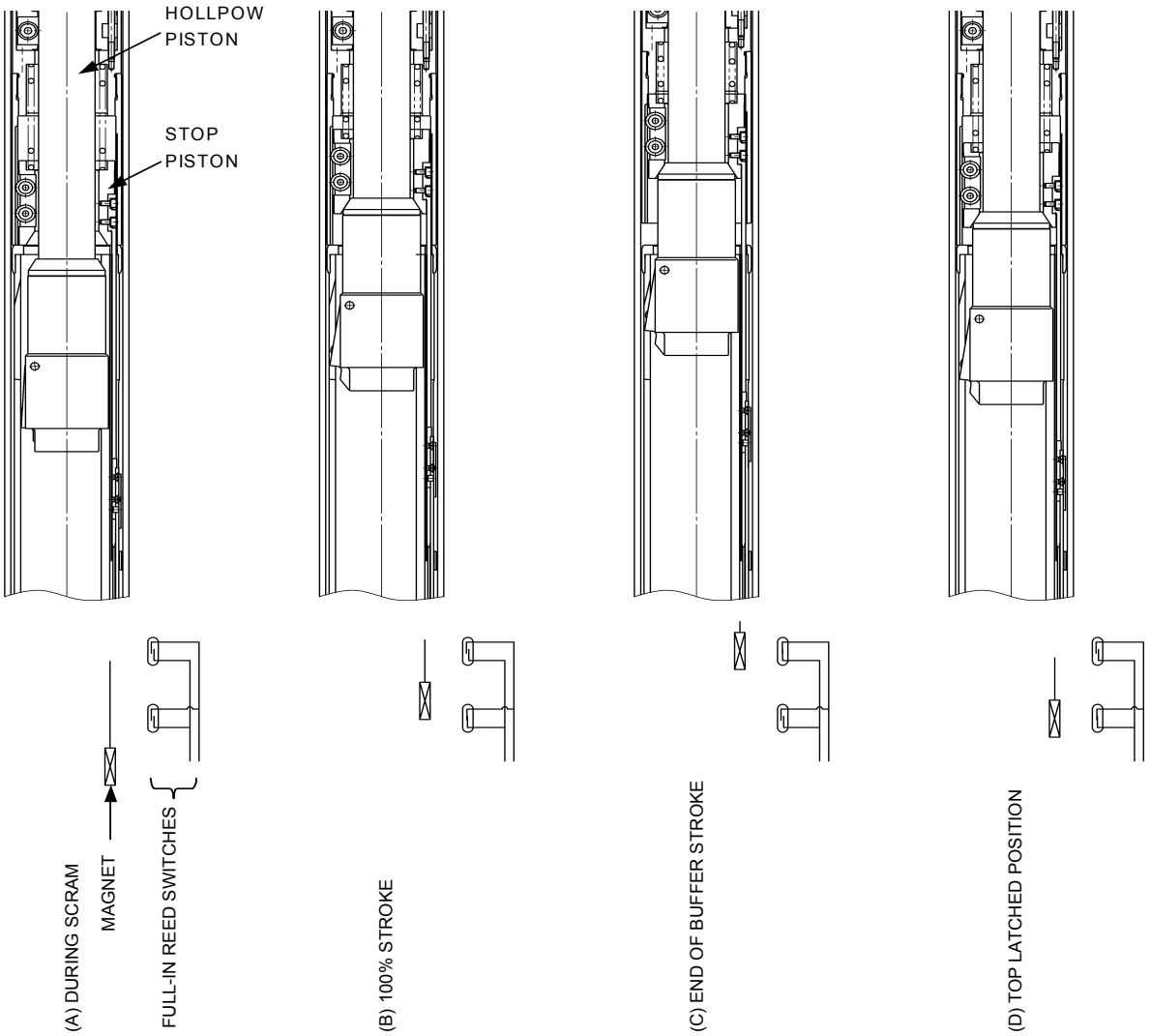

Figure 4.6-3. Continuous Full-in Indicating Device

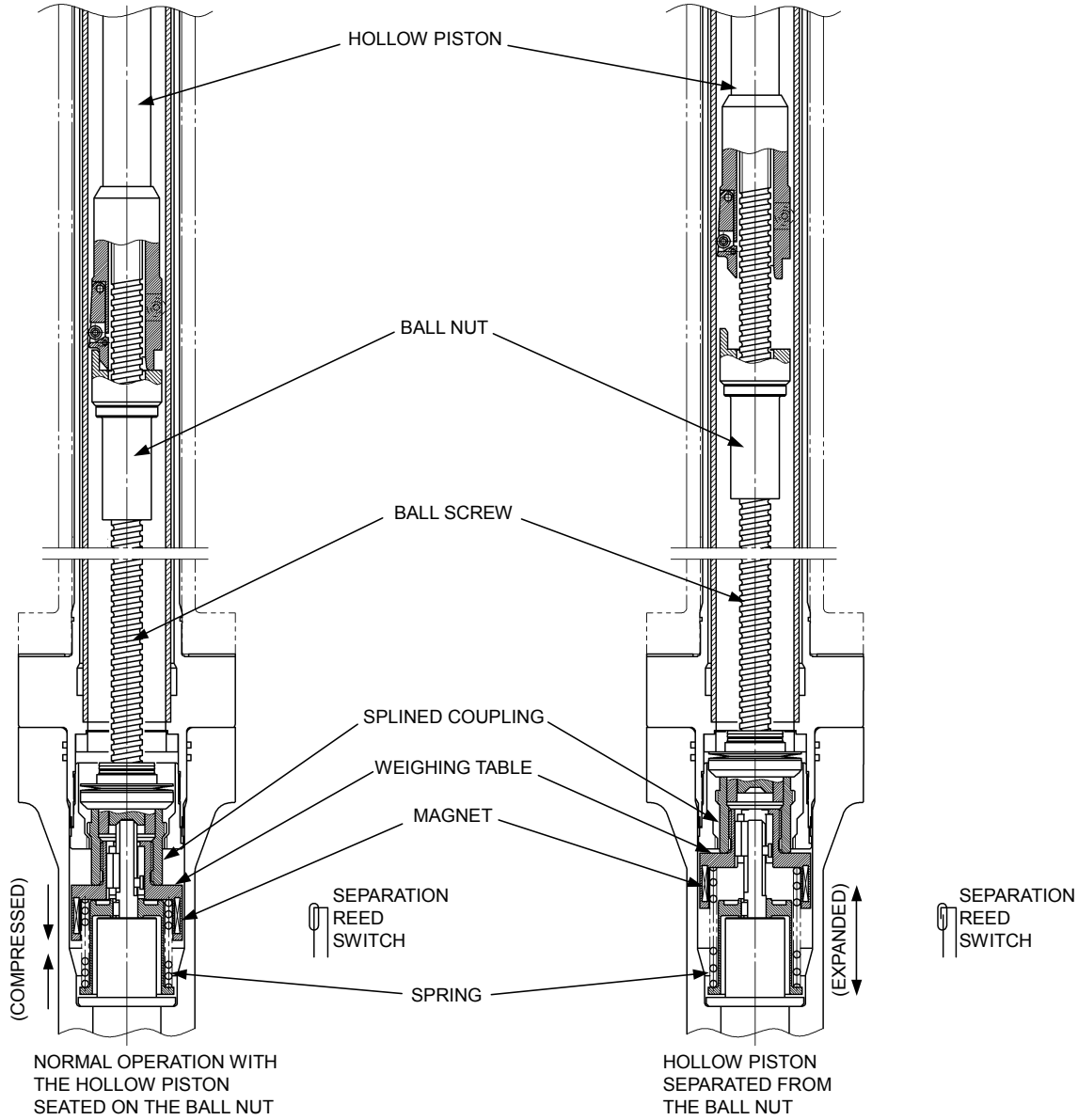

Figure 4.6-4. Control Rod Separation Detection

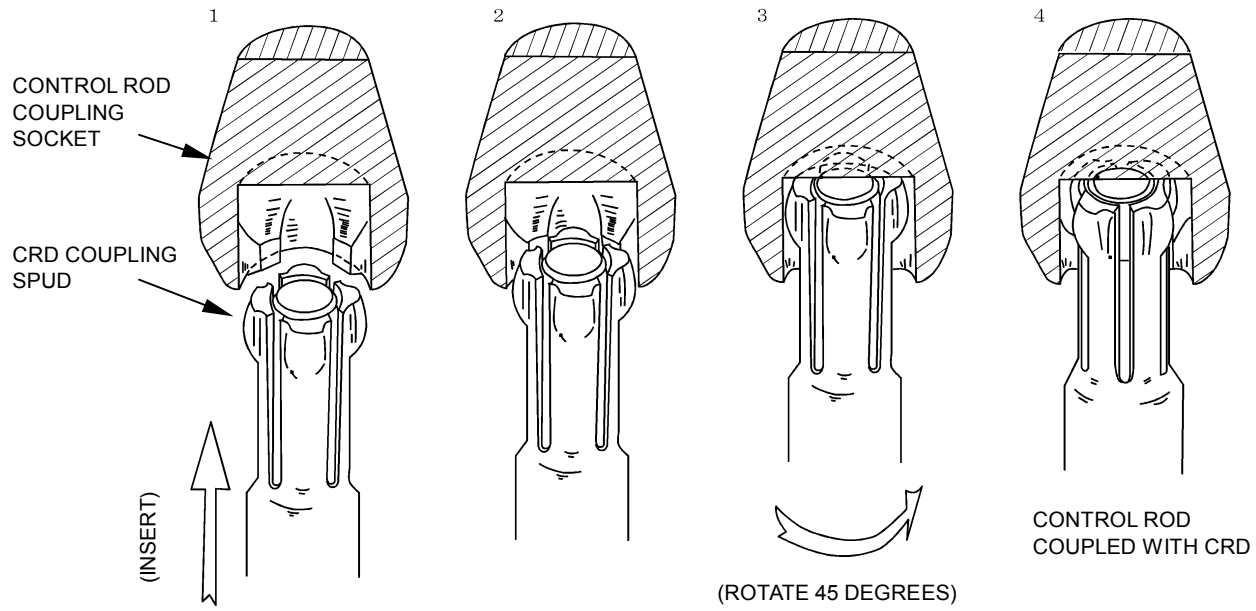

Figure 4.6-5. Control Rod to Control Rod Drive Coupling

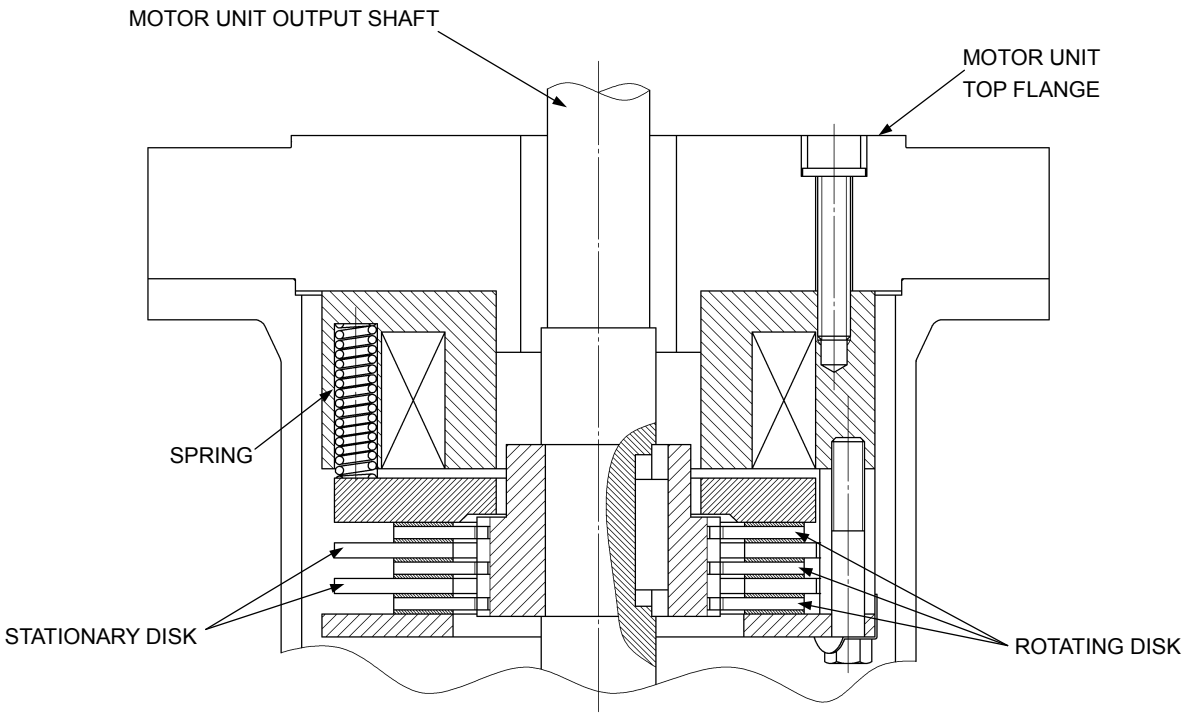

Figure 4.6-6. FMCRD Electro-mechanical Brake

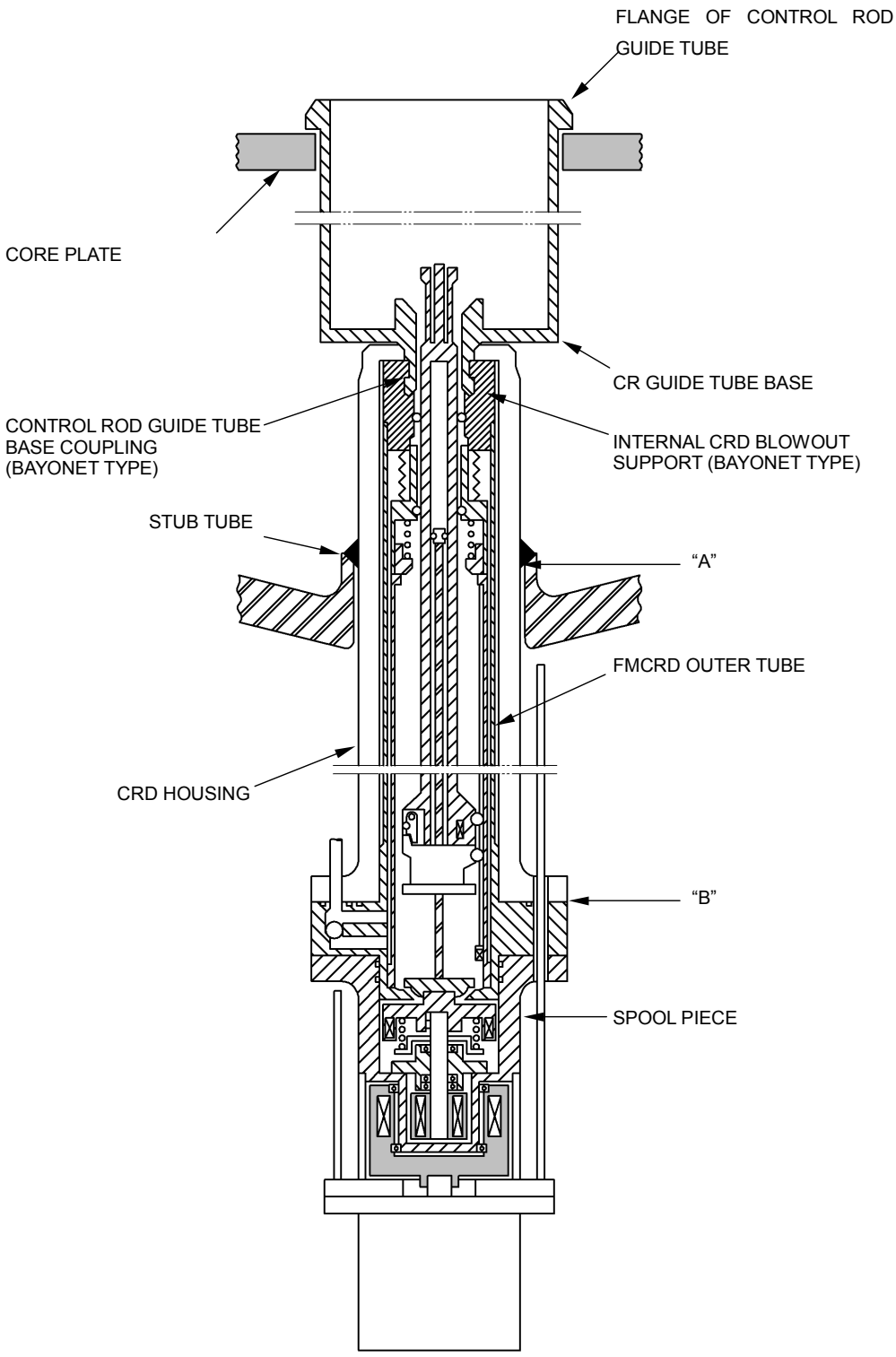

Figure 4.6-7. Internal CRD Blowout Support Schematic

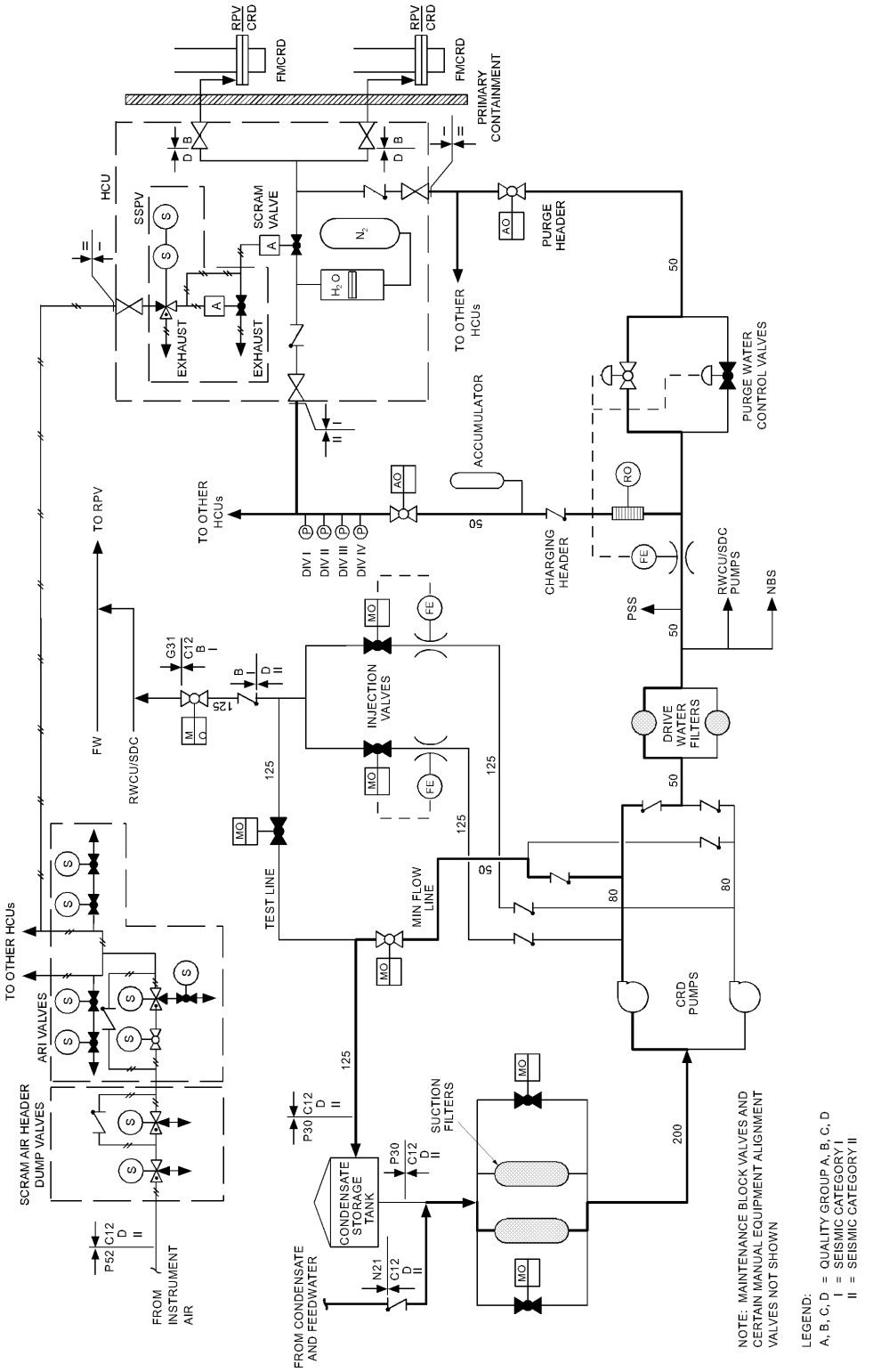

Figure 4.6-8. Control Rod Drive System Simplified Process and Instrumentation Diagram

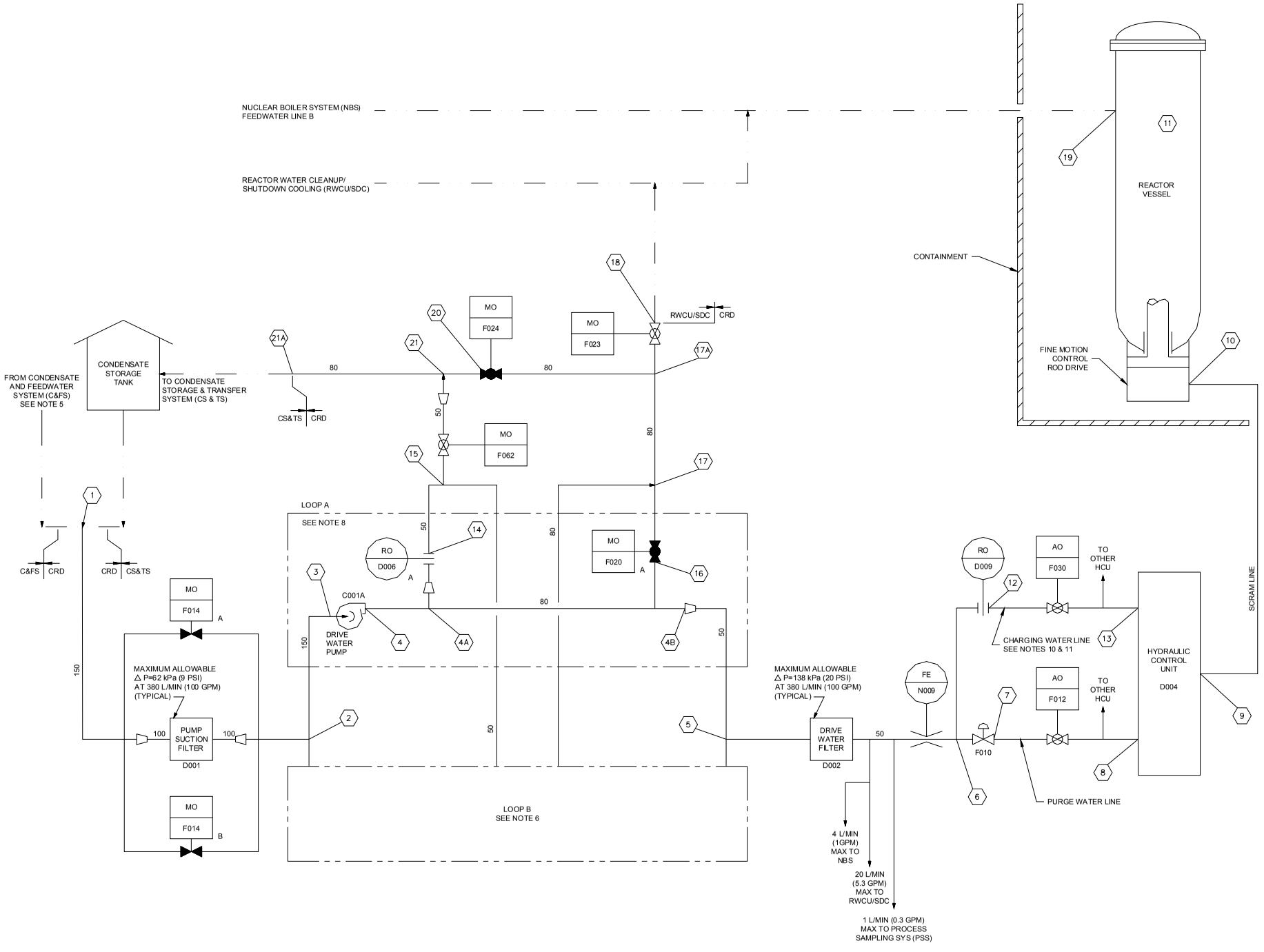

1. ALL EQUIPMENT NUMBERS SHOWN ON THIS DIAGRAM ARE PREFIXED BY C12- UNLESS OTHERWISE INDICATED.
2. LINE SIZES ARE SPECIFIED ON THE PIPING AND INSTRUMENTATION DIAGRAM (MPL NO. C12-1010).
3. ALL VALUES ARE NOMINAL UNLESS NOTED OTHERWISE.
4. THE TERM PR DENOTES REACTOR PRESSURE IMMEDIATELY ABOVE THE CORE PLATE.
5. THE CST WILL PROVIDE AN ALTERNATE SOURCE OF WATER FOR THE CRD SYSTEM IF THE CONDENSATE AND FEEDWATER SYSTEM IS NOT AVAILABLE.
6. ONE PUMP IS RUNNING AND ONE IS ON STANDBY DURING OPERATING MODES A, B, AND C. THE OPERATOR WILL SELECT WHICH PUMP IS TO RUN. PUMP A IS USED TO DEFINE THE PROCESS CONDITIONS FOR THE OPERATING PUMP. BOTH PUMPS RUN DURING OPERATING MODES D AND E. FOR THESE MODES, THE PROCESS CONDITIONS OF PUMP B ARE IDENTICAL TO THOSE OF PUMP A.
7. DURING NORMAL MOTOR-DRIVEN ROD INSERTIONS (SINGLE ROD OR GANGED MOVEMENTS) IN MODE A, THE PURGE WATER FLOW AT LOCATION 8 IS INCREASED TO A MINIMUM OF 8.2 L/MIN (2.2 GPM) TO EACH HCU ASSOCIATED WITH A MOVING DRIVE. THIS IS ACCOMPLISHED BY AUTOMATIC OPENING OF THE PURGE WATER MAKE-UP VALVE IN THE HCU. THE FLOW FROM EACH HCU THEN DIVIDES EVENLY BETWEEN THE TWO DRIVES SUCH THAT THE FLOW AT LOCATIONS 9 AND 10 IS A MINIMUM OF 4.1 L/MIN (1.1 GPM). THE PURGE WATER FLOW TO THE STATIONARY DRIVES CORRESPONDINGLY DECREASES SINCE THE TOTAL PURGE WATER HEADER FLOW RATE AT LOCATION 7 REMAINS CONSTANT.
8. IN MODE A, THE MINIMUM DRIVE PURGE FLOW RATE AT LOCATIONS 9 AND 10 SHALL NOT BE LESS THAN 0.7 L/MIN (0.18 GPM) TO ANY DRIVE WHILE ALL DRIVES ARE STATIONARY. THE PURGE FLOW RATE TO THE STATIONARY DRIVES IN MODE A MAY BE LESS THAN THIS LIMIT FOR BRIEF PERIODS OF TIME DURING GANG ROD MOVEMENTS AS DESCRIBED IN NOTE 7.
9. SYSTEM OPERATION IS POSSIBLE WITH INTERMEDIATE PRESSURES IN THE REACTOR VESSEL. HOWEVER, THESE CONDITIONS DO NOT CONTROL PIPE OR VALVE SIZING OR SPECIFICATION, AND NO DATA IS SHOWN.
10. PUMP FLOW OF 767 L/MIN (203 GPM) SHALL NOT BE EXCEEDED. ORIFICE D009 REDUCES THE PRESSURE AT THE INSERT LINE SO THAT NO GREATER THAN A TOTAL OF 455 L/MIN (120 GPM) WILL LEAK THROUGH ALL THE DRIVES WHEN PR = 0 MPa GAUGE (0 PSIG). FLOW AT LOCATIONS 9 AND 10 IS EQUAL TO 455 L/MIN (120 GPM) DIVIDED BY 269 (THE NUMBER OF DRIVES).
11. RESTRICTING ORIFICES D006 AND D009 ARE COMPOSED OF MULTIPLE ORIFICES CONNECTED IN SERIES.
12. THE SPECIFIED LINE LOSSES ARE FOR SCRAM LINE ONLY. TOTAL COMBINED LOSSES FOR THE HCU PLUS SCRAM LINE ARE 1.68 MPa (243 PSI) MINIMUM AND 2.12 MPa (307 PSI) MAXIMUM AT THE SPECIFIED FLOW RATE.
13. FCV-F020 LIMITS FLOW TO THE REACTOR IN THE VESSEL INJECTION MODE TO 1960 L/MIN (518 GPM) SO THAT PUMP RUNOUT CAPACITY OF 1973 L/MIN (521 GPM) SHALL NOT BE EXCEEDED.
14. THE PRESSURE CONDITIONS IDENTIFIED IN THIS DRAWING ARE BASED ON PREVIOUS BWR SYSTEM DESIGN OF SIMILAR CONFIGURATION AND ARE REPRESENTATIVE OF TYPICAL EXPECTED VALUES.

Figure 4.6-9. Control Rod Drive System Process Flow Diagram
(Sheet 1 of 2)

MODE A NORMAL OPERATION - SIZES PURGE WATER HEADER

LOCATION ⬡		1	2	3	4	5	6	7	8	9	10	11	12	13	14	15	16	17	18	19	20	21
FLOW	L/MIN (GPM)	662 (175)	662 (175)	662 (175)	662 (175)	375 (99)	350 (92.5)	350 (92.5)	2.6 (0.68)	1.3 (0.34) MAX	1.3 (0.34) MAX	---	0	0	287 (76)	287 (76)	0	0	0	0	0	287 (76)
PRESSURE	MPa GAUGE (PSIG)			*	*	*	*	PR+0.25 (PR+36) MIN	PR+0.25 (PR+36) MIN	PR+0.20 (PR+29) MIN	PR+0.20 (PR+29) MIN	PR			*							
									SEE NOTE 7													

CONDITIONS:
1. NORMAL DRIVE OPERATION
2. MAXIMUM PURGE FLOW TO DRIVES (SEE NOTE 8)
3. REACTOR PRESSURE PR = 7.067 MPa GAUGE (1025 PSIG)(SEE NOTE 9)

MODE B SCRAM - SIZES SCRAM INSERT LINE

LOCATION ⬡		1	2	3	4	5	6	7	8	9	10	11	12	13	14	15	16	17	18	19	20	21
FLOW	L/MIN (GPM)	312 (82)	312 (82)	312 (82)	312 (82)	25 (6.6)	0	0	0	473 (125)	473 (125)	---	0	0	287 (76)	287 (76)	0	0	0	0	0	287 (76)
PRESSURE	MPa GAUGE (PSIG)									*	*	PR			*							

CONDITIONS:
1. DRIVES SCRAMMING
2. SCRAM INSERT LINE LOSSES AT SPECIFIED LIMITS
3. REACTOR PRESSURE PR = 7.067 MPa GAUGE (1025 PSIG) (SEE NOTE 9)

MODE C SCRAM COMPLETED - SIZES THE PUMP SUCTION FILTER LINES AND CHARGING THE WATER HEADER

LOCATION ⬡		1	2	3	4	5	6	7	8	9	10	11	12	13	14	15	16	17	18	19	20	21
FLOW	L/MIN (GPM)	767 (203)	767 (203)	767 (203)	767 (203)	480 (127)	455 (120)	0	0	SEE NOTES 10 AND 11		---	455 (120) MAX	3.4 (0.9) MAX	287 (76)	287 (76)	0	0	0	0	0	287 (76)
PRESSURE	MPa GAUGE (PSIG)			*	*							PR			*							

CONDITIONS:
1. SCRAMMING OF DRIVES COMPLETED
2. MAXIMUM CRD SUPPLY PUMP FLOW THROUGH PUMP SUCTION FILTER
3. REACTOR PRESSURE PR = 0 MPa GAUGE (0 PSIG) (SEE NOTE 9)

MODE D REACTOR VESSEL INJECTION - SIZES THE PUMP SUCTION AND VESSEL INJECTION LINES

LOCATION ⬡		1	2	3	4	5	6	7	8	9	10	11	12	13	14	15	16	17	18	19	20	21
FLOW	L/MIN (GPM)	3945 (1042)	3945 (1042)	1973 (521)	1973 (521)	25 (6.6)	0	0	0	0	0	---	0	0	0	0	1960 (518)	3920 (1036)	3920 (1036)	3920 (1036)	0	0
PRESSURE	MPa GAUGE (PSIG)			*	*							PR			*		SEE NOTE 13					

CONDITIONS:
1. SCRAMMING OF DRIVES COMPLETED
2. MAXIMUM CRD SUPPLY PUMP FLOW (PUMP RUNOUT)
3. REACTOR PRESSURE PR = 8.619 MPa GAUGE (1250 PSIG) (SEE NOTE 9)

MODE E TEST MODE

LOCATION ⬡		1	2	3	4	5	6	7	8	9	10	11	12	13	14	15	16	17	18	19	20	21
FLOW	L/MIN (GPM)	3945 (1042)	3945 (1042)	1973 (521)	1973 (521)	25 (6.6)	0	0	0	0	0	---	0	0	0	0	1960 (518)	3920 (1036)	0	0	3920 (1036)	3920 (1036)
PRESSURE	MPa GAUGE (PSIG)			*	*							PR			*						*	*

CONDITIONS:
1. PURGE FLOW TO DRIVES INTERRUPTED
2. DISCHARGE TO CONDENSATE STORAGE
3. NORMAL REACTOR OPERATION

DESIGN PRESSURE / TEMPERATURE

LOCATION ⬡		1-2	2-3	4-5	5-6	6-7	7-8	9-10	6-12	12-13	4A-14	14-15	15-21	4B-16	16-17	17-18	17A-20	20-21	21-21A
PRESSURE	MPa GAUGE (PSIG)	2.82 (409)	2.82 (409)	18.6 (2700)	18.6 (2700)	18.6 (2700)	18.6 (2700)	23.54 (3410)	18.6 (2700)	18.6 (2700)	18.6 (2700)	18.6 (2700)	18.6 (2700)	18.6 (2700)	18.6 (2700)	18.6 (2700)	18.6 (2700)	18.6 (2700)	18.6 (2700)
TEMPERATURE	°C (°F)	66 (150)	66 (150)	66 (150)	66 (150)	66 (150)	66 (150)	66 (150)	66 (150)	66 (150)	66 (150)	66 (150)	66 (150)	66 (150)	302 (575)	302 (575)	302 (575)	66 (150)	66 (150)

EQUIPMENT OPERATIONAL CONDITITIONS

EQUIPMENT IDENTIFICATION	EQUIPMENT DESCRIPTION	MODE A	MODE B	MODE C	MODE D	MODE E
C001A, B	CRD PUMP (NO. RUNNING)	1	1	1	2	2
F010	FCV	0	0	C	0	0
F012	AO VALVE	0	0	0	C	C
F014A, B	MO VALVE	C	C	C	0	0
F020A, B	FCV	C	C	C	0	0
F023	MO VALVE	0	0	0	0	C
F024	MO VALVE	C	C	C	C	0
F030	AO VALVE	0	0	0	C	C
F062	MO VALVE	0	0	0	C	C

* THE PRESSURE AT THIS LOCATION DEPENDS ON PIPING ARRANGEMENT, AND MAY BE VARIED WITHIN THE FOLLOWING LIMITS. SEE NOTE 14.

LOCATION:

⬡3 MINIMUM NPSH AT PUMP SUCTION = 11 METER (36 FEET) AT 1973 L/MIN (521 GPM)
MAXIMUM SUCTION PRESSURE 0.34 MPa (50 PSIG)

⬡4 MINIMUM PUMP TOTAL DYNAMIC HEAD (TDH):
1560 METER (5120 FEET) FOR MODES A AND B
1200 METER (3940 FEET) FOR MODE C
1000 METER (3280 FEET) FOR MODES D AND E

⬡6 MAXIMUM PRESSURE DROP BETWEEN LOCATIONS
⬡4 AND ⬡6 = 0.50 MPa (72 PSIG) FOR MODE A

⬡9 ⬡10 LINE LOSS BETWEEN LOCATIONS
⬡9 AND ⬡10 FOR MODE B
0.72 MPa (104 PSI) MINIMUM
1.16 MPa (168 PSI) MAXIMUM
AT THE SPECIFIED FLOW RATE (SEE NOTE 12).

⬡14 SUFFICIENT PRESSURE TO RETURN FLOW TO CONDENSATE STORAGE.

⬡20 ⬡21 SUFFICIENT PRESSURE TO RETURN FLOW TO CONDENSATE STORAGE.

Figure 4.6-9. Control Rod Drive System Process Flow Diagram
(Sheet 2 of 2)

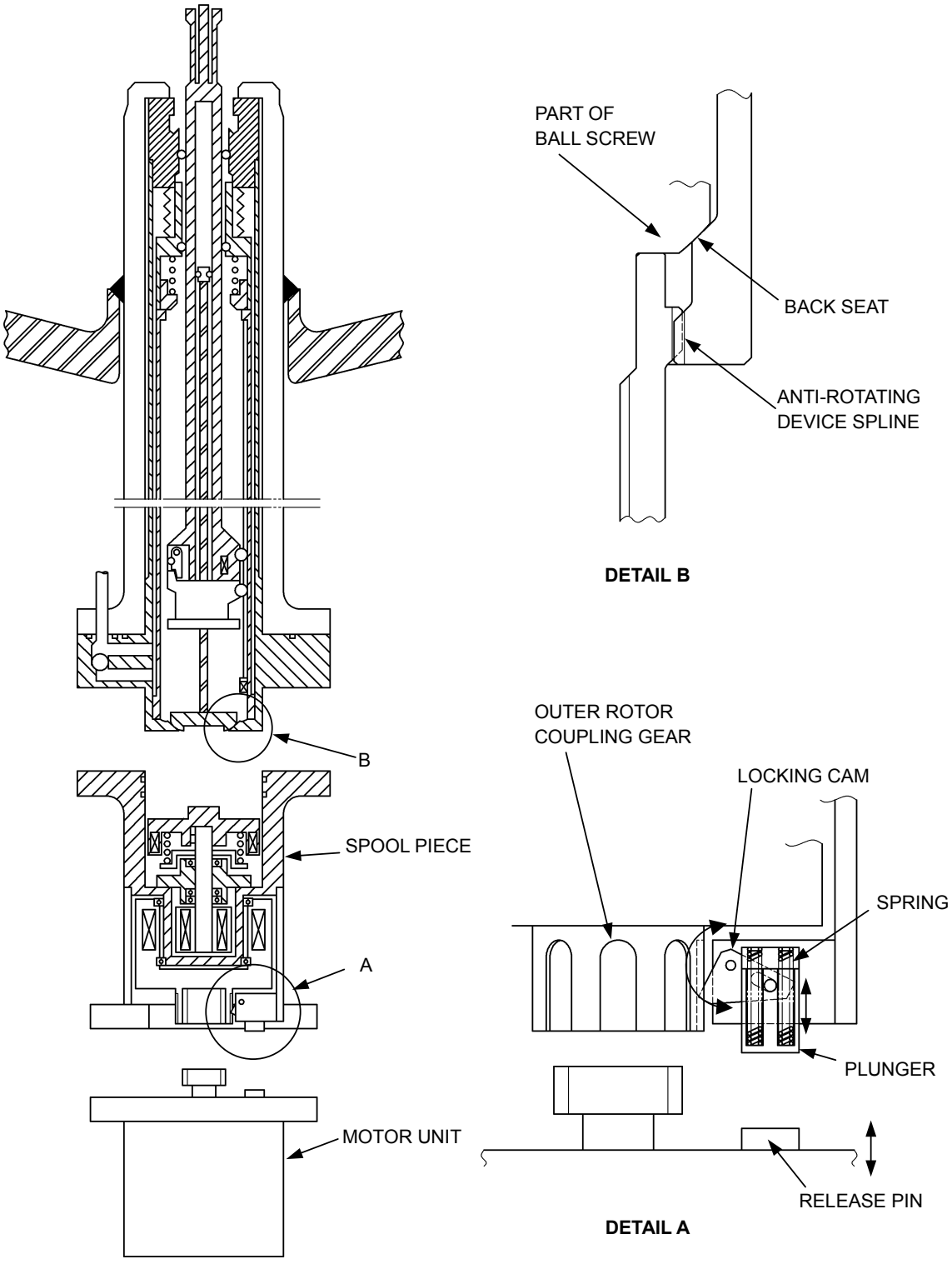

Figure 4.6-10. Control Rod Drive System Separation Mechanism

4A. TYPICAL CONTROL ROD PATTERNS AND ASSOCIATED POWER DISTRIBUTION FOR ESBWR

4A.1 INTRODUCTION

This appendix contains a typical simulation of an equilibrium cycle. The control rod patterns used are just one example of a set of control rod patterns which could be used to provide the radial and axial power shaping needed to meet the required operating thermal limits.

The basic control rod strategy for this case consists of control rod patterns used only to compensate for excess reactivity and to aid in shaping the axial power profile.

4A.2 RESULTS OF CORE SIMULATION STUDIES

Table 4A-1 itemizes the stepwise rod pattern for exposure steps and their related figure numbers. Control rod patterns, relative axial power, axial exposure, relative integrated power per bundle, and average bundle exposure for a range of exposure are shown on Figures 4A-1 through 4A-18. The detailed data presented demonstrate that this design can be operated throughout this cycle with adequate margins to allow for operating flexibility. The variation of the minimum critical power ratio (MCPR) with cycle exposure is shown in Figure 4A-19. Similarly, adequate margin is indicated with respect to the expected MCPR operating limit.

4A.3 COL UNIT-SPECIFIC INFORMATION

Results within this section identify the example rod patterns, loading pattern, bundle description, and mechanical design of a fuel bundle assembly that demonstrates certification of the ESBWR plant description. In the event the COL applicant chooses a fuel design different than that described herein, the rod patterns and associated power distribution consistent with the chosen loading patterns, bundle descriptions, and the mechanical design of the fuel bundle assembly shall satisfy the criteria identified in Section 4B.

Table 4A-1

Incremental Exposure Steps and Related Figure Numbers

Incremental Exposure (GWd/MT)	Figure Numbers
0.0	4A-1a through 4A-1e
1.1	4A-2a through 4A-2e
2.2	4A-3a through 4A-3e
3.3	4A-4a through 4A-4e
4.4	4A-5a through 4A-5e
5.5	4A-6a through 4A-6e
6.6	4A-7a through 4A-7e
7.7	4A-8a through 4A-8e
8.8	4A-9a through 4A-9e
9.9	4A-10a through 4A-10e
11.0	4A-11a through 4A-11e
12.1	4A-12a through 4A-12e
13.2	4A-13a through 4A-13e
14.3	4A-14a through 4A-14e
15.4	4A-15a through 4A-15e
16.5	4A-16a through 4A-16e
17.9	4A-17a through 4A-17e
18.5	4A-18a through 4A-18e

```
        ( ROD PATTERN DEPLETION

NITER    0  POWER           IMAX  19  POWER(MWT)           4.5000E+03  ( 100.0 %)
IBOUN    1  1/4             JMAX  19  PRESSURE(PSIA)       1.0550E+03
IRN      1  MIRROR          KMAX  25  FLOW(*10E-6LB/HR)    7.8508E+01  ( 100.0 %)
ILPA     0                  NSMAX 10  BYPASS(LB/HR)        1.1742E+07  (  15.0 %)          CONTROL ROD CONFIGURATION
IFLW     2  DETAIL          LMAX  20  ENTHALPY(BTU/LB)             512.30                    IN NOTCHES WITHDRAWN
RSTART   0  NEW             LVDCT  8  INLET TEMP(DEG F)            520.47
NEWPHY   2                  IPFTL  0  BEGINNING EXPOSURE          13105.1                 1  3  5  7  9 11 13 15 17 19
NEXO     3  CALC.                    DELTA EXPOS.(DELTE)              0.0
RBOCA    0                  IALPRM 0  DELBRN                           0.0              1
IACF     0                  IFAST  0  TOTAL NOTCHES                 1394
             IPDOME   1     IAHB   0  CORE FUEL MASS          MTU:162.928              3                              40
                                      CORE FUEL MASS          STU:179.596
ENERGY (MWD) (DELTE)                0. ENERGY (MWD) (DELBRN)             0.            5
CYCLE ENERGY (MWD)                  0. CYCLE EXPOSURE                    0.0
CORE AVG. POWER DENSITY      54.328033                                                    7                          59
NEUTRON MULTIPLICATION      1.00738621 FINAL AVG. EXPOSURE          13105.1
DIFP    (EPS5 = 0.00200)    0.00134337 CORE AVG. NEUTRON FLUX    1.424E+14               9
AVERAGE VOID FRACTION         0.547263 CORE AVG. GD WORTH             -0.121
CORE PRESSURE DROP,PSI        8.192794 CORE AVG. GD RESIDUAL WORTH  0.000              11                  47              16
EXP RATIO INDEX (INER-II)       0.0000 CORE AVERAGE XENON WORTH   -0.0216
                                                                                      13
CORE HISTORY MAX. VALUES:       LOCATION: I   J   K
  NODAL EXPOSURE, MWD/T    47824.          7   7   5   METRIC    52716.              15            59              50
  BUNDLE EXPOSURE, MWD/T   39032.         13   2       METRIC    43025.
  EXPOSURE RATIO, NEXRAT   0.0000          0   0   0                                  17
  AXIAL POWER PEAK         1.4253                  5
                                                                                      19  40              16              22
```

Figure 4A-1a. Control Rod Pattern Summary at 0.0 GWd/MT Exposure

0.0 GWD/MT

Node	Axial Power
25	0.124
24	0.246
23	0.365
22	0.484
21	0.597
20	0.692
19	0.778
18	0.848
17	0.904
16	0.998
15	1.156
14	1.227
13	1.285
12	1.321
11	1.347
10	1.361
9	1.356
8	1.367
7	1.388
6	1.411
5	1.425
4	1.408
3	1.308
2	1.056
1	0.546

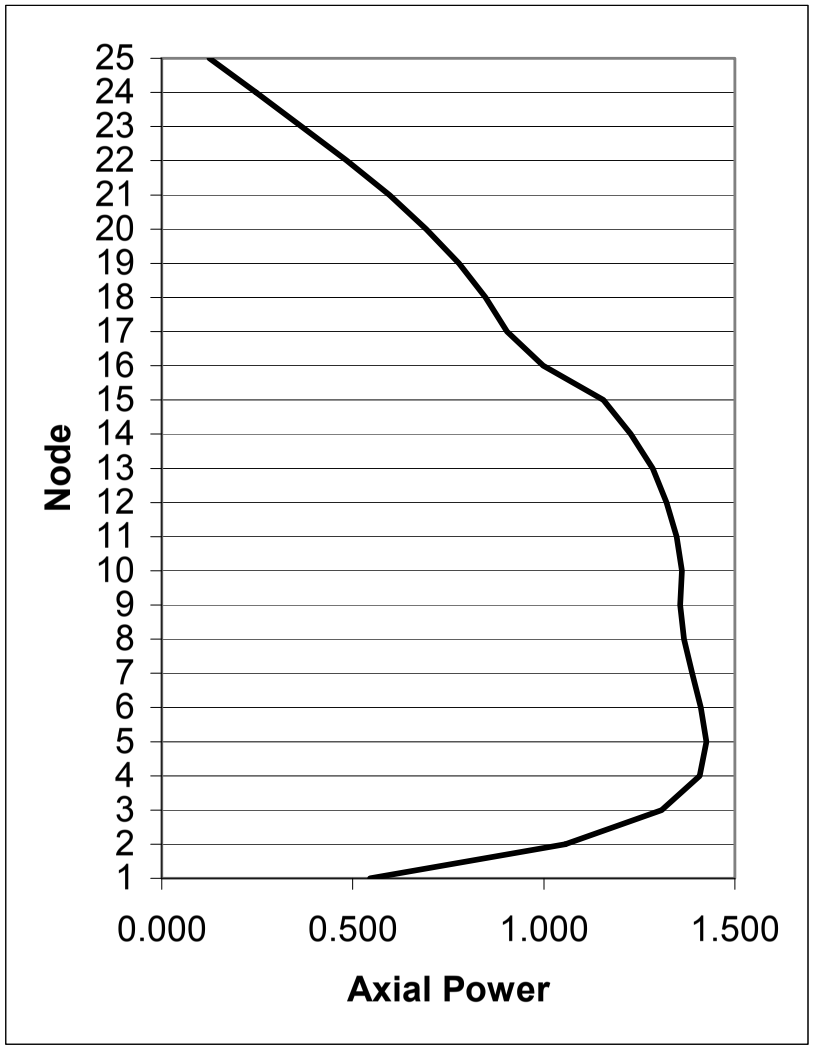

Figure 4A-1b. Relative Axial Power at 0.0 GWd/MT

0.0GWD/MT

Node	Axial Exposure (MWD/MT)
25	3064.4
24	5314.1
23	7426.4
22	9532.7
21	11406.6
20	12957.8
19	14216.4
18	15117.2
17	15652.8
16	15999.9
15	15447.7
14	16013.1
13	16500.0
12	16865.0
11	17193.6
10	17465.8
9	17613.4
8	17804.7
7	18064.1
6	18307.6
5	18383.4
4	17976.8
3	16406.0
2	12947.7
1	6569.7

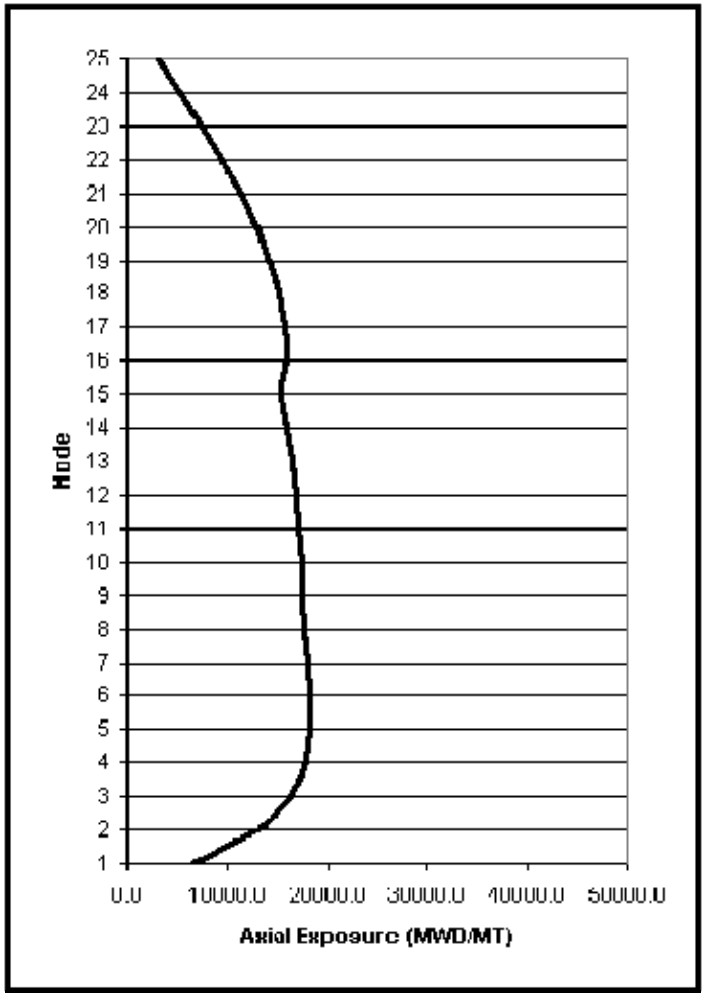

Figure 4A-1c. Axial Exposure at 0.0 GWd/MT Exposure

	1	2	3	4	5	6	7	8	9	10	11	12	13	14	15	16	17	18	19
1															0.37	0.42	0.44	0.43	0.40
2													0.37	0.49	0.58	0.76	0.78	0.72	0.62
3											0.40	0.49	0.67	0.76	0.88	0.92	0.94	0.85	0.63
4									0.36	0.47	0.66	0.75	0.85	0.91	0.97	1.04	1.02	0.95	0.84
5								0.43	0.62	0.71	0.82	0.92	0.99	1.02	1.05	1.09	0.98	1.09	1.06
6							0.42	0.65	0.78	0.86	0.96	1.04	1.08	1.07	1.09	1.11	1.15	1.14	1.16
7						0.42	0.54	0.79	0.92	1.00	0.97	1.14	1.09	1.12	1.02	1.12	1.19	1.22	1.23
8					0.43	0.65	0.79	0.89	1.01	1.05	1.16	1.06	1.15	1.21	1.15	1.14	1.21	1.25	1.29
9				0.36	0.62	0.78	0.92	1.01	1.07	1.08	1.09	1.14	1.20	1.21	1.20	1.20	1.22	1.24	1.25
10				0.47	0.71	0.86	1.00	1.05	1.08	1.09	1.10	1.14	1.19	1.20	1.21	1.20	1.21	1.18	1.14
11			0.40	0.66	0.82	0.96	0.97	1.16	1.09	1.10	0.94	1.03	1.19	1.20	1.17	1.26	1.20	1.12	0.85
12			0.49	0.75	0.92	1.04	1.14	1.06	1.14	1.14	1.03	1.02	1.16	1.19	1.26	1.25	1.19	1.09	0.86
13		0.37	0.67	0.85	0.99	1.08	1.09	1.15	1.20	1.19	1.19	1.16	1.18	1.21	1.23	1.23	1.19	1.16	1.13
14		0.49	0.76	0.91	1.02	1.07	1.12	1.21	1.21	1.20	1.20	1.19	1.21	1.19	1.19	1.19	1.18	1.18	1.18
15	0.37	0.58	0.88	0.98	1.05	1.09	1.02	1.15	1.20	1.21	1.17	1.26	1.23	1.19	1.00	1.05	1.15	1.20	1.17
16	0.42	0.76	0.92	1.04	1.09	1.11	1.12	1.14	1.20	1.20	1.26	1.25	1.23	1.19	1.05	1.05	1.18	1.24	1.28
17	0.44	0.78	0.94	1.02	0.98	1.15	1.19	1.21	1.22	1.21	1.20	1.19	1.19	1.19	1.15	1.18	1.20	1.23	1.24
18	0.43	0.72	0.85	0.95	1.09	1.14	1.22	1.25	1.24	1.18	1.12	1.09	1.16	1.18	1.20	1.24	1.23	1.18	1.15
19	0.40	0.62	0.63	0.84	1.06	1.16	1.23	1.29	1.25	1.14	0.85	0.86	1.13	1.18	1.17	1.28	1.24	1.15	0.89

Figure 4A-1d. Relative Integrated Power Per Bundle at 0.0 GWd/MT Exposure

	1	2	3	4	5	6	7	8	9	10	11	12	13	14	15	16	17	18	19
1															36.86	35.60	38.91	35.94	37.24
2													43.03	37.56	36.70	19.13	17.65	16.90	0.00
3											39.40	36.77	19.76	0.00	21.57	22.59	19.88	0.00	33.57
4									39.21	37.16	17.70	0.00	0.00	0.00	22.56	20.50	0.00	0.00	14.76
5								41.07	14.88	0.00	0.00	0.00	18.69	0.00	0.00	0.00	32.42	0.00	22.59
6							38.26	16.34	0.00	0.00	0.00	21.39	0.00	22.80	0.00	23.28	0.00	22.99	0.00
7						38.26	38.90	0.00	18.39	0.00	32.15	20.06	0.00	0.00	27.24	20.84	21.99	0.00	23.61
8					41.08	16.34	0.00	0.00	0.00	22.12	17.29	31.50	0.00	13.40	15.39	16.11	0.00	21.89	23.07
9				39.21	14.88	0.00	18.39	0.00	18.59	0.00	0.00	0.00	21.10	0.00	21.96	0.00	22.04	0.00	21.94
10				37.17	0.00	0.00	0.00	22.12	0.00	23.11	0.00	21.88	0.00	22.55	0.00	0.00	0.00	22.08	0.00
11			39.41	17.69	0.00	0.00	32.15	17.28	0.00	0.00	30.65	21.94	21.72	0.00	30.82	21.97	22.36	0.00	23.35
12			36.78	0.00	0.00	21.39	20.05	31.51	0.00	21.87	21.94	22.98	0.00	0.00	21.79	22.39	0.00	0.00	22.15
13		43.00	19.76	0.00	18.68	0.00	0.00	0.00	21.09	0.00	21.72	0.00	23.10	0.00	22.20	0.00	22.59	0.00	22.44
14		37.56	0.00	0.00	0.00	22.80	0.00	13.41	0.00	22.54	0.00	0.00	0.00	22.98	0.00	22.21	0.00	22.06	0.00
15	36.86	36.72	21.57	22.55	0.00	0.00	27.25	15.38	21.96	0.00	30.83	21.79	22.20	0.00	30.65	22.77	0.00	0.00	29.09
16	35.60	19.13	22.58	20.50	0.00	23.27	20.84	16.11	0.00	0.00	21.97	22.39	0.00	22.20	22.76	22.98	0.00	21.48	22.69
17	38.91	17.65	19.88	0.00	32.43	0.00	21.99	0.00	22.04	0.00	22.36	0.00	22.58	0.00	0.00	0.00	22.98	0.00	22.60
18	35.95	16.90	0.00	0.00	0.00	22.98	0.00	21.89	0.00	22.07	0.00	0.00	0.00	22.06	0.00	21.48	0.00	23.11	0.00
19	37.24	0.00	33.58	14.76	22.58	0.00	23.60	23.06	21.94	0.00	23.34	22.15	22.44	0.00	29.09	22.69	22.60	0.00	23.11

Figure 4A-1e. Average Bundle Exposure at 0.0 GWd/MT Exposure

```
      ( ROD PATTERN DEPLETION

NITER   0  POWER           IMAX  19  POWER(MWT)          4.5000E+03  ( 100.0 %)
IBOUN   1  1/4             JMAX  19  PRESSURE(PSIA)      1.0550E+03
IRN     1  MIRROR          KMAX  25  FLOW(*10E-6LB/HR)   7.8508E+01  ( 100.0 %)
ILPA    0                  NSMAX 10  BYPASS(LB/HR)       1.1742E+07  (  15.0 %)
IFLW    2  DETAIL          LMAX  20  ENTHALPY(BTU/LB)            512.30
RSTART  0  NEW             LVDCT  6  INLET TEMP(DEG F)           520.47
NEWPHY  2                  IPFTL  0  BEGINNING EXPOSURE         13105.1
NEXO    3  CALC.                     DELTA EXPOS.(DELTE)            0.0
RBOCA   1                  IALPRM 0  DELBRN                     1000.0
IACF    0                  IFAST  0  TOTAL NOTCHES                1394
             IPDOME   1    IAHB   0  CORE FUEL MASS         MTU:162.928
                                     CORE FUEL MASS         STU:179.596
ENERGY (MWD) (DELTE)              0. ENERGY (MWD) (DELBRN)      179596.
CYCLE ENERGY (MWD)           179598. CYCLE EXPOSURE             1000.0
CORE AVG. POWER DENSITY     54.328033
NEUTRON MULTIPLICATION     1.00571263 FINAL AVG. EXPOSURE       14105.1
DIFP    (EPS5 = 0.00200)   0.00152212 CORE AVG. NEUTRON FLUX   1.430E+14
AVERAGE VOID FRACTION        0.538596 CORE AVG. GD WORTH          -0.114
CORE PRESSURE DROP,PSI       8.128463 CORE AVG. GD RESIDUAL WORTH  0.000
EXP RATIO INDEX (INER-II)       0.0000 CORE AVERAGE XENON WORTH   -0.0216

CORE HISTORY MAX. VALUES:       LOCATION: I   J   K
  NODAL EXPOSURE, MWD/T   48513.          7   7   5   METRIC    53476.
  BUNDLE EXPOSURE, MWD/T  39404.         13   2       METRIC    43435.
  EXPOSURE RATIO, NEXRAT  0.0000          0   0   0
  AXIAL POWER PEAK        1.3669                  6
```

CONTROL ROD CONFIGURATION
IN NOTCHES WITHDRAWN

	1	3	5	7	9	11	13	15	17	19
1										
3										40
5										
7								59		
9										
11						47				16
13										
15			59					50		
17										
19	40					16				22

Figure 4A-2a. Control Rod Pattern Summary at 1.1 GWd/MT Exposure

1.1 GWD/MT

Node	Axial Power
25	0.133
24	0.264
23	0.392
22	0.517
21	0.633
20	0.730
19	0.816
18	0.885
17	0.941
16	1.035
15	1.191
14	1.257
13	1.310
12	1.340
11	1.359
10	1.365
9	1.352
8	1.353
7	1.360
6	1.367
5	1.364
4	1.328
3	1.218
2	0.979
1	0.510

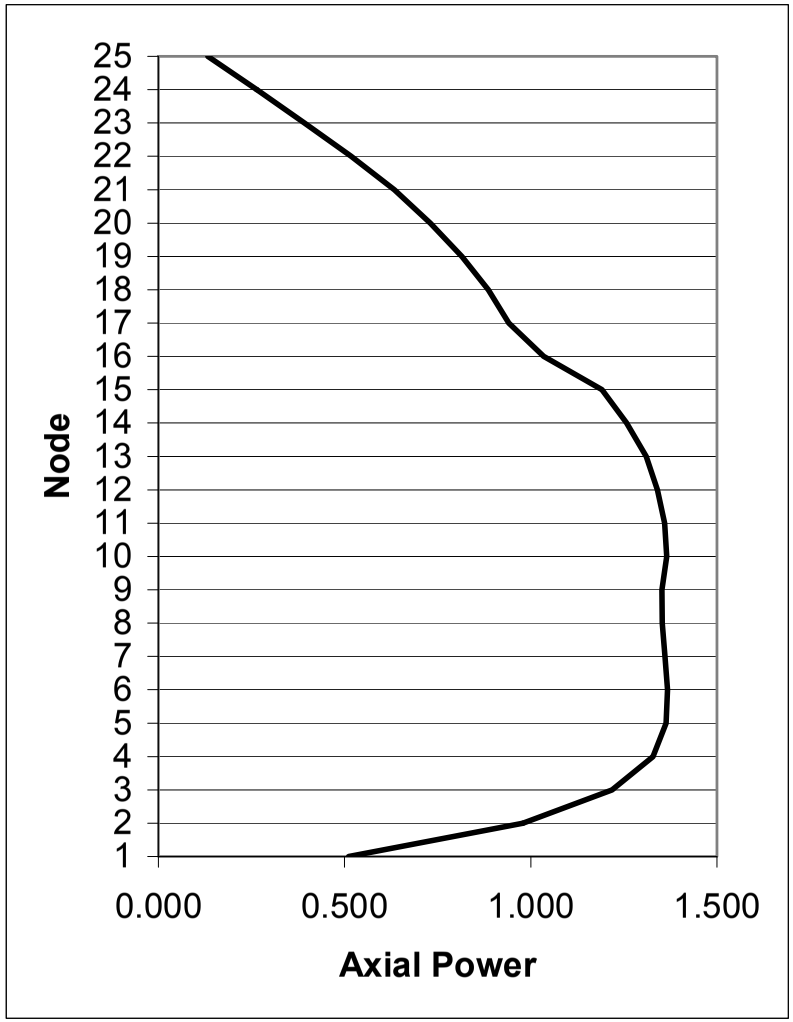

Figure 4A-2b. Relative Axial Power at 1.1 GWd/MT Exposure

1.1 GWD/MT

Node	Axial Exposure (MWD/MT)
25	3243.8
24	5625.9
23	7870.9
22	10121.8
21	12132.7
20	13800.1
19	15162.5
18	16148.4
17	16752.4
16	17170.3
15	16637.1
14	17275.5
13	17822.2
12	18224.4
11	18579.8
10	18866.4
9	19010.0
8	19213.0
7	19493.8
6	19760.6
5	19851.5
4	19426.8
3	17753.2
2	14035.7
1	7120.2

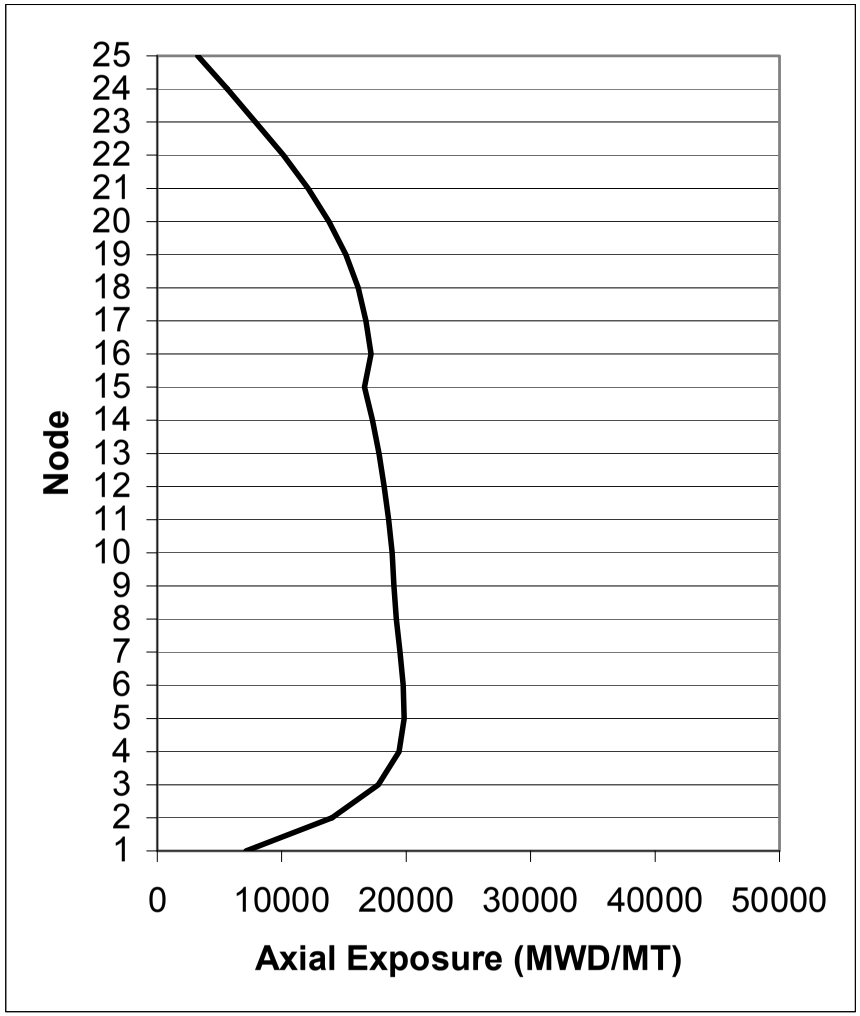

Figure 4A-2c. Axial Exposure at 1.1 GWd/MT Exposure

														0.37	0.41	0.44	0.43	0.4
												0.37	0.48	0.58	0.75	0.78	0.72	0.62
										0.39	0.49	0.67	0.76	0.87	0.91	0.93	0.85	0.64
							0.36	0.47	0.66	0.74	0.84	0.91	0.97	1.03	1.01	0.96	0.85	
						0.43	0.62	0.71	0.82	0.92	0.99	1.02	1.05	1.09	0.98	1.09	1.06	
					0.42	0.65	0.78	0.86	0.96	1.04	1.08	1.07	1.09	1.11	1.15	1.13	1.16	
				0.42	0.54	0.79	0.92	1	0.96	1.14	1.1	1.13	1.03	1.13	1.18	1.22	1.22	
			0.43	0.65	0.79	0.89	1.01	1.05	1.16	1.06	1.16	1.23	1.17	1.16	1.22	1.24	1.27	
		0.36	0.62	0.78	0.92	1.01	1.08	1.09	1.1	1.15	1.21	1.22	1.21	1.21	1.22	1.24	1.24	
		0.47	0.71	0.86	1	1.05	1.09	1.09	1.1	1.14	1.2	1.2	1.22	1.21	1.21	1.18	1.14	
	0.39	0.66	0.82	0.96	0.96	1.16	1.1	1.1	0.94	1.03	1.2	1.21	1.17	1.25	1.2	1.12	0.85	
	0.49	0.75	0.92	1.04	1.14	1.06	1.15	1.14	1.03	1.02	1.17	1.2	1.25	1.24	1.2	1.1	0.86	
0.37	0.67	0.84	0.99	1.08	1.1	1.16	1.21	1.2	1.2	1.17	1.18	1.21	1.22	1.23	1.18	1.16	1.12	
0.48	0.76	0.91	1.02	1.07	1.13	1.23	1.22	1.2	1.21	1.2	1.21	1.19	1.19	1.19	1.19	1.18	1.18	
0.37	0.58	0.87	0.97	1.05	1.09	1.03	1.17	1.21	1.22	1.17	1.25	1.22	1.19	1.01	1.05	1.15	1.2	1.16
0.41	0.75	0.91	1.03	1.09	1.11	1.13	1.16	1.21	1.21	1.25	1.24	1.23	1.19	1.05	1.05	1.18	1.23	1.26
0.44	0.78	0.93	1.01	0.98	1.15	1.18	1.22	1.22	1.21	1.2	1.2	1.18	1.19	1.15	1.18	1.19	1.23	1.22
0.43	0.72	0.85	0.96	1.09	1.13	1.22	1.24	1.24	1.18	1.12	1.1	1.16	1.18	1.2	1.23	1.23	1.17	1.14
0.4	0.62	0.64	0.85	1.06	1.16	1.22	1.27	1.24	1.14	0.85	0.86	1.12	1.18	1.16	1.26	1.22	1.14	0.89

Figure 4A-2d. Relative Integrated Power Per Bundle at 1.1 GWd/MT Exposure

	1	2	3	4	5	6	7	8	9	10	11	12	13	14	15	16	17	18	19
1															37.26	36.05	39.35	36.38	37.70
2													43.43	38.14	37.37	19.95	18.52	17.75	0.66
3											39.79	37.37	20.50	0.88	22.60	23.59	20.94	0.99	34.28
4									39.57	37.70	18.41	0.77	0.88	0.99	23.59	21.61	1.10	1.10	15.65
5								41.56	15.54	0.77	0.88	0.99	19.73	1.10	1.21	1.21	33.51	1.21	23.81
6							38.69	17.09	0.88	0.99	1.10	22.49	1.21	24.03	1.21	24.47	1.21	24.25	1.32
7						38.69	39.46	0.88	19.40	1.10	33.18	21.27	1.21	1.21	28.33	22.05	23.26	1.32	24.91
8					41.56	17.09	0.88	0.99	1.10	23.26	18.52	32.63	1.21	14.77	16.64	17.42	1.32	23.26	24.47
9				39.57	15.54	0.88	19.40	1.10	19.73	1.21	1.21	1.21	22.38	1.32	23.26	1.32	23.37	1.32	23.37
10				37.70	0.77	0.99	1.10	23.26	1.21	24.36	1.21	23.15	1.32	23.92	1.32	1.32	1.32	23.37	1.21
11			39.90	18.41	0.88	1.10	33.18	18.52	1.21	1.21	31.64	23.04	23.04	1.32	32.08	23.37	23.70	1.21	24.25
12			37.37	0.77	0.99	22.49	21.27	32.74	1.21	23.15	23.04	24.14	1.32	1.32	23.15	23.81	1.32	1.21	23.15
13		43.43	20.50	0.88	19.73	1.21	1.21	1.21	22.38	1.32	23.04	1.32	24.36	1.32	23.59	1.32	23.92	1.32	23.70
14		38.14	0.88	0.99	1.10	23.92	1.21	14.77	1.32	23.81	1.32	1.32	1.32	24.25	1.32	23.48	1.32	23.37	1.32
15	37.26	37.37	22.49	23.59	1.21	1.21	28.33	16.64	23.26	1.32	32.08	23.15	23.59	1.32	31.75	23.92	1.21	1.32	30.42
16	36.05	19.95	23.59	21.61	1.21	24.47	22.05	17.42	1.32	1.32	23.37	23.81	1.32	23.48	23.92	24.14	1.32	22.82	24.14
17	39.35	18.52	20.94	1.10	33.51	1.21	23.26	1.32	23.37	1.32	23.70	1.32	23.92	1.32	1.21	1.32	24.36	1.32	23.92
18	36.38	17.75	0.99	1.10	1.21	24.25	1.32	23.26	1.32	23.37	1.21	1.21	1.32	23.37	1.32	22.82	1.32	24.36	1.21
19	37.70	0.66	34.28	15.65	23.81	1.32	24.91	24.47	23.37	1.21	24.25	23.15	23.70	1.32	30.42	24.14	23.92	1.21	24.03

Figure 4A-2e. Average Bundle Exposure at 1.1 GWd/MT Exposure

```
        ( ROD PATTERN DEPLETION

NITER   0  POWER           IMAX  19  POWER(MWT)          4.5000E+03  ( 100.0 %)
IBOUN   1  1/4             JMAX  19  PRESSURE(PSIA)      1.0550E+03
IRN     1  MIRROR          KMAX  25  FLOW(*10E-6LB/HR)   7.8508E+01  ( 100.0 %)
ILPA    0                  NSMAX 10  BYPASS(LB/HR)       1.1742E+07  (  15.0 %)          CONTROL ROD CONFIGURATION
IFLW    2  DETAIL          LMAX  20  ENTHALPY(BTU/LB)            512.30                    IN NOTCHES WITHDRAWN
RSTART  0  NEW             LVDCT  7  INLET TEMP(DEG F)           520.47
NEWPHY  2                  IPFTL  0  BEGINNING EXPOSURE         14105.1                1  3  5  7  9 11 13 15 17 19
NEXO    3  CALC.                    DELTA EXPOS.(DELTE)            0.0
RBOCA   1                  IALPRM 0  DELBRN                      1000.0              1
IACF    0                  IFAST  0  TOTAL NOTCHES                 1393
             IPDOME   1    IAHB   0  CORE FUEL MASS         MTU:162.928              3                           46
                                     CORE FUEL MASS         STU:179.596
ENERGY (MWD) (DELTE)              0. ENERGY (MWD) (DELBRN)      179596.              5
CYCLE ENERGY (MWD)             359195. CYCLE EXPOSURE             2000.0
CORE AVG. POWER DENSITY     54.328033                                               7                       65
NEUTRON MULTIPLICATION     1.00590336 FINAL AVG. EXPOSURE        15105.1
DIFP    (EPS5 = 0.00200)   0.00114340 CORE AVG. NEUTRON FLUX   1.434E+14            9
AVERAGE VOID FRACTION         0.539311 CORE AVG. GD WORTH          -0.109
CORE PRESSURE DROP,PSI        8.113272 CORE AVG. GD RESIDUAL WORTH  0.000           11                21           12
EXP RATIO INDEX (INER-II)       0.0000 CORE AVERAGE XENON WORTH   -0.0217
                                                                                    13
CORE HISTORY MAX. VALUES:       LOCATION: I   J   K
  NODAL EXPOSURE, MWD/T    49163.          7   7   5   METRIC    54192.           15         65           67
  BUNDLE EXPOSURE, MWD/T   39773.         13   2       METRIC    43842.
  EXPOSURE RATIO, NEXRAT   0.0000          0   0   0                              17
  AXIAL POWER PEAK         1.4242                  9
                                                                                    19  46           12            3
```

Figure 4A-3a. Control Rod Pattern Summary at 2.2 GWd/MT Exposure

2.2 GWD/MT

Node	Axial Power
25	0.132
24	0.260
23	0.385
22	0.506
21	0.613
20	0.706
19	0.785
18	0.852
17	0.908
16	1.003
15	1.162
14	1.241
13	1.307
12	1.358
11	1.397
10	1.423
9	1.424
8	1.407
7	1.392
6	1.382
5	1.365
4	1.318
3	1.202
2	0.964
1	0.507

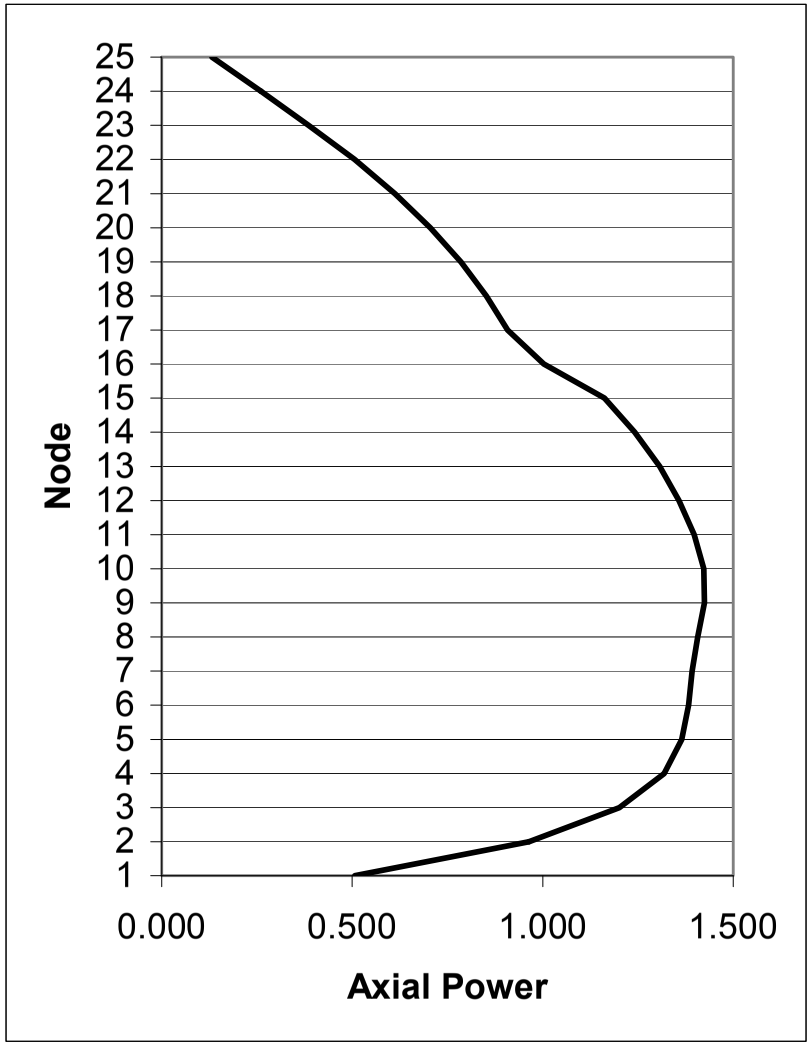

Figure 4A-3b.

Relative Axial Power at 2.2 GWd/MT Exposure

2.2 GWD/MT

Node	Axial Exposure (MWD/MT)
25	3436.3
24	5960.2
23	8347.5
22	10751.4
21	12903.3
20	14688.4
19	16154.8
18	17225.8
17	17897.2
16	18383.0
15	17862.3
14	18568.9
13	19170.0
12	19603.0
11	19978.2
10	20271.1
9	20402.3
8	20606.1
7	20894.5
6	21168.4
5	21255.9
4	20794.8
3	19007.9
2	15043.7
1	7635.2

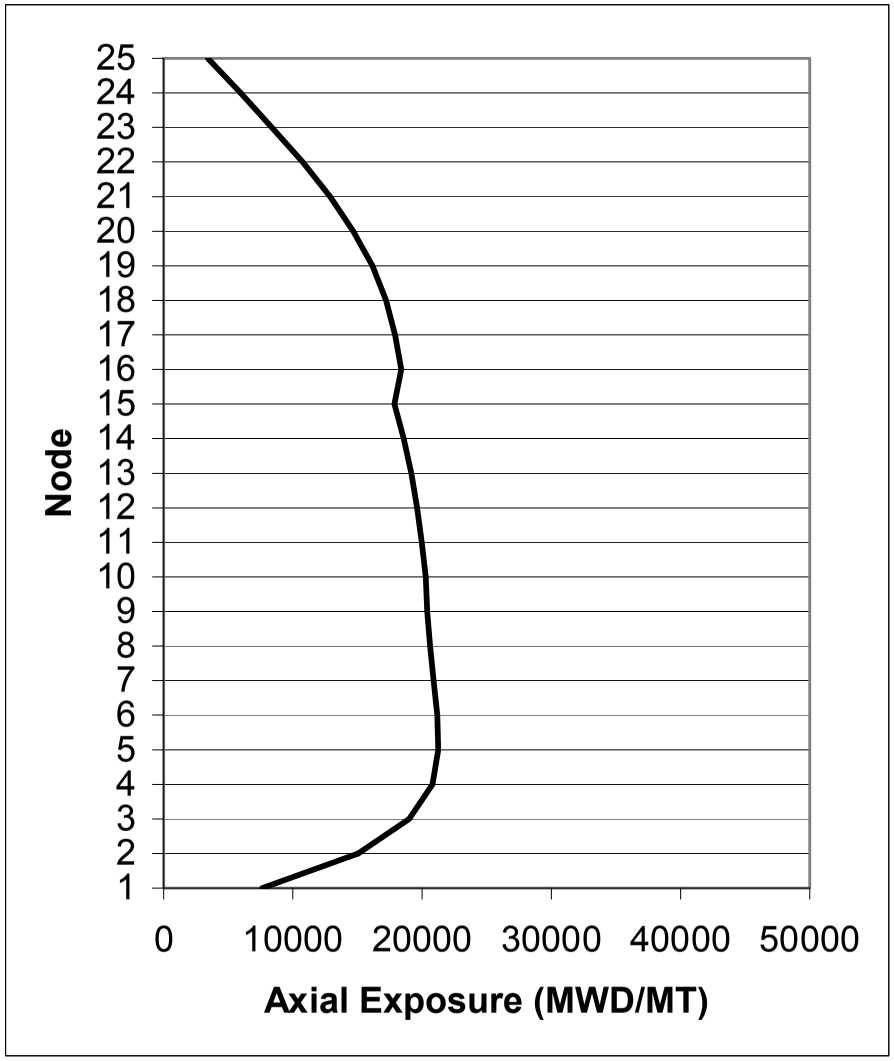

Figure 4A-3c. Axial Exposure at 2.2 GWd/MT Exposure

	1	2	3	4	5	6	7	8	9	10	11	12	13	14	15	16	17	18	19
1															0.37	0.41	0.44	0.44	0.41
2													0.37	0.48	0.57	0.75	0.78	0.74	0.65
3											0.39	0.49	0.67	0.76	0.87	0.91	0.94	0.88	0.67
4									0.36	0.47	0.66	0.75	0.85	0.92	0.97	1.04	1.03	0.99	0.90
5								0.43	0.62	0.71	0.82	0.92	0.99	1.04	1.07	1.11	0.99	1.11	1.07
6							0.41	0.64	0.78	0.86	0.96	1.03	1.10	1.07	1.12	1.12	1.17	1.14	1.18
7						0.41	0.53	0.78	0.90	0.99	0.94	1.12	1.11	1.16	1.06	1.16	1.19	1.24	1.21
8					0.43	0.64	0.78	0.89	1.00	1.02	1.13	1.03	1.17	1.24	1.21	1.20	1.25	1.23	1.25
9				0.36	0.62	0.78	0.90	1.00	1.05	1.06	1.07	1.12	1.18	1.23	1.20	1.24	1.22	1.25	1.22
10				0.47	0.71	0.86	0.99	1.02	1.06	1.03	1.04	1.06	1.16	1.17	1.23	1.22	1.23	1.17	1.15
11			0.39	0.66	0.82	0.96	0.94	1.13	1.07	1.04	0.77	0.84	1.12	1.19	1.14	1.23	1.19	1.13	0.83
12			0.49	0.75	0.92	1.03	1.12	1.03	1.12	1.06	0.84	0.84	1.12	1.18	1.23	1.22	1.21	1.11	0.84
13		0.37	0.67	0.85	0.99	1.10	1.11	1.17	1.18	1.16	1.12	1.12	1.14	1.21	1.22	1.25	1.19	1.18	1.12
14		0.48	0.76	0.92	1.04	1.07	1.16	1.24	1.23	1.17	1.19	1.18	1.21	1.19	1.23	1.21	1.23	1.19	1.20
15	0.37	0.57	0.87	0.97	1.07	1.12	1.06	1.21	1.20	1.23	1.14	1.23	1.22	1.23	1.09	1.15	1.21	1.23	1.16
16	0.41	0.75	0.91	1.04	1.11	1.12	1.16	1.20	1.24	1.22	1.23	1.22	1.25	1.21	1.15	1.15	1.23	1.23	1.25
17	0.44	0.78	0.94	1.03	0.99	1.17	1.19	1.25	1.22	1.23	1.19	1.21	1.19	1.23	1.21	1.23	1.21	1.25	1.21
18	0.44	0.74	0.88	0.99	1.11	1.14	1.24	1.23	1.25	1.17	1.13	1.11	1.18	1.19	1.23	1.23	1.25	1.16	1.14
19	0.41	0.65	0.67	0.90	1.07	1.18	1.21	1.25	1.22	1.15	0.83	0.84	1.12	1.20	1.16	1.25	1.21	1.14	0.81

Figure 4A-3d. Relative Integrated Power Per Bundle at 2.2 GWd/MT Exposure

	1	2	3	4	5	6	7	8	9	10	11	12	13	14	15	16	17	18	19
1															37.70	36.49	39.90	36.93	38.14
2													43.87	38.58	38.03	20.83	19.40	18.52	1.32
3											40.23	37.81	21.27	1.65	23.48	24.58	21.94	1.87	34.94
4									40.01	38.25	19.18	1.65	1.87	1.98	24.69	22.82	2.20	2.09	16.64
5								42.00	16.20	1.54	1.76	1.98	20.83	2.20	2.31	2.43	34.61	2.43	24.91
6							39.24	17.75	1.76	1.87	2.09	23.70	2.43	25.13	2.43	25.68	2.54	25.46	2.54
7						39.24	40.12	1.76	20.39	2.20	34.28	22.60	2.43	2.43	29.54	23.37	24.58	2.65	26.35
8					42.00	17.75	1.76	1.98	2.20	24.47	19.84	33.84	2.54	16.09	17.97	18.63	2.65	24.58	25.90
9				40.01	16.20	1.76	20.39	2.20	20.94	2.43	2.43	2.54	23.70	2.65	24.58	2.65	24.69	2.76	24.69
10				38.25	1.54	1.87	2.20	24.47	2.43	25.46	2.43	24.36	2.65	25.24	2.65	2.65	2.65	24.69	2.54
11			40.23	19.18	1.76	2.09	34.28	19.84	2.43	2.43	32.74	24.25	24.36	2.65	33.40	24.69	25.02	2.43	25.24
12			37.92	1.65	1.98	23.70	22.60	33.84	2.54	24.36	24.25	25.24	2.54	2.65	24.58	25.13	2.65	2.43	24.03
13		43.76	21.27	1.87	20.83	2.43	2.43	2.54	23.70	2.65	24.36	2.54	25.68	2.65	24.91	2.76	25.24	2.54	24.91
14		38.58	1.65	1.98	2.20	25.13	2.43	16.09	2.65	25.13	2.65	2.65	2.65	25.57	2.65	24.80	2.65	24.69	2.65
15	37.70	38.03	23.48	24.69	2.31	2.43	29.54	17.97	24.58	2.65	33.40	24.58	24.91	2.65	32.85	25.13	2.54	2.65	31.64
16	36.49	20.83	24.58	22.82	2.43	25.68	23.37	18.63	2.65	2.65	24.69	25.13	2.76	24.80	25.13	25.24	2.65	24.25	25.46
17	39.90	19.40	21.94	2.20	34.61	2.54	24.58	2.65	24.69	2.65	25.02	2.65	25.24	2.65	2.54	2.65	25.57	2.76	25.35
18	36.93	18.52	1.87	2.09	2.43	25.46	2.65	24.58	2.76	24.69	2.43	2.43	2.54	24.69	2.65	24.25	2.76	25.68	2.54
19	38.14	1.32	34.94	16.64	24.91	2.54	26.35	25.90	24.69	2.54	25.24	24.03	24.91	2.65	31.64	25.46	25.35	2.54	25.02

Figure 4A-3e. Average Bundle Exposure at 2.2 GWd/MT Exposure

```
( ROD PATTERN DEPLETION

NITER   0  POWER          IMAX  19  POWER(MWT)          4.5000E+03  ( 100.0 %)
IBOUN   1  1/4            JMAX  19  PRESSURE(PSIA)       1.0550E+03
IRN     1  MIRROR         KMAX  25  FLOW(*10E-6LB/HR)    7.8508E+01  ( 100.0 %)
ILPA    0                 NSMAX 10  BYPASS(LB/HR)        1.1742E+07  (  15.0 %)
IFLW    2  DETAIL         LMAX  20  ENTHALPY(BTU/LB)             512.30
RSTART  0  NEW            LVDCT  6  INLET TEMP(DEG F)            520.47
NEWPHY  2                 IPFTL  0  BEGINNING EXPOSURE          15105.1
NEXO    3  CALC.                   DELTA EXPOS.(DELTE)             0.0
RBOCA   1                 IALPRM 0  DELBRN                      1000.0
IACF    0                 IFAST  0  TOTAL NOTCHES                 1393
             IPDOME   1   IAHB   0  CORE FUEL MASS          MTU:162.928
                                    CORE FUEL MASS          STU:179.596
ENERGY (MWD) (DELTE)              0. ENERGY (MWD) (DELBRN)       179596.
CYCLE ENERGY (MWD)           538793. CYCLE EXPOSURE              3000.0
CORE AVG. POWER DENSITY     54.328033
NEUTRON MULTIPLICATION     1.00554347 FINAL AVG. EXPOSURE         16105.1
DIFP    (EPS5 = 0.00200)   0.00115973 CORE AVG. NEUTRON FLUX    1.438E+14
AVERAGE VOID FRACTION        0.534040 CORE AVG. GD WORTH           -0.104
CORE PRESSURE DROP,PSI       8.093865 CORE AVG. GD RESIDUAL WORTH  0.000
EXP RATIO INDEX (INER-II)       0.0000 CORE AVERAGE XENON WORTH    -0.0218

CORE HISTORY MAX. VALUES:       LOCATION: I   J   K
  NODAL EXPOSURE, MWD/T   49804.          7   7   5   METRIC    54899.
  BUNDLE EXPOSURE, MWD/T  40142.         13   2       METRIC    44248.
  EXPOSURE RATIO, NEXRAT  0.0000          0   0   0
  AXIAL POWER PEAK        1.4071                 10
```

CONTROL ROD CONFIGURATION
IN NOTCHES WITHDRAWN

	1	3	5	7	9	11	13	15	17	19
1										
3										46
5										
7								65		
9										
11						21				12
13										
15			65					67		
17										
19	46					12				3

Figure 4A-4a. Control Rod Pattern Summary at 3.3 GWd/MT Exposure

3.3 GWD/MT

Node	Axial Power
25	0.142
24	0.279
23	0.412
22	0.538
21	0.647
20	0.740
19	0.819
18	0.883
17	0.936
16	1.026
15	1.180
14	1.251
13	1.310
12	1.354
11	1.387
10	1.407
9	1.405
8	1.385
7	1.365
6	1.350
5	1.327
4	1.276
3	1.159
2	0.929
1	0.493

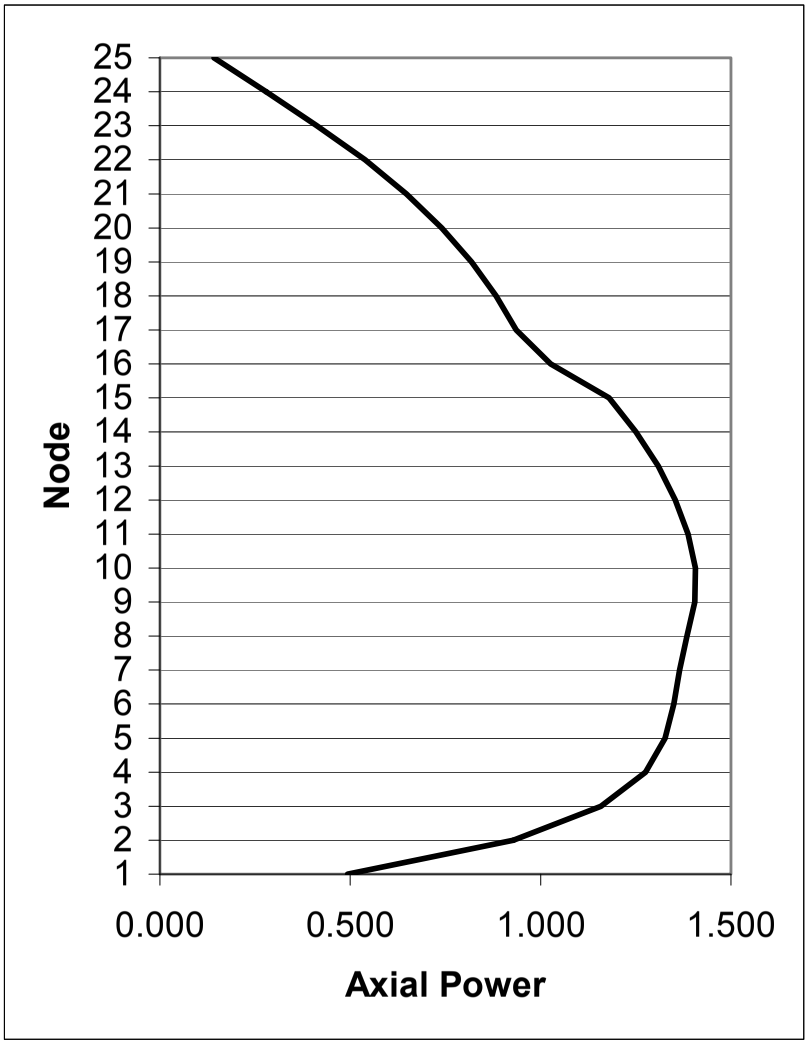

Figure 4A-4b. Relative Axial Power at 3.3 GWd/MT Exposure

3.3 GWD/MT

Node	Axial Exposure (MWD/MT)
25	3626.9
24	6290.0
23	8816.3
22	11366.9
21	13648.8
20	15547.2
19	17110.0
18	18262.4
17	19002.3
16	19558.5
15	19058.0
14	19845.9
13	20514.7
12	21000.0
11	21415.6
10	21734.6
9	21868.8
8	22055.6
7	22328.1
6	22592.1
5	22661.6
4	22152.4
3	20245.4
2	16036.5
1	8147.0

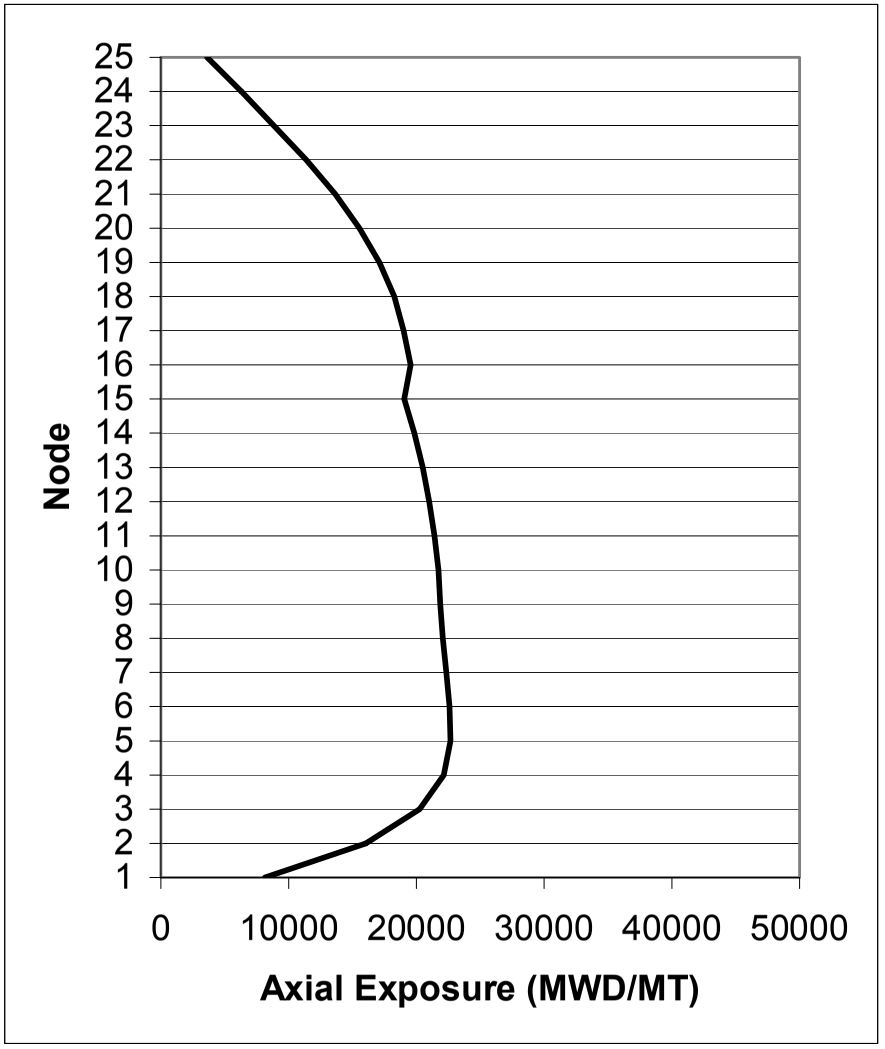

Figure 4A-4c. Axial Exposure at 3.3 GWd/MT Exposure

	1	2	3	4	5	6	7	8	9	10	11	12	13	14	15	16	17	18	19
1															0.36	0.40	0.44	0.44	0.40
2													0.37	0.48	0.57	0.74	0.77	0.73	0.65
3											0.40	0.49	0.67	0.77	0.86	0.90	0.93	0.88	0.67
4									0.36	0.47	0.66	0.76	0.86	0.93	0.96	1.03	1.04	0.99	0.91
5								0.43	0.63	0.73	0.83	0.93	1.00	1.05	1.08	1.11	0.98	1.12	1.06
6							0.42	0.65	0.79	0.87	0.97	1.03	1.11	1.07	1.13	1.11	1.18	1.12	1.18
7						0.42	0.53	0.80	0.91	1.00	0.94	1.12	1.13	1.17	1.06	1.15	1.18	1.24	1.19
8					0.43	0.65	0.80	0.90	1.01	1.02	1.13	1.03	1.18	1.24	1.21	1.20	1.25	1.22	1.23
9				0.36	0.63	0.79	0.91	1.01	1.05	1.08	1.08	1.14	1.18	1.24	1.20	1.25	1.20	1.25	1.20
10				0.47	0.73	0.87	1.00	1.02	1.08	1.03	1.06	1.06	1.18	1.17	1.24	1.23	1.24	1.16	1.15
11			0.40	0.66	0.83	0.97	0.94	1.13	1.08	1.06	0.77	0.85	1.12	1.20	1.13	1.22	1.18	1.14	0.83
12			0.49	0.76	0.93	1.03	1.12	1.03	1.14	1.06	0.85	0.84	1.13	1.19	1.22	1.21	1.22	1.12	0.84
13		0.37	0.67	0.86	1.00	1.11	1.13	1.18	1.18	1.18	1.12	1.13	1.13	1.22	1.20	1.26	1.18	1.19	1.11
14		0.48	0.77	0.93	1.05	1.07	1.17	1.24	1.24	1.17	1.20	1.19	1.22	1.18	1.24	1.20	1.24	1.18	1.20
15	0.36	0.57	0.86	0.96	1.08	1.13	1.06	1.21	1.20	1.24	1.13	1.22	1.20	1.24	1.08	1.14	1.21	1.23	1.14
16	0.40	0.74	0.90	1.03	1.11	1.11	1.15	1.20	1.25	1.23	1.22	1.21	1.26	1.20	1.14	1.13	1.24	1.21	1.22
17	0.44	0.77	0.93	1.04	0.98	1.18	1.18	1.25	1.20	1.24	1.18	1.22	1.18	1.24	1.21	1.24	1.19	1.24	1.18
18	0.44	0.73	0.88	0.99	1.12	1.12	1.24	1.22	1.25	1.16	1.14	1.12	1.19	1.18	1.23	1.21	1.24	1.14	1.13
19	0.40	0.65	0.67	0.91	1.06	1.18	1.19	1.23	1.20	1.15	0.83	0.84	1.11	1.20	1.14	1.22	1.18	1.13	0.80

Figure 4A-4d. Relative Integrated Power Per Bundle at 3.3 GWd/MT Exposure

	1	2	3	4	5	6	7	8	9	10	11	12	13	14	15	16	17	18	19
1															38.08	36.96	40.37	37.38	38.56
2													44.25	39.16	38.62	21.62	20.23	19.31	2.09
3											40.71	38.40	21.97	2.52	24.47	25.61	22.97	2.85	35.72
4									40.40	38.72	19.87	2.48	2.81	3.03	25.76	23.93	3.38	3.20	17.62
5								42.50	16.93	2.36	2.71	3.04	21.97	3.41	3.50	3.63	35.68	3.64	26.11
6							39.65	18.47	2.58	2.84	3.17	24.81	3.60	26.34	3.64	26.95	3.82	26.75	3.85
7						39.65	40.67	2.61	21.41	3.29	35.32	23.81	3.64	3.75	30.68	24.60	25.91	4.05	27.64
8					42.50	18.47	2.61	2.95	3.33	25.55	21.09	34.98	3.84	17.46	19.28	19.97	4.06	25.99	27.27
9				40.41	16.93	2.58	21.41	3.33	22.11	3.56	3.58	3.76	25.05	4.02	25.93	4.01	26.06	4.10	26.03
10				38.73	2.36	2.84	3.29	25.55	3.56	26.64	3.57	25.56	3.91	26.48	4.03	3.99	4.02	25.96	3.77
11			40.72	19.87	2.71	3.17	35.33	21.08	3.58	3.57	33.57	25.14	25.60	3.96	34.66	26.10	26.31	3.72	26.13
12			38.41	2.48	3.04	24.81	23.81	34.99	3.76	25.56	25.13	26.14	3.80	3.92	25.92	26.48	3.96	3.64	24.97
13		44.22	21.96	2.81	21.96	3.60	3.64	3.84	25.05	3.91	25.59	3.80	26.95	4.00	26.24	4.09	26.51	3.86	26.16
14		39.16	2.52	3.03	3.41	26.33	3.75	17.46	4.02	26.48	3.96	3.92	4.00	26.91	3.98	26.15	3.97	25.98	3.92
15	38.08	38.63	24.47	25.76	3.50	3.64	30.68	19.28	25.93	4.04	34.67	25.91	26.24	3.98	34.07	26.36	3.86	4.00	32.95
16	36.97	21.62	25.60	23.93	3.63	26.94	24.60	19.97	4.01	3.99	26.09	26.48	4.09	26.15	26.35	26.55	3.96	25.56	26.86
17	40.37	20.23	22.97	3.38	35.69	3.82	25.91	4.06	26.05	4.02	26.31	3.96	26.50	3.97	3.86	3.96	26.95	4.08	26.64
18	37.39	19.31	2.85	3.20	3.64	26.74	4.05	25.99	4.11	25.95	3.72	3.64	3.86	25.98	4.00	25.56	4.08	26.98	3.78
19	38.56	2.09	35.72	17.62	26.10	3.85	27.63	27.26	26.02	3.77	26.12	24.97	26.16	3.92	32.95	26.86	26.64	3.78	25.95

Figure 4A-4e. Average Bundle Exposure at 3.3 GWd/MT Exposure

```
        ( ROD PATTERN DEPLETION

NITER   0  POWER           IMAX  19  POWER(MWT)          4.5000E+03  ( 100.0 %)
IBOUN   1  1/4             JMAX  19  PRESSURE(PSIA)      1.0550E+03
IRN     1  MIRROR          KMAX  25  FLOW(*10E-6LB/HR)   7.8508E+01  ( 100.0 %)
ILPA    0                  NSMAX 10  BYPASS(LB/HR)       1.1742E+07  (  15.0 %)          CONTROL ROD CONFIGURATION
IFLW    2  DETAIL          LMAX  20  ENTHALPY(BTU/LB)            512.30                    IN NOTCHES WITHDRAWN
RSTART  0  NEW             LVDCT  7  INLET TEMP(DEG F)           520.47
NEWPHY  2                  IPFTL  0  BEGINNING EXPOSURE         16105.1                 1  3  5  7  9 11 13 15 17 19
NEXO    3  CALC.                    DELTA EXPOS.(DELTE)             0.0
RBOCA   1                  IALPRM 0  DELBRN                      1000.0              1
IACF    0                  IFAST  0  TOTAL NOTCHES                 1506
             IPDOME   1    IAHB   0  CORE FUEL MASS         MTU:162.928              3                           76
                                     CORE FUEL MASS         STU:179.596
ENERGY (MWD) (DELTE)              0. ENERGY (MWD) (DELBRN)      179596.              5
CYCLE ENERGY (MWD)              718391. CYCLE EXPOSURE             4000.0
CORE AVG. POWER DENSITY       54.328033                                              7                       48
NEUTRON MULTIPLICATION     1.00330818 FINAL AVG. EXPOSURE        17105.1
DIFP    (EPS5 = 0.00200)   0.00131285 CORE AVG. NEUTRON FLUX   1.439E+14              9
AVERAGE VOID FRACTION         0.532918 CORE AVG. GD WORTH          -0.099
CORE PRESSURE DROP,PSI        8.081792 CORE AVG. GD RESIDUAL WORTH  0.000            11                52             9
EXP RATIO INDEX (INER-II)       0.0000 CORE AVERAGE XENON WORTH   -0.0219
                                                                                     13
CORE HISTORY MAX. VALUES:       LOCATION: I   J   K
  NODAL EXPOSURE, MWD/T    50435.          7   7   5   METRIC    55594.            15          48           12
  BUNDLE EXPOSURE, MWD/T   40509.         13   2       METRIC    44653.
  EXPOSURE RATIO, NEXRAT   0.0000          0   0   0                                17
  AXIAL POWER PEAK         1.3389                  7
                                                                                     19  76            9           14
```

Figure 4A-5a. Control Rod Pattern Summary at 4.4 GWd/MT Exposure

4.4 GWD/MT

Node	Axial Power
25	0.156
24	0.304
23	0.449
22	0.579
21	0.689
20	0.784
19	0.866
18	0.930
17	0.978
16	1.060
15	1.202
14	1.257
13	1.297
12	1.310
11	1.317
10	1.327
9	1.329
8	1.334
7	1.339
6	1.336
5	1.315
4	1.267
3	1.152
2	0.926
1	0.496

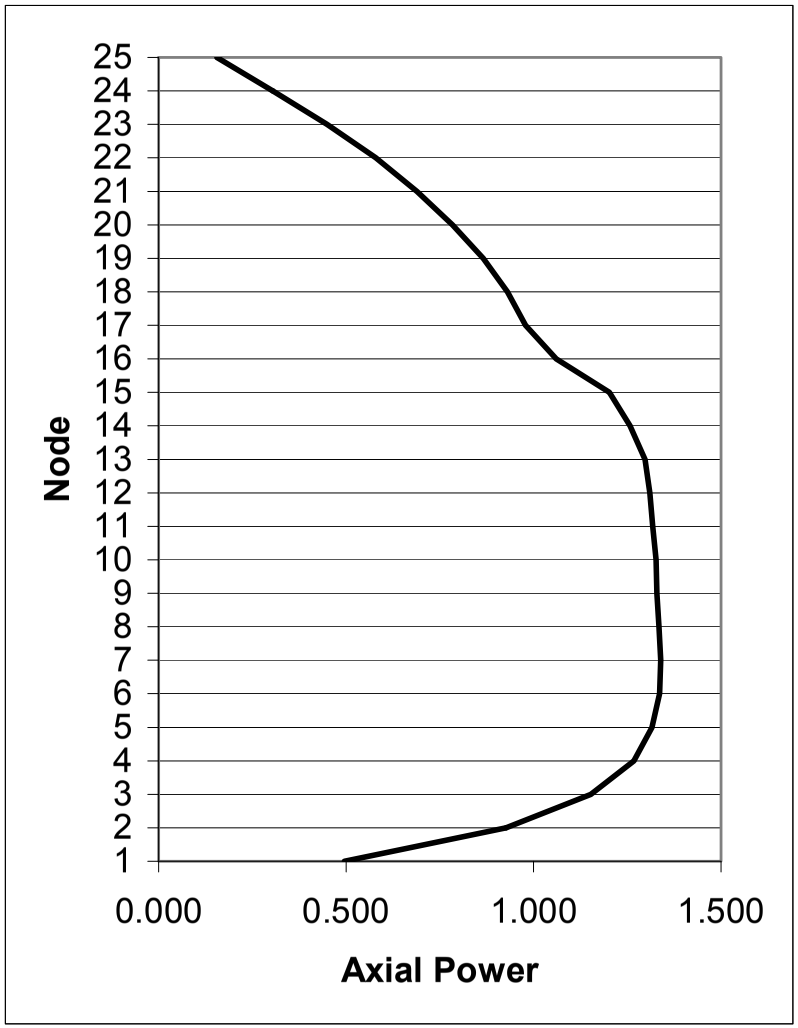

Figure 4A-5b. Relative Axial Power at 4.4 GWd/MT Exposure

4.4 GWD/MT

Node	Axial Exposure (MWD/MT)
25	3832.1
24	6643.2
23	9318.0
22	12021.9
21	14436.5
20	16448.2
19	18105.9
18	19337.1
17	20141.2
16	20761.4
15	20271.5
14	21133.0
13	21862.1
12	22392.8
11	22842.5
10	23182.2
9	23315.3
8	23481.7
7	23733.9
6	23982.8
5	24028.7
4	23466.6
3	21438.7
2	16993.1
1	8644.2

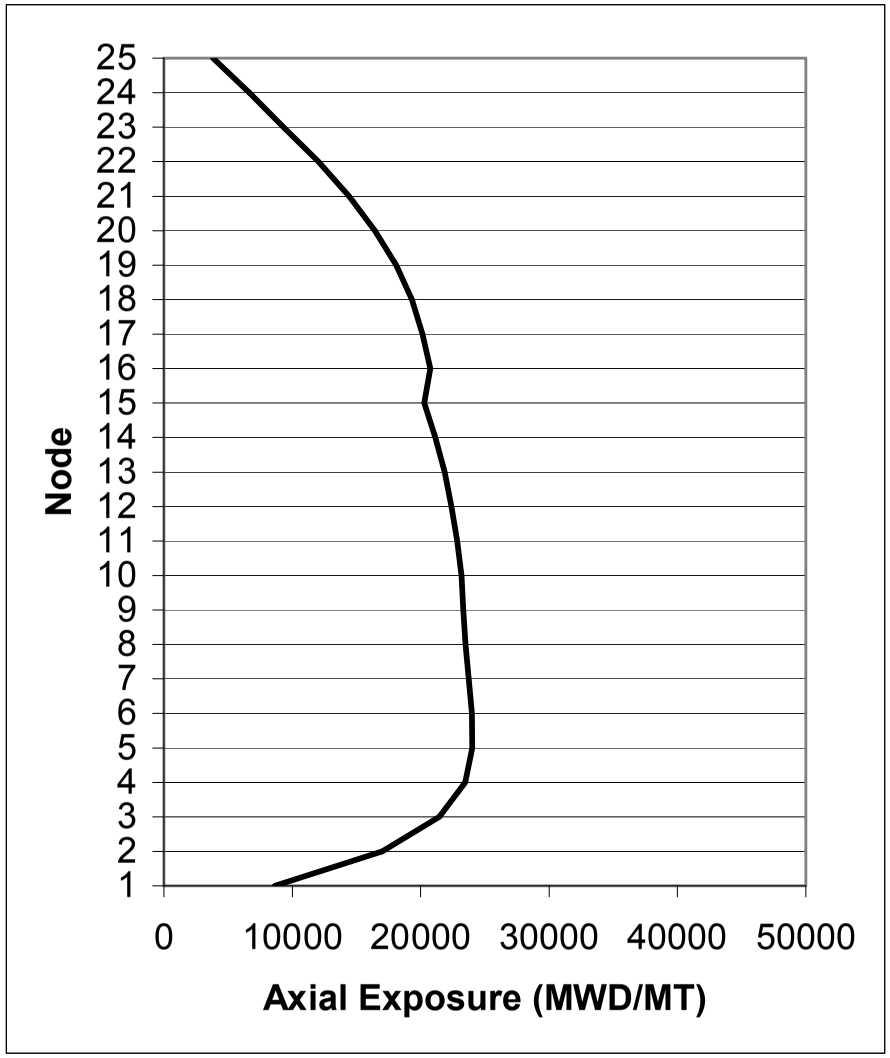

Figure 4A-5c. Axial Exposure at 4.4 GWd/MT Exposure

	1	2	3	4	5	6	7	8	9	10	11	12	13	14	15	16	17	18	19
1															0.37	0.42	0.46	0.48	0.45
2													0.38	0.49	0.58	0.76	0.81	0.80	0.75
3											0.41	0.51	0.69	0.79	0.88	0.92	0.97	0.97	0.83
4									0.38	0.50	0.69	0.79	0.89	0.96	0.97	1.05	1.09	1.08	1.10
5								0.46	0.66	0.77	0.87	0.97	1.02	1.07	1.10	1.13	1.00	1.18	1.13
6							0.45	0.68	0.84	0.92	1.01	1.05	1.14	1.07	1.13	1.09	1.19	1.14	1.22
7						0.45	0.57	0.85	0.96	1.06	0.98	1.15	1.16	1.17	0.98	1.06	1.15	1.24	1.18
8					0.46	0.68	0.85	0.96	1.08	1.07	1.18	1.07	1.22	1.23	1.12	1.10	1.23	1.19	1.20
9				0.38	0.66	0.84	0.96	1.08	1.12	1.17	1.18	1.22	1.22	1.26	1.18	1.23	1.18	1.24	1.18
10				0.50	0.77	0.92	1.06	1.07	1.17	1.12	1.18	1.16	1.25	1.19	1.25	1.23	1.23	1.13	1.13
11			0.41	0.69	0.87	1.01	0.98	1.18	1.18	1.18	1.00	1.07	1.20	1.24	1.12	1.19	1.14	1.12	0.80
12			0.51	0.79	0.97	1.05	1.15	1.07	1.22	1.16	1.07	1.06	1.21	1.22	1.18	1.16	1.18	1.08	0.79
13		0.38	0.69	0.89	1.02	1.14	1.16	1.22	1.22	1.25	1.20	1.21	1.15	1.21	1.13	1.18	1.10	1.13	1.04
14		0.49	0.79	0.96	1.08	1.07	1.17	1.23	1.26	1.19	1.24	1.22	1.21	1.10	1.11	1.04	1.12	1.07	1.12
15	0.37	0.58	0.88	0.97	1.10	1.13	0.98	1.12	1.18	1.25	1.12	1.18	1.13	1.11	0.74	0.77	1.05	1.12	1.03
16	0.42	0.76	0.92	1.05	1.13	1.09	1.06	1.10	1.23	1.23	1.19	1.16	1.18	1.04	0.77	0.76	1.05	1.07	1.09
17	0.46	0.81	0.97	1.09	1.00	1.19	1.15	1.23	1.18	1.23	1.14	1.18	1.10	1.12	1.05	1.05	1.04	1.12	1.07
18	0.48	0.80	0.97	1.08	1.18	1.14	1.24	1.19	1.24	1.13	1.12	1.08	1.13	1.07	1.12	1.07	1.12	1.03	1.05
19	0.45	0.75	0.83	1.10	1.13	1.22	1.18	1.20	1.18	1.14	0.80	0.79	1.04	1.12	1.03	1.09	1.07	1.05	0.76

Figure 4A-5d. Relative Integrated Power Per Bundle at 4.4 GWd/MT Exposure

	1	2	3	4	5	6	7	8	9	10	11	12	13	14	15	16	17	18	19
1															38.48	37.41	40.85	37.87	39.01
2													44.65	39.68	39.24	22.44	21.09	20.12	2.80
3											41.15	38.95	22.70	3.36	25.42	26.59	23.99	3.82	36.46
4									40.80	39.24	20.60	3.32	3.76	4.06	26.82	25.06	4.52	4.29	18.62
5								42.97	17.62	3.16	3.62	4.07	23.07	4.57	4.69	4.86	36.77	4.87	27.28
6							40.11	19.18	3.46	3.80	4.24	25.94	4.82	27.52	4.89	28.17	5.11	27.98	5.15
7						40.11	41.25	3.48	22.42	4.39	36.36	25.04	4.88	5.04	31.84	25.87	27.21	5.41	28.94
8					42.97	19.18	3.48	3.94	4.45	26.67	22.33	36.12	5.14	18.82	20.61	21.29	5.43	27.33	28.62
9				40.81	17.62	3.46	22.42	4.45	23.27	4.75	4.78	5.01	26.35	5.39	27.25	5.39	27.38	5.48	27.35
10				39.25	3.16	3.80	4.39	26.67	4.75	27.77	4.73	26.73	5.20	27.77	5.40	5.35	5.38	27.24	5.03
11			41.16	20.60	3.62	4.24	36.36	22.33	4.78	4.73	34.42	26.07	26.83	5.29	35.90	27.44	27.61	4.98	27.04
12			38.96	3.32	4.07	25.94	25.04	36.13	5.01	26.73	26.07	27.07	5.04	5.23	27.26	27.81	5.30	4.87	25.89
13		44.62	22.70	3.76	23.06	4.82	4.88	5.14	26.35	5.20	26.83	5.04	28.20	5.35	27.57	5.47	27.81	5.17	27.38
14		39.69	3.36	4.06	4.57	27.51	5.04	18.83	5.39	27.76	5.29	5.23	5.35	28.21	5.35	27.47	5.33	27.28	5.24
15	38.48	39.25	25.42	26.82	4.69	4.89	31.85	20.61	27.25	5.40	35.91	27.25	27.57	5.35	35.26	27.61	5.20	5.36	34.21
16	37.41	22.44	26.59	25.06	4.86	28.16	25.87	21.29	5.39	5.35	27.44	27.81	5.47	27.47	27.61	27.80	5.32	26.89	28.21
17	40.85	21.09	23.99	4.52	36.77	5.11	27.21	5.43	27.38	5.38	27.60	5.30	27.80	5.33	5.20	5.32	28.26	5.44	27.95
18	37.88	20.12	3.82	4.29	4.87	27.98	5.41	27.33	5.48	27.23	4.98	4.87	5.17	27.27	5.36	26.89	5.44	28.23	5.02
19	39.01	2.80	36.47	18.62	27.27	5.15	28.94	28.61	27.35	5.04	27.04	25.89	27.38	5.24	34.21	28.20	27.94	5.02	26.83

Figure 4A-5e. Average Bundle Exposure at 4.4 GWd/MT Exposure

```
        ( ROD PATTERN DEPLETION

NITER    0  POWER           IMAX  19  POWER(MWT)          4.5000E+03  ( 100.0 %)
IBOUN    1  1/4             JMAX  19  PRESSURE(PSIA)      1.0550E+03
IRN      1  MIRROR          KMAX  25  FLOW(*10E-6LB/HR)   7.8508E+01  ( 100.0 %)
ILPA     0                  NSMAX 10  BYPASS(LB/HR)       1.1742E+07  (  15.0 %)          CONTROL ROD CONFIGURATION
IFLW     2  DETAIL          LMAX  20  ENTHALPY(BTU/LB)            512.30                    IN NOTCHES WITHDRAWN
RSTART   0  NEW             LVDCT  5  INLET TEMP(DEG F)           520.47
NEWPHY   2                  IPFTL  0  BEGINNING EXPOSURE         17105.2                1  3  5  7  9 11 13 15 17 19
NEXO     3  CALC.                    DELTA EXPOS.(DELTE)             0.0
RBOCA    1                  IALPRM 0  DELBRN                     1000.0                1
IACF     0                  IFAST  0  TOTAL NOTCHES                1506
             IPDOME   1     IAHB   0  CORE FUEL MASS         MTU:162.928                3                          76
                                      CORE FUEL MASS         STU:179.596
ENERGY (MWD) (DELTE)              0.  ENERGY (MWD) (DELBRN)      179596.                5
CYCLE ENERGY (MWD)             897988.  CYCLE EXPOSURE              5000.0
CORE AVG. POWER DENSITY      54.328033                                                    7                      48
NEUTRON MULTIPLICATION      1.00301719  FINAL AVG. EXPOSURE        18105.2
DIFP    (EPS5 = 0.00200)    0.00165296  CORE AVG. NEUTRON FLUX   1.442E+14               9
AVERAGE VOID FRACTION         0.529501  CORE AVG. GD WORTH          -0.094
CORE PRESSURE DROP,PSI        8.086356  CORE AVG. GD RESIDUAL WORTH  0.000               11              52            9
EXP RATIO INDEX (INER-II)       0.0000  CORE AVERAGE XENON WORTH   -0.0220
                                                                                        13
CORE HISTORY MAX. VALUES:       LOCATION: I   J   K
  NODAL EXPOSURE, MWD/T    51080.          7   7   5   METRIC    56306.               15       48           12
  BUNDLE EXPOSURE, MWD/T   40886.         13   2       METRIC    45069.
  EXPOSURE RATIO, NEXRAT   0.0000          0   0   0                                   17
  AXIAL POWER PEAK         1.3231                  7
                                                                                        19 76            9           14
```

Figure 4A-6a. Control Rod Pattern Summary at 5.5 GWd/MT Exposure

5.5 GWD/MT

Node	Axial Power
25	0.165
24	0.321
23	0.473
22	0.605
21	0.716
20	0.809
19	0.888
18	0.949
17	0.993
16	1.070
15	1.204
14	1.253
13	1.289
12	1.298
11	1.304
10	1.312
9	1.314
8	1.319
7	1.323
6	1.320
5	1.298
4	1.248
3	1.132
2	0.909
1	0.489

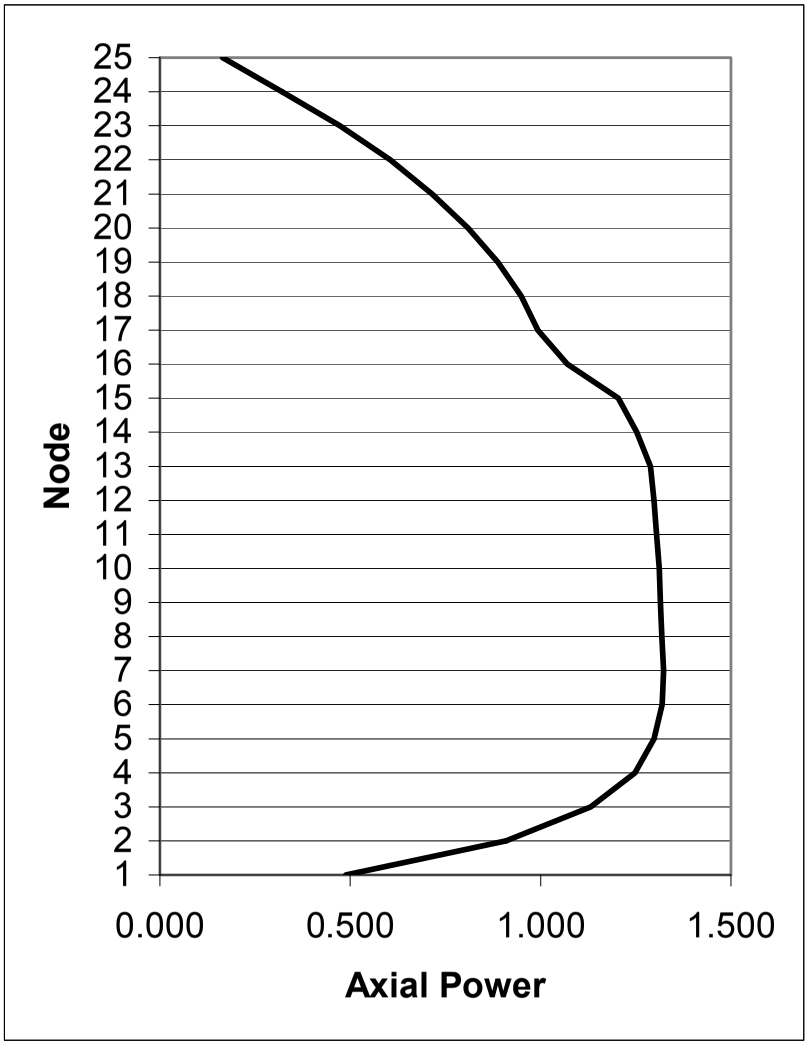

Figure 4A-6b. Relative Axial Power at 5.5 GWd/MT Exposure

Node	*5.5 GWD/MT* Axial Exposure (MWD/MT)
25	4056.6
24	7028.7
23	9864.0
22	12726.1
21	15275.3
20	17402.5
19	19159.6
18	20469.0
17	21331.4
16	22004.2
15	21507.8
14	22426.3
13	23196.6
12	23740.2
11	24197.7
10	24547.0
9	24683.7
8	24855.5
7	25112.9
6	25359.1
5	25383.5
4	24771.5
3	22625.6
2	17947.1
1	9144.2

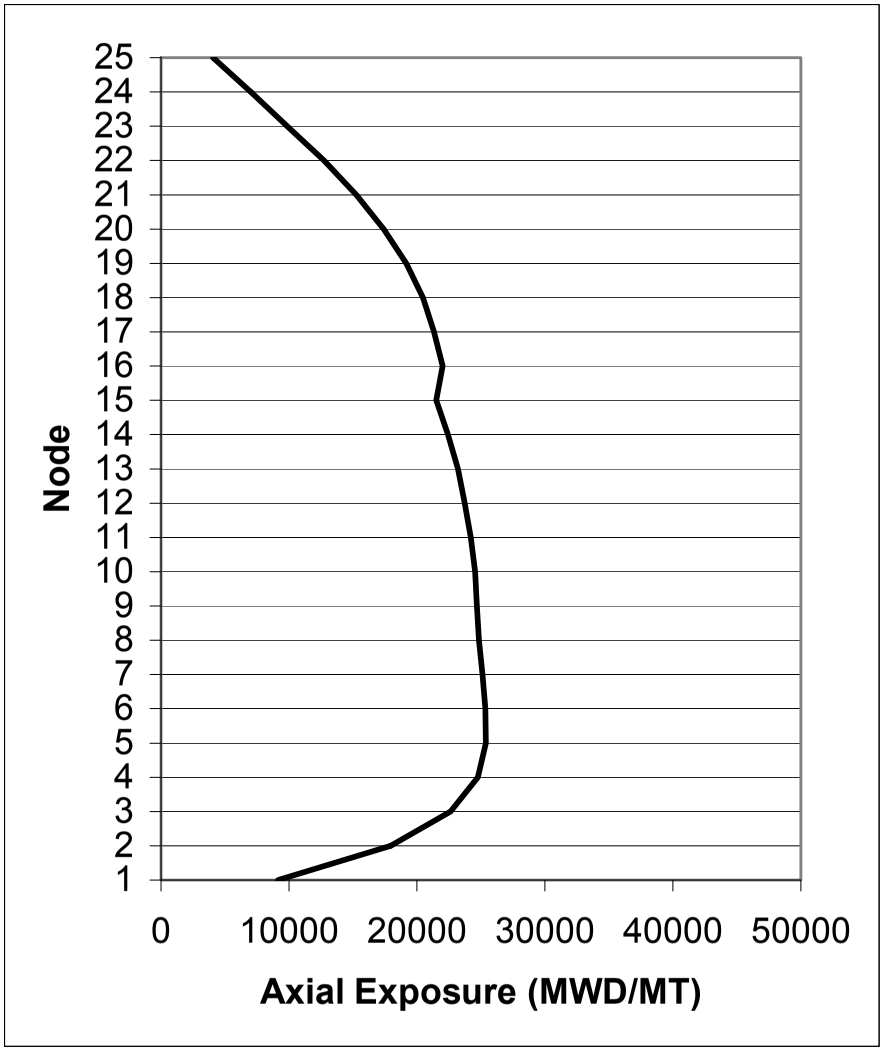

Figure 4A-6c. Axial Exposure at 5.5 GWd/MT Exposure

	1	2	3	4	5	6	7	8	9	10	11	12	13	14	15	16	17	18	19
1															0.36	0.41	0.45	0.47	0.45
2													0.37	0.49	0.57	0.75	0.80	0.79	0.74
3											0.41	0.51	0.68	0.79	0.86	0.90	0.96	0.97	0.82
4									0.39	0.50	0.69	0.80	0.90	0.96	0.97	1.04	1.09	1.08	1.09
5								0.46	0.66	0.78	0.88	0.98	1.02	1.09	1.10	1.14	1.00	1.18	1.11
6							0.45	0.69	0.85	0.93	1.02	1.05	1.15	1.07	1.14	1.08	1.19	1.13	1.22
7						0.45	0.57	0.86	0.96	1.07	0.97	1.14	1.17	1.19	0.98	1.05	1.14	1.24	1.16
8					0.46	0.69	0.86	0.98	1.09	1.07	1.18	1.07	1.23	1.23	1.11	1.09	1.23	1.18	1.18
9				0.39	0.66	0.85	0.96	1.09	1.12	1.19	1.19	1.23	1.21	1.28	1.17	1.24	1.17	1.25	1.16
10				0.50	0.78	0.93	1.07	1.07	1.19	1.12	1.20	1.16	1.26	1.19	1.26	1.24	1.24	1.13	1.14
11			0.41	0.69	0.88	1.02	0.97	1.18	1.19	1.20	0.99	1.07	1.20	1.25	1.11	1.18	1.14	1.13	0.79
12			0.51	0.80	0.98	1.05	1.14	1.07	1.23	1.16	1.07	1.05	1.23	1.23	1.17	1.15	1.19	1.10	0.79
13		0.37	0.68	0.90	1.02	1.15	1.17	1.23	1.21	1.26	1.20	1.23	1.15	1.22	1.13	1.19	1.09	1.14	1.03
14		0.49	0.79	0.96	1.09	1.07	1.19	1.23	1.28	1.19	1.25	1.23	1.22	1.10	1.12	1.03	1.13	1.07	1.13
15	0.36	0.57	0.86	0.97	1.10	1.14	0.98	1.11	1.17	1.26	1.11	1.17	1.13	1.12	0.74	0.77	1.06	1.12	1.02
16	0.41	0.75	0.90	1.04	1.14	1.08	1.05	1.09	1.24	1.24	1.18	1.15	1.19	1.04	0.77	0.76	1.06	1.06	1.08
17	0.45	0.80	0.96	1.09	1.00	1.19	1.14	1.23	1.17	1.24	1.14	1.19	1.09	1.13	1.06	1.06	1.03	1.12	1.05
18	0.47	0.79	0.97	1.08	1.18	1.13	1.24	1.18	1.25	1.13	1.13	1.10	1.14	1.07	1.12	1.06	1.12	1.02	1.05
19	0.45	0.74	0.82	1.09	1.11	1.22	1.16	1.18	1.16	1.14	0.79	0.79	1.03	1.13	1.02	1.08	1.05	1.05	0.76

Figure 4A-6d. Relative Integrated Power Per Bundle at 5.5 GWd/MT Exposure

	1	2	3	4	5	6	7	8	9	10	11	12	13	14	15	16	17	18	19
1															38.89	37.87	41.35	38.39	39.51
2													45.07	40.22	39.88	23.28	21.98	21.00	3.62
3											41.60	39.51	23.46	4.23	26.39	27.60	25.07	4.89	37.37
4									41.22	39.80	21.36	4.19	4.74	5.11	27.89	26.22	5.73	5.48	19.84
5								43.47	18.35	4.01	4.59	5.14	24.19	5.76	5.90	6.11	37.87	6.17	28.52
6							40.61	19.94	4.38	4.81	5.36	27.11	6.07	28.70	6.13	29.37	6.42	29.24	6.49
7						40.61	41.88	4.42	23.48	5.56	37.44	26.31	6.16	6.33	32.92	27.04	28.47	6.78	30.25
8					43.48	19.94	4.42	5.00	5.65	27.85	23.64	37.30	6.48	20.18	21.84	22.50	6.78	28.64	29.95
9				41.23	18.35	4.38	23.48	5.65	24.51	6.04	6.08	6.35	27.69	6.78	28.55	6.74	28.68	6.85	28.65
10				39.80	4.01	4.81	5.56	27.85	6.04	29.01	6.03	28.01	6.58	29.08	6.77	6.70	6.73	28.48	6.28
11			41.61	21.36	4.59	5.36	37.44	23.63	6.08	6.03	35.52	27.25	28.16	6.65	37.14	28.75	28.87	6.21	27.92
12			39.52	4.19	5.14	27.10	26.31	37.31	6.35	28.00	27.25	28.23	6.38	6.57	28.56	29.09	6.60	6.07	26.77
13		45.04	23.46	4.74	24.19	6.07	6.16	6.48	27.69	6.58	28.15	6.38	29.47	6.68	28.82	6.77	29.01	6.41	28.53
14		40.23	4.23	5.12	5.76	28.70	6.33	20.18	6.78	29.07	6.65	6.57	6.68	29.42	6.57	28.62	6.57	28.46	6.47
15	38.89	39.89	26.39	27.89	5.90	6.13	32.93	21.84	28.55	6.78	37.15	28.56	28.82	6.57	36.08	28.46	6.35	6.59	35.34
16	37.87	23.28	27.60	26.22	6.11	29.36	27.04	22.50	6.74	6.70	28.75	29.09	6.77	28.61	28.46	28.63	6.48	28.07	29.41
17	41.35	21.98	25.07	5.73	37.88	6.42	28.47	6.78	28.68	6.73	28.86	6.60	29.01	6.57	6.35	6.48	29.40	6.68	29.12
18	38.40	21.00	4.89	5.48	6.17	29.23	6.78	28.64	6.85	28.48	6.21	6.07	6.41	28.46	6.59	28.07	6.68	29.37	6.18
19	39.51	3.62	37.38	19.84	28.52	6.49	30.24	29.94	28.64	6.29	27.91	26.77	28.52	6.47	35.34	29.41	29.12	6.18	27.67

Figure 4A-6e. Average Bundle Exposure at 5.5 GWd/MT Exposure

```
        ( ROD PATTERN DEPLETION

NITER   0  POWER           IMAX  19  POWER(MWT)          4.5000E+03  ( 100.0 %)
IBOUN   1  1/4             JMAX  19  PRESSURE(PSIA)      1.0550E+03
IRN     1  MIRROR          KMAX  25  FLOW(*10E-6LB/HR)   7.8508E+01  ( 100.0 %)
ILPA    0                  NSMAX 10  BYPASS(LB/HR)       1.1742E+07  (  15.0 %)          CONTROL ROD CONFIGURATION
IFLW    2  DETAIL          LMAX  20  ENTHALPY(BTU/LB)            512.30                    IN NOTCHES WITHDRAWN
RSTART  0  NEW             LVDCT  5  INLET TEMP(DEG F)           520.47
NEWPHY  2                  IPFTL  0  BEGINNING EXPOSURE         18105.1                 1  3  5  7  9 11 13 15 17 19
NEXO    3  CALC.                    DELTA EXPOS.(DELTE)             0.0
RBOCA   1                  IALPRM 0  DELBRN                      1000.0              1
IACF    0                  IFAST  0  TOTAL NOTCHES                 1506
             IPDOME   1    IAHB   0  CORE FUEL MASS         MTU:162.928              3                           76
                                     CORE FUEL MASS         STU:179.596
ENERGY (MWD) (DELTE)              0. ENERGY (MWD) (DELBRN)      179596.              5
CYCLE ENERGY (MWD)          1077586. CYCLE EXPOSURE              6000.0
CORE AVG. POWER DENSITY    54.328033                                                 7                      48
NEUTRON MULTIPLICATION    1.00301743 FINAL AVG. EXPOSURE        19105.1
DIFP    (EPS5 = 0.00200)  0.00133491 CORE AVG. NEUTRON FLUX   1.445E+14             9
AVERAGE VOID FRACTION       0.526596 CORE AVG. GD WORTH          -0.088
CORE PRESSURE DROP,PSI      8.082481 CORE AVG. GD RESIDUAL WORTH  0.000            11               52            9
EXP RATIO INDEX (INER-II)     0.0000 CORE AVERAGE XENON WORTH   -0.0222
                                                                                   13
CORE HISTORY MAX. VALUES:       LOCATION: I   J   K
  NODAL EXPOSURE, MWD/T   51720.          7   7   5   METRIC    57011.            15         48           12
  BUNDLE EXPOSURE, MWD/T  41261.         13   2       METRIC    45482.
  EXPOSURE RATIO, NEXRAT  0.0000          0   0   0                                17
  AXIAL POWER PEAK        1.3100                  7
                                                                                   19  76           9           14
```

Figure 4A-7a. Control Rod Pattern Summary at 6.6 GWd/MT Exposure

6.6 GWD/MT

Node	Axial Power
25	0.173
24	0.337
23	0.495
22	0.629
21	0.739
20	0.831
19	0.907
18	0.965
17	1.004
16	1.076
15	1.202
14	1.245
13	1.277
12	1.285
11	1.289
10	1.297
9	1.300
8	1.305
7	1.310
6	1.308
5	1.287
4	1.236
3	1.120
2	0.898
1	0.485

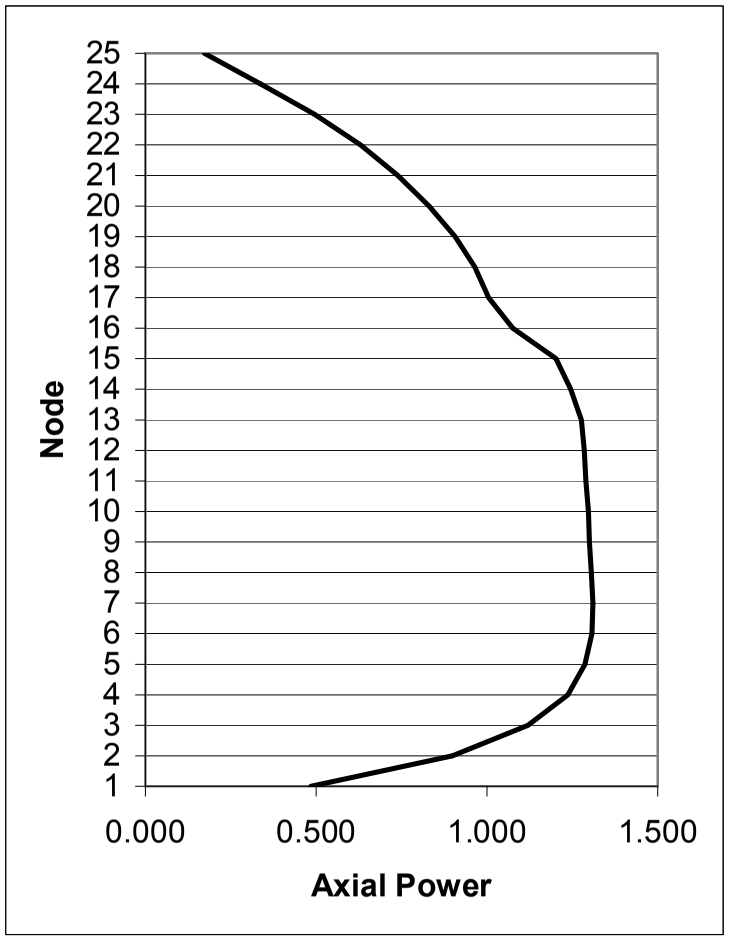

Figure 4A-7b. Relative Axial Power at 6.6 GWd/MT Exposure

6.6 GWD/MT

Node	Axial Exposure (MWD/MT)
25	4294.4
24	7435.5
23	10439.1
22	13462.6
21	16146.2
20	18387.0
19	20240.2
18	21624.0
17	22539.5
16	23258.1
15	22746.1
14	23715.2
13	24522.2
12	25076.0
11	25539.5
10	25897.1
9	26037.1
8	26213.9
7	26475.6
6	26718.3
5	26720.1
4	26056.4
3	23791.4
2	18883.3
1	9637.3

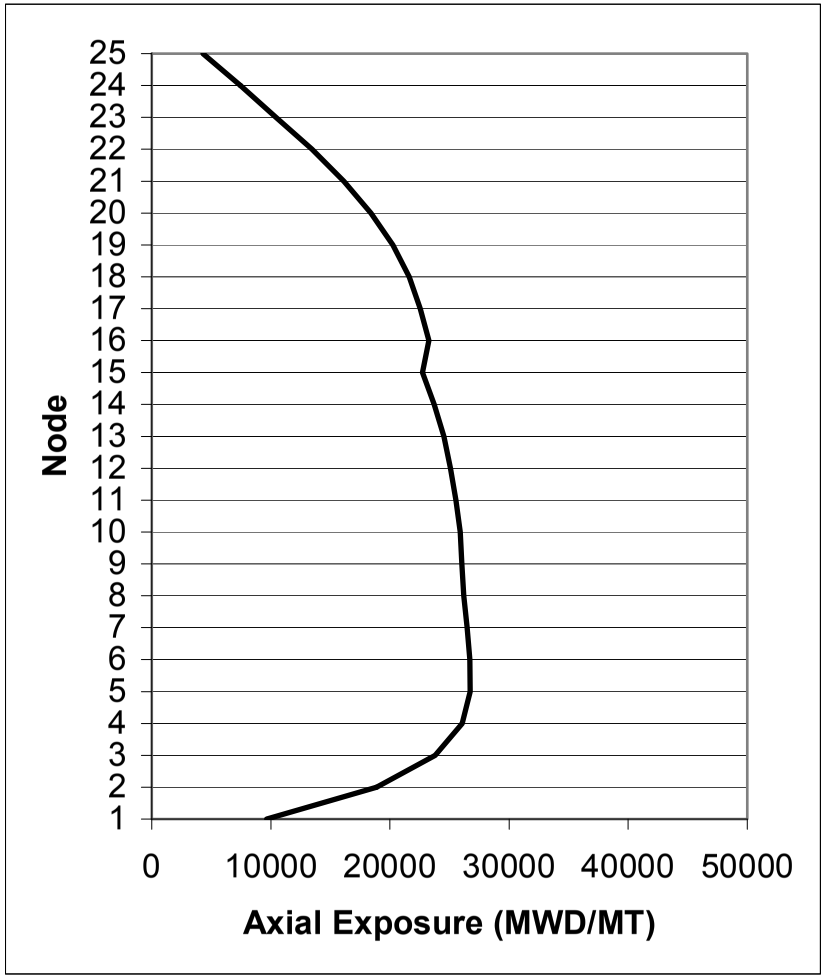

Figure 4A-7c. Axial Exposure at 6.6 GWd/MT Exposure

	1	2	3	4	5	6	7	8	9	10	11	12	13	14	15	16	17	18	19
1															0.35	0.40	0.44	0.46	0.44
2													0.37	0.48	0.56	0.73	0.78	0.78	0.74
3											0.41	0.51	0.68	0.79	0.85	0.88	0.94	0.97	0.81
4									0.39	0.50	0.70	0.81	0.91	0.97	0.95	1.02	1.09	1.08	1.08
5								0.46	0.67	0.79	0.89	0.99	1.02	1.10	1.11	1.14	0.99	1.18	1.10
6							0.45	0.69	0.86	0.94	1.03	1.05	1.16	1.07	1.15	1.07	1.19	1.11	1.22
7						0.45	0.57	0.87	0.96	1.08	0.97	1.14	1.19	1.20	0.97	1.04	1.12	1.24	1.14
8					0.46	0.69	0.87	0.99	1.11	1.07	1.17	1.06	1.25	1.22	1.11	1.09	1.24	1.16	1.16
9				0.39	0.67	0.86	0.96	1.11	1.13	1.20	1.21	1.25	1.21	1.29	1.17	1.25	1.16	1.25	1.14
10				0.50	0.79	0.94	1.08	1.07	1.20	1.12	1.21	1.15	1.28	1.18	1.28	1.25	1.25	1.12	1.15
11			0.41	0.70	0.89	1.03	0.97	1.17	1.21	1.21	0.99	1.06	1.19	1.27	1.11	1.17	1.13	1.14	0.79
12			0.51	0.81	0.99	1.05	1.14	1.06	1.25	1.15	1.06	1.05	1.24	1.25	1.17	1.14	1.20	1.11	0.79
13		0.37	0.68	0.91	1.02	1.16	1.19	1.25	1.21	1.28	1.19	1.24	1.15	1.24	1.12	1.20	1.09	1.15	1.02
14		0.48	0.79	0.97	1.10	1.07	1.20	1.22	1.29	1.18	1.27	1.25	1.24	1.10	1.13	1.03	1.15	1.07	1.14
15	0.35	0.56	0.85	0.95	1.11	1.15	0.97	1.11	1.17	1.28	1.11	1.17	1.12	1.13	0.74	0.77	1.07	1.13	1.01
16	0.40	0.73	0.88	1.02	1.14	1.07	1.04	1.09	1.25	1.25	1.17	1.14	1.20	1.03	0.77	0.76	1.07	1.05	1.06
17	0.44	0.78	0.94	1.09	0.99	1.19	1.12	1.24	1.16	1.25	1.13	1.20	1.09	1.15	1.07	1.07	1.03	1.13	1.04
18	0.46	0.78	0.97	1.08	1.18	1.11	1.24	1.16	1.25	1.12	1.14	1.11	1.15	1.07	1.13	1.05	1.13	1.02	1.05
19	0.44	0.74	0.81	1.08	1.10	1.22	1.14	1.16	1.14	1.15	0.79	0.79	1.03	1.14	1.01	1.06	1.04	1.05	0.76

Figure 4A-7d. Relative Integrated Power Per Bundle at 6.6 GWd/MT Exposure

	1	2	3	4	5	6	7	8	9	10	11	12	13	14	15	16	17	18	19
1															39.29	38.32	41.85	38.91	40.00
2													45.48	40.76	40.51	24.11	22.86	21.87	4.44
3											42.06	40.07	24.22	5.10	27.34	28.60	26.13	5.96	38.28
4									41.65	40.35	22.13	5.07	5.74	6.18	28.96	27.36	6.93	6.68	21.04
5								43.98	19.08	4.86	5.56	6.22	25.31	6.96	7.12	7.37	38.97	7.47	29.75
6							41.10	20.70	5.32	5.84	6.49	28.26	7.34	29.88	7.38	30.56	7.73	30.48	7.84
7						41.10	42.51	5.37	24.54	6.74	38.51	27.57	7.45	7.64	34.00	28.20	29.72	8.15	31.53
8					43.98	20.70	5.37	6.08	6.85	29.03	24.94	38.48	7.84	21.53	23.07	23.71	8.14	29.94	31.25
9				41.65	19.08	5.32	24.54	6.85	25.75	7.35	7.39	7.70	29.03	8.18	29.84	8.10	29.97	8.22	29.92
10				40.35	4.86	5.84	6.74	29.03	7.35	30.25	7.35	29.28	7.97	30.38	8.16	8.06	8.10	29.72	7.54
11			42.06	22.12	5.56	6.49	38.52	24.94	7.39	7.35	36.61	28.43	29.47	8.04	38.37	30.05	30.12	7.45	28.79
12			40.09	5.07	6.22	28.26	27.57	38.49	7.70	29.28	28.42	29.39	7.73	7.93	29.86	30.35	7.91	7.28	27.64
13		45.45	24.21	5.74	25.31	7.34	7.45	7.84	29.03	7.97	29.47	7.73	30.74	8.03	30.06	8.08	30.22	7.67	29.66
14		40.76	5.10	6.18	6.96	29.88	7.64	21.54	8.18	30.38	8.04	7.93	8.03	30.63	7.79	29.76	7.81	29.64	7.71
15	39.29	40.52	27.34	28.95	7.12	7.38	34.00	23.07	29.84	8.16	38.38	29.85	30.06	7.79	36.89	29.31	7.51	7.83	36.47
16	38.32	24.11	28.59	27.36	7.37	30.55	28.20	23.71	8.10	8.06	30.05	30.35	8.08	29.75	29.31	29.47	7.65	29.24	30.59
17	41.85	22.86	26.13	6.93	38.98	7.73	29.72	8.14	29.96	8.10	30.11	7.91	30.21	7.82	7.51	7.65	30.53	7.92	30.28
18	38.92	21.87	5.96	6.68	7.47	30.47	8.15	29.94	8.23	29.72	7.45	7.28	7.67	29.64	7.83	29.24	7.92	30.50	7.33
19	40.00	4.44	38.29	21.04	29.74	7.84	31.52	31.24	29.92	7.54	28.79	27.64	29.66	7.72	36.47	30.59	30.27	7.33	28.51

Figure 4A-7e. Average Bundle Exposure at 6.6 GWd/MT Exposure

```
        ( ROD PATTERN DEPLETION

NITER   0  POWER           IMAX  19  POWER(MWT)          4.5000E+03  ( 100.0 %)
IBOUN   1  1/4             JMAX  19  PRESSURE(PSIA)      1.0550E+03
IRN     1  MIRROR          KMAX  25  FLOW(*10E-6LB/HR)   7.8508E+01  ( 100.0 %)
ILPA    0                  NSMAX 10  BYPASS(LB/HR)       1.1742E+07  (  15.0 %)          CONTROL ROD CONFIGURATION
IFLW    2  DETAIL          LMAX  20  ENTHALPY(BTU/LB)            512.30                    IN NOTCHES WITHDRAWN
RSTART  0  NEW             LVDCT  7  INLET TEMP(DEG F)            520.47
NEWPHY  2                  IPFTL  0  BEGINNING EXPOSURE         19105.1                 1  3  5  7  9 11 13 15 17 19
NEXO    3  CALC.                     DELTA EXPOS.(DELTE)             0.0
RBOCA   1                  IALPRM 0  DELBRN                      1000.0                1
IACF    0                  IFAST  0  TOTAL NOTCHES                 1515
             IPDOME   1    IAHB   0  CORE FUEL MASS         MTU:162.928                3
                                     CORE FUEL MASS         STU:179.596
ENERGY (MWD) (DELTE)              0. ENERGY (MWD) (DELBRN)      179596.                5
CYCLE ENERGY (MWD)          1257184. CYCLE EXPOSURE              7000.0
CORE AVG. POWER DENSITY    54.328033                                                    7                     45
NEUTRON MULTIPLICATION    1.00171769 FINAL AVG. EXPOSURE        20105.1
DIFP   (EPS5 = 0.00200)   0.00138611 CORE AVG. NEUTRON FLUX   1.449E+14                9
AVERAGE VOID FRACTION       0.531062 CORE AVG. GD WORTH          -0.082
CORE PRESSURE DROP,PSI      8.079891 CORE AVG. GD RESIDUAL WORTH  0.000               11              19           4
EXP RATIO INDEX (INER-II)     0.0000 CORE AVERAGE XENON WORTH   -0.0224
                                                                                      13
CORE HISTORY MAX. VALUES:      LOCATION: I   J   K
  NODAL EXPOSURE, MWD/T   52358.         7   7   5   METRIC    57714.               15        45          26
  BUNDLE EXPOSURE, MWD/T  41633.        13   2       METRIC    45892.
  EXPOSURE RATIO, NEXRAT  0.0000         0   0   0                                   17
  AXIAL POWER PEAK        1.3294                 5
                                                                                      19               4          29
```

Figure 4A-8a. Control Rod Pattern Summary at 7.7 GWd/MT Exposure

7.7 GWD/MT

Node	Axial Power
25	0.185
24	0.357
23	0.522
22	0.661
21	0.775
20	0.860
19	0.923
18	0.964
17	0.985
16	1.040
15	1.146
14	1.176
13	1.195
12	1.214
11	1.235
10	1.254
9	1.269
8	1.287
7	1.307
6	1.324
5	1.329
4	1.300
3	1.196
2	0.970
1	0.528

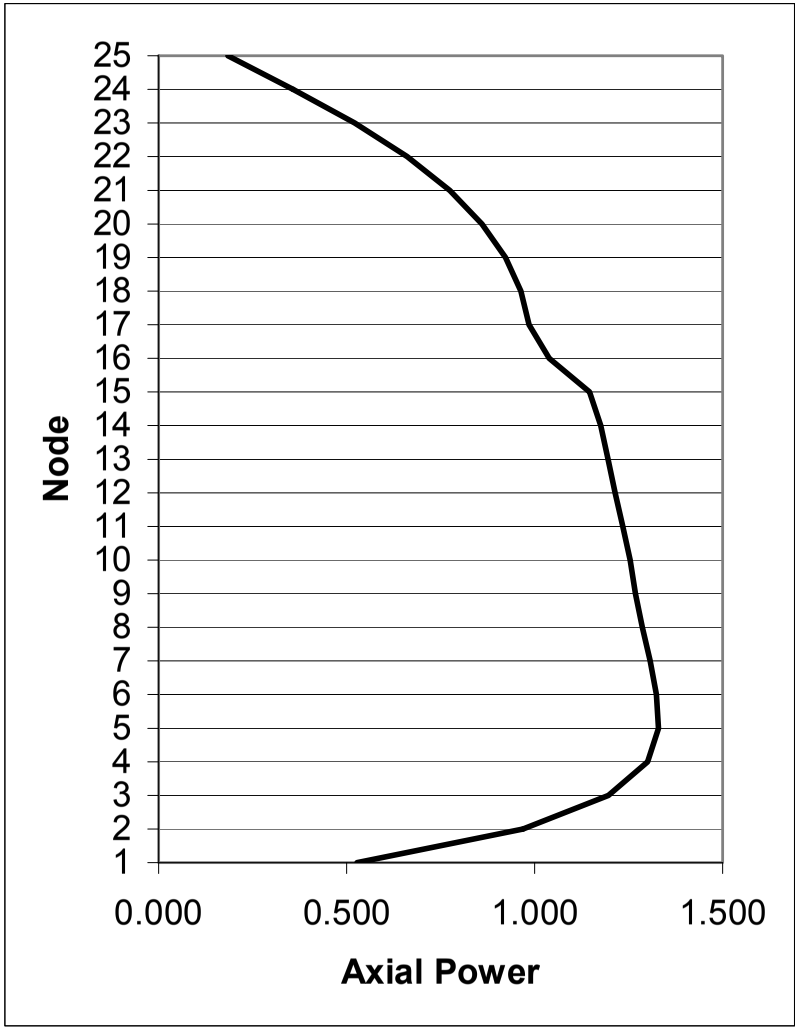

Figure 4A-8b. Relative Axial Power at 7.7 GWd/MT Exposure

7.7 GWD/MT

Node	Axial Exposure (MWD/MT)
25	4544.6
24	7862.4
23	11041.6
22	14228.5
21	17045.6
20	19397.7
19	21343.8
18	22797.8
17	23761.6
16	24518.7
15	23982.5
14	24996.1
13	25835.8
12	26397.8
11	26866.1
10	27231.5
9	27375.4
8	27557.9
7	27824.8
6	28065.1
5	28045.2
4	27329.9
3	24944.9
2	19808.5
1	10126.7

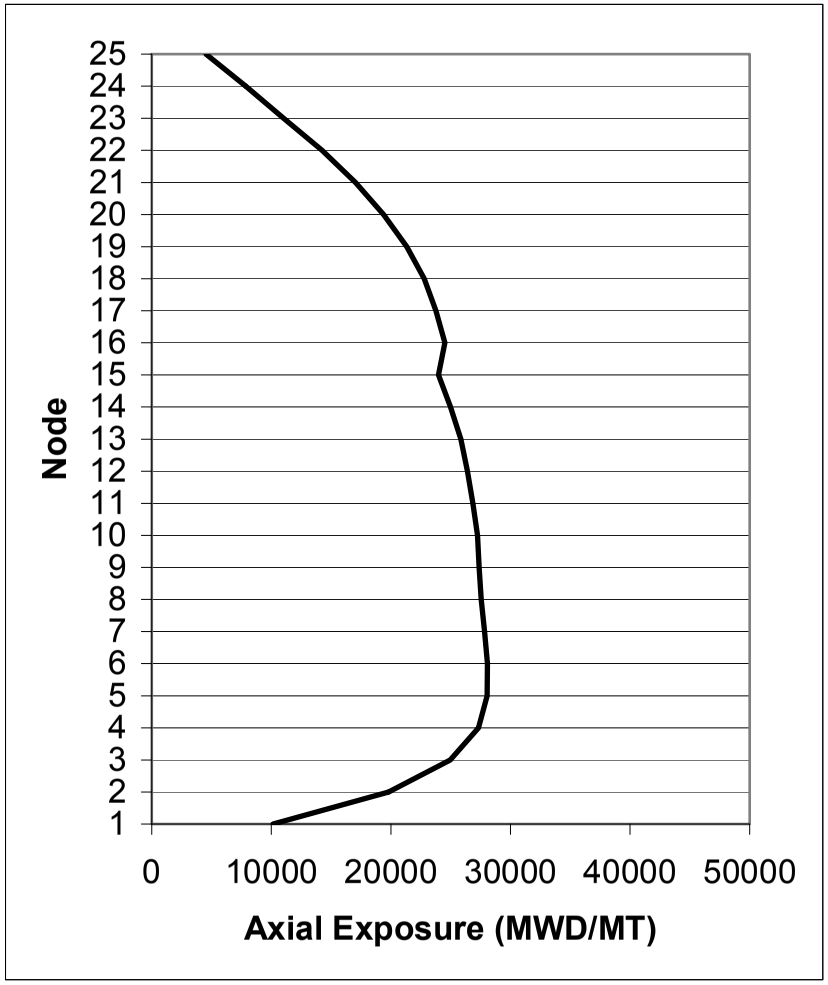

Figure 4A-8c. Axial Exposure at 7.7 GWd/MT Exposure

	1	2	3	4	5	6	7	8	9	10	11	12	13	14	15	16	17	18	19
1															0.35	0.39	0.44	0.46	0.45
2													0.37	0.47	0.55	0.72	0.78	0.78	0.76
3											0.41	0.51	0.68	0.79	0.84	0.87	0.94	0.98	0.84
4									0.38	0.50	0.69	0.81	0.91	0.97	0.94	1.01	1.10	1.10	1.12
5								0.45	0.66	0.79	0.90	0.99	1.01	1.10	1.11	1.14	0.98	1.19	1.10
6							0.44	0.68	0.86	0.94	1.03	1.03	1.16	1.06	1.14	1.05	1.20	1.10	1.23
7						0.44	0.56	0.86	0.95	1.07	0.95	1.11	1.18	1.19	0.94	1.01	1.10	1.24	1.13
8					0.45	0.68	0.86	0.98	1.10	1.03	1.13	1.03	1.23	1.19	1.07	1.05	1.23	1.14	1.14
9				0.38	0.66	0.86	0.95	1.10	1.09	1.18	1.17	1.21	1.17	1.27	1.14	1.25	1.15	1.26	1.13
10				0.50	0.79	0.94	1.07	1.03	1.18	1.06	1.14	1.06	1.23	1.14	1.27	1.26	1.27	1.12	1.16
11			0.41	0.69	0.90	1.03	0.95	1.13	1.17	1.14	0.78	0.84	1.10	1.24	1.09	1.16	1.13	1.17	0.79
12			0.51	0.81	0.99	1.03	1.11	1.02	1.21	1.06	0.84	0.84	1.18	1.23	1.15	1.14	1.23	1.15	0.79
13		0.37	0.68	0.91	1.01	1.16	1.18	1.23	1.17	1.23	1.10	1.18	1.11	1.24	1.13	1.24	1.12	1.20	1.05
14		0.47	0.79	0.97	1.10	1.06	1.19	1.19	1.27	1.14	1.24	1.23	1.24	1.11	1.18	1.08	1.21	1.11	1.20
15	0.35	0.55	0.84	0.94	1.11	1.14	0.94	1.07	1.14	1.27	1.09	1.15	1.13	1.18	0.84	0.88	1.16	1.21	1.06
16	0.39	0.72	0.87	1.01	1.14	1.05	1.01	1.05	1.25	1.26	1.16	1.14	1.24	1.08	0.88	0.87	1.17	1.12	1.12
17	0.44	0.78	0.94	1.10	0.98	1.20	1.10	1.23	1.15	1.27	1.13	1.23	1.12	1.21	1.16	1.17	1.10	1.22	1.11
18	0.46	0.78	0.98	1.10	1.19	1.10	1.25	1.14	1.26	1.12	1.17	1.15	1.20	1.12	1.21	1.12	1.22	1.10	1.17
19	0.45	0.76	0.84	1.12	1.10	1.23	1.13	1.14	1.13	1.16	0.79	0.79	1.05	1.20	1.07	1.12	1.11	1.17	0.90

Figure 4A-8d. Relative Integrated Power Per Bundle at 7.7 GWd/MT Exposure

	1	2	3	4	5	6	7	8	9	10	11	12	13	14	15	16	17	18	19
1															39.68	38.76	42.34	39.42	40.49
2													45.89	41.29	41.12	24.92	23.73	22.73	5.26
3											42.51	40.64	24.97	5.97	28.28	29.57	27.17	7.03	39.17
4									42.07	40.90	22.89	5.97	6.74	7.25	30.01	28.49	8.13	7.87	22.23
5								44.48	19.82	5.73	6.54	7.31	26.44	8.16	8.34	8.62	40.06	8.76	30.95
6							41.59	21.46	6.26	6.88	7.63	29.42	8.62	31.06	8.64	31.73	9.05	31.70	9.18
7						41.59	43.14	6.32	25.60	7.93	39.58	28.82	8.76	8.96	35.07	29.35	30.96	9.52	32.78
8					44.49	21.46	6.32	7.17	8.07	30.21	26.23	39.65	9.22	22.88	24.30	24.91	9.50	31.22	32.52
9				42.08	19.81	6.26	25.60	8.07	26.99	8.68	8.72	9.08	30.37	9.60	31.13	9.48	31.24	9.60	31.18
10				40.91	5.73	6.88	7.93	30.20	8.68	31.48	8.69	30.55	9.38	31.69	9.57	9.44	9.48	30.96	8.80
11			42.52	22.89	6.54	7.63	39.59	26.23	8.72	8.69	37.70	29.59	30.79	9.43	39.59	31.34	31.36	8.71	29.67
12			40.65	5.97	7.31	29.42	28.82	39.66	9.08	30.54	29.59	30.54	9.10	9.30	31.14	31.61	9.23	8.50	28.51
13		45.86	24.97	6.74	26.43	8.62	8.76	9.22	30.37	9.38	30.78	9.10	32.01	9.39	31.29	9.40	31.42	8.94	30.79
14		41.29	5.97	7.25	8.16	31.05	8.96	22.88	9.60	31.68	9.44	9.30	9.39	31.84	9.04	30.90	9.08	30.81	8.97
15	39.68	41.13	28.28	30.01	8.35	8.64	35.07	24.29	31.13	9.57	39.60	31.14	31.29	9.04	37.71	30.16	8.69	9.07	37.58
16	38.77	24.92	29.56	28.49	8.63	31.73	29.35	24.91	9.48	9.45	31.34	31.61	9.40	30.89	30.16	30.30	8.83	30.40	31.76
17	42.34	23.73	27.17	8.13	40.07	9.05	30.96	9.50	31.24	9.48	31.36	9.23	31.41	9.08	8.69	8.83	31.66	9.16	31.42
18	39.43	22.73	7.03	7.87	8.76	31.70	9.52	31.22	9.60	30.95	8.71	8.50	8.94	30.81	9.07	30.40	9.16	31.62	8.49
19	40.49	5.26	39.18	22.23	30.95	9.19	32.78	32.52	31.18	8.81	29.66	28.51	30.78	8.97	37.58	31.76	31.42	8.49	29.34

Figure 4A-8e. Average Bundle Exposure at 7.7 GWd/MT Exposure

```
        ( ROD PATTERN DEPLETION

NITER   0  POWER           IMAX  19  POWER(MWT)          4.5000E+03  ( 100.0 %)
IBOUN   1  1/4             JMAX  19  PRESSURE(PSIA)      1.0550E+03
IRN     1  MIRROR          KMAX  25  FLOW(*10E-6LB/HR)   7.8508E+01  ( 100.0 %)
ILPA    0                  NSMAX 10  BYPASS(LB/HR)       1.1742E+07  (  15.0 %)          CONTROL ROD CONFIGURATION
IFLW    2  DETAIL          LMAX  20  ENTHALPY(BTU/LB)            512.30                    IN NOTCHES WITHDRAWN
RSTART  0  NEW             LVDCT  5  INLET TEMP(DEG F)           520.47
NEWPHY  2                  IPFTL  0  BEGINNING EXPOSURE         20105.1                1  3  5  7  9 11 13 15 17 19
NEXO    3  CALC.                    DELTA EXPOS.(DELTE)            0.0
RBOCA   1                  IALPRM 0  DELBRN                      1000.0                1
IACF    0                  IFAST  0  TOTAL NOTCHES                 1515
             IPDOME   1    IAHB   0  CORE FUEL MASS         MTU:162.928                3
                                     CORE FUEL MASS         STU:179.596
ENERGY (MWD) (DELTE)              0. ENERGY (MWD) (DELBRN)      179596.                5
CYCLE ENERGY (MWD)          1436781. CYCLE EXPOSURE              8000.0
CORE AVG. POWER DENSITY    54.328033                                                    7                    45
NEUTRON MULTIPLICATION    1.00232935 FINAL AVG. EXPOSURE        21105.1
DIFP    (EPS5 = 0.00200)  0.00135982 CORE AVG. NEUTRON FLUX   1.451E+14                9
AVERAGE VOID FRACTION       0.530853 CORE AVG. GD WORTH          -0.071
CORE PRESSURE DROP,PSI      8.099077 CORE AVG. GD RESIDUAL WORTH  0.000               11              19           4
EXP RATIO INDEX (INER-II)     0.0000 CORE AVERAGE XENON WORTH   -0.0226
                                                                                      13
CORE HISTORY MAX. VALUES:       LOCATION: I   J   K
  NODAL EXPOSURE, MWD/T   53011.          7   7   5   METRIC    58434.               15
      45          26
  BUNDLE EXPOSURE, MWD/T  42000.         13   2       METRIC    46297.
  EXPOSURE RATIO, NEXRAT  0.0000          0   0   0                                   17
  AXIAL POWER PEAK        1.3400                  5
                                                                          19              4          29
```

Figure 4A-9a. Control Rod Pattern Summary at 8.8 GWd/MT Exposure

8.8 GWD/MT

Node	Axial Power
25	0.189
24	0.366
23	0.533
22	0.672
21	0.783
20	0.867
19	0.927
18	0.966
17	0.986
16	1.035
15	1.134
14	1.160
13	1.178
12	1.196
11	1.217
10	1.238
9	1.257
8	1.279
7	1.305
6	1.328
5	1.340
4	1.316
3	1.211
2	0.981
1	0.535

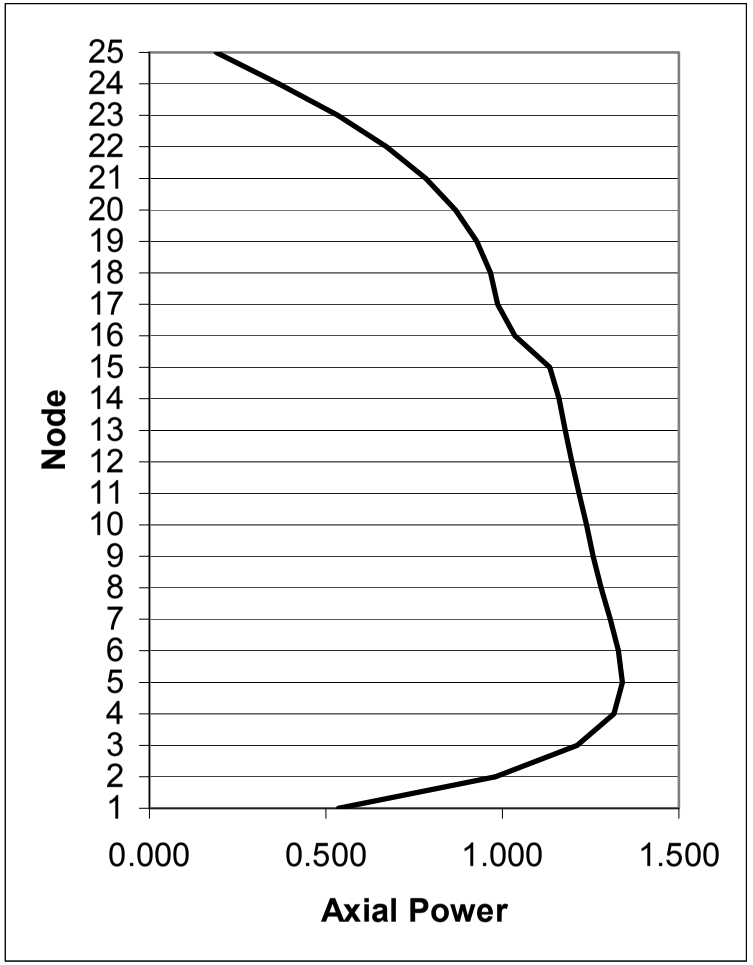

Figure 4A-9b. Relative Axial Power at 8.8 GWd/MT Exposure

Node	*8.8 GWD/MT* Axial Exposure (MWD/MT)
25	4811.0
24	8314.8
23	11676.3
22	15033.0
21	17988.2
20	20444.3
19	22466.5
18	23970.3
17	24960.5
16	25737.2
15	25161.4
14	26205.6
13	27065.2
12	27647.1
11	28136.2
10	28521.3
9	28681.5
8	28883.1
7	29170.8
6	29428.9
5	29414.5
4	28669.3
3	26177.0
2	20807.1
1	10659.4

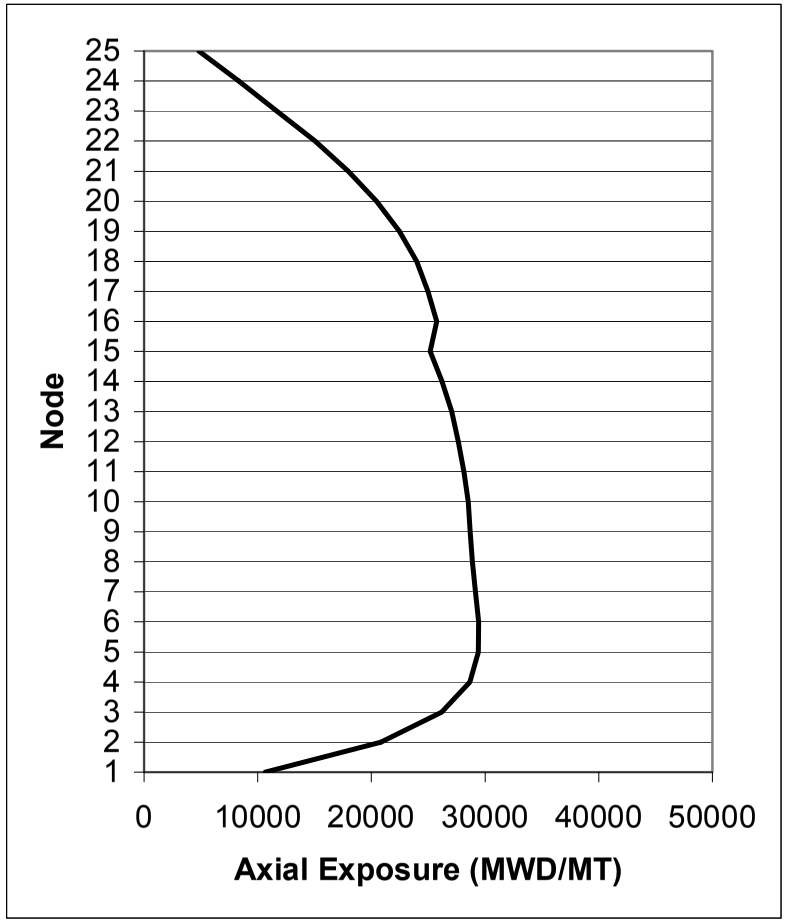

Figure 4A-9c. Axial Exposure at 8.8 GWd/MT Exposure

	1	2	3	4	5	6	7	8	9	10	11	12	13	14	15	16	17	18	19
1															0.34	0.38	0.42	0.45	0.44
2													0.36	0.47	0.54	0.70	0.76	0.77	0.75
3											0.41	0.51	0.67	0.79	0.82	0.85	0.92	0.98	0.83
4									0.38	0.50	0.69	0.82	0.92	0.98	0.93	1.00	1.09	1.10	1.10
5								0.45	0.67	0.80	0.91	1.00	1.01	1.11	1.12	1.14	0.97	1.19	1.08
6							0.44	0.68	0.87	0.96	1.04	1.03	1.17	1.05	1.15	1.04	1.20	1.09	1.23
7						0.44	0.56	0.87	0.95	1.08	0.94	1.10	1.20	1.21	0.93	0.99	1.09	1.25	1.11
8					0.45	0.68	0.87	1.00	1.11	1.03	1.13	1.02	1.25	1.19	1.06	1.05	1.24	1.13	1.12
9				0.38	0.67	0.87	0.95	1.11	1.09	1.19	1.19	1.22	1.16	1.29	1.13	1.26	1.14	1.27	1.11
10				0.50	0.80	0.96	1.08	1.03	1.19	1.06	1.15	1.06	1.25	1.14	1.29	1.28	1.28	1.11	1.17
11			0.41	0.69	0.91	1.04	0.94	1.13	1.19	1.15	0.78	0.84	1.10	1.26	1.08	1.15	1.13	1.18	0.79
12			0.51	0.82	1.00	1.03	1.10	1.02	1.22	1.06	0.84	0.84	1.20	1.25	1.14	1.13	1.25	1.16	0.79
13		0.36	0.67	0.92	1.01	1.17	1.20	1.25	1.16	1.25	1.10	1.20	1.11	1.26	1.12	1.25	1.12	1.22	1.05
14		0.47	0.79	0.98	1.11	1.05	1.21	1.19	1.29	1.14	1.26	1.25	1.26	1.11	1.19	1.08	1.23	1.11	1.21
15	0.34	0.54	0.82	0.93	1.12	1.15	0.93	1.06	1.13	1.29	1.08	1.14	1.12	1.19	0.84	0.88	1.17	1.22	1.05
16	0.38	0.70	0.85	1.00	1.14	1.04	0.99	1.05	1.26	1.28	1.15	1.13	1.25	1.08	0.88	0.87	1.18	1.11	1.10
17	0.42	0.76	0.92	1.09	0.97	1.20	1.09	1.24	1.14	1.28	1.13	1.25	1.12	1.23	1.17	1.18	1.10	1.23	1.10
18	0.45	0.77	0.98	1.10	1.19	1.09	1.25	1.13	1.27	1.11	1.18	1.16	1.22	1.11	1.22	1.11	1.23	1.09	1.17
19	0.44	0.75	0.83	1.10	1.08	1.23	1.11	1.12	1.11	1.17	0.79	0.79	1.05	1.21	1.05	1.10	1.10	1.17	0.90

Figure 4A-9d. Relative Integrated Power Per Bundle at 8.8 GWd/MT Exposure

	1	2	3	4	5	6	7	8	9	10	11	12	13	14	15	16	17	18	19
1															40.06	39.19	42.82	39.92	40.98
2													46.30	41.81	41.73	25.72	24.58	23.59	6.09
3											42.96	41.20	25.72	6.84	29.20	30.53	28.20	8.11	40.10
4									42.50	41.46	23.66	6.86	7.74	8.32	31.05	29.61	9.33	9.09	23.47
5								44.98	20.55	6.60	7.53	8.41	27.55	9.38	9.57	9.88	41.14	10.08	32.16
6							42.08	22.21	7.21	7.92	8.76	30.56	9.90	32.22	9.90	32.89	10.36	32.92	10.54
7						42.08	43.76	7.28	26.65	9.11	40.62	30.04	10.06	10.27	36.10	30.46	32.18	10.89	34.03
8					44.99	22.21	7.28	8.26	9.28	31.35	27.48	40.78	10.58	24.19	25.47	26.07	10.86	32.48	33.78
9				42.50	20.55	7.21	26.64	9.28	28.20	9.97	10.01	10.41	31.66	11.00	32.39	10.85	32.51	10.99	32.43
10				41.46	6.60	7.92	9.11	31.34	9.97	32.65	9.94	31.72	10.73	32.95	10.97	10.84	10.87	32.19	10.08
11			42.97	23.66	7.53	8.76	40.63	27.48	10.01	9.94	38.57	30.52	32.01	10.81	40.79	32.62	32.61	9.99	30.54
12			41.21	6.86	8.41	30.55	30.04	40.79	10.41	31.71	30.51	31.46	10.40	10.65	32.41	32.87	10.59	9.76	29.38
13		46.27	25.71	7.74	27.55	9.90	10.06	10.58	31.65	10.74	32.00	10.40	33.23	10.76	32.53	10.76	32.65	10.26	31.95
14		41.82	6.84	8.32	9.38	32.22	10.27	24.20	11.00	32.94	10.81	10.65	10.76	33.06	10.33	32.09	10.42	32.04	10.29
15	40.06	41.74	29.20	31.05	9.57	9.90	36.11	25.47	32.39	10.97	40.80	32.41	32.53	10.33	38.63	31.13	9.97	10.41	38.76
16	39.20	25.71	30.52	29.61	9.88	32.88	30.46	26.07	10.85	10.84	32.62	32.87	10.77	32.08	31.12	31.26	10.11	31.63	33.00
17	42.82	24.58	28.20	9.34	41.15	10.37	32.18	10.86	32.51	10.87	32.61	10.59	32.65	10.42	9.97	10.11	32.88	10.51	32.65
18	39.93	23.59	8.12	9.09	10.08	32.91	10.89	32.48	10.99	32.19	10.00	9.76	10.26	32.04	10.41	31.63	10.51	32.83	9.78
19	40.98	6.09	40.11	23.47	32.16	10.55	34.02	33.77	32.42	10.08	30.53	29.38	31.95	10.29	38.76	32.99	32.64	9.78	30.34

Figure 4A-9e. Average Bundle Exposure at 8.8 GWd/MT Exposure

```
        ( ROD PATTERN DEPLETION

NITER   0  POWER           IMAX  19  POWER(MWT)          4.5000E+03  ( 100.0 %)
IBOUN   1  1/4             JMAX  19  PRESSURE(PSIA)      1.0550E+03
IRN     1  MIRROR          KMAX  25  FLOW(*10E-6LB/HR)   7.8508E+01  ( 100.0 %)
ILPA    0                  NSMAX 10  BYPASS(LB/HR)       1.1742E+07  (  15.0 %)          CONTROL ROD CONFIGURATION
IFLW    2  DETAIL          LMAX  20  ENTHALPY(BTU/LB)            512.30                    IN NOTCHES WITHDRAWN
RSTART  0  NEW             LVDCT  7  INLET TEMP(DEG F)           520.47
NEWPHY  2                  IPFTL  0  BEGINNING EXPOSURE         21105.1                1  3  5  7  9 11 13 15 17 19
NEXO    3  CALC.                    DELTA EXPOS.(DELTE)             0.0
RBOCA   1                  IALPRM 0  DELBRN                      1000.0                1
IACF    0                  IFAST  0  TOTAL NOTCHES                 2176
             IPDOME   1    IAHB   0  CORE FUEL MASS         MTU:162.928                3                    63
                                     CORE FUEL MASS         STU:179.596
ENERGY (MWD) (DELTE)              0. ENERGY (MWD) (DELBRN)      179596.                5
CYCLE ENERGY (MWD)          1616379. CYCLE EXPOSURE              9000.0
CORE AVG. POWER DENSITY    54.328033                                                    7              43           18
NEUTRON MULTIPLICATION    1.00039327 FINAL AVG. EXPOSURE        22105.1
DIFP    (EPS5 = 0.00200)  0.00138080 CORE AVG. NEUTRON FLUX   1.461E+14               9
AVERAGE VOID FRACTION       0.530555 CORE AVG. GD WORTH          -0.061
CORE PRESSURE DROP,PSI      8.031613 CORE AVG. GD RESIDUAL WORTH  0.000              11       43            2
EXP RATIO INDEX (INER-II)     0.0000 CORE AVERAGE XENON WORTH   -0.0229
                                                                                     13
CORE HISTORY MAX. VALUES:       LOCATION: I   J   K
  NODAL EXPOSURE, MWD/T   53673.          7   7   5   METRIC    59164.              15 63           2           22
  BUNDLE EXPOSURE, MWD/T  42363.         13   2       METRIC    46697.
  EXPOSURE RATIO, NEXRAT  0.0000          0   0   0                                  17
  AXIAL POWER PEAK        1.3700                  5
                                                                                     19       18          22
```

Figure 4A-10a. Control Rod Pattern Summary at 9.9 GWd/MT Exposure

9.9 GWD/MT

Node	Axial Power
25	0.183
24	0.354
23	0.515
22	0.646
21	0.752
20	0.832
19	0.891
18	0.934
17	0.962
16	1.015
15	1.114
14	1.142
13	1.168
12	1.197
11	1.225
10	1.250
9	1.267
8	1.286
7	1.315
6	1.346
5	1.370
4	1.360
3	1.269
2	1.038
1	0.569

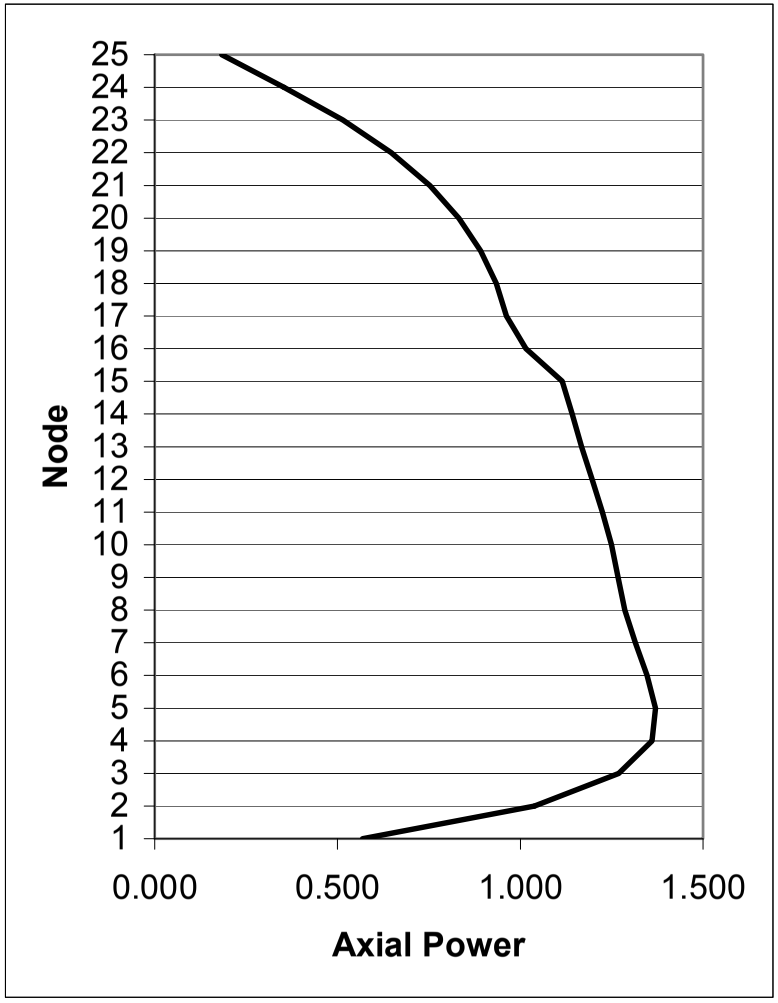

Figure 4A-10b. Relative Axial Power at 9.9 GWd/MT Exposure

9.9 GWD/MT

Node	Axial Exposure (MWD/MT)
25	5083.9
24	8778.1
23	12325.0
22	15850.3
21	18941.3
20	21499.0
19	23594.7
18	25146.1
17	26159.7
16	26950.7
15	26328.5
14	27399.0
13	28276.6
12	28877.7
11	29388.3
10	29795.0
9	29975.3
8	30200.8
7	30514.9
6	30797.1
5	30794.6
4	30024.2
3	27424.6
2	21817.4
1	11199.6

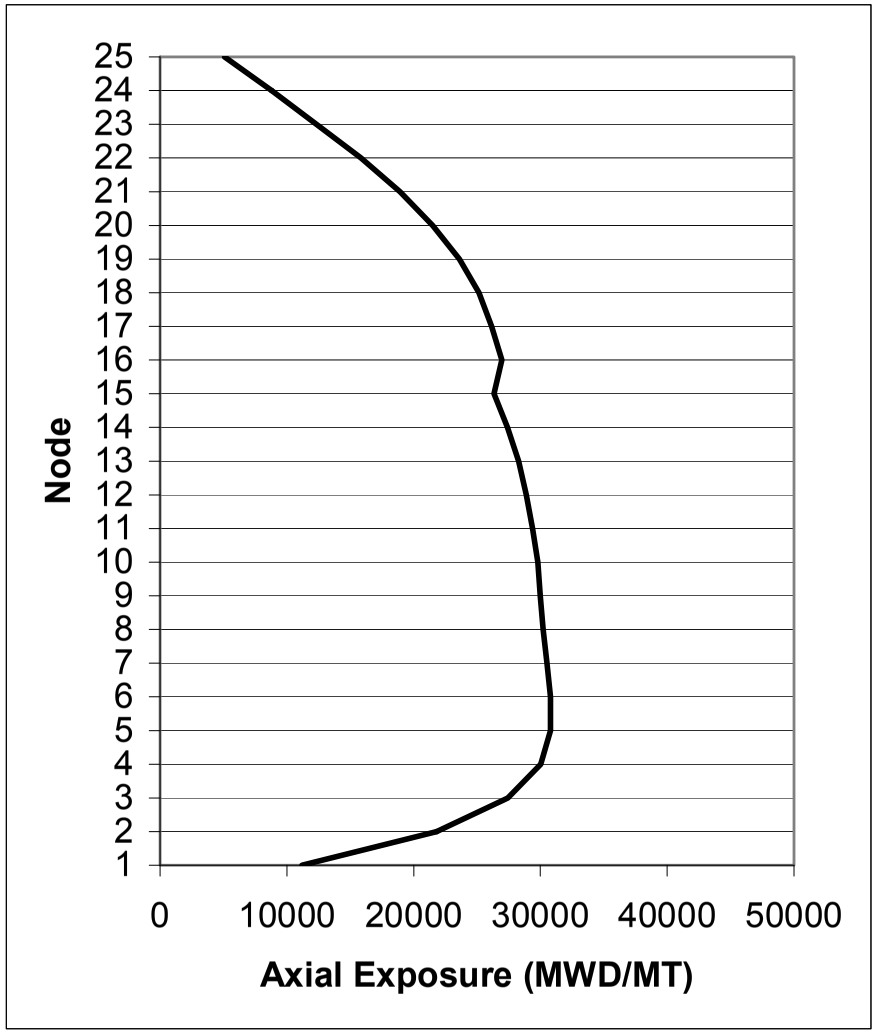

Figure 4A-10c. Axial Exposure at 9.9 GWd/MT Exposure

	1	2	3	4	5	6	7	8	9	10	11	12	13	14	15	16	17	18	19
1															0.31	0.36	0.40	0.43	0.42
2													0.35	0.45	0.50	0.66	0.72	0.74	0.73
3											0.40	0.50	0.66	0.76	0.73	0.76	0.87	0.95	0.80
4									0.38	0.49	0.68	0.82	0.92	0.97	0.85	0.90	1.06	1.07	1.05
5								0.44	0.65	0.78	0.89	0.99	1.00	1.13	1.14	1.15	0.95	1.16	1.01
6							0.43	0.67	0.85	0.92	0.98	0.97	1.18	1.08	1.24	1.08	1.21	1.03	1.12
7						0.43	0.56	0.87	0.92	1.02	0.77	0.90	1.20	1.29	1.12	1.19	1.10	1.17	0.77
8					0.44	0.67	0.87	1.00	1.10	0.99	0.93	0.86	1.26	1.24	1.28	1.25	1.29	1.06	0.79
9				0.38	0.65	0.85	0.92	1.10	1.09	1.22	1.21	1.25	1.18	1.33	1.16	1.32	1.15	1.27	1.07
10				0.49	0.78	0.92	1.02	0.99	1.22	1.11	1.28	1.15	1.32	1.13	1.24	1.23	1.29	1.15	1.29
11			0.40	0.68	0.89	0.98	0.77	0.93	1.21	1.28	1.11	1.19	1.18	1.23	0.73	0.78	1.08	1.31	1.20
12			0.50	0.82	0.99	0.97	0.90	0.86	1.25	1.15	1.19	1.18	1.30	1.22	0.77	0.77	1.23	1.30	1.22
13		0.35	0.66	0.92	1.00	1.18	1.20	1.26	1.18	1.32	1.18	1.30	1.14	1.28	1.06	1.21	1.12	1.31	1.16
14		0.45	0.76	0.97	1.13	1.08	1.29	1.24	1.33	1.13	1.23	1.22	1.28	1.12	1.27	1.13	1.30	1.14	1.22
15	0.31	0.50	0.73	0.85	1.14	1.24	1.12	1.28	1.16	1.24	0.73	0.77	1.06	1.27	1.10	1.18	1.29	1.23	0.81
16	0.36	0.66	0.76	0.90	1.15	1.08	1.19	1.25	1.32	1.23	0.78	0.77	1.21	1.13	1.18	1.18	1.29	1.09	0.84
17	0.40	0.72	0.87	1.06	0.95	1.22	1.10	1.29	1.15	1.29	1.08	1.23	1.12	1.30	1.29	1.29	1.14	1.27	1.07
18	0.43	0.74	0.95	1.07	1.16	1.03	1.17	1.06	1.27	1.15	1.31	1.30	1.31	1.14	1.23	1.09	1.27	1.13	1.28
19	0.42	0.73	0.80	1.05	1.01	1.12	0.77	0.79	1.07	1.29	1.20	1.22	1.16	1.22	0.81	0.84	1.07	1.28	1.19

Figure 4A-10d. Relative Integrated Power Per Bundle at 9.9 GWd/MT Exposure

	1	2	3	4	5	6	7	8	9	10	11	12	13	14	15	16	17	18	19
1															40.43	39.61	43.29	40.42	41.46
2													46.70	42.32	42.32	26.49	25.42	24.43	6.92
3											43.41	41.76	26.46	7.70	30.11	31.47	29.21	9.19	41.01
4									42.92	42.01	24.42	7.76	8.76	9.40	32.08	30.71	10.54	10.31	24.69
5								45.48	21.28	7.49	8.53	9.52	28.66	10.60	10.81	11.15	42.21	11.39	33.35
6							42.56	22.97	8.16	8.97	9.91	31.69	11.19	33.38	11.17	34.04	11.69	34.12	11.90
7						42.56	44.39	8.24	27.69	10.30	41.66	31.26	11.38	11.60	37.13	31.55	33.38	12.26	35.25
8					45.49	22.97	8.24	9.36	10.51	32.48	28.72	41.91	11.95	25.50	26.64	27.23	12.23	33.72	35.01
9				42.93	21.28	8.16	27.69	10.51	29.40	11.29	11.32	11.75	32.94	12.42	33.64	12.25	33.77	12.38	33.65
10				42.01	7.49	8.97	10.30	32.48	11.29	33.82	11.21	32.88	12.11	34.20	12.39	12.25	12.28	33.42	11.37
11			43.42	24.42	8.53	9.91	41.67	28.72	11.32	11.21	39.43	31.44	33.22	12.19	41.99	33.89	33.85	11.29	31.40
12			41.77	7.76	9.52	31.68	31.25	41.92	11.75	32.88	31.44	32.39	11.71	12.03	33.67	34.11	11.97	11.04	30.25
13		46.67	26.46	8.76	28.66	11.19	11.38	11.95	32.94	12.11	33.22	11.71	34.45	12.16	33.77	12.14	33.89	11.61	33.10
14		42.33	7.70	9.40	10.60	33.38	11.60	25.50	12.42	34.20	12.20	12.03	12.16	34.28	11.64	33.27	11.77	33.27	11.62
15	40.43	42.33	30.11	32.07	10.81	11.17	37.14	26.64	33.64	12.39	42.00	33.67	33.77	11.64	39.55	32.09	11.26	11.76	39.92
16	39.62	26.49	31.46	30.71	11.15	34.03	31.55	27.23	12.25	12.25	33.89	34.11	12.14	33.27	32.09	32.22	11.41	32.85	34.21
17	43.29	25.42	29.21	10.54	42.22	11.69	33.38	12.23	33.77	12.29	33.85	11.97	33.88	11.77	11.26	11.41	34.08	11.87	33.86
18	40.43	24.43	9.19	10.31	11.39	34.12	12.26	33.72	12.39	33.41	11.30	11.05	11.61	33.27	11.76	32.85	11.87	34.03	11.07
19	41.46	6.92	41.02	24.69	33.35	11.91	35.24	35.00	33.65	11.37	31.40	30.25	33.10	11.62	39.92	34.21	33.85	11.07	31.32

Figure 4A-10e. Average Bundle Exposure at 9.9 GWd/MT Exposure

```
        ( ROD PATTERN DEPLETION

NITER   0  POWER           IMAX  19  POWER(MWT)          4.5000E+03  ( 100.0 %)
IBOUN   1  1/4             JMAX  19  PRESSURE(PSIA)      1.0550E+03
IRN     1  MIRROR          KMAX  25  FLOW(*10E-6LB/HR)   7.8508E+01  ( 100.0 %)
ILPA    0                  NSMAX 10  BYPASS(LB/HR)       1.1742E+07  (  15.0 %)
IFLW    2  DETAIL          LMAX  20  ENTHALPY(BTU/LB)           512.30
RSTART  0  NEW             LVDCT  5  INLET TEMP(DEG F)          520.47
NEWPHY  2                  IPFTL  0  BEGINNING EXPOSURE        22105.1
NEXO    3  CALC.                    DELTA EXPOS.(DELTE)           0.0
RBOCA   1                  IALPRM 0  DELBRN                    1000.0
IACF    0                  IFAST  0  TOTAL NOTCHES               2176
             IPDOME   1    IAHB   0  CORE FUEL MASS        MTU:162.928
                                     CORE FUEL MASS        STU:179.596
ENERGY (MWD) (DELTE)              0. ENERGY (MWD) (DELBRN)     179596.
CYCLE ENERGY (MWD)          1795977. CYCLE EXPOSURE            10000.0
CORE AVG. POWER DENSITY    54.328033
NEUTRON MULTIPLICATION    1.00122511 FINAL AVG. EXPOSURE       23105.1
DIFP   (EPS5 = 0.00200)   0.00131738 CORE AVG. NEUTRON FLUX  1.462E+14
AVERAGE VOID FRACTION       0.530505 CORE AVG. GD WORTH         -0.052
CORE PRESSURE DROP,PSI      8.042318 CORE AVG. GD RESIDUAL WORTH  0.000
EXP RATIO INDEX (INER-II)     0.0000 CORE AVERAGE XENON WORTH   -0.0232

CORE HISTORY MAX. VALUES:      LOCATION: I   J   K
  NODAL EXPOSURE, MWD/T   54292.         7   7   5   METRIC    59847.
  BUNDLE EXPOSURE, MWD/T  42715.        13   2       METRIC    47085.
  EXPOSURE RATIO, NEXRAT  0.0000         0   0   0
  AXIAL POWER PEAK        1.3741                 5
```

CONTROL ROD CONFIGURATION
IN NOTCHES WITHDRAWN

```
    1  3  5  7  9 11 13 15 17 19
 1
 3                    63
 5
 7              43           18
 9
11        43            2
13
15 63            2           22
17
19        18           22
```

Figure 4A-11a. Control Rod Pattern Summary at 11.0 GWd/MT Exposure

11.0 GWD/MT

Node	Axial Power
25	0.186
24	0.360
23	0.523
22	0.655
21	0.760
20	0.839
19	0.898
18	0.940
17	0.966
16	1.014
15	1.106
14	1.129
13	1.152
12	1.179
11	1.207
10	1.232
9	1.253
8	1.275
7	1.308
6	1.345
5	1.374
4	1.372
3	1.289
2	1.056
1	0.579

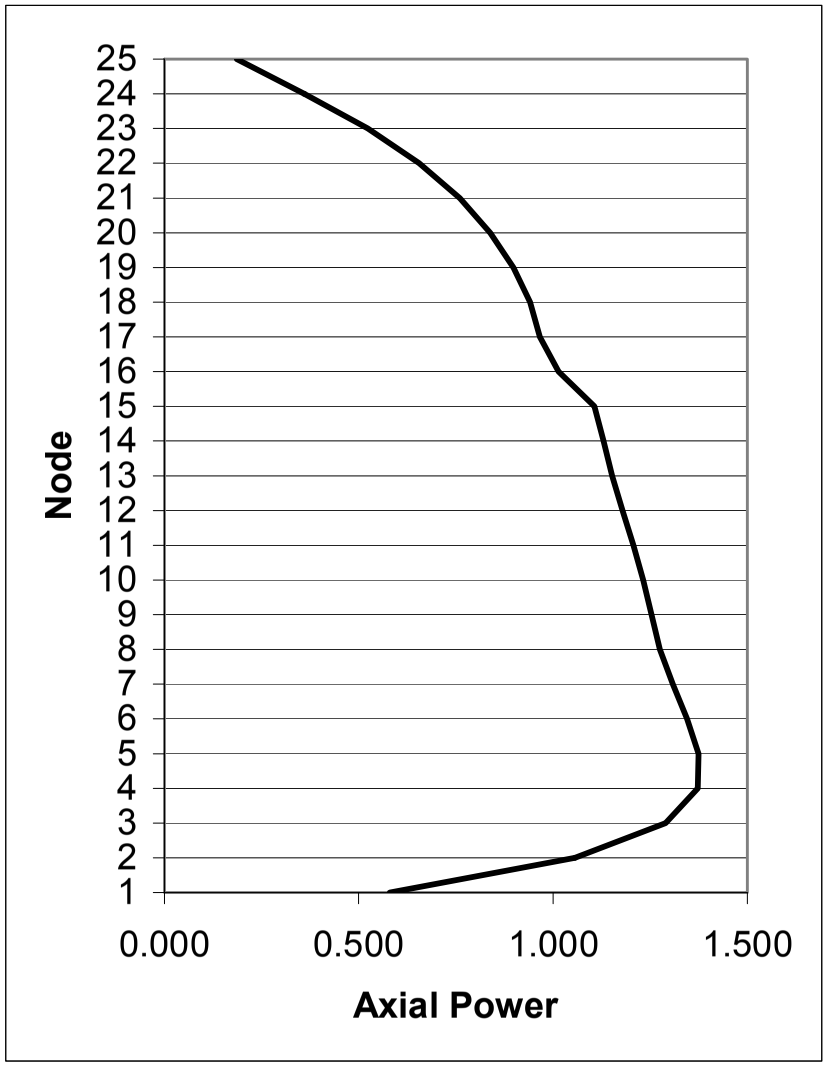

Figure 4A-11b. Relative Axial Power at 11.0 GWd/MT Exposure

11.0 GWD/MT

Node	Axial Exposure (MWD/MT)
25	5347.9
24	9226.0
23	12951.5
22	16636.9
21	19856.9
20	22510.9
19	24678.8
18	26282.9
17	27330.1
16	28140.6
15	27475.0
14	28574.0
13	29477.7
12	30108.8
11	30648.2
10	31080.6
9	31280.1
8	31524.8
7	31868.9
6	32183.9
5	32205.7
4	31425.4
3	28732.0
2	22886.8
1	11773.3

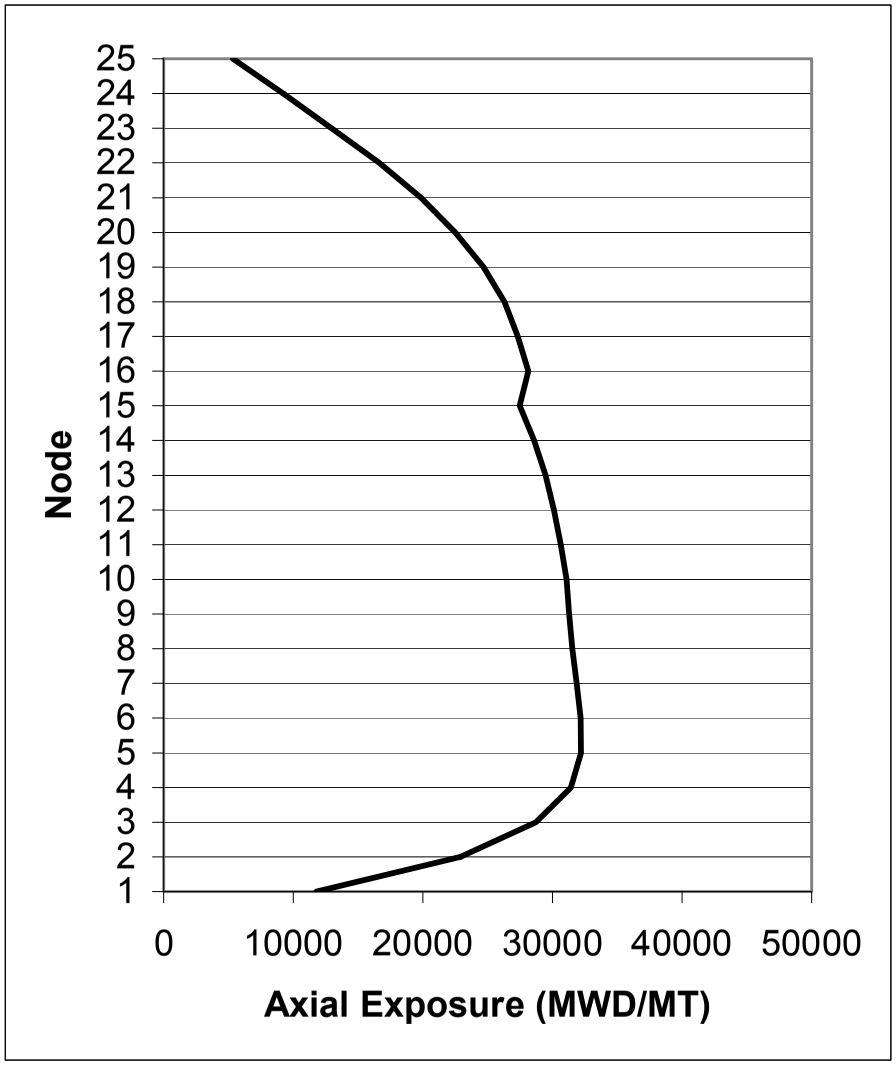

Figure 4A-11c. Axial Exposure at 11.0 GWd/MT Exposure

	1	2	3	4	5	6	7	8	9	10	11	12	13	14	15	16	17	18	19
1															0.30	0.35	0.39	0.42	0.41
2													0.35	0.44	0.49	0.64	0.70	0.72	0.73
3											0.40	0.50	0.66	0.76	0.72	0.74	0.86	0.94	0.78
4									0.37	0.49	0.68	0.82	0.93	0.98	0.84	0.89	1.06	1.07	1.03
5								0.44	0.65	0.80	0.90	1.00	1.00	1.14	1.15	1.15	0.94	1.16	1.00
6							0.43	0.67	0.86	0.94	1.00	0.97	1.19	1.07	1.24	1.07	1.22	1.02	1.12
7						0.43	0.56	0.88	0.92	1.04	0.77	0.90	1.21	1.29	1.10	1.17	1.09	1.17	0.77
8					0.44	0.67	0.88	1.01	1.12	0.99	0.93	0.86	1.27	1.22	1.26	1.23	1.29	1.04	0.78
9				0.37	0.65	0.86	0.92	1.12	1.09	1.23	1.23	1.26	1.17	1.34	1.15	1.33	1.14	1.27	1.05
10				0.49	0.80	0.94	1.04	0.99	1.23	1.11	1.30	1.14	1.32	1.13	1.25	1.25	1.30	1.14	1.30
11			0.40	0.68	0.90	1.00	0.77	0.93	1.23	1.30	1.10	1.18	1.17	1.24	0.73	0.78	1.08	1.32	1.19
12			0.50	0.82	1.00	0.97	0.90	0.86	1.26	1.14	1.18	1.17	1.32	1.24	0.77	0.77	1.24	1.32	1.21
13		0.35	0.66	0.93	1.00	1.19	1.21	1.27	1.17	1.32	1.17	1.32	1.14	1.29	1.06	1.22	1.12	1.33	1.15
14		0.44	0.76	0.98	1.14	1.07	1.29	1.22	1.34	1.13	1.24	1.24	1.29	1.12	1.29	1.13	1.32	1.14	1.24
15	0.30	0.49	0.72	0.84	1.15	1.24	1.10	1.26	1.15	1.25	0.73	0.77	1.06	1.29	1.10	1.17	1.31	1.25	0.81
16	0.35	0.64	0.74	0.89	1.15	1.07	1.17	1.23	1.33	1.25	0.78	0.77	1.22	1.13	1.17	1.17	1.31	1.09	0.83
17	0.39	0.70	0.86	1.06	0.94	1.22	1.09	1.29	1.14	1.30	1.08	1.24	1.12	1.32	1.31	1.31	1.14	1.28	1.07
18	0.42	0.72	0.94	1.07	1.16	1.02	1.17	1.04	1.27	1.14	1.32	1.32	1.33	1.14	1.25	1.09	1.28	1.13	1.30
19	0.41	0.73	0.78	1.03	1.00	1.12	0.77	0.78	1.05	1.30	1.19	1.21	1.15	1.24	0.81	0.83	1.07	1.30	1.18

Figure 4A-11d. Relative Integrated Power Per Bundle at 11.0 GWd/MT Exposure

	1	2	3	4	5	6	7	8	9	10	11	12	13	14	15	16	17	18	19
1															40.77	40.01	43.73	40.90	41.93
2													47.09	42.82	42.87	27.22	26.21	25.25	7.73
3											43.85	42.31	27.19	8.54	30.92	32.30	30.18	10.24	41.89
4									43.33	42.55	25.18	8.66	9.77	10.47	33.01	31.70	11.71	11.49	25.85
5								45.97	22.00	8.35	9.51	10.61	29.77	11.85	12.07	12.42	43.26	12.66	34.47
6							43.04	23.71	9.10	9.99	11.00	32.76	12.49	34.57	12.53	35.23	13.03	35.26	13.14
7						43.04	45.01	9.20	28.71	11.42	42.51	32.25	12.70	13.02	38.37	32.87	34.59	13.55	36.10
8					45.98	23.71	9.20	10.46	11.72	33.57	29.76	42.85	13.33	26.86	28.05	28.61	13.64	34.88	35.88
9				43.34	22.00	9.10	28.70	11.72	30.61	12.63	12.66	13.13	34.24	13.89	34.92	13.70	35.03	13.78	34.83
10				42.56	8.35	9.99	11.42	33.57	12.63	35.05	12.62	34.15	13.56	35.45	13.75	13.60	13.71	34.69	12.79
11			43.86	25.17	9.51	11.00	42.52	29.75	12.66	12.62	40.66	32.76	34.52	13.55	42.80	34.75	35.04	12.73	32.73
12			42.32	8.67	10.61	32.76	32.25	42.86	13.13	34.15	32.75	33.69	13.15	13.37	34.52	34.96	13.32	12.48	31.59
13		47.06	27.19	9.77	29.77	12.49	12.70	13.34	34.24	13.56	34.52	13.15	35.71	13.56	34.94	13.48	35.12	13.05	34.38
14		42.82	8.54	10.47	11.85	34.56	13.02	26.87	13.89	35.45	13.55	13.38	13.56	35.52	13.05	34.52	13.20	34.52	12.97
15	40.78	42.88	30.92	33.01	12.07	12.54	38.37	28.05	34.92	13.75	42.81	34.52	34.94	13.05	40.77	33.39	12.68	13.11	40.82
16	40.01	27.21	32.29	31.70	12.42	35.22	32.87	28.61	13.70	13.61	34.75	34.96	13.48	34.51	33.38	33.52	12.84	34.05	35.13
17	43.73	26.22	30.18	11.71	43.27	13.03	34.59	13.65	35.03	13.71	35.04	13.32	35.12	13.21	12.68	12.84	35.34	13.26	35.04
18	40.90	25.25	10.24	11.49	12.67	35.25	13.55	34.88	13.78	34.68	12.74	12.48	13.05	34.52	13.11	34.05	13.26	35.28	12.47
19	41.93	7.73	41.90	25.85	34.46	13.14	36.10	35.88	34.83	12.80	32.72	31.59	34.38	12.97	40.82	35.13	35.03	12.48	32.63

Figure 4A-11e. Average Bundle Exposure at 11.0 GWd/MT Exposure

```
        ( ROD PATTERN DEPLETION

NITER   0  POWER           IMAX  19  POWER(MWT)          4.5000E+03  ( 100.0 %)
IBOUN   1  1/4             JMAX  19  PRESSURE(PSIA)      1.0550E+03
IRN     1  MIRROR          KMAX  25  FLOW(*10E-6LB/HR)   7.8508E+01  ( 100.0 %)
ILPA    0                  NSMAX 10  BYPASS(LB/HR)       1.1742E+07  (  15.0 %)          CONTROL ROD CONFIGURATION
IFLW    2  DETAIL          LMAX  20  ENTHALPY(BTU/LB)            512.30                    IN NOTCHES WITHDRAWN
RSTART  0  NEW             LVDCT  7  INLET TEMP(DEG F)           520.47
NEWPHY  2                  IPFTL  0  BEGINNING EXPOSURE         23105.1                1  3  5  7  9 11 13 15 17 19
NEXO    3  CALC.                    DELTA EXPOS.(DELTE)            0.0
RBOCA   1                  IALPRM 0  DELBRN                     1000.0                1
IACF    0                  IFAST  0  TOTAL NOTCHES                2220
             IPDOME   1    IAHB   0  CORE FUEL MASS         MTU:162.928                3                    83
                                     CORE FUEL MASS         STU:179.596
ENERGY (MWD) (DELTE)              0. ENERGY (MWD) (DELBRN)      179596.                5
CYCLE ENERGY (MWD)          1975574. CYCLE EXPOSURE             11000.0
CORE AVG. POWER DENSITY    54.328033                                                    7              28            6
NEUTRON MULTIPLICATION    0.99892431 FINAL AVG. EXPOSURE        24105.1
DIFP    (EPS5 = 0.00200)  0.00093365 CORE AVG. NEUTRON FLUX   1.467E+14                9
AVERAGE VOID FRACTION       0.541181 CORE AVG. GD WORTH          -0.044
CORE PRESSURE DROP,PSI      8.078023 CORE AVG. GD RESIDUAL WORTH  0.000               11       28            7
EXP RATIO INDEX (INER-II)      0.0000 CORE AVERAGE XENON WORTH   -0.0235
                                                                                      13
CORE HISTORY MAX. VALUES:       LOCATION: I   J   K
  NODAL EXPOSURE, MWD/T   54927.          7   7   5   METRIC    60546.               15 83           7           3
  BUNDLE EXPOSURE, MWD/T  43063.         13   2       METRIC    47468.
  EXPOSURE RATIO, NEXRAT  0.0000          0   0   0                                   17
  AXIAL POWER PEAK        1.4387                  4
                                                                                      19        6           3
```

Figure 4A-12a. Control Rod Pattern Summary at 12.1 GWd/MT Exposure

12.1 GWD/MT

Node	Axial Power
25	0.182
24	0.352
23	0.505
22	0.622
21	0.721
20	0.800
19	0.863
18	0.905
17	0.919
16	0.961
15	1.049
14	1.081
13	1.119
12	1.156
11	1.194
10	1.232
9	1.271
8	1.315
7	1.361
6	1.404
5	1.438
4	1.439
3	1.362
2	1.127
1	0.621

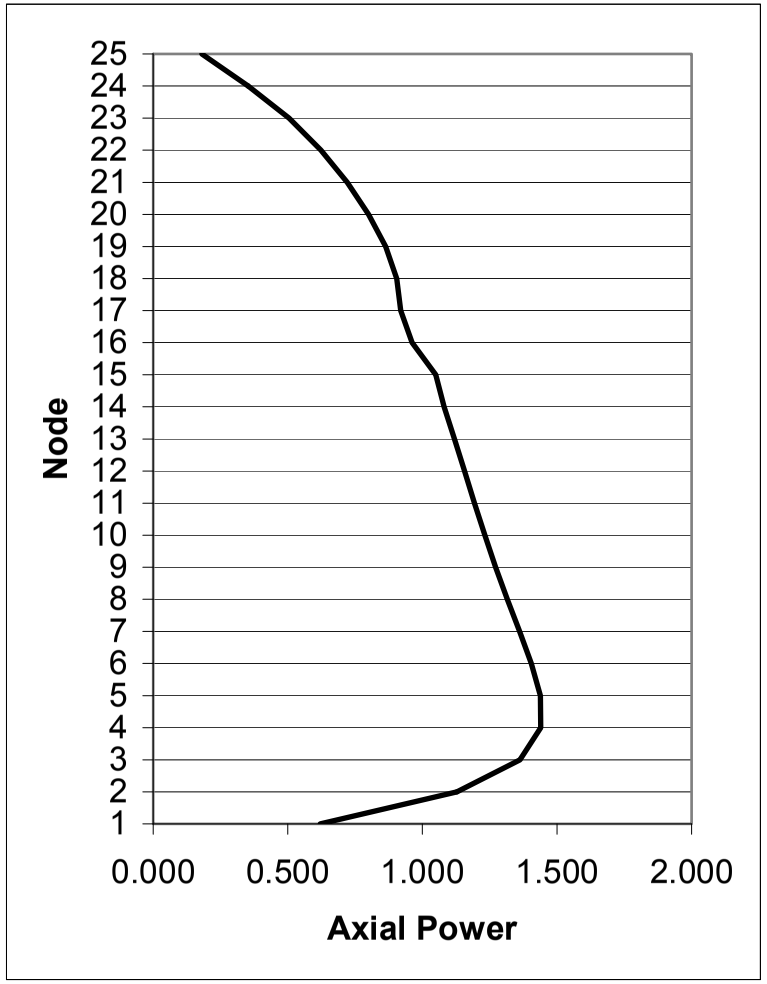

Figure 4A-12b. Relative Axial Power at 12.1 GWd/MT Exposure

12.1 GWD/MT

Node	Axial Exposure (MWD/MT)
25	5616.5
24	9682.3
23	13588.3
22	17433.5
21	20781.7
20	23531.4
19	25771.3
18	27427.1
17	28505.0
16	29329.3
15	28612.9
14	29735.8
13	30662.8
12	31321.9
11	31889.6
10	32348.5
9	32570.2
8	32838.3
7	33216.6
6	33569.1
5	33620.9
4	32838.8
3	30060.0
2	23974.6
1	12358.0

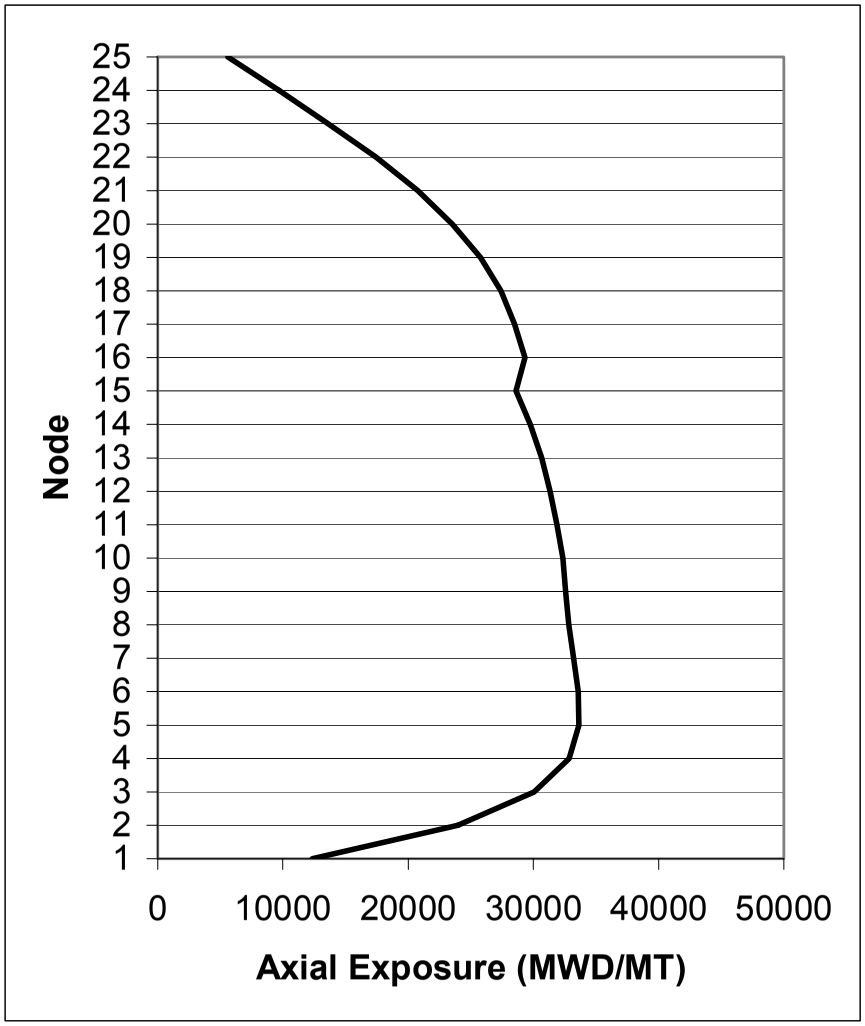

Figure 4A-12c. Axial Exposure at 12.1 GWd/MT Exposure

	1	2	3	4	5	6	7	8	9	10	11	12	13	14	15	16	17	18	19
1															0.31	0.36	0.40	0.43	0.42
2													0.36	0.46	0.51	0.66	0.72	0.74	0.74
3											0.41	0.51	0.68	0.81	0.78	0.80	0.88	0.98	0.79
4									0.38	0.49	0.69	0.85	0.97	1.03	0.92	0.96	1.11	1.11	1.04
5								0.44	0.66	0.81	0.92	1.02	1.01	1.19	1.20	1.20	0.95	1.18	0.99
6							0.43	0.67	0.87	0.95	0.99	0.95	1.20	1.08	1.27	1.07	1.23	1.02	1.12
7						0.43	0.56	0.89	0.91	1.02	0.70	0.82	1.21	1.30	1.10	1.16	1.07	1.16	0.71
8					0.44	0.67	0.89	1.02	1.11	0.96	0.85	0.78	1.25	1.20	1.24	1.21	1.29	1.02	0.73
9				0.38	0.66	0.87	0.91	1.11	1.07	1.22	1.21	1.24	1.15	1.33	1.14	1.33	1.13	1.27	1.03
10				0.49	0.81	0.95	1.02	0.96	1.22	1.09	1.29	1.12	1.32	1.12	1.26	1.26	1.31	1.13	1.31
11			0.41	0.69	0.92	0.99	0.70	0.85	1.21	1.29	1.08	1.15	1.16	1.25	0.75	0.79	1.08	1.33	1.18
12			0.51	0.85	1.02	0.95	0.82	0.78	1.24	1.12	1.15	1.15	1.33	1.25	0.79	0.78	1.26	1.33	1.19
13		0.36	0.68	0.97	1.01	1.20	1.21	1.25	1.15	1.32	1.16	1.33	1.14	1.31	1.06	1.24	1.12	1.33	1.13
14		0.46	0.81	1.03	1.19	1.08	1.30	1.20	1.33	1.12	1.25	1.25	1.31	1.12	1.30	1.12	1.33	1.12	1.23
15	0.31	0.51	0.78	0.92	1.20	1.27	1.10	1.24	1.14	1.26	0.75	0.79	1.06	1.30	1.09	1.16	1.32	1.23	0.73
16	0.36	0.66	0.80	0.96	1.20	1.07	1.16	1.21	1.33	1.26	0.79	0.78	1.24	1.12	1.16	1.15	1.31	1.05	0.74
17	0.40	0.72	0.88	1.11	0.95	1.23	1.07	1.29	1.13	1.31	1.08	1.26	1.12	1.33	1.32	1.31	1.11	1.26	1.02
18	0.43	0.74	0.98	1.11	1.18	1.02	1.16	1.02	1.27	1.14	1.33	1.33	1.33	1.12	1.23	1.05	1.26	1.10	1.28
19	0.42	0.74	0.79	1.04	0.99	1.12	0.71	0.73	1.03	1.31	1.18	1.19	1.13	1.23	0.73	0.74	1.02	1.28	1.15

Figure 4A-12d. Relative Integrated Power Per Bundle at 12.1 GWd/MT Exposure

	1	2	3	4	5	6	7	8	9	10	11	12	13	14	15	16	17	18	19
1															41.11	40.39	44.16	41.36	42.39
2													47.47	43.30	43.41	27.92	26.99	26.05	8.53
3											44.30	42.86	27.92	9.38	31.71	33.12	31.12	11.29	42.75
4									43.75	43.09	25.93	9.57	10.80	11.54	33.94	32.68	12.88	12.68	26.99
5								46.46	22.72	9.23	10.51	11.71	30.88	13.11	13.34	13.69	44.30	13.94	35.57
6							43.52	24.46	10.05	11.03	12.10	33.83	13.80	35.75	13.90	36.40	14.36	36.38	14.37
7						43.52	45.63	10.17	29.73	12.57	43.35	33.24	14.04	14.44	39.59	34.16	35.79	14.83	36.94
8					46.46	24.46	10.17	11.57	12.95	34.66	30.78	43.80	14.73	28.21	29.44	29.96	15.06	36.03	36.74
9				43.75	22.72	10.05	29.72	12.95	31.82	13.99	14.01	14.51	35.54	15.37	36.18	15.16	36.29	15.19	35.99
10				43.10	9.23	11.03	12.57	34.66	13.99	36.27	14.05	35.41	15.01	36.69	15.13	14.98	15.15	35.95	14.23
11			44.30	25.93	10.51	12.10	43.36	30.78	14.01	14.05	41.87	34.05	35.81	14.91	43.60	35.61	36.22	14.19	34.04
12			42.87	9.57	11.71	33.83	33.24	43.81	14.51	35.41	34.05	34.98	14.60	14.74	35.37	35.81	14.69	13.93	32.92
13		47.44	27.92	10.80	30.88	13.80	14.04	14.73	35.54	15.02	35.81	14.60	36.96	14.99	36.10	14.82	36.36	14.51	35.65
14		43.31	9.38	11.54	13.11	35.74	14.44	28.22	15.37	36.69	14.92	14.74	14.99	36.75	14.47	35.77	14.66	35.77	14.33
15	41.11	43.42	31.71	33.93	13.34	13.90	39.59	29.44	36.18	15.13	43.61	35.37	36.10	14.47	41.98	34.68	14.12	14.48	41.72
16	40.39	27.92	33.11	32.68	13.69	36.39	34.16	29.96	15.16	14.98	35.61	35.81	14.83	35.76	34.67	34.81	14.29	35.25	36.05
17	44.16	26.99	31.12	12.88	44.31	14.37	35.79	15.06	36.28	15.15	36.22	14.69	36.36	14.66	14.12	14.29	36.59	14.67	36.21
18	41.37	26.05	11.29	12.68	13.94	36.38	14.84	36.03	15.19	35.94	14.19	13.93	14.51	35.77	14.49	35.25	14.67	36.52	13.90
19	42.39	8.53	42.76	26.99	35.56	14.38	36.94	36.74	35.99	14.23	34.04	32.92	35.64	14.34	41.71	36.05	36.21	13.90	33.94

Figure 4A-12e. Average Bundle Exposure at 12.1 GWd/MT Exposure

```
        ( ROD PATTERN DEPLETION

NITER   0  POWER           IMAX  19  POWER(MWT)          4.5000E+03  ( 100.0 %)
IBOUN   1  1/4             JMAX  19  PRESSURE(PSIA)      1.0550E+03
IRN     1  MIRROR          KMAX  25  FLOW(*10E-6LB/HR)   7.8508E+01  ( 100.0 %)
ILPA    0                  NSMAX 10  BYPASS(LB/HR)       1.1742E+07  (  15.0 %)
IFLW    2  DETAIL          LMAX  20  ENTHALPY(BTU/LB)            512.30
RSTART  0  NEW             LVDCT  7  INLET TEMP(DEG F)           520.47
NEWPHY  2                  IPFTL  0  BEGINNING EXPOSURE         24105.1
NEXO    3  CALC.                    DELTA EXPOS.(DELTE)            0.0
RBOCA   1                  IALPRM 0  DELBRN                     1000.0
IACF    0                  IFAST  0  TOTAL NOTCHES                2220
             IPDOME   1    IAHB   0  CORE FUEL MASS         MTU:162.928
                                     CORE FUEL MASS         STU:179.596
ENERGY (MWD) (DELTE)              0. ENERGY (MWD) (DELBRN)      179596.
CYCLE ENERGY (MWD)          2155172. CYCLE EXPOSURE             12000.0
CORE AVG. POWER DENSITY    54.328033
NEUTRON MULTIPLICATION    0.99814355 FINAL AVG. EXPOSURE        25105.1
DIFP   (EPS5 = 0.00200)   0.00133348 CORE AVG. NEUTRON FLUX   1.468E+14
AVERAGE VOID FRACTION       0.529696 CORE AVG. GD WORTH          -0.038
CORE PRESSURE DROP,PSI      8.065024 CORE AVG. GD RESIDUAL WORTH  0.000
EXP RATIO INDEX (INER-II)     0.0000 CORE AVERAGE XENON WORTH   -0.0236

CORE HISTORY MAX. VALUES:      LOCATION: I   J   K
  NODAL EXPOSURE, MWD/T   55610.         7   7   5   METRIC    61299.
  BUNDLE EXPOSURE, MWD/T  43424.        13   2       METRIC    47867.
  EXPOSURE RATIO, NEXRAT  0.0000         0   0   0
  AXIAL POWER PEAK        1.3380                 5
```

CONTROL ROD CONFIGURATION
IN NOTCHES WITHDRAWN

```
    1  3  5  7  9 11 13 15 17 19
 1
 3                      83
 5
 7               28             6
 9
11        28             7
13
15 83             7             3
17
19         6             3
```

Figure 4A-13a. Control Rod Pattern Summary at 13.2 GWd/MT Exposure

13.2 GWD/MT

Node	Axial Power
25	0.200
24	0.389
23	0.556
22	0.682
21	0.789
20	0.872
19	0.937
18	0.976
17	0.982
16	1.017
15	1.098
14	1.117
13	1.143
12	1.168
11	1.192
10	1.217
9	1.242
8	1.270
7	1.298
6	1.323
5	1.338
4	1.327
3	1.252
2	1.041
1	0.573

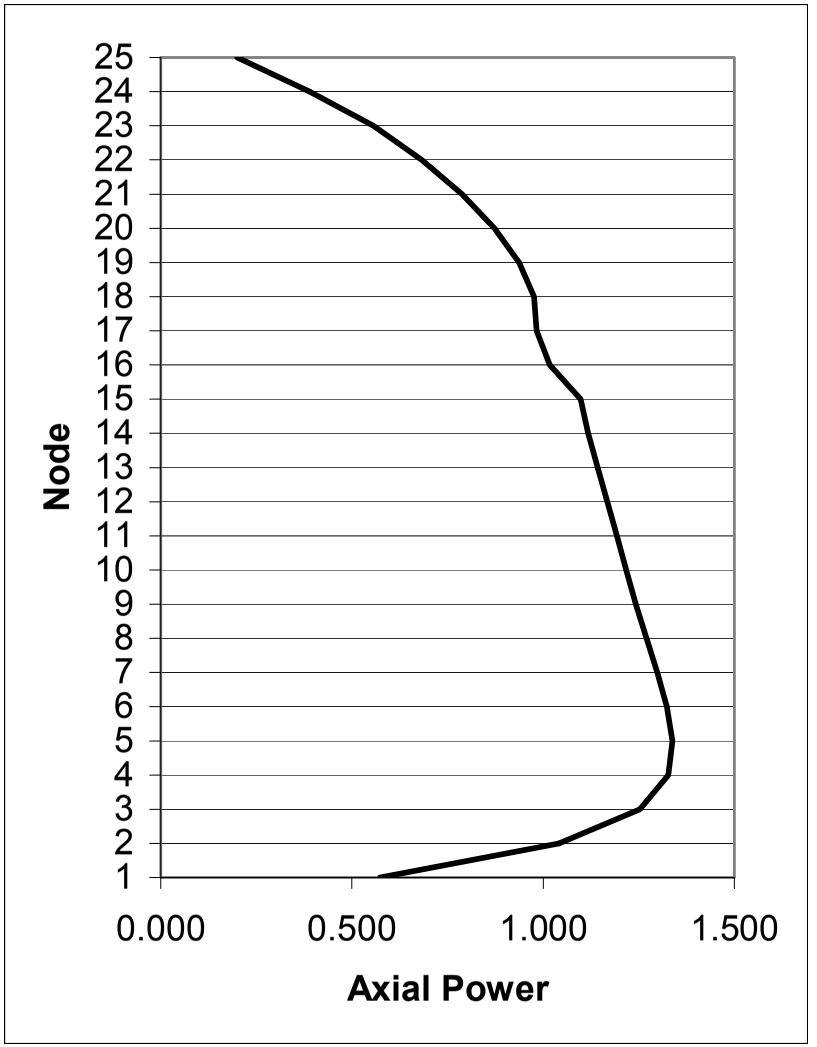

Figure 4A-13b. Relative Axial Power at 13.2 GWd/MT Exposure

13.2 GWD/MT

Node	Axial Exposure (MWD/MT)
25	5878.4
24	10128.0
23	14202.6
22	18190.7
21	21659.4
20	24505.2
19	26821.5
18	28527.8
17	29623.2
16	30455.9
15	29692.3
14	30847.5
13	31813.5
12	32511.5
11	33118.0
10	33616.4
9	33879.4
8	34193.0
7	34618.5
6	35015.6
5	35101.5
4	34320.6
3	31462.8
2	25135.6
1	12984.5

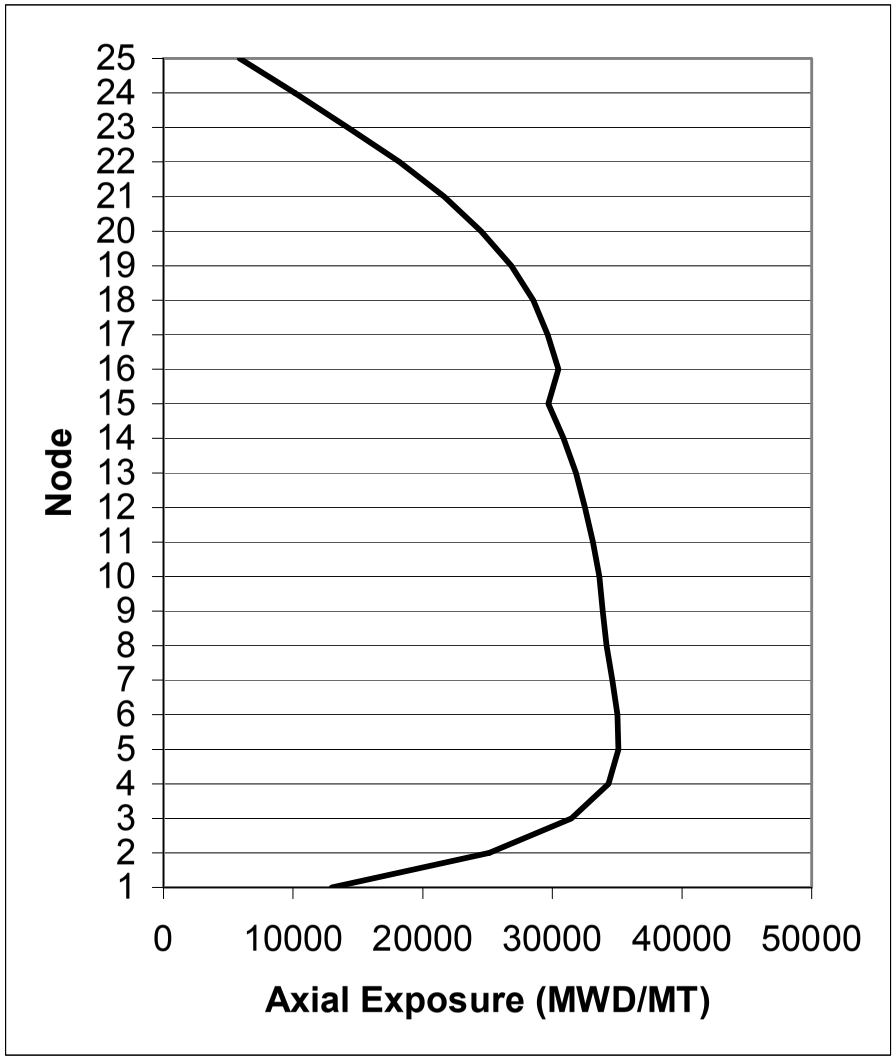

Figure 4A-13c. Axial Exposure at 13.2 GWd/MT Exposure

	1	2	3	4	5	6	7	8	9	10	11	12	13	14	15	16	17	18	19
1															0.31	0.36	0.40	0.43	0.42
2													0.37	0.46	0.51	0.66	0.72	0.74	0.75
3											0.42	0.52	0.69	0.83	0.79	0.80	0.88	0.99	0.79
4									0.39	0.51	0.71	0.88	0.99	1.06	0.92	0.96	1.12	1.12	1.03
5								0.45	0.67	0.84	0.95	1.05	1.03	1.21	1.22	1.21	0.95	1.19	0.99
6							0.44	0.69	0.90	0.98	1.03	0.97	1.22	1.08	1.28	1.06	1.23	1.01	1.12
7						0.44	0.57	0.92	0.93	1.05	0.71	0.83	1.21	1.30	1.08	1.14	1.06	1.15	0.71
8					0.45	0.69	0.92	1.05	1.14	0.97	0.86	0.79	1.25	1.19	1.21	1.19	1.27	1.00	0.72
9				0.39	0.67	0.90	0.93	1.14	1.08	1.23	1.22	1.24	1.14	1.32	1.12	1.31	1.11	1.25	1.01
10				0.51	0.84	0.98	1.05	0.97	1.23	1.09	1.29	1.11	1.31	1.10	1.24	1.25	1.30	1.12	1.29
11			0.42	0.71	0.95	1.03	0.71	0.86	1.22	1.29	1.07	1.14	1.14	1.24	0.74	0.79	1.06	1.32	1.16
12			0.52	0.88	1.05	0.97	0.83	0.79	1.24	1.11	1.14	1.14	1.32	1.25	0.78	0.78	1.25	1.33	1.17
13		0.37	0.69	0.99	1.03	1.22	1.21	1.25	1.14	1.31	1.14	1.32	1.12	1.30	1.05	1.23	1.11	1.32	1.12
14		0.46	0.83	1.06	1.21	1.08	1.30	1.19	1.32	1.10	1.24	1.25	1.30	1.11	1.29	1.11	1.32	1.11	1.22
15	0.31	0.51	0.79	0.92	1.22	1.28	1.08	1.21	1.12	1.24	0.74	0.78	1.05	1.29	1.07	1.14	1.31	1.23	0.72
16	0.36	0.66	0.80	0.96	1.21	1.06	1.14	1.19	1.31	1.25	0.79	0.78	1.23	1.11	1.14	1.14	1.30	1.04	0.73
17	0.40	0.72	0.88	1.12	0.95	1.23	1.06	1.27	1.11	1.30	1.06	1.25	1.11	1.32	1.31	1.30	1.10	1.26	1.01
18	0.43	0.74	0.99	1.12	1.19	1.01	1.15	1.00	1.25	1.12	1.32	1.33	1.32	1.11	1.23	1.04	1.26	1.09	1.28
19	0.42	0.75	0.79	1.03	0.99	1.12	0.71	0.72	1.01	1.29	1.16	1.17	1.12	1.22	0.72	0.73	1.01	1.28	1.13

Figure 4A-13d. Relative Integrated Power Per Bundle at 13.2 GWd/MT Exposure

	1	2	3	4	5	6	7	8	9	10	11	12	13	14	15	16	17	18	19
1															41.45	40.78	44.60	41.83	42.85
2													47.87	43.81	43.97	28.65	27.78	26.86	9.35
3											44.74	43.42	28.67	10.28	32.58	34.00	32.09	12.36	43.62
4									44.16	43.64	26.69	10.51	11.86	12.68	34.94	33.74	14.10	13.90	28.13
5								46.95	23.45	10.12	11.52	12.84	32.00	14.42	14.66	15.02	45.35	15.24	36.66
6							44.00	25.20	11.01	12.07	13.20	34.89	15.13	36.93	15.30	37.58	15.72	37.50	15.61
7						44.00	46.24	11.15	30.73	13.69	44.12	34.15	15.36	15.87	40.79	35.44	36.97	16.11	37.73
8					46.95	25.20	11.15	12.70	14.18	35.72	31.72	44.66	16.10	29.54	30.80	31.30	16.48	37.15	37.55
9				44.17	23.45	11.01	30.73	14.18	33.00	15.33	15.34	15.88	36.81	16.83	37.43	16.63	37.53	16.58	37.13
10				43.65	10.12	12.07	13.70	35.71	15.33	37.47	15.47	36.65	16.47	37.92	16.51	16.36	16.59	37.20	15.67
11			44.75	26.69	11.52	13.20	44.13	31.71	15.34	15.47	43.06	35.32	37.09	16.29	44.43	36.48	37.41	15.66	35.34
12			43.43	10.51	12.84	34.88	34.15	44.67	15.88	36.64	35.32	36.25	16.06	16.12	36.24	36.67	16.07	15.40	34.24
13		47.84	28.67	11.86	31.99	15.13	15.36	16.10	36.81	16.47	37.08	16.06	38.22	16.43	37.27	16.19	37.59	15.98	36.89
14		43.81	10.28	12.68	14.42	36.93	15.87	29.54	16.83	37.92	16.29	16.12	16.43	37.99	15.90	37.00	16.12	37.00	15.69
15	41.45	43.98	32.57	34.94	14.67	15.31	40.80	30.80	37.43	16.51	44.44	36.24	37.27	15.90	43.18	35.95	15.57	15.84	42.52
16	40.79	28.65	33.99	33.75	15.02	37.58	35.43	31.30	16.63	16.36	36.48	36.67	16.19	37.00	35.94	36.08	15.73	36.40	36.87
17	44.60	27.79	32.09	14.10	45.36	15.73	36.97	16.48	37.53	16.59	37.41	16.08	37.59	16.13	15.57	15.73	37.82	16.07	37.33
18	41.84	26.86	12.36	13.90	15.25	37.50	16.12	37.15	16.59	37.19	15.66	15.40	15.98	37.00	15.85	36.40	16.07	37.73	15.31
19	42.85	9.35	43.63	28.13	36.66	15.61	37.73	37.54	37.12	15.67	35.34	34.24	36.89	15.69	42.51	36.86	37.33	15.31	35.20

Figure 4A-13e. Average Bundle Exposure at 13.2 GWd/MT Exposure

```
        ( ROD PATTERN DEPLETION

NITER   0  POWER           IMAX  19  POWER(MWT)          4.5000E+03  ( 100.0 %)
IBOUN   1  1/4             JMAX  19  PRESSURE(PSIA)      1.0550E+03
IRN     1  MIRROR          KMAX  25  FLOW(*10E-6LB/HR)   7.8508E+01  ( 100.0 %)
ILPA    0                  NSMAX 10  BYPASS(LB/HR)       1.1742E+07  (  15.0 %)          CONTROL ROD CONFIGURATION
IFLW    2  DETAIL          LMAX  20  ENTHALPY(BTU/LB)            512.30                    IN NOTCHES WITHDRAWN
RSTART  0  NEW             LVDCT  8  INLET TEMP(DEG F)           520.47
NEWPHY  2                  IPFTL  0  BEGINNING EXPOSURE         25105.1                1  3  5  7  9 11 13 15 17 19
NEXO    3  CALC.                    DELTA EXPOS.(DELTE)            0.0
RBOCA   1                  IALPRM 0  DELBRN                      1000.0                1
IACF    0                  IFAST  0  TOTAL NOTCHES                 2024
             IPDOME   1    IAHB   0  CORE FUEL MASS         MTU:162.928                3
                                     CORE FUEL MASS         STU:179.596
ENERGY (MWD) (DELTE)              0. ENERGY (MWD) (DELBRN)      179596.                5
CYCLE ENERGY (MWD)          2334770. CYCLE EXPOSURE             13000.0
CORE AVG. POWER DENSITY    54.328033                                                    7              32            9
NEUTRON MULTIPLICATION    0.99741405 FINAL AVG. EXPOSURE        26105.1
DIFP   (EPS5 = 0.00200)   0.00114769 CORE AVG. NEUTRON FLUX   1.467E+14                9
AVERAGE VOID FRACTION       0.515585 CORE AVG. GD WORTH          -0.034
CORE PRESSURE DROP,PSI      7.989760 CORE AVG. GD RESIDUAL WORTH  0.000               11       32           10
EXP RATIO INDEX (INER-II)     0.0000 CORE AVERAGE XENON WORTH   -0.0237
                                                                                      13
CORE HISTORY MAX. VALUES:       LOCATION: I   J   K
  NODAL EXPOSURE, MWD/T   56294.          7   7   5   METRIC    62052.               15              10            1
  BUNDLE EXPOSURE, MWD/T  43792.         13   2       METRIC    48272.
  EXPOSURE RATIO, NEXRAT  0.0000          0   0   0                                   17
  AXIAL POWER PEAK        1.2201                  5
                                                                                      19        9           1
```

Figure 4A-14a. Control Rod Pattern Summary at 14.3 GWd/MT Exposure

14.3 GWD/MT

Node	Axial Power
25	0.228
24	0.442
23	0.634
22	0.773
21	0.883
20	0.970
19	1.034
18	1.067
17	1.065
16	1.078
15	1.144
14	1.145
13	1.153
12	1.161
11	1.169
10	1.178
9	1.188
8	1.199
7	1.211
6	1.218
5	1.220
4	1.206
3	1.143
2	0.960
1	0.531

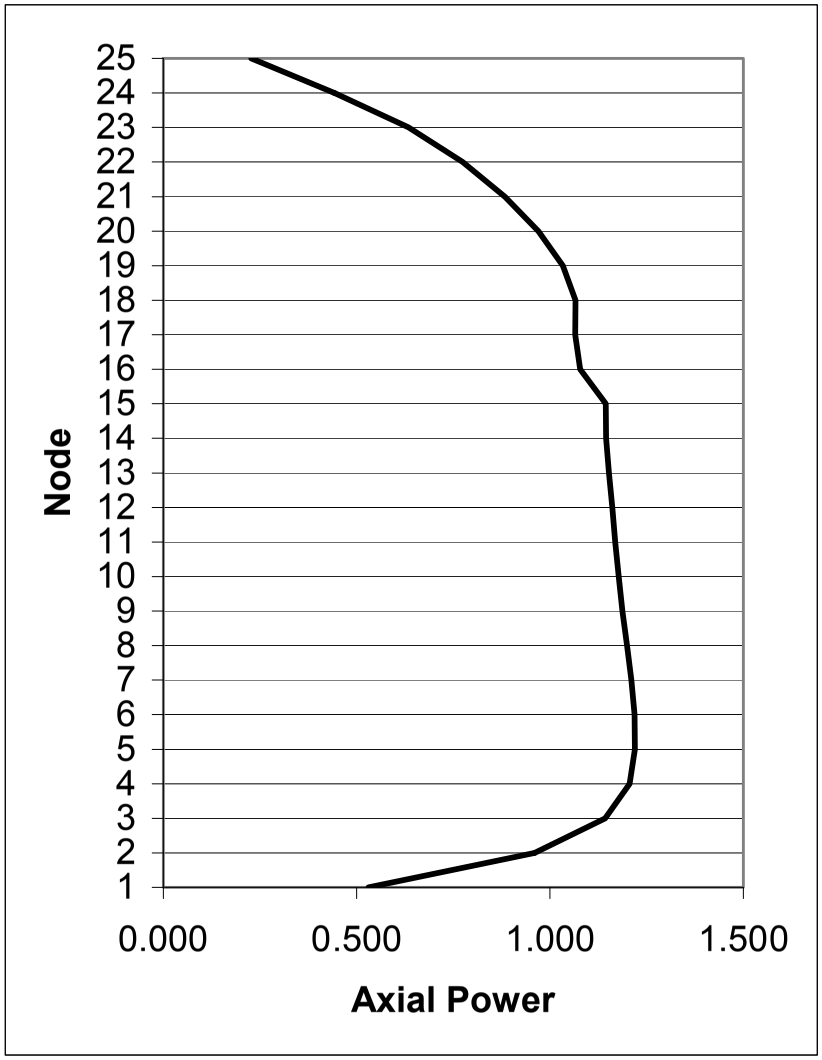

Figure 4A-14b. Relative Axial Power at 14.3 GWd/MT Exposure

14.3 GWD/MT

Node	Axial Exposure (MWD/MT)
25	6167.4
24	10620.3
23	14878.7
22	19020.9
21	22619.0
20	25566.9
19	27962.0
18	29715.5
17	30818.5
16	31647.6
15	30821.6
14	31996.8
13	32989.4
12	33713.3
11	34344.8
10	34868.5
9	35158.5
8	35501.1
7	35955.5
6	36378.1
5	36479.6
4	35687.1
3	32752.3
2	26207.6
1	13562.6

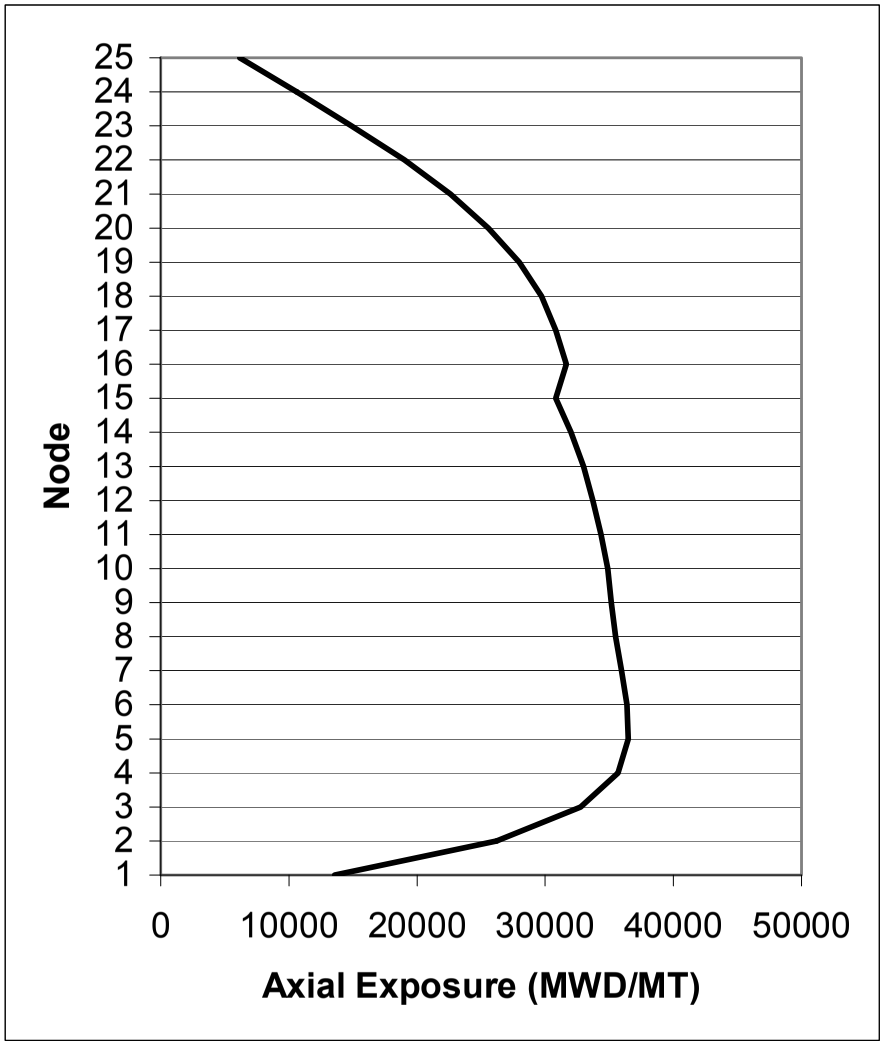

Figure 4A-14c. Axial Exposure at 14.3 GWd/MT Exposure

	1	2	3	4	5	6	7	8	9	10	11	12	13	14	15	16	17	18	19
1															0.32	0.36	0.40	0.43	0.42
2													0.38	0.47	0.52	0.67	0.72	0.74	0.76
3											0.43	0.54	0.71	0.85	0.81	0.82	0.89	1.00	0.79
4									0.40	0.53	0.73	0.91	1.02	1.08	0.95	0.99	1.13	1.13	1.03
5								0.47	0.69	0.87	0.98	1.08	1.04	1.22	1.23	1.22	0.96	1.19	0.98
6							0.46	0.71	0.93	1.02	1.06	0.99	1.23	1.08	1.28	1.06	1.22	1.00	1.12
7						0.46	0.59	0.95	0.96	1.09	0.75	0.87	1.23	1.30	1.07	1.12	1.04	1.14	0.72
8					0.47	0.71	0.95	1.08	1.17	0.99	0.90	0.82	1.25	1.17	1.19	1.17	1.25	0.99	0.72
9				0.40	0.69	0.93	0.96	1.17	1.10	1.25	1.24	1.25	1.14	1.30	1.10	1.29	1.09	1.23	1.00
10				0.53	0.87	1.02	1.09	0.99	1.25	1.10	1.29	1.11	1.30	1.09	1.23	1.23	1.28	1.10	1.27
11			0.43	0.73	0.98	1.06	0.75	0.90	1.24	1.29	1.07	1.12	1.13	1.23	0.75	0.79	1.05	1.30	1.13
12			0.54	0.91	1.08	0.99	0.87	0.82	1.25	1.11	1.12	1.12	1.30	1.23	0.79	0.78	1.23	1.30	1.14
13		0.38	0.71	1.02	1.04	1.23	1.23	1.25	1.14	1.30	1.13	1.30	1.11	1.28	1.03	1.21	1.09	1.30	1.09
14		0.48	0.85	1.08	1.22	1.08	1.30	1.17	1.30	1.09	1.23	1.23	1.28	1.09	1.27	1.09	1.29	1.08	1.20
15	0.32	0.52	0.81	0.95	1.23	1.28	1.07	1.19	1.10	1.23	0.75	0.79	1.03	1.27	1.05	1.11	1.28	1.20	0.71
16	0.36	0.67	0.82	0.99	1.22	1.06	1.12	1.17	1.29	1.23	0.79	0.78	1.21	1.09	1.11	1.11	1.28	1.01	0.71
17	0.40	0.72	0.89	1.13	0.96	1.22	1.04	1.25	1.09	1.28	1.05	1.23	1.09	1.29	1.28	1.28	1.08	1.23	0.98
18	0.43	0.74	1.00	1.13	1.19	1.00	1.14	0.99	1.23	1.10	1.30	1.30	1.30	1.08	1.20	1.01	1.23	1.06	1.25
19	0.42	0.76	0.79	1.03	0.98	1.12	0.72	0.72	1.00	1.27	1.13	1.14	1.09	1.20	0.71	0.71	0.98	1.25	1.10

Figure 4A-14d. Relative Integrated Power Per Bundle at 14.3 GWd/MT Exposure

	1	2	3	4	5	6	7	8	9	10	11	12	13	14	15	16	17	18	19
1															41.80	41.17	45.04	42.30	43.31
2													48.27	44.32	44.54	29.38	28.57	27.67	10.18
3											45.20	44.00	29.43	11.19	33.44	34.88	33.07	13.45	44.49
4									44.59	44.20	27.47	11.48	12.96	13.85	35.96	34.81	15.34	15.13	29.27
5								47.45	24.19	11.04	12.57	14.00	33.13	15.75	16.01	16.36	46.41	16.56	37.75
6							44.48	25.96	12.00	13.16	14.33	35.96	16.47	38.12	16.71	38.75	17.08	38.61	16.85
7						44.48	46.88	12.16	31.76	14.86	44.91	35.07	16.70	17.30	41.99	36.69	38.14	17.38	38.51
8					47.45	25.96	12.16	13.86	15.43	36.79	32.66	45.53	17.48	30.84	32.14	32.62	17.88	38.26	38.34
9				44.59	24.19	12.00	31.76	15.43	34.19	16.69	16.68	17.24	38.07	18.29	38.67	18.07	38.75	17.96	38.24
10				44.21	11.04	13.16	14.86	36.78	16.69	38.68	16.89	37.87	17.91	39.14	17.88	17.73	18.02	38.43	17.09
11			45.21	27.47	12.57	14.33	44.92	32.66	16.68	16.89	44.25	36.58	38.35	17.66	45.25	37.35	38.58	17.12	36.62
12			44.01	11.48	14.00	35.95	35.07	45.54	17.24	37.87	36.57	37.50	17.52	17.49	37.10	37.53	17.45	16.86	35.53
13		48.24	29.43	12.96	33.13	16.48	16.70	17.48	38.07	17.91	38.35	17.52	39.46	17.86	38.42	17.54	38.81	17.43	38.12
14		44.32	11.19	13.85	15.75	38.12	17.31	30.85	18.29	39.13	17.66	17.49	17.86	39.21	17.32	38.23	17.58	38.22	17.03
15	41.80	44.55	33.44	35.96	16.01	16.71	42.00	32.14	38.67	17.88	45.26	37.10	38.42	17.32	44.36	37.20	17.01	17.20	43.31
16	41.18	29.38	34.87	34.81	16.36	38.75	36.69	32.62	18.07	17.74	37.35	37.53	17.54	38.22	37.20	37.33	17.17	37.55	37.68
17	45.04	28.58	33.07	15.34	46.41	17.08	38.14	17.88	38.75	18.02	38.58	17.45	38.81	17.58	17.02	17.17	39.03	17.45	38.45
18	42.31	27.67	13.46	15.14	16.56	38.61	17.39	38.26	17.97	38.42	17.12	16.86	17.44	38.23	17.20	37.55	17.45	38.93	16.72
19	43.31	10.18	44.50	29.27	37.75	16.85	38.51	38.33	38.24	17.10	36.61	35.53	38.12	17.03	43.31	37.67	38.44	16.72	36.45

Figure 4A-14e. Average Bundle Exposure at 14.3 GWd/MT Exposure

```
        ( ROD PATTERN DEPLETION

NITER    0  POWER           IMAX  19  POWER(MWT)          4.5000E+03  ( 100.0 %)
IBOUN    1  1/4             JMAX  19  PRESSURE(PSIA)      1.0550E+03
IRN      1  MIRROR          KMAX  25  FLOW(*10E-6LB/HR)   7.8508E+01  ( 100.0 %)
ILPA     0                  NSMAX 10  BYPASS(LB/HR)       1.1742E+07  (  15.0 %)          CONTROL ROD CONFIGURATION
IFLW     2  DETAIL          LMAX  20  ENTHALPY(BTU/LB)            512.30                    IN NOTCHES WITHDRAWN
RSTART   0  NEW             LVDCT  8  INLET TEMP(DEG F)           520.47
NEWPHY   2                  IPFTL  0  BEGINNING EXPOSURE        26105.1               1  3  5  7  9 11 13 15 17 19
NEXO     3  CALC.                    DELTA EXPOS.(DELTE)           0.0
RBOCA    1                  IALPRM 0  DELBRN                    1000.0               1
IACF     0                  IFAST  0  TOTAL NOTCHES               1788
             IPDOME   1     IAHB   0  CORE FUEL MASS         MTU:162.928            3
                                      CORE FUEL MASS         STU:179.596
ENERGY (MWD) (DELTE)              0.  ENERGY (MWD) (DELBRN)      179596.               5
CYCLE ENERGY (MWD)          2514367.  CYCLE EXPOSURE            14000.0
CORE AVG. POWER DENSITY    54.328033                                                   7                    30
NEUTRON MULTIPLICATION    0.99675190 FINAL AVG. EXPOSURE        27105.1
DIFP    (EPS5 = 0.00200)  0.00142914 CORE AVG. NEUTRON FLUX   1.464E+14               9
AVERAGE VOID FRACTION       0.498509 CORE AVG. GD WORTH          -0.031
CORE PRESSURE DROP,PSI      7.903288 CORE AVG. GD RESIDUAL WORTH  0.000              11             13           1
EXP RATIO INDEX (INER-II)     0.0000 CORE AVERAGE XENON WORTH   -0.0239
                                                                                     13
CORE HISTORY MAX. VALUES:      LOCATION: I   J   K
  NODAL EXPOSURE, MWD/T   56955.         7   7   5   METRIC    62782.               15       30           4
  BUNDLE EXPOSURE, MWD/T  44168.        13   2       METRIC    48687.
  EXPOSURE RATIO, NEXRAT  0.0000         0   0   0                                   17
  AXIAL POWER PEAK        1.1887                15
                                                                                     19              1           0
```

Figure 4A-15a. Control Rod Pattern Summary at 15.4 GWd/MT Exposure

15.4 GWD/MT

Node	Axial Power
25	0.254
24	0.494
23	0.705
22	0.866
21	0.988
20	1.075
19	1.131
18	1.147
17	1.123
16	1.127
15	1.189
14	1.178
13	1.175
12	1.170
11	1.165
10	1.160
9	1.154
8	1.148
7	1.139
6	1.124
5	1.103
4	1.071
3	1.003
2	0.844
1	0.469

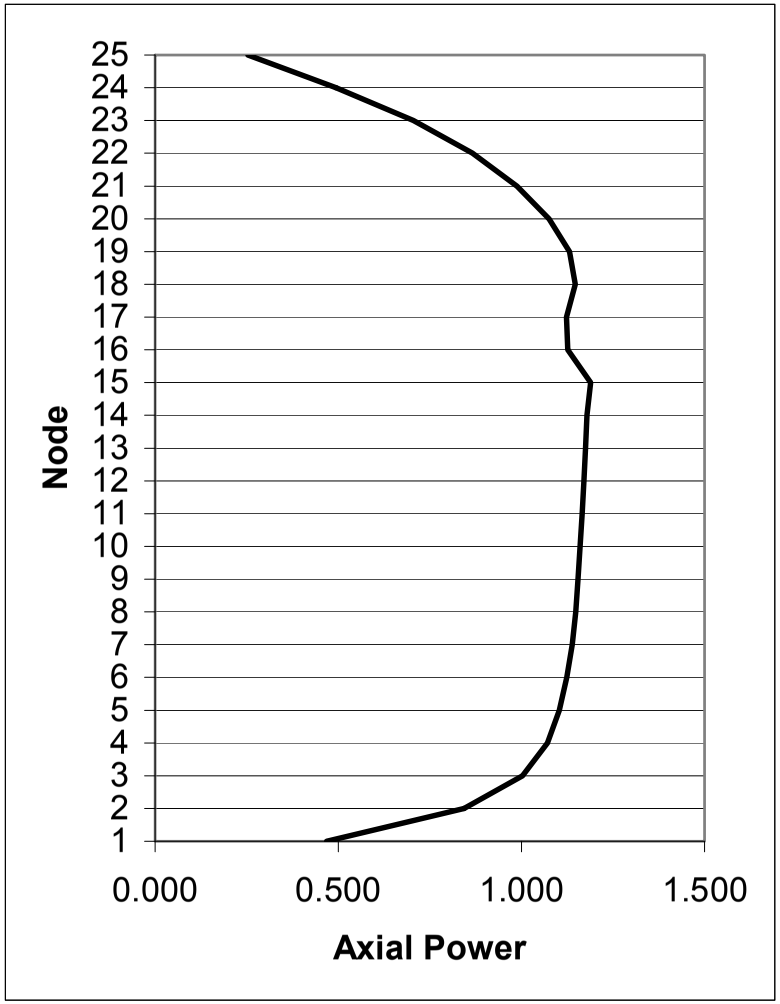

Figure 4A-15b. Relative Axial Power at 15.4 GWd/MT Exposure

15.4 GWD/MT

Node	Axial Exposure (MWD/MT)
25	6495.8
24	11180.6
23	15650.3
22	19962.1
21	23693.6
20	26747.2
19	29219.8
18	31013.1
17	32114.7
16	32910.9
15	31998.9
14	33174.9
13	34175.7
12	34907.6
11	35547.2
10	36080.2
9	36381.3
8	36736.5
7	37202.3
6	37632.9
5	37736.2
4	36929.0
3	33929.3
2	27196.3
1	14098.5

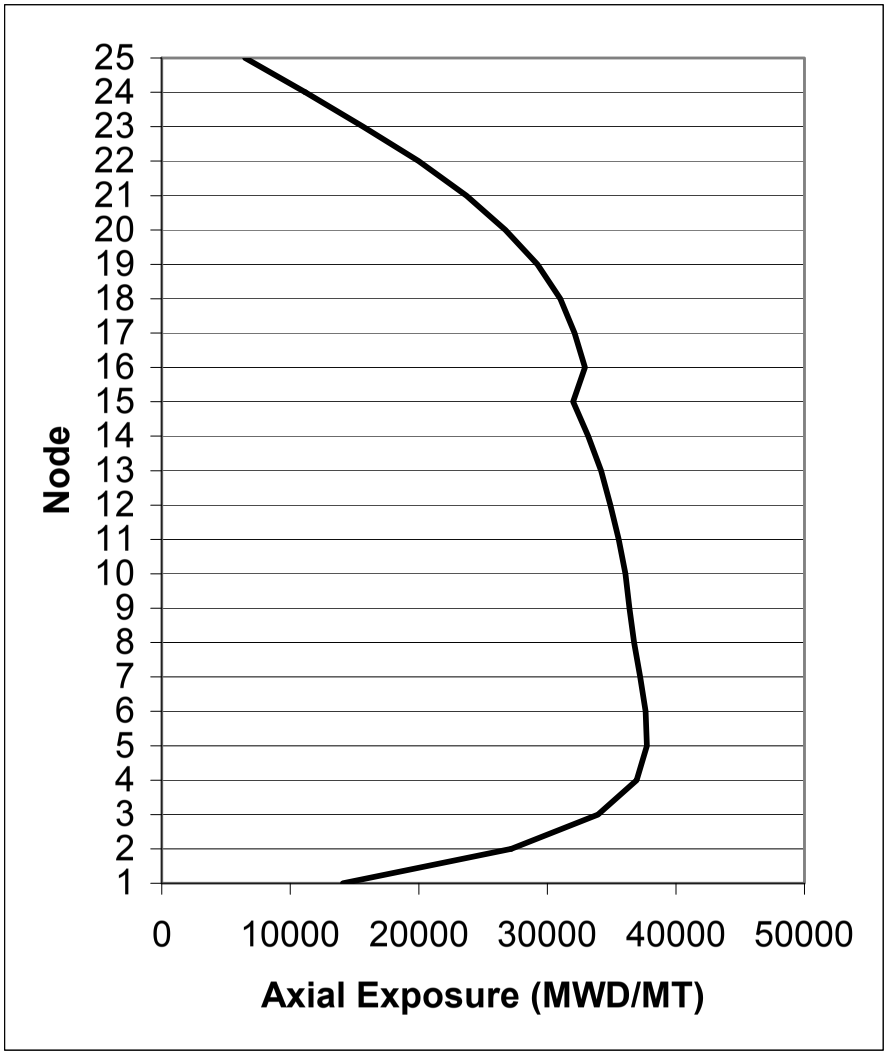

Figure 4A-15c. Axial Exposure at 15.4 GWd/MT Exposure

	1	2	3	4	5	6	7	8	9	10	11	12	13	14	15	16	17	18	19
1															0.32	0.36	0.40	0.44	0.43
2													0.38	0.48	0.52	0.67	0.72	0.75	0.78
3											0.45	0.56	0.72	0.86	0.81	0.82	0.89	1.02	0.80
4									0.43	0.57	0.77	0.95	1.05	1.09	0.94	0.98	1.14	1.15	1.05
5								0.51	0.75	0.95	1.07	1.15	1.06	1.22	1.20	1.19	0.96	1.22	1.03
6							0.49	0.76	1.01	1.12	1.19	1.07	1.27	1.06	1.19	0.99	1.20	1.04	1.23
7						0.49	0.63	1.02	1.03	1.22	0.99	1.12	1.27	1.23	0.85	0.88	1.01	1.22	1.05
8					0.51	0.76	1.02	1.16	1.25	1.07	1.15	1.03	1.28	1.12	0.94	0.93	1.19	1.05	1.03
9				0.43	0.75	1.01	1.03	1.25	1.14	1.29	1.28	1.27	1.13	1.27	1.06	1.23	1.07	1.23	1.03
10				0.57	0.95	1.12	1.22	1.07	1.29	1.08	1.21	1.03	1.25	1.09	1.28	1.28	1.27	1.05	1.16
11			0.45	0.77	1.07	1.19	0.99	1.15	1.28	1.21	0.75	0.78	1.05	1.27	1.05	1.10	1.07	1.19	0.74
12			0.56	0.95	1.15	1.07	1.12	1.03	1.27	1.03	0.78	0.78	1.20	1.27	1.09	1.08	1.25	1.18	0.74
13		0.38	0.72	1.05	1.06	1.27	1.27	1.28	1.13	1.25	1.05	1.20	1.06	1.26	1.05	1.23	1.06	1.22	0.98
14		0.48	0.86	1.09	1.22	1.06	1.23	1.12	1.27	1.09	1.27	1.27	1.26	1.04	1.15	0.98	1.22	1.05	1.21
15	0.32	0.52	0.81	0.94	1.20	1.19	0.85	0.94	1.06	1.28	1.05	1.09	1.05	1.15	0.69	0.72	1.16	1.21	1.00
16	0.36	0.67	0.82	0.98	1.19	0.99	0.88	0.93	1.23	1.28	1.10	1.08	1.23	0.98	0.72	0.72	1.14	1.01	1.00
17	0.40	0.72	0.89	1.14	0.96	1.20	1.01	1.19	1.07	1.27	1.07	1.25	1.06	1.22	1.16	1.14	1.00	1.18	0.98
18	0.44	0.75	1.02	1.15	1.22	1.04	1.22	1.05	1.23	1.05	1.19	1.18	1.22	1.05	1.21	1.01	1.18	0.98	1.10
19	0.43	0.78	0.80	1.05	1.03	1.23	1.05	1.04	1.03	1.16	0.74	0.74	0.98	1.21	1.00	1.00	0.98	1.10	0.69

Figure 4A-15d. Relative Integrated Power Per Bundle at 15.4 GWd/MT Exposure

	1	2	3	4	5	6	7	8	9	10	11	12	13	14	15	16	17	18	19
1															42.15	41.57	45.48	42.77	43.78
2													48.69	44.84	45.11	30.12	29.37	28.49	11.02
3											45.67	44.59	30.21	12.13	34.34	35.78	34.04	14.56	45.36
4									45.03	44.78	28.27	12.48	14.08	15.04	37.00	35.90	16.59	16.38	30.41
5								47.97	24.96	12.01	13.65	15.19	34.28	17.10	17.37	17.71	47.46	17.87	38.83
6							44.99	26.74	13.03	14.28	15.50	37.05	17.84	39.31	18.12	39.92	18.43	39.71	18.08
7						44.99	47.53	13.21	32.82	16.06	45.74	36.03	18.05	18.73	43.18	37.93	39.29	18.64	39.30
8					47.97	26.74	13.21	15.05	16.72	37.88	33.66	46.44	18.86	32.14	33.46	33.90	19.25	39.35	39.13
9				45.03	24.95	13.03	32.81	16.72	35.41	18.07	18.04	18.61	39.32	19.72	39.88	19.49	39.95	19.32	39.34
10				44.79	12.01	14.28	16.06	37.87	18.07	39.89	18.32	39.09	19.34	40.34	19.23	19.09	19.42	39.64	18.49
11			45.68	28.27	13.65	15.50	45.75	33.65	18.04	18.32	45.42	37.81	39.60	19.01	46.08	38.22	39.73	18.55	37.87
12			44.60	12.48	15.19	37.04	36.03	46.45	18.62	39.09	37.81	38.74	18.95	18.85	37.97	38.39	18.80	18.30	36.79
13		48.66	30.21	14.08	34.27	17.84	18.05	18.86	39.32	19.34	39.59	18.95	40.68	19.27	39.56	18.87	40.01	18.86	39.33
14		44.85	12.13	15.04	17.10	39.31	18.73	32.14	19.72	40.34	19.01	18.85	19.27	40.41	18.72	39.42	19.00	39.42	18.35
15	42.15	45.13	34.34	37.00	17.37	18.12	43.18	33.45	39.88	19.23	46.09	37.97	39.56	18.72	45.52	38.42	18.43	18.52	44.10
16	41.57	30.12	35.78	35.90	17.71	39.91	37.92	33.91	19.50	19.09	38.22	38.39	18.87	39.42	38.42	38.55	18.57	38.66	38.46
17	45.48	29.37	34.05	16.59	47.47	18.43	39.29	19.25	39.94	19.43	39.73	18.81	40.01	19.01	18.43	18.58	40.22	18.80	39.53
18	42.78	28.49	14.56	16.38	17.87	39.71	18.64	39.35	19.32	39.63	18.55	18.30	18.87	39.42	18.53	38.66	18.80	40.10	18.09
19	43.78	11.02	45.37	30.40	38.83	18.08	39.30	39.13	39.34	18.50	37.86	36.79	39.33	18.35	44.10	38.46	39.52	18.10	37.67

Figure 4A-15e. Average Bundle Exposure at 15.4 GWd/MT Exposure

```
        ( ROD PATTERN DEPLETION

NITER   0  POWER           IMAX  19  POWER(MWT)          4.5000E+03  ( 100.0 %)
IBOUN   1  1/4             JMAX  19  PRESSURE(PSIA)      1.0550E+03
IRN     1  MIRROR          KMAX  25  FLOW(*10E-6LB/HR)   7.8508E+01  ( 100.0 %)
ILPA    0                  NSMAX 10  BYPASS(LB/HR)       1.1742E+07  (  15.0 %)          CONTROL ROD CONFIGURATION
IFLW    2  DETAIL          LMAX  20  ENTHALPY(BTU/LB)            512.30                    IN NOTCHES WITHDRAWN
RSTART  0  NEW             LVDCT  6  INLET TEMP(DEG F)           520.47
NEWPHY  2                  IPFTL  0  BEGINNING EXPOSURE         27105.2               1  3  5  7  9 11 13 15 17 19
NEXO    3  CALC.                    DELTA EXPOS.(DELTE)            0.0
RBOCA   1                  IALPRM 0  DELBRN                     1000.0               1
IACF    0                  IFAST  0  TOTAL NOTCHES                1224
             IPDOME   1    IAHB   0  CORE FUEL MASS         MTU:162.928               3
                                     CORE FUEL MASS         STU:179.596
ENERGY (MWD) (DELTE)              0. ENERGY (MWD) (DELBRN)      179596.               5
CYCLE ENERGY (MWD)          2693965. CYCLE EXPOSURE             15000.0
CORE AVG. POWER DENSITY    54.328033                                                  7                    98
NEUTRON MULTIPLICATION    0.99618727 FINAL AVG. EXPOSURE        28105.2
DIFP   (EPS5 = 0.00200)   0.00142044 CORE AVG. NEUTRON FLUX   1.466E+14               9
AVERAGE VOID FRACTION       0.493528 CORE AVG. GD WORTH          -0.028
CORE PRESSURE DROP,PSI      7.918104 CORE AVG. GD RESIDUAL WORTH  0.000              11             12            0
EXP RATIO INDEX (INER-II)     0.0000 CORE AVERAGE XENON WORTH   -0.0240
                                                                                    13
CORE HISTORY MAX. VALUES:      LOCATION: I   J   K
  NODAL EXPOSURE, MWD/T   57658.         7   7   5   METRIC    63557.              15       98           11
  BUNDLE EXPOSURE, MWD/T  44551.        13   2       METRIC    49109.
  EXPOSURE RATIO, NEXRAT  0.0000         0   0   0                                  17
  AXIAL POWER PEAK        1.2120                15
                                                                                    19              0            0
```

Figure 4A-16a. Control Rod Pattern Summary at 16.5 GWd/MT Exposure

16.5 GWD/MT

Node	Axial Power
25	0.262
24	0.512
23	0.730
22	0.889
21	1.002
20	1.082
19	1.129
18	1.142
17	1.126
16	1.141
15	1.212
14	1.204
13	1.200
12	1.193
11	1.183
10	1.171
9	1.158
8	1.142
7	1.120
6	1.092
5	1.060
4	1.022
3	0.958
2	0.815
1	0.457

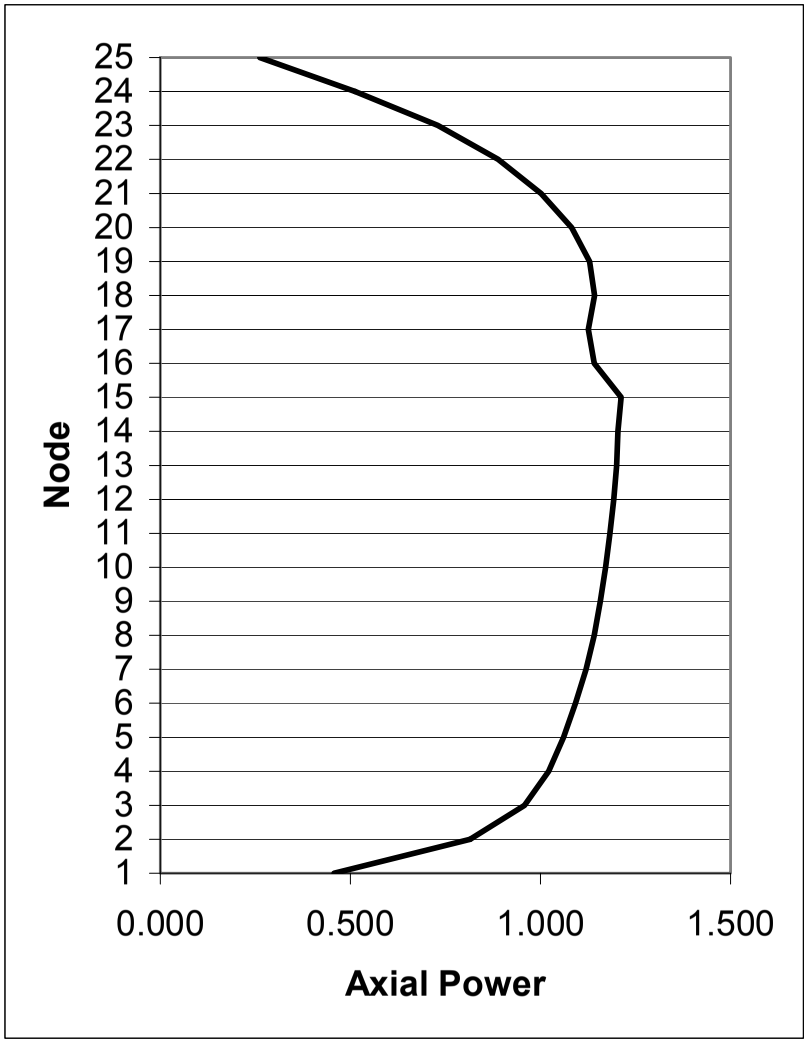

Figure 4A-16b. Relative Axial Power at 16.5 GWd/MT Exposure

16.5 GWD/MT

Node	Axial Exposure (MWD/MT)
25	6861.6
24	11805.8
23	16507.8
22	21015.4
21	24895.3
20	28055.7
19	30596.1
18	32409.0
17	33480.7
16	34231.8
15	33221.8
14	34387.1
13	35384.3
12	36111.8
11	36746.1
10	37273.5
9	37569.9
8	37919.1
7	38375.0
6	38790.3
5	38872.2
4	38031.7
3	34962.4
2	28065.5
1	14571.4

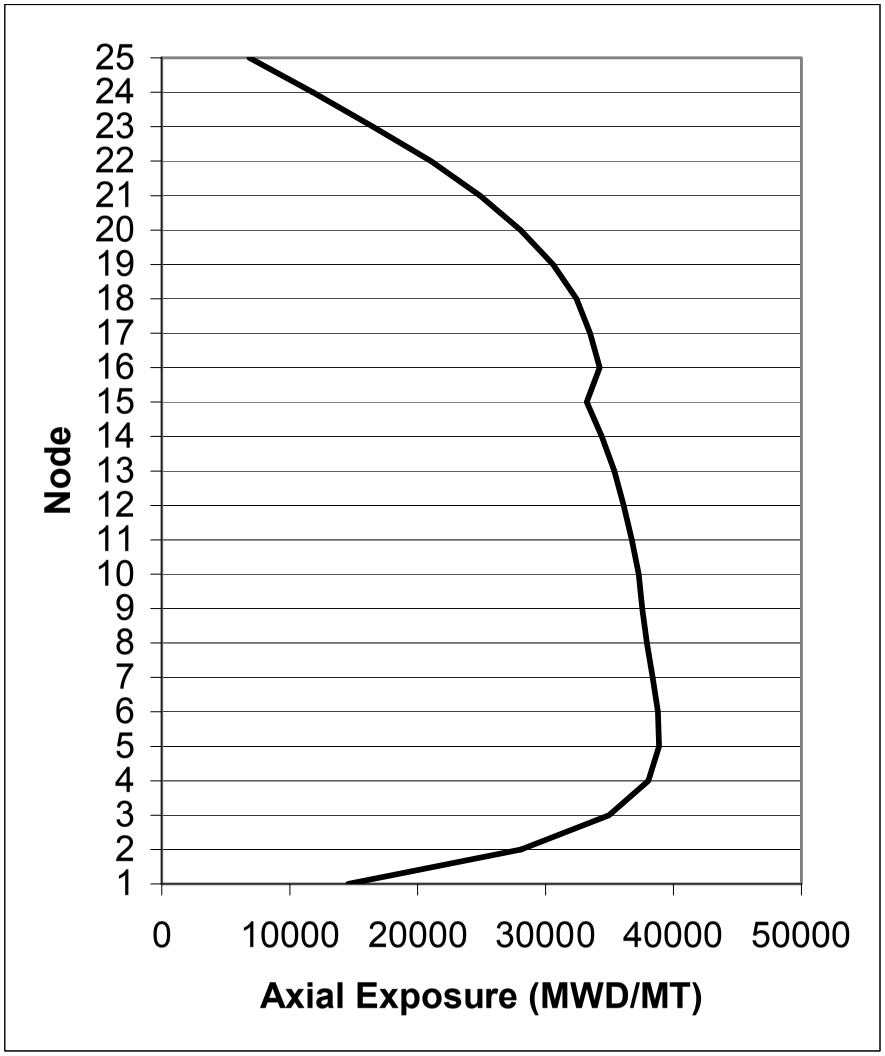

Figure 4A-16c. Axial Exposure at 16.5 GWd/MT Exposure

	1	2	3	4	5	6	7	8	9	10	11	12	13	14	15	16	17	18	19
1															0.32	0.36	0.40	0.43	0.43
2													0.39	0.48	0.52	0.66	0.72	0.75	0.79
3											0.46	0.56	0.73	0.88	0.81	0.81	0.89	1.02	0.80
4									0.43	0.57	0.77	0.97	1.07	1.12	0.95	0.99	1.15	1.16	1.04
5								0.50	0.74	0.96	1.08	1.16	1.07	1.25	1.25	1.23	0.97	1.23	1.02
6							0.49	0.75	1.01	1.13	1.20	1.07	1.29	1.09	1.28	1.05	1.24	1.05	1.23
7						0.49	0.63	1.02	1.01	1.21	0.98	1.11	1.29	1.31	1.07	1.12	1.06	1.24	1.04
8					0.50	0.75	1.02	1.15	1.23	1.05	1.13	1.02	1.30	1.17	1.18	1.16	1.26	1.05	1.02
9				0.43	0.74	1.01	1.01	1.23	1.12	1.26	1.25	1.25	1.12	1.29	1.10	1.29	1.08	1.23	1.02
10				0.57	0.96	1.13	1.21	1.05	1.26	1.05	1.18	1.00	1.23	1.08	1.28	1.28	1.26	1.03	1.14
11			0.46	0.77	1.08	1.20	0.98	1.13	1.25	1.18	0.73	0.76	1.02	1.23	1.02	1.08	1.04	1.15	0.71
12			0.56	0.97	1.16	1.07	1.11	1.02	1.25	1.00	0.76	0.76	1.16	1.22	1.06	1.05	1.21	1.14	0.71
13		0.39	0.73	1.07	1.07	1.29	1.29	1.30	1.12	1.23	1.02	1.16	1.02	1.21	1.01	1.18	1.02	1.17	0.94
14		0.48	0.88	1.12	1.25	1.09	1.31	1.17	1.29	1.08	1.23	1.22	1.21	1.00	1.11	0.95	1.17	1.01	1.16
15	0.32	0.52	0.81	0.95	1.25	1.28	1.07	1.18	1.10	1.28	1.02	1.06	1.01	1.11	0.70	0.73	1.12	1.16	0.95
16	0.36	0.66	0.81	0.99	1.23	1.05	1.12	1.16	1.29	1.28	1.08	1.05	1.18	0.95	0.73	0.72	1.10	0.97	0.96
17	0.40	0.72	0.89	1.15	0.97	1.24	1.06	1.26	1.08	1.26	1.04	1.21	1.02	1.17	1.12	1.10	0.96	1.12	0.94
18	0.43	0.75	1.02	1.16	1.23	1.05	1.24	1.05	1.23	1.03	1.15	1.14	1.17	1.01	1.16	0.97	1.12	0.94	1.05
19	0.43	0.79	0.80	1.04	1.02	1.23	1.04	1.02	1.02	1.14	0.71	0.71	0.94	1.16	0.95	0.96	0.94	1.05	0.66

Figure 4A-16d. Relative Integrated Power Per Bundle at 16.5 GWd/MT Exposure

	1	2	3	4	5	6	7	8	9	10	11	12	13	14	15	16	17	18	19
1															42.50	41.97	45.93	43.26	44.26
2													49.11	45.37	45.69	30.86	30.16	29.32	11.89
3											46.17	45.20	31.00	13.08	35.23	36.68	35.03	15.69	46.24
4									45.51	45.41	29.12	13.53	15.24	16.25	38.04	36.98	17.85	17.65	31.56
5								48.52	25.78	13.06	14.83	16.46	35.45	18.44	18.70	19.02	48.51	19.22	39.96
6							45.53	27.58	14.15	15.52	16.82	38.23	19.24	40.47	19.43	41.01	19.75	40.86	19.44
7						45.53	48.23	14.33	33.95	17.40	46.84	37.27	19.45	20.09	44.11	38.90	40.39	19.98	40.46
8					48.53	27.58	14.33	16.33	18.10	39.06	34.93	47.57	20.27	33.36	34.49	34.93	20.57	40.50	40.27
9				45.51	25.78	14.15	33.95	18.10	36.67	19.49	19.45	20.02	40.57	21.12	41.05	20.85	41.12	20.68	40.48
10				45.42	13.06	15.52	17.40	39.06	19.49	41.07	19.66	40.22	20.71	41.54	20.64	20.50	20.82	40.80	19.77
11			46.18	29.12	14.83	16.82	46.84	34.92	19.45	19.66	46.25	38.67	40.75	20.41	47.24	39.44	40.91	19.86	38.68
12			45.21	13.53	16.46	38.22	37.26	47.58	20.02	40.22	38.67	39.60	20.28	20.24	39.18	39.58	20.18	19.60	37.60
13		49.08	31.00	15.24	35.45	19.24	19.45	20.27	40.56	20.71	40.75	20.28	41.85	20.65	40.72	20.22	41.18	20.21	40.41
14		45.38	13.08	16.25	18.44	40.47	20.09	33.37	21.12	41.53	20.41	20.24	20.65	41.55	19.98	40.50	20.35	40.58	19.68
15	42.50	45.70	35.23	38.03	18.70	19.43	44.12	34.49	41.05	20.64	47.24	39.18	40.71	19.98	46.29	39.22	19.71	19.86	45.20
16	41.97	30.85	36.68	36.98	19.02	41.01	38.90	34.93	20.85	20.50	39.43	39.58	20.23	40.50	39.22	39.34	19.83	39.78	39.57
17	45.93	30.17	35.03	17.85	48.52	19.75	40.40	20.57	41.12	20.82	40.91	20.19	41.17	20.35	19.71	19.83	41.32	20.10	40.61
18	43.26	29.32	15.69	17.66	19.22	40.86	19.99	40.51	20.68	40.79	19.86	19.60	20.21	40.58	19.86	39.78	20.10	41.18	19.31
19	44.26	11.89	46.25	31.56	39.96	19.44	40.45	40.27	40.48	19.77	38.68	37.60	40.41	19.68	45.20	39.57	40.61	19.31	38.43

Figure 4A-16e. Average Bundle Exposure at 16.5 GWd/MT Exposure

```
        ( ROD PATTERN DEPLETION

NITER   0  POWER           IMAX  19  POWER(MWT)          4.5000E+03  ( 100.0 %)
IBOUN   1  1/4             JMAX  19  PRESSURE(PSIA)      1.0550E+03
IRN     1  MIRROR          KMAX  25  FLOW(*10E-6LB/HR)   7.8508E+01  ( 100.0 %)
ILPA    0                  NSMAX 10  BYPASS(LB/HR)       1.1742E+07  (  15.0 %)          CONTROL ROD CONFIGURATION
IFLW    2  DETAIL          LMAX  20  ENTHALPY(BTU/LB)            512.30                    IN NOTCHES WITHDRAWN
RSTART  0  NEW             LVDCT  8  INLET TEMP(DEG F)           520.47
NEWPHY  2                  IPFTL  0  BEGINNING EXPOSURE         28105.2               1  3  5  7  9 11 13 15 17 19
NEXO    3  CALC.                    DELTA EXPOS.(DELTE)            0.0
RBOCA   1                  IALPRM 0  DELBRN                     1200.0               1
IACF    0                  IFAST  0  TOTAL NOTCHES                 483
             IPDOME   1    IAHB   0  CORE FUEL MASS         MTU:162.928               3
                                     CORE FUEL MASS         STU:179.596
ENERGY (MWD) (DELTE)              0. ENERGY (MWD) (DELBRN)      215515.               5
CYCLE ENERGY (MWD)          2909482. CYCLE EXPOSURE             16200.0
CORE AVG. POWER DENSITY    54.328033                                                   7
NEUTRON MULTIPLICATION    0.99613780 FINAL AVG. EXPOSURE        29305.2
DIFP   (EPS5 = 0.00200)   0.00120246 CORE AVG. NEUTRON FLUX   1.467E+14               9
AVERAGE VOID FRACTION       0.474274 CORE AVG. GD WORTH          -0.025
CORE PRESSURE DROP,PSI      7.838247 CORE AVG. GD RESIDUAL WORTH  0.000              11
EXP RATIO INDEX (INER-II)     0.0000 CORE AVERAGE XENON WORTH   -0.0242
                                                                                     13
CORE HISTORY MAX. VALUES:      LOCATION: I   J   K
  NODAL EXPOSURE, MWD/T   58431.         7   7   5   METRIC    64409.               15                    4
  BUNDLE EXPOSURE, MWD/T  45179.         5  17       METRIC    49801.
  EXPOSURE RATIO, NEXRAT  0.0000         0   0   0                                   17
  AXIAL POWER PEAK        1.2529                15
                                                                                     19                        1
```

Figure 4A-17a. Control Rod Pattern Summary at 17.9 GWd/MT Exposure

17.9 GWD/MT

Node	Axial Power
25	0.291
24	0.572
23	0.808
22	0.982
21	1.108
20	1.181
19	1.216
18	1.214
17	1.182
16	1.187
15	1.253
14	1.233
13	1.218
12	1.200
11	1.177
10	1.152
9	1.124
8	1.091
7	1.050
6	1.002
5	0.949
4	0.892
3	0.822
2	0.698
1	0.395

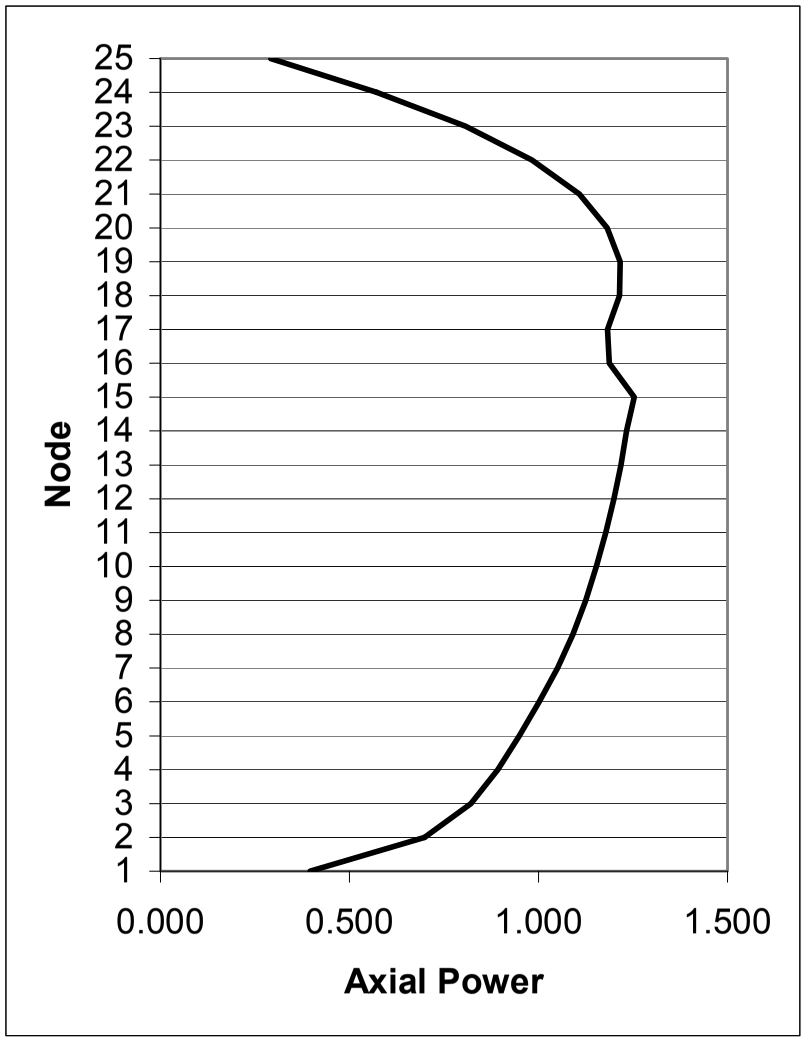

Figure 4A-17b. Relative Axial Power at 17.9 GWd/MT Exposure

17.9 GWD/MT

Node	Axial Exposure (MWD/MT)
25	7315.2
24	12583.7
23	17573.2
22	22313.0
21	26358.8
20	29635.7
19	32244.5
18	34076.4
17	35124.6
16	35837.0
15	34718.0
14	35873.2
13	36865.6
12	37584.3
11	38206.4
10	38719.3
9	39000.5
8	39330.2
7	39759.1
6	40139.9
5	40182.3
4	39294.3
3	36146.2
2	29072.7
1	15125.0

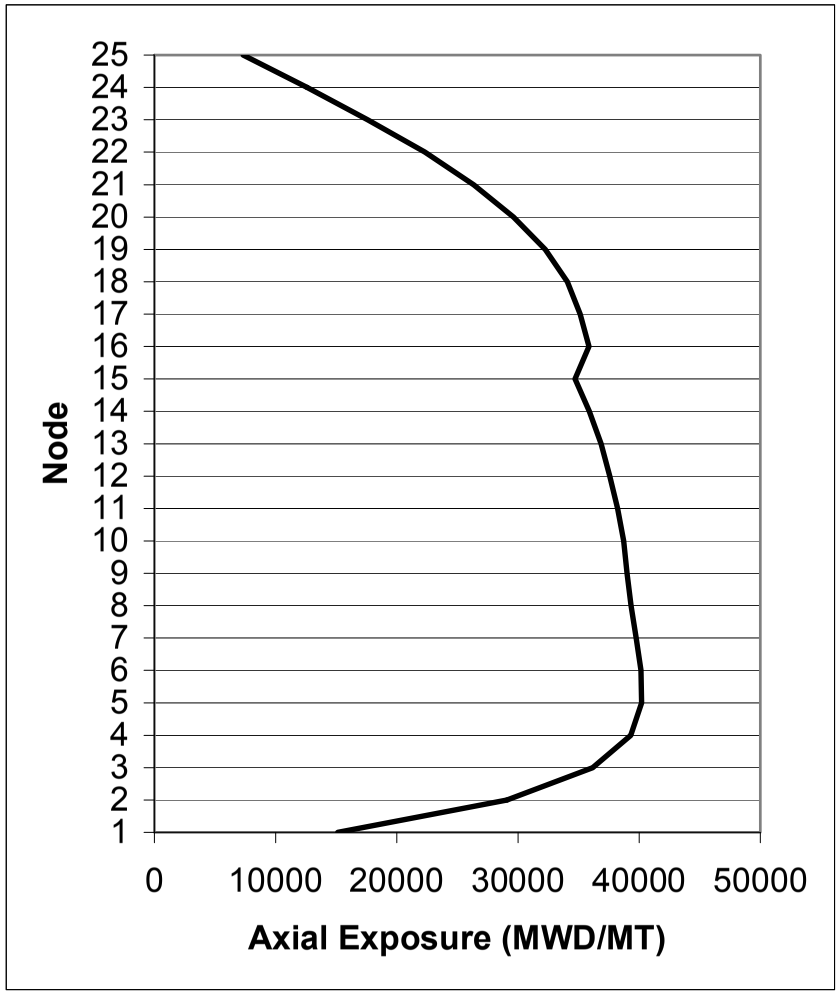

Figure 4A-17c. Axial Exposure at 17.9 GWd/MT Exposure

	1	2	3	4	5	6	7	8	9	10	11	12	13	14	15	16	17	18	19
1															0.30	0.34	0.38	0.42	0.42
2													0.37	0.47	0.50	0.63	0.69	0.72	0.77
3											0.45	0.55	0.71	0.86	0.78	0.78	0.85	0.99	0.77
4									0.43	0.57	0.76	0.95	1.04	1.08	0.91	0.94	1.10	1.11	0.99
5								0.50	0.74	0.96	1.07	1.14	1.04	1.21	1.20	1.18	0.93	1.17	0.97
6							0.49	0.75	1.01	1.12	1.18	1.05	1.25	1.05	1.22	1.01	1.18	1.00	1.17
7						0.49	0.63	1.02	1.01	1.20	0.97	1.09	1.26	1.26	1.03	1.07	1.02	1.19	1.00
8					0.50	0.75	1.02	1.15	1.23	1.05	1.13	1.01	1.27	1.13	1.14	1.12	1.22	1.03	1.01
9				0.43	0.74	1.01	1.01	1.23	1.13	1.28	1.28	1.27	1.12	1.27	1.08	1.26	1.07	1.23	1.04
10				0.57	0.96	1.12	1.20	1.05	1.28	1.09	1.28	1.08	1.27	1.08	1.27	1.27	1.27	1.08	1.26
11			0.45	0.76	1.07	1.18	0.97	1.13	1.28	1.28	1.05	1.09	1.11	1.26	1.03	1.08	1.08	1.28	1.11
12			0.55	0.95	1.14	1.05	1.09	1.01	1.27	1.08	1.09	1.09	1.27	1.26	1.06	1.05	1.25	1.27	1.11
13		0.37	0.71	1.04	1.04	1.25	1.26	1.27	1.12	1.27	1.11	1.27	1.07	1.22	1.01	1.18	1.04	1.24	1.05
14		0.47	0.86	1.08	1.21	1.05	1.26	1.13	1.27	1.08	1.26	1.26	1.22	0.99	1.09	0.93	1.16	1.02	1.19
15	0.30	0.50	0.78	0.91	1.20	1.22	1.03	1.14	1.08	1.27	1.03	1.06	1.01	1.09	0.66	0.68	1.08	1.13	0.94
16	0.34	0.63	0.78	0.94	1.18	1.01	1.07	1.12	1.26	1.27	1.08	1.05	1.18	0.93	0.68	0.67	1.05	0.92	0.91
17	0.38	0.69	0.85	1.10	0.93	1.18	1.02	1.22	1.07	1.27	1.08	1.25	1.04	1.16	1.08	1.05	0.91	1.06	0.88
18	0.42	0.72	0.99	1.11	1.17	1.00	1.19	1.03	1.23	1.08	1.28	1.27	1.24	1.02	1.13	0.92	1.06	0.88	0.99
19	0.42	0.77	0.77	0.99	0.97	1.17	1.00	1.01	1.04	1.26	1.11	1.11	1.05	1.19	0.94	0.91	0.88	0.99	0.63

Figure 4A-17d. Relative Integrated Power Per Bundle at 17.9 GWd/MT Exposure

	1	2	3	4	5	6	7	8	9	10	11	12	13	14	15	16	17	18	19
1															42.92	42.44	46.46	43.83	44.83
2													49.62	46.01	46.38	31.73	31.11	30.31	12.93
3											46.78	45.95	31.96	14.24	36.31	37.76	36.20	17.04	47.30
4									46.08	46.17	30.14	14.81	16.65	17.72	39.29	38.29	19.37	19.19	32.94
5								49.19	26.77	14.33	16.26	17.99	36.87	20.09	20.35	20.65	49.79	20.84	41.31
6							46.18	28.58	15.50	17.01	18.40	39.65	20.95	41.92	21.12	42.40	21.39	42.24	21.06
7						46.18	49.06	15.68	35.29	19.01	48.13	38.74	21.16	21.82	45.53	40.37	41.80	21.62	41.84
8					49.19	28.58	15.68	17.86	19.73	40.45	36.42	48.92	21.98	34.91	36.06	36.47	22.23	41.90	41.63
9				46.09	26.76	15.50	35.29	19.73	38.16	21.16	21.10	21.67	42.05	22.83	42.51	22.56	42.55	22.30	41.82
10				46.17	14.33	17.01	19.01	40.45	21.16	42.46	21.22	41.54	22.33	42.96	22.33	22.19	22.49	42.16	21.27
11			46.78	30.14	16.26	18.40	48.14	36.42	21.10	21.22	47.22	39.68	42.10	22.04	48.59	40.86	42.29	21.38	39.63
12			45.96	14.81	17.99	39.64	38.74	48.93	21.67	41.54	39.67	40.60	21.81	21.86	40.57	40.97	21.78	21.11	38.53
13		49.59	31.96	16.65	36.87	20.95	21.16	21.99	42.04	22.33	42.10	21.81	43.20	22.25	42.06	21.79	42.53	21.76	41.65
14		46.02	14.24	17.73	20.10	41.91	21.82	34.91	22.83	42.96	22.04	21.86	22.26	42.88	21.46	41.76	21.90	41.91	21.21
15	42.92	46.39	36.31	39.29	20.35	21.12	45.54	36.05	42.51	22.33	48.60	40.57	42.05	21.46	47.21	40.18	21.18	21.39	46.46
16	42.44	31.73	37.75	38.29	20.65	42.40	40.37	36.47	22.56	22.19	40.86	40.97	21.79	41.76	40.18	40.29	21.29	41.06	40.83
17	46.46	31.11	36.20	19.37	49.80	21.39	41.80	22.24	42.55	22.49	42.28	21.79	42.52	21.90	21.18	21.29	42.59	21.58	41.85
18	43.84	30.31	17.04	19.19	20.84	42.24	21.62	41.90	22.30	42.16	21.39	21.12	21.76	41.91	21.39	41.06	21.58	42.42	20.70
19	44.83	12.93	47.31	32.94	41.30	21.06	41.83	41.63	41.82	21.28	39.62	38.53	41.65	21.21	46.46	40.83	41.84	20.70	39.31

Figure 4A-17e. Average Bundle Exposure at 17.9 GWd/MT Exposure

```
        ( ROD PATTERN DEPLETION

NITER   0  POWER           IMAX  19  POWER(MWT)          4.5000E+03  ( 100.0 %)
IBOUN   1  1/4             JMAX  19  PRESSURE(PSIA)      1.0550E+03
IRN     1  MIRROR          KMAX  25  FLOW(*10E-6LB/HR)   7.8508E+01  ( 100.0 %)
ILPA    0                  NSMAX 10  BYPASS(LB/HR)       1.1742E+07  (  15.0 %)          CONTROL ROD CONFIGURATION
IFLW    2  DETAIL          LMAX  20  ENTHALPY(BTU/LB)            512.30                    IN NOTCHES WITHDRAWN
RSTART  0  NEW             LVDCT  7  INLET TEMP(DEG F)           520.47
NEWPHY  2                  IPFTL  0  BEGINNING EXPOSURE         29305.1                1  3  5  7  9 11 13 15 17 19
NEXO    3  CALC.                    DELTA EXPOS.(DELTE)            0.0
RBOCA   1                  IALPRM 0  DELBRN                      571.7                1
IACF    0                  IFAST  0  TOTAL NOTCHES                  0
             IPDOME   1    IAHB   0  CORE FUEL MASS         MTU:162.928                3
                                     CORE FUEL MASS         STU:179.596
ENERGY (MWD) (DELTE)              0. ENERGY (MWD) (DELBRN)      102666.                5
CYCLE ENERGY (MWD)          3012149. CYCLE EXPOSURE             16771.7
CORE AVG. POWER DENSITY    54.328033                                                     7
NEUTRON MULTIPLICATION    0.99644077 FINAL AVG. EXPOSURE        29876.8
DIFP   (EPS5 = 0.00200)   0.00122178 CORE AVG. NEUTRON FLUX   1.467E+14                9
AVERAGE VOID FRACTION       0.465628 CORE AVG. GD WORTH          -0.024
CORE PRESSURE DROP,PSI      7.820546 CORE AVG. GD RESIDUAL WORTH  0.000               11
EXP RATIO INDEX (INER-II)     0.0000 CORE AVERAGE XENON WORTH   -0.0243
                                                                                       13
CORE HISTORY MAX. VALUES:      LOCATION: I   J   K
  NODAL EXPOSURE, MWD/T   58746.         7   7   5   METRIC    64756.                15
  BUNDLE EXPOSURE, MWD/T  45709.         5  17       METRIC    50385.
  EXPOSURE RATIO, NEXRAT  0.0000         0   0   0                                    17
  AXIAL POWER PEAK        1.2624                15
                                                                                       19
```

Figure 4A-18a. Control Rod Pattern Summary at 18.5 GWd/MT Exposure

18.5 GWD/MT

Node	Axial Power
25	0.309
24	0.607
23	0.858
22	1.039
21	1.162
20	1.227
19	1.253
18	1.241
17	1.200
16	1.200
15	1.262
14	1.238
13	1.218
12	1.195
11	1.168
10	1.138
9	1.105
8	1.066
7	1.019
6	0.964
5	0.903
4	0.840
3	0.766
2	0.651
1	0.370

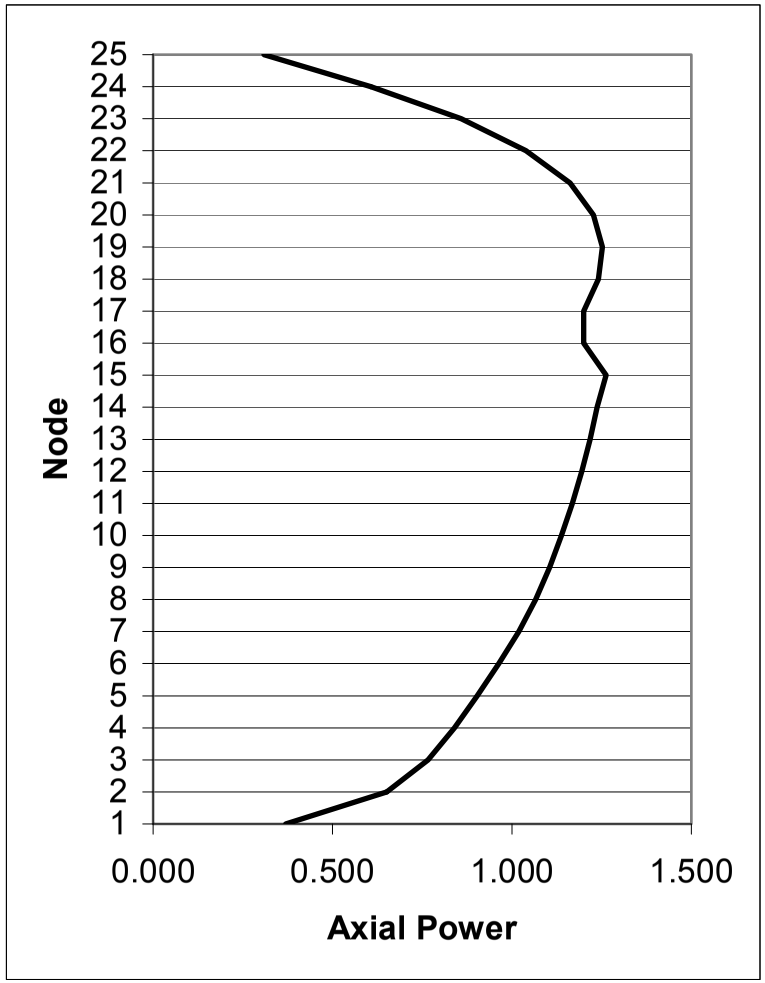

Figure 4A-18b. Relative Axial Power at 18.5 GWd/MT Exposure

18.5 GWD/MT

Node	Axial Exposure (MWD/MT)
25	7555.4
24	12997.8
23	18134.9
22	22996.1
21	27129.3
20	30457.4
19	33090.3
18	34921.0
17	35947.0
16	36632.4
15	35454.9
14	36598.4
13	37581.9
12	38289.8
11	38898.9
10	39396.9
9	39662.3
8	39972.7
7	40377.5
6	40730.0
5	40741.1
4	39819.7
3	36630.0
2	29483.8
1	15353.0

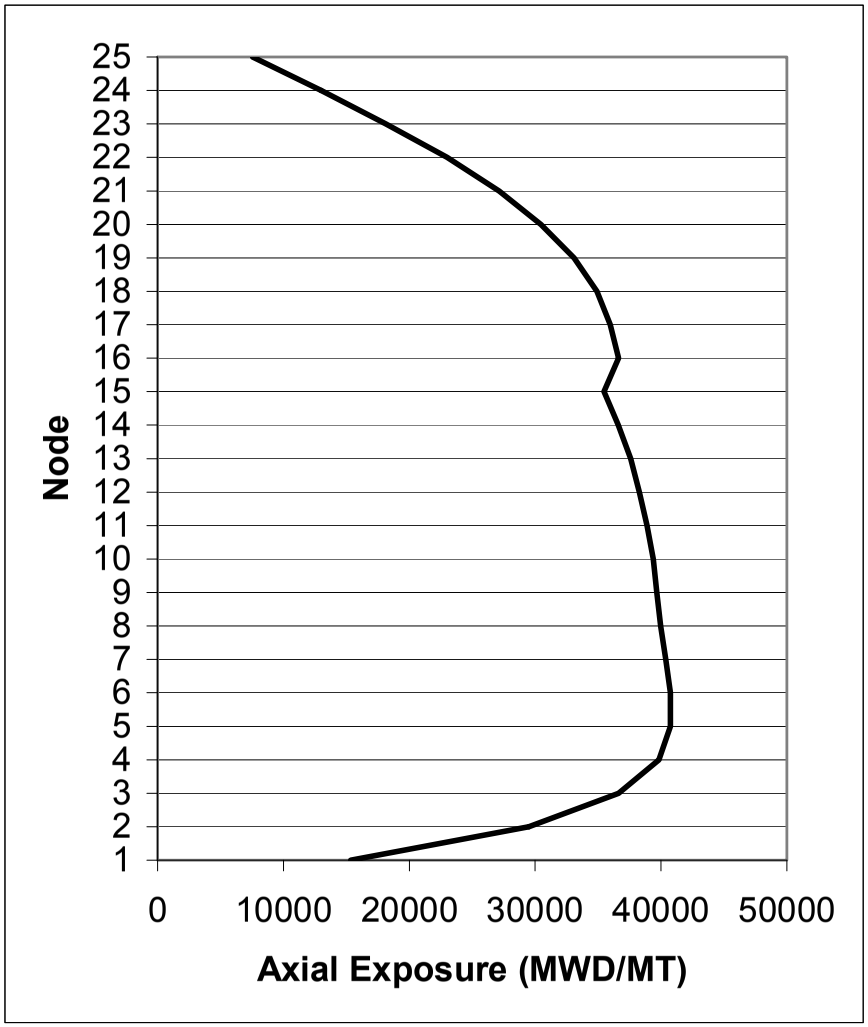

Figure 4A-18c. Axial Exposure at 18.5 GWd/MT Exposure

	1	2	3	4	5	6	7	8	9	10	11	12	13	14	15	16	17	18	19
1															0.29	0.33	0.37	0.40	0.40
2													0.36	0.45	0.48	0.61	0.66	0.70	0.75
3											0.43	0.53	0.69	0.84	0.75	0.75	0.82	0.96	0.74
4									0.42	0.55	0.74	0.93	1.02	1.05	0.88	0.91	1.06	1.07	0.95
5								0.48	0.72	0.93	1.04	1.11	1.01	1.17	1.15	1.13	0.89	1.12	0.93
6							0.47	0.73	0.99	1.09	1.15	1.01	1.21	1.01	1.17	0.97	1.13	0.96	1.12
7						0.47	0.61	0.99	0.98	1.17	0.94	1.05	1.21	1.21	0.99	1.02	0.98	1.14	0.96
8					0.48	0.73	0.99	1.12	1.19	1.02	1.08	0.97	1.22	1.09	1.09	1.08	1.17	0.99	0.97
9				0.42	0.72	0.99	0.98	1.19	1.09	1.23	1.23	1.22	1.08	1.22	1.04	1.22	1.03	1.19	1.01
10				0.55	0.93	1.09	1.17	1.02	1.23	1.05	1.24	1.05	1.22	1.05	1.23	1.24	1.24	1.06	1.23
11			0.43	0.74	1.04	1.15	0.94	1.08	1.23	1.24	1.01	1.05	1.08	1.24	1.01	1.07	1.07	1.27	1.09
12			0.53	0.93	1.11	1.01	1.05	0.97	1.22	1.05	1.05	1.06	1.25	1.25	1.07	1.07	1.27	1.28	1.11
13		0.36	0.69	1.02	1.01	1.21	1.21	1.22	1.08	1.22	1.08	1.25	1.07	1.26	1.06	1.25	1.08	1.28	1.08
14		0.45	0.84	1.05	1.17	1.01	1.21	1.09	1.22	1.05	1.24	1.25	1.26	1.06	1.24	1.07	1.28	1.09	1.25
15	0.29	0.48	0.75	0.88	1.15	1.17	0.99	1.09	1.04	1.23	1.01	1.07	1.06	1.24	1.04	1.09	1.28	1.26	1.03
16	0.33	0.61	0.75	0.91	1.13	0.97	1.02	1.08	1.22	1.24	1.07	1.07	1.25	1.07	1.09	1.09	1.27	1.06	1.04
17	0.37	0.66	0.82	1.06	0.89	1.13	0.98	1.17	1.03	1.24	1.07	1.27	1.08	1.28	1.28	1.27	1.07	1.24	1.04
18	0.40	0.70	0.96	1.07	1.12	0.96	1.14	0.99	1.19	1.06	1.27	1.28	1.28	1.09	1.26	1.06	1.24	1.06	1.25
19	0.40	0.75	0.74	0.95	0.93	1.12	0.96	0.97	1.01	1.23	1.09	1.11	1.08	1.25	1.03	1.04	1.04	1.25	1.10

Figure 4A-18d. Relative Integrated Power Per Bundle at 18.5 GWd/MT Exposure

	1	2	3	4	5	6	7	8	9	10	11	12	13	14	15	16	17	18	19
1															43.11	42.65	46.70	44.09	45.09
2													49.86	46.31	46.70	32.13	31.54	30.76	13.42
3											47.06	46.29	32.41	14.78	36.80	38.25	36.73	17.67	47.78
4									46.35	46.52	30.63	15.41	17.31	18.41	39.87	38.88	20.07	19.89	33.56
5								49.50	27.23	14.93	16.94	18.71	37.53	20.86	21.11	21.39	50.38	21.58	41.92
6							46.48	29.05	16.13	17.72	19.15	40.31	21.74	42.58	21.88	43.04	22.13	42.87	21.80
7						46.48	49.46	16.32	35.93	19.77	48.75	39.43	21.95	22.61	46.18	41.05	42.44	22.37	42.47
8					49.51	29.05	16.32	18.58	20.50	41.11	37.13	49.56	22.78	35.62	36.77	37.17	23.00	42.55	42.26
9				46.36	27.23	16.14	35.92	20.50	38.87	21.97	21.91	22.47	42.75	23.62	43.18	23.36	43.22	23.07	42.48
10				46.53	14.93	17.72	19.77	41.11	21.97	43.15	22.03	42.22	23.13	43.64	23.13	22.99	23.29	42.84	22.07
11			47.07	30.62	16.94	19.15	48.75	37.13	21.91	22.03	47.89	40.36	42.80	22.83	49.24	41.54	42.96	22.19	40.33
12			46.30	15.41	18.71	40.30	39.43	49.57	22.47	42.22	40.36	41.28	22.61	22.65	41.24	41.63	22.57	21.92	39.23
13		49.83	32.41	17.31	37.53	21.74	21.95	22.78	42.75	23.13	42.80	22.61	43.87	23.03	42.69	22.53	43.18	22.54	42.31
14		46.31	14.78	18.41	20.86	42.57	22.61	35.63	23.63	43.64	22.84	22.65	23.03	43.50	22.14	42.35	22.63	42.55	21.96
15	43.11	46.71	36.80	39.87	21.11	21.89	46.18	36.77	43.19	23.13	49.25	41.24	42.69	22.14	47.63	40.61	21.86	22.10	47.06
16	42.66	32.13	38.25	38.88	21.40	43.03	41.04	37.18	23.36	22.99	41.54	41.63	22.53	42.34	40.61	40.71	21.95	41.64	41.41
17	46.70	31.55	36.74	20.07	50.39	22.14	42.44	23.00	43.22	23.29	42.96	22.57	43.18	22.63	21.87	21.95	43.16	22.25	42.40
18	44.10	30.76	17.67	19.89	21.58	42.87	22.37	42.55	23.08	42.84	22.19	21.92	22.54	42.55	22.10	41.64	22.25	42.98	21.33
19	45.09	13.42	47.79	33.56	41.92	21.80	42.46	42.26	42.48	22.07	40.32	39.23	42.31	21.96	47.06	41.41	42.40	21.33	39.70

Figure 4A-18e. Average Bundle Exposure at 18.5 GWd/MT Exposure

Exposure (MWD/MT)	MCPR
0	1.435
1102	1.442
2205	1.426
3307	1.443
4409	1.385
5512	1.409
6614	1.443
7716	1.468
8818	1.503
9921	1.491
11023	1.490
12125	1.499
13228	1.508
14330	1.529
15432	1.538
16535	1.506
17857	1.515
18488	1.514

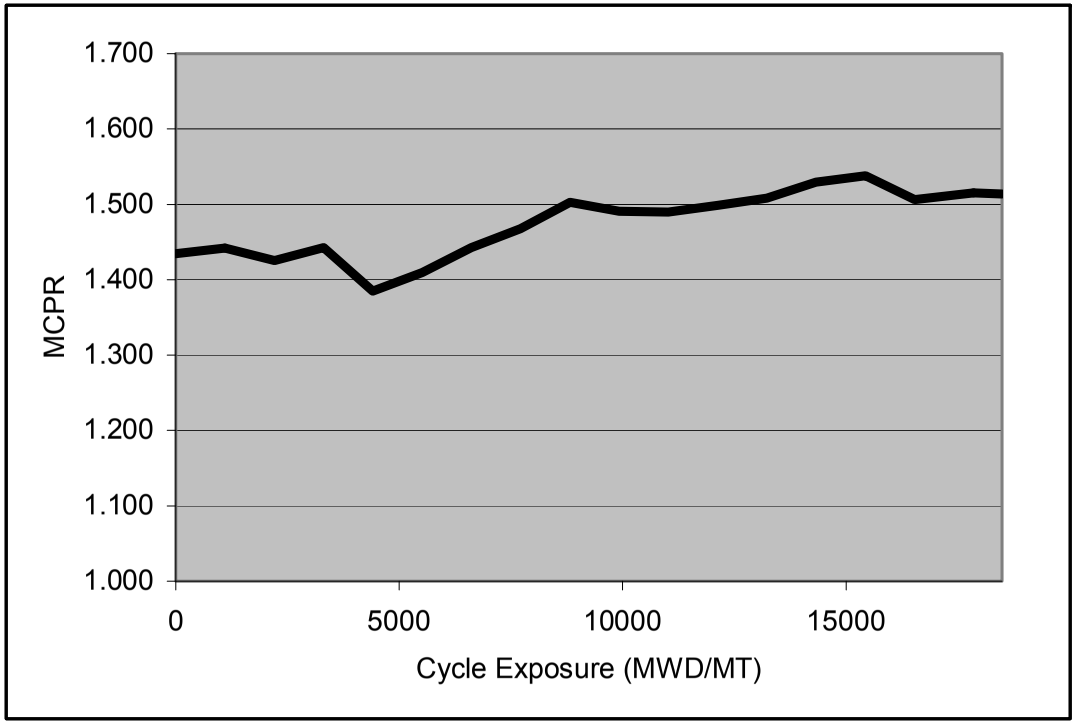

Figure 4A-19. Minimum Critical Power Ratio (MCPR) as a Function of Exposure

4B. FUEL LICENSING ACCEPTANCE CRITERIA

The fuel licensing acceptance criteria are presented in the following subsections.

4B.1 GENERAL CRITERIA

This section has been deleted.

4B.2 THERMAL-MECHANICAL

A set of design limits are defined, and applied in the fuel rod thermal-mechanical design analyses, to ensure that fuel rod mechanical integrity is maintained throughout the fuel rod design lifetime. The design criteria were developed by GNF and other specific industry groups to focus on the parameters most significant to fuel performance and operating occurrences that can realistically limit fuel performance. The specific criteria are patterned after ANSI/ANS-57.5-1981 (Reference 4B-1) and NUREG-0800 Rev. 2 (Reference 4B-2). Table 4B.1-1 presents a summary of the design criteria. The bases for the design criteria listed in Table 4B.1-1 are presented below.

Table 4B.1-1 Fuel Rod Thermal-Mechanical Design Criteria

Criterion	Governing Equation
1. [*The cladding creepout rate ($\dot{\varepsilon}$ cladding creepout), due to fuel rod internal pressure, shall not exceed the fuel pellet irradiation swelling rate ($\dot{\varepsilon}$ fuel swelling).*]*	$\dot{\varepsilon}_{cladding\_creepout} \le \dot{\varepsilon}_{fuel\_swelling}$
2. [*The maximum fuel center temperature (T_{center}) shall remain below the fuel melting point (T_{melt}).*]*	$T_{center} < T_{melt}$
3. [*The cladding circumferential plastic strain (ε_θ^P) during an anticipated operational occurrence shall not exceed 1.00%*]*.	$\varepsilon_\theta^P \le 1.00\%$
4. [*The fuel rod cladding fatigue life usage ($\sum_i \frac{n_i}{n_f}$ where n_i=number of applied strain cycles at amplitude ε_i and n_f=number of cycles to failure at amplitude ε_i) shall not exceed the material fatigue capability.*]*	$\sum_i \frac{n_i}{n_f} \le 1.0$
5. [*Cladding structural instability, as evidenced by rapid ovality changes, shall not occur.*]*	No creep collapse
6. [*Cladding effective stresses(σ_e)/strains(ε_e) shall not exceed the failure stress(σ_f)/strain(ε_f).*]*	$\sigma_e < \sigma_f, \quad \varepsilon_e < \varepsilon_f$
7. [*The as-fabricated fuel pellet evolved hydrogen (C_H is content of hydrogen) at greater than 1800 ℃ shall not exceed prescribed limits.*]*	$C_H \le$ *Manufacturing Specifications*

Cladding Lift-Off / Fuel Rod Internal Pressure (Item 1 of Table 4B.1-1)

The fuel rod is filled with helium during manufacture to a specified fill gas pressure. With the initial rise to power, this fuel rod internal pressure increases due to the corresponding increase in the gas average temperature and the reduction in the fuel rod void volume due to fuel pellet expansion and inward cladding elastic deflection due to the higher reactor coolant pressure. With continued irradiation, the fuel rod internal pressure will progressively increase further due to the release of gaseous fission products from the fuel pellets to the fuel rod void volume. With further irradiation, a potential adverse thermal feedback condition may arise due to excessive fuel rod internal pressure.

In this case, the tensile cladding stress resulting from a fuel rod internal pressure greater than the coolant pressure causes the cladding to deform outward (cladding creep-out). If the rate of the cladding outward deformation (cladding creep-out rate) exceeds the rate at which the fuel pellet expands due to irradiation swelling (fuel swelling rate), the pellet-cladding gap will begin to open (or increase if already open). An increase in the pellet-cladding gap will reduce the pellet-cladding thermal conductance thereby increasing fuel temperatures. The increased fuel temperatures will result in further fuel pellet fission gas release, greater fuel rod internal pressure, and correspondingly a faster rate of cladding creep-out and gap opening.

This potential adverse thermal feedback condition is avoided by limiting the cladding creep-out rate, due to fuel rod internal pressure, to less than or equal to the fuel pellet irradiation swelling rate. This is confirmed through the calculation of a design ratio (of internal pressure to critical pressure) and ensuring that the calculated design ratio is less than 1.00 at any point in time for all fuel rod types.

Fuel Temperature (Melting, Item 2 of Table 4B.1-1)

Numerous irradiation experiments have demonstrated that extended operation with significant fuel pellet central melting does not result in damage to the fuel rod cladding. However, the fuel rod performance is evaluated to ensure that fuel melting will not occur. To achieve this objective, the fuel rod is evaluated to ensure that fuel melting during normal steady-state operation and whole core anticipated operational occurrences is not expected to occur.

Cladding Strain

After the initial rise to power and the establishment of steady-state operating conditions, the pellet-cladding gap will eventually close due to the combined effects of cladding creep-down, fuel pellet irradiation swelling, and fuel pellet fragment outward relocation. Once hard pellet-cladding contact (PCMI) has occurred, cladding outward diametral deformation can occur. The consequences of this cladding deformation are dependent on the deformation rate (strain rate).

High Strain Rate (Anticipated Operational Occurrences, Item 3 of Table 4B.1-1)

Depending on the extent of irradiation exposure, the magnitude of the power increase, and the final peak power level, the cladding can be strained due to the fuel pellet thermal expansion occurring during rapid power ramps. This high strain rate deformation can be a combination of (a) plastic deformation during the power increase due to the cladding stress exceeding the cladding material yield strength, and (b) creep deformation during the elevated power hold time due to creep-assisted relaxation of the high cladding stresses. This cladding permanent (plastic plus creep) deformation during anticipated operational occurrences is limited to a maximum of 1.00%.

In non-barrier cladding, fast power ramps can also cause a chemical/mechanical pellet cladding interaction commonly known as PCI/SCC. To prevent PCI/SCC failures in non-barrier cladding, reactor operational restrictions must be imposed. To eliminate PCI/SCC failures without imposing reactor operational restrictions, GNF invented and developed barrier cladding. Barrier cladding utilizes a thin zirconium layer on the inner surface of Zircaloy tubes. The minimum thickness of the zirconium layer is specified to ensure that small cracks which are known to initiate on the inner surface of barrier cladding (the surface layer subject to hardening by absorption of fission products during irradiation) will not propagate through the zirconium

barrier into the Zircaloy tube. The barrier concept has been demonstrated by experimental irradiation testing and extensive commercial reactor operation to be an effective preventive measure for PCI/SCC failure without imposing reactor operating restrictions.

Low Strain Rate (Steady-State Operation, no limit in Table 4B.1-1)

During normal steady-state operation, once the cladding has come into hard contact with the fuel, subsequent fuel pellet irradiation swelling causes the cladding to deform gradually outward. The fuel pellet swelling rate is very slow. The effect of this slow fuel pellet expansion is the relaxation of low stresses imposed by the fuel swelling, resulting in a low strain-rate outward creep deformation of the cladding. Similarly, when the fuel rod internal pressure exceeds the external pressure exerted by the reactor coolant, the cladding will also slowly creep outward. Under both of these conditions, irradiated Zircaloy exhibits substantial creep ductility. Therefore, no specific limit is applied to low-strain rate cladding deformation.

Dynamic Loads / Cladding Fatigue (Item 4 of Table 4B.1-1)

As a result of normal operational variations, cyclic loadings are applied to the fuel rod cladding by the fuel pellet. Therefore, the fuel rod is evaluated to ensure that the cumulative duty from cladding strains due to these cyclic loadings will not exceed the cladding fatigue capability. The Zircaloy fatigue curve employed represents a statistical lower bound to the existing fatigue experimental measurements. The design limit for fatigue cycling, to assure that the design basis is met, is that the value of calculated fatigue usage must be less than the material fatigue capability (fatigue usage < 1.0).

Elastic Buckling / Cladding Creep Collapse (Item 5 of Table 4B.1-1)

The condition of an external coolant pressure greater than the fuel rod internal pressure provides the potential for elastic buckling or possibly even plastic deformation if the stresses exceed the material yield strength. Fuel rod failure due to elastic buckling or plastic collapse has never been observed in commercial nuclear reactors. However, a more limiting condition that has been observed in commercial nuclear reactors is cladding creep collapse. This condition occurs at cladding stress levels far below that required for elastic buckling or plastic deformation. In the early 1970s, excessive in-reactor fuel pellet densification resulted in the production of large fuel column axial gaps in some PWR fuel rods. The high PWR coolant pressure in conjunction with thin cladding tubes and low helium fill gas pressure resulted in excessive fuel rod cladding creep and subsequent cladding collapse over fuel column axial gaps. Such collapse occurs due to a slow increase of cladding initial ovality due to creep resulting from the combined effect of reactor coolant pressure, temperature and fast neutron flux on the cladding over the axial gap. Since the cladding is unsupported by fuel pellets in the axial gap region, the ovality can become large enough to result in elastic instability and cladding collapse.

Fuel Rod Stresses (Item 6 of Table 4B.1-1)

The fuel rod is evaluated to ensure that fuel rod failure will not occur due to stresses or strains exceeding the fuel rod mechanical capability. In addition to the loads imposed by the difference between the external coolant pressure and the fuel rod internal gas pressure, a number of other stresses or strains can occur in the cladding tube. These stresses or strains are combined through application of the distortion energy theory to determine an effective stress or strain. The applied

limit is patterned after ANSI/ANS-57.5-1981 (Reference 4B-1). The figure of merit employed is termed the Design Ratio where

$$Design\ Ratio = \frac{Effective\ Stress}{Stress\ Limit}\ or\ \frac{Effective\ Strain}{Strain\ Limit}$$

where the stress or strain limit is the failure stress or strain. The value of the Design Ratio must be less than 1.00.

Fuel Rod Hydrogen (Item 7 of Table 4B.1-1)

GNF experience has demonstrated that excessive fuel rod internal hydrogen content due to hydrogenous impurities can result in fuel rod failure due to localized hydriding. The potential for primary hydriding fuel rod failure is limited by the application of specification limits on the fuel pellets in conjunction with fabrication practices that eliminate hydrogenous contaminants from all sources during the manufacturing process.

4B.3 NUCLEAR

[*A negative Doppler reactivity coefficient is maintained for any operating condition.*]* The Doppler reactivity coefficient is of high importance in reactor safety. The Doppler coefficient of the core is a measure of the reactivity change associated with an increase in the absorption of resonance-energy neutrons caused by a change in the temperature of the material and is a function of the average of the bundle Doppler coefficients. A negative Doppler coefficient provides instantaneous negative reactivity feedback to any rise in fuel temperature, on a gross or local basis and thus assures the tendency of self-control .

[*A negative core moderator void reactivity coefficient resulting from boiling in the active flow channels is maintained for any operating conditions.*]* The core moderator void coefficient resulting from boiling in the active flow channels is maintained negative over the complete range of ESBWR operation. This flattens the radial power distribution and provides ease of reactor control due to the negative void feedback mechanism.

[*A negative moderator temperature reactivity coefficient is maintained for temperatures equal or greater than hot standby.*]* The moderator temperature coefficient is associated with a change in the moderating capability of the water. Once the reactor reaches the power producing range, boiling begins and the moderator temperature remains essentially constant. The moderator temperature reactivity coefficient is negative during power operation.

[*To prevent a super prompt critical reactivity insertion accident originating from any operating condition, the net prompt reactivity feedback due to prompt heating of the moderator and fuel is negative.]** The mechanical and nuclear designs of the fuel are such that the prompt reactivity feedback (requiring no conductive or convective heat transfer and no operator action) provides an automatic shutdown mechanism in the event of a super prompt reactivity incident. This characteristic ensures rapid termination of super prompt critical accidents, with additional long-term shutdown capability due to negative void coefficient, for those cases where conductive heat transfer from the fuel to the water results in boiling in the active channel region.

[*A negative power reactivity coefficient (as determined by calculating the reactivity change due to an incremental power change) from a steady-state base power level) is maintained for all operating power levels above hot standby.*]* A negative power coefficient provides an inherent

negative feedback mechanism to provide more reliable control of the plant as the operator performs power maneuvers. It is particularly effective in preventing xenon initiated power oscillations in the core. The power coefficient is effectively the combination of Doppler, void and moderator temperature reactivity coefficients.

[*The core is capable of being made subcritical with margin in the most reactive condition throughout an operating cycle with the most reactive control rod, or rod pair, in the full-out position and all other rods fully inserted.*]* This parameter is dependent upon the core loading and is calculated for each plant cycle prior to plant operation of that cycle.

4B.4 HYDRAULIC

This section has been deleted.

4B.5 OPERATING LIMIT MCPR

This section has been deleted.

4B.6 CRITICAL POWER CORRELATION

[*The currently approved critical power correlation will be confirmed or a new correlation is established when there is a change in wetted parameters of the flow geometry in the active region of the assembly; this specifically includes fuel and water rod diameter, channel sizing and spacer design.*]*

- The criteria for establishing the new correlation are as follows:
- The new correlation shall be based on full-scale prototypical test assemblies.
- Tests shall be performed on assemblies with typical rod-to-rod peaking factors.
- The functional form of the currently approved correlations shall be maintained.
- Correlation fit to data shall be best fit.
- The correlation's range of application shall be determined.
- One or more additional assemblies must be tested to verify correlation accuracy (i.e., test data not used to determine the new correlation coefficients).
- The uncertainty of the resulting correlation shall be determined and included in establishing the operating limits.

The basis of the correlation is a best fit of data taken of prototypical test assemblies with typical rod-to-rod peaking factors.

4B.7 STABILITY

This section has been deleted.

4B.8 OVERPRESSURE PROTECTION ANALYSIS

This section has been deleted.

4B.9 REFUELING ACCIDENT ANALYSIS

This section has been deleted.

4B.10 ANTICIPATED TRANSIENT WITHOUT SCRAM

This section has been deleted.

4B.11 COL UNIT-SPECIFIC INFORMATION

None.

4B.12 REFERENCES

4B-1 American National Standard for Light Water Reactors Fuel Assembly Mechanical Design and Evaluation, American Nuclear Society Standards Committee Working Group ANS 57.5, ANSI/ANS-57.5-1981.

4B-2 US Nuclear Regulatory Commission Standard Review Plan 4.2 – Fuel System Design, (USNRC SRP 4.2), NUREG-0800 Rev. 2, July 1981.

4C. CONTROL ROD LICENSING ACCEPTANCE CRITERIA

A set of acceptance criteria has been established for evaluating control rod designs. Control rod compliance with these criteria constitutes the basis for NRC acceptance and approval of the design . The control rod licensing acceptance criteria and their bases are provided below. Any change to these criteria must have prior NRC review and approval.

4C.1 GENERAL CRITERIA

[*The control rod will meet following acceptance criteria:*

- *The control rod stresses, strains, and cumulative fatigue shall be evaluated to not exceed the ultimate stress or strain limit of the material.*
- *The control rod shall be evaluated to be capable of insertion into the core during all modes of plant operation within the limits assumed in the plant analyses.*
- *The material of the control rod shall be shown to be compatible with the reactor environment.*
- *The reactivity worth of the control rod shall be included in the plant core analyses.*]*

4C.2 BASIS FOR ACCEPTANCE CRITERIA

The following licensing bases is provided for the acceptance criteria given in Section 4C.1:

Stress, Strain and Fatigue

The control rod is evaluated to assure that it does not fail because of loads due to shipping, handling, normal operation, including the effects of anticipated operational occurrences (AOOs), infrequent incidents and accidents. To ensure that the control rod does not fail, these loads must not exceed the ultimate stress and strain limit of the material, structure, or welded connection. Fatigue must not exceed a fatigue usage factor of 1.0.

The loads evaluated include those due to normal operational transients (scram and jogging), pressure differentials, thermal gradients, flow and system induced vibration, and irradiation growth in addition to the lateral and vertical loads expected for each condition. Fatigue usage is based upon the cumulative effect of the cyclic loadings. The analyses include corrosion and crud deposition as a function of time, as appropriate.

Conservatism is included in the analyses by including margin to the limit or by assuming loads greater than expected for each condition. Higher loads can be incorporated into the analyses by increasing the load itself or by statistically considering the uncertainties in the value of the load.

Control Rod Insertion

The control rod is evaluated to be sure that it can be inserted during normal operations including the effects of anticipated operational occurrences (AOOs), infrequent incidents and accidents. These evaluations include a combination of analyses of the geometrical clearance and actual testing. The analyses consider the effects of manufacturing tolerances, swelling and irradiation growth. Tests may be performed to demonstrate control rod insertion capability for conditions such as control rod or fuel channel deformation and vibrations due to safe shutdown earthquakes.

Control Rod Material

The external control rod materials must be capable of withstanding the reactor coolant environment for the life of the control rod. Effects of crudding, crevices, stress corrosion and irradiation upon the material must be included in the control rod and core evaluations. Irradiation effects to be considered include material hardening and absorber depletion and swelling.

Reactivity

The reactivity worth of the control rod is determined by the initial amount and type of absorber material and irradiation depletion. Scram time insertion performance must also be included in the plant core analyses including normal operations, including the effects of anticipated operational occurrences (AOOs), and accidents.

4C.3 COL UNIT-SPECIFIC INFORMATION

None.

4D. STABILITY EVALUATION

The stability licensing criterion for all nuclear power plants is set forth in 10 CFR 50 Appendix A, General Design Criterion 12 (GDC-12). As discussed in Section 4B.8, this requires assurance that power oscillations, which can result in conditions exceeding specified acceptable fuel design limits, are either not possible or can be reliably detected and suppressed. Because the most limiting stability condition in the ESBWR normal operating region is at the rated power/flow condition, the ESBWR is designed so that power oscillations are not possible (i.e., remains stable) throughout the whole operating region, including plant startup. In addition, the ESBWR is designed to be stable during anticipated operational occurrences (AOOs). As a backup, the ESBWR will implement a Detect and Suppress solution as a defense-in-depth system. The details of the solution will be developed during the ESBWR Construction and Operating License (COL) phase.

This appendix summarizes the stability evaluation of the ESBWR design. Section 4D.1 presents the stability performance during power operation and Section 4D.2 presents the stability performance during plant startup.

4D.1 STABILITY PERFORMANCE DURING POWER OPERATION

4D.1.1 Stability Criteria

Compliance with General Design Criterion 12 is assured by implementing design criteria for the decay ratio. GE uses a stability criteria map of core decay ratio vs. channel decay ratio to establish margins to stability. Stability acceptance criteria for BWRs are established on this map at core decay ratio = 0.8 and limiting channel decay ratio = 0.8, with an allowance for regional mode oscillations in the top right corner of the defined rectangle. These boundaries were established considering model uncertainties of the order of 0.2 in the core and channel decay ratio in the GE analysis methods (FABLE and ODYSY). There is also margin in the regional boundary, which is drawn below available plant regional oscillation data, though the amount of conservatism has not been quantified. The NRC has approved application of ODYSY to the E1A Long Term Stability Solution [4D-1, 4D-2].

The ESBWR core size of 1132 bundles is significantly larger than the largest operating BWR (ABWR with 872 bundles). The sub-criticality of the azimuth harmonic, which is relevant for regional oscillations, decreases with core size. The regional stability boundary is expected to move inwards in the Core Decay ratio vs. Channel Decay Ratio plane as the sub-criticality decreases. Rather than modifying the operating plant stability map, the regional decay ratio will be calculated directly and compared with an acceptance criterion of 0.8. The margin of 0.2 in the calculation of the regional decay ratio is reasonable and consistent with the values for the channel and core decay ratios. Figure 4.D-1 shows the three-dimensional stability map and the design criteria for channel, core and regional stability.

The design goal is for the nominal values of the core, channel and regional decay ratios at rated power and flow to be less than 0.4, or about half the design criteria. This is consistent with the BWR design philosophy of maintaining the decay ratios in the flow control range approximately half of the limiting values.

The design requirement is for the core, channel and regional decay ratios to be less than the acceptance criteria of 0.8 at the 2σ level of uncertainty. Because the ESBWR is a new plant and there are no plant data, the uncertainties includes operating state and model uncertainties, even though there is already an explicit allowance for model uncertainty in the acceptance criteria.

4D.1.2 Analysis Methods

The TRACG computer code is used for the analysis of ESBWR stability margins. TRACG is a General Electric (GE) proprietary version of the Transient Reactor Analysis Code (TRAC). TRACG uses advanced one-dimensional and three-dimensional methods to model the phenomena that are important in evaluating the operation of BWRs. The NRC has approved TRACG for ESBWR LOCA (ECCS and containment) analysis. [4D-3]. The application of TRACG for Anticipated Operational Occurrences (AOOs) and for ATWS overpressure calculations for operating BWRs has also been approved by the NRC [4D-4, 4D-5].

TRACG has a multi-dimensional, two-fluid model for the reactor thermal hydraulics and a three-dimensional reactor kinetics model. The models can be used to accurately simulate a large variety of test and reactor configurations. These features allow for realistic simulation of a wide range of BWR phenomena, and are described in detail in the TRACG Model Description Licensing Topical Report [4D-6].

TRACG has been extensively qualified against separate effects tests, component performance data, integral system effects tests and operating BWR plant data. The details are presented in the TRACG Qualification Licensing Topical Report [4D-7]. Specific qualification studies for tests simulating passive BWR design features are reported in References 4D-8 and 4D-9.

The stability analysis statistically accounts for the uncertainties and biases in the models and plant parameters using a Monte Carlo method for the Normal Distribution One-Sided Upper Tolerance Limit (ND-OSUTL) if the output distribution is normal, or the Order Statistics method if it is not. Conservative values are used in place of probability distributions for some plant parameters for convenience. The uncertainties and biases considered include the following:

- Model uncertainties
- Experimental uncertainties and any uncertainties related to test scale-up
- Plant uncertainties
- Process measurement errors
- Manufacturing tolerances

The overall analysis approach followed is consistent with the Code Scaling Applicability and Uncertainty (CSAU) analysis methodology [4D-10].

The application methodology is described in Reference 4D-11, Licensing Topical Report, NEDE-33083P, Supplement 1, “TRACG Application for ESBWR Stability Analysis”.

4D.1.3 Steady State Stability Performance

4D.1.3.1 Baseline Analysis

A baseline analysis was performed for the ESBWR at rated conditions, which are the most limiting from the perspective of stability due to the highest power/flow ratio [4D-11]. Analysis was conducted for equilibrium GE14 core at various points in the cycle: Beginning of Cycle (BOC), Middle of Cycle (MOC) near the peak reactivity state, and End of Cycle (EOC). The initial conditions are tabulated in Table 4D-1. The core average axial power shapes for the three exposure points are shown in Figure 4D-2.

Channel Stability

Channel stability is evaluated for the highest power channels by perturbing the inlet flow velocity while maintaining constant channel power.

Super Bundle Stability

A super bundle is defined as a group of 16 bundles below a common chimney cell. The hydrodynamic stability of the highest power super bundle was analyzed by perturbing the inlet flow to the group of 16 bundles while maintaining constant power. The calculation was performed at BOC conditions because this is the most limiting for channel hydrodynamic stability.

Core wide Stability

Core stability was evaluated at BOC, MOC and EOC conditions. The calculations were made with the 3-D kinetics model interacting with the thermal hydraulics parameters. The response to a pressure perturbation in the steam line was analyzed to obtain the decay ratio.

Regional Stability

The 'nominal' decay ratio for out-of-phase regional oscillations was calculated by perturbing the core in the out-of-phase mode about the line of symmetry for the azimuthal harmonic mode.

The initial conditions were the same as for the channel and core stability cases. The decay ratio calculations were made at BOC conditions because of the lowest value of the sub-criticality and highest bottom peaking at these conditions. The channel decay ratio is also the highest at BOC because of the bottom peaked axial flux shape. The decay ratio and oscillation frequency were extracted from the responses for the individual channel groups.

Results

The results for channel, super bundle, core and regional stability are tabulated in Table 4D-2. The channel decay ratio was the highest at BOC because of the bottom peaked axial power shape. The channel decay ratios meet the design goal of 0.4. The oscillation time period is approximately twice the transit time for the void propagation through the channel. The transit time through the chimney does not contribute to the oscillation time period. There is pressure equalization at the top of the bypass region, which reduces the importance of the chimney. Moreover, there are insignificant frictional losses in the chimney and the static head does not affect the stability performance.

The super bundle decay ratio was lower than that for the single high power bundle, because of the lower average power for the group of 16 bundles. Again, the transit time through the chimney does not contribute to the oscillation time period. The slightly larger time period relative to the hot bundle is also due to the lower average power level.

The core decay ratio was the highest at MOC conditions due to the combination of axial power shape and void coefficient. The oscillation time period corresponds to twice the vapor transit time through the core region. The core decay ratios meet the design goal of 0.4.

The decay ratio and oscillation frequency for regional stability were extracted from the responses for the individual channel groups. The results for the limiting channel group are tabulated in Table 4.D-2. Several other channel groups were within 0.01 of the highest group. The regional decay ratio meets the design goal of 0.4.

4D.1.4 Statistical Analysis of ESBWR Stability

4D.1.4.1 Channel Decay Ratio Statistical Analysis

A Monte Carlo analysis of channel stability was performed at rated power and flow and BOC conditions that were determined to be limiting. A total of 59 trials were made. In each trial, random draws are made for each of the parameters determined to be important for stability. Some of these parameters are not important for channel stability per se, but the same set of parameters was perturbed for both channel and core stability. These parameters and their individual probability distributions are listed in Reference 4D-11. The value for each of these parameters is drawn from the individual probability distribution for that parameter. A TRACG calculation is made with this perturbed set of parameters to obtain a new steady state. The channel decay ratio for the highest power channel is then calculated by applying a perturbation in inlet velocity. This constitutes one trial in the Monte Carlo process. A One-Sided Upper Tolerance Limit with 95% content and 95% confidence level (OSUTL95/95) is calculated from the Monte Carlo distribution. Table 4D-3 shows the value of the OSUTL95/95 for the channel decay ratio.

4D.1.4.2 Core Wide Decay Ratio Statistical Analysis

The Monte Carlo analysis of core stability was performed at rated power and flow and MOC conditions that were determined to be limiting. As for channel stability, a total of 59 trials were made. In each trial, random draws are made for each of the parameters determined to be important for stability. A TRACG calculation is made with this perturbed set of parameters to obtain a new steady state. The core decay ratio is then calculated by applying a pressure perturbation in turbine inlet pressure. This constitutes one trial in the Monte Carlo process. An OSUTL95/95 is calculated from the Monte Carlo distribution. Table 4D-3 shows the value of the OSUTL95/95 for the core decay ratio.

4D.1.4.3 Regional Decay Ratio Statistical Analysis

The Monte Carlo analysis of regional stability was performed at rated power and flow and BOC conditions that were determined to be limiting. As for core-wide stability, a total of 59 trials were made. In each trial, random draws are made for each of the parameters determined to be important for regional stability. A TRACG calculation is made with this perturbed set of

parameters to obtain a new steady state. The regional decay ratio is then calculated by applying an instantaneous inlet velocity perturbation. A positive perturbation is applied to all channel groups on one side of the line of symmetry of the harmonic mode; a negative perturbation is applied to the channel groups on the other side. The decay ratio was extracted for the high power channel group from the transient response. This constitutes one trial in the Monte Carlo process. An OSUTL95/95 is calculated from the Monte Carlo distribution. Table 4D-3 shows the value of the OSUTL95/95 for the regional decay ratio.

4D.1.4.4 Comparison with Design Limits

Figure 4D-3 shows the stability map with the design criteria. The baseline results for core, channel and regional decay ratios are compared against the design goal. The OSUTL95/95 values for core, channel and regional decay ratios are compared against the design criteria. Note that these values are calculated at different times in the cycle and represent the highest individual values. The combination of these decay ratios at the same time is not possible. Nevertheless, the limiting core, channel and regional decay ratios (OSUTL95/95) are simultaneously compared against the design limits. Figure 4D-3 shows that both the design goals and design limits are satisfied for the ESBWR core.

The demonstration of stability margins has been performed for an equilibrium GE14 core design. The COL applicant will need to verify that the final core design is at least as stable as the GE14 core design used in the analysis in this section. If the nominal decay ratios are higher than the calculated values, the statistical analysis of decay ratios will need to be performed and the results checked versus the design criteria.

4D.1.5 Stability Performance During AOOs

In general, the stability margin reduces when the reactor power increases and/or core flow reduces. Because the ESBWR design relies on natural circulation for core flow circulation, the core flow during full power operation is only dependent upon the vessel water level. Higher water level means higher core flow, and vice versa. During normal operation, the water level is tightly controlled within a pre-set range (between Level 4 and Level 7 setpoints) through the feedwater and level control system. During AOOs, a reactor scram is initiated when the water level is too high (higher than Level 8 setpoint) or too low (below Level 3 setpoint). In addition, high neutron flux scram and high-simulated thermal power scram are initiated to prevent the reactor from operating at high power. Therefore, the stability during AOOs is assured by the scram protection.

Two limiting AOOs were identified based on the above discussion: Loss-of Feedwater Heater (LOFWH), which results in increased power; and Loss of Feedwater Flow (LOFW), which results in a lower flow. The trajectories of the transients in the power – flow map are shown in Figure 4D-4. The curve A-A corresponds to operation with a reduced level in the downcomer. The lower level leads to a reduction in flow. Different points on A – A correspond to changes in control reactivity or changes in core inlet subcooling.

LOFWH is a slow transient, in which the power increases slowly as the feedwater temperature drops. If the operator takes no action, the power would increase until a high thermal power scram occurs at 115% of rated power. The worst operating point would be one where the drop in

feedwater temperature is such that the power increases to just below the setpoint (115%) and levels off at that value.

Stability analysis was performed at the pre-scram conditions due to the loss of the feedwater heating at MOC conditions. Decreasing the feedwater temperature simulated the transient. The power increased to approximately 116% (slightly above the scram conditions of 115%) due to the feedwater temperature reduction. The circulation flow increased slightly and the average core void fraction stayed almost constant.

Stability analysis was performed at new power/flow/feedwater conditions after a steady state was achieved (Table 4D-4). Under these conditions the feedwater temperature had dropped from 488 to 447°K and reactor power had increased from 4500 to 5221 MWt. The transient response to a pressure perturbation was analyzed to determine the decay ratio. The core decay ratio and channel decay ratio at the pre-scram conditions are shown in Table 4D-4, and are well below the stability design criteria.

Analysis of the LOFW transient turned out to be more complex. The transient is rapid and unless the feedwater flow is restored, will scram in a few seconds on a trip at L3. In this period, the flow, power and subcooling are dropping and pressure is responding to the pressure controller. Rather than imposing a pressure perturbation on top of the transient response to evaluate the decay ratio, the following approach was adopted. When the level had fallen below L3, the feedwater flow was restored to maintain a reduced level. This eventually led to a new steady state where the circulation flow was reduced slightly and the power stabilized close to the initial value with a reduced core inlet temperature. This operating point is more severe than the rated condition as the flow is reduced at the same power level. It provides a conservative evaluation of the LOFW transient, as the power is higher than would occur during a LOFW.

Results of stability analysis for the reduced level case are shown in Table 4D-4. The results from these studies show that adequate margin is maintained to the stability design criteria even for these more severe operating states.

4D.1.6 Stability Performance During Anticipated Transients Without Scram

The Anticipated Transients Without Scram (ATWS) mitigation design for the ESBWR is summarized in Subsection 15.5.4. This includes automatic feedwater runback and automatic boron injection. The TRACG analysis results presented in Subsection 15.5.4 confirm the conclusion that there are no stability issues during the ATWS transient.

4D.2 STABILITY PERFORMANCE DURING PLANT STARTUP

In contrast to operating BWRs, the ESBWR plant starts up without recirculation pumps. At low pressure, the initiation of voiding in the core and chimney causes perceptible changes in the driving head because of the large difference between liquid and vapor densities. Consequently, startup procedures are developed to assure smooth ascension in pressure and power.

Tests in experimental natural circulation loops [4D-12, 4D-13, 4D-14] have identified two mechanisms for potential flow oscillations at low pressure. First, at very low flows, a periodic “geysering” flow oscillation was found to occur due to condensation of core exit vapor in the subcooled chimney region. Condensation–induced oscillations may occur under these conditions. The chimney subcooling and the rate of vapor production in the core determine the

condensation rate. Oscillations of this kind are unlikely given the ESBWR startup procedures, which are designed to avoid vapor generation in the core prior to reaching saturated conditions in the chimney, and are similar to those of the natural circulation Dodewaard reactor. Dodewaard experienced no "geysering" oscillation in its 22 refuel cycles of operation. Second, initiation of vapor production in the chimney region leads to a reduction in hydrostatic head in the chimney and a resultant core flow increase. This, in turn, could cause voids to collapse in the chimney, leading to a reduction in flow. Oscillations of this second kind (known in the literature as Type 1 instability [4D-15], (Figure 4D-5) are unavoidable in a natural circulation reactor as the Type 1 instability region has to be crossed prior to establishing a steady two-phase voided region in the chimney. However, the magnitude of the flow oscillations is typically very small and this phenomenon had also never been observed at Dodewaard. In the final cycle of its operation, a special startup test was performed to probe the low-pressure portion of the startup trajectory. Though no oscillations were detectable on the APRMs, it was possible to infer the presence of small oscillations in core velocity from the auto correlation function of the APRM signal (Figure 4D-6) [4D-16]. These were small oscillations superposed on the core velocity with little, if any, reactivity impact, as the core flow is single phase in this phase of the startup transient. Reference 4D-11 provides more discussion of the applicability of the Dodewaard experience to the ESBWR.

In this section, the mechanism of the hydrostatic oscillations is examined and startup trajectories are analyzed with TRACG. The results show that large margins to boiling transition are maintained throughout the startup scenario.

4D.2.1 Phenomena Governing Oscillations during Startup

During startup, the water in the ESBWR vessel is initially heated to about 85˚C by decay heat supplemented by auxiliary heaters. Following de-aeration, control rods are pulled to criticality and nuclear heatup begins at a low core power. As the water circulates through the core and downcomer by natural circulation, it is gradually heated up. The RWCU system removes a portion of the heat by draining water from the downcomer and lower plenum, cooling it in heat exchangers and returning it through the feedwater sparger. Because of the large height of the ESBWR vessel, the pressure at the water level (near the top of the separators) is lower than the core pressure by about 1 bar. Figure 4D-7 shows a schematic of the vessel and the axial pressure profile. At low pressures corresponding to startup conditions, the pressure gradient gives rise to a significant difference in the saturation temperature between the core exit and the top of the separators. The saturation temperature profile is shown on the right side of the figure. As the circulating water is slowly heated up, saturation temperature is first reached at the top of the separators. Vapor generation at the top of the separators results in a reduction in the density head in the separators, and the voids propagate downwards. The formation of voids also results in a larger driving head for natural circulation flow. The increase in natural circulation flow reduces the core exit temperature and leads to a collapse of the voids. This completes one cycle of the hydrostatic head oscillation. The sequence of events for one cycle is illustrated in the right hand portion of Figure 4D-7. These oscillations persist until the inlet temperature to the core increases and a steady void fraction is established in the separators. Small oscillations in the flow rate are harmless when the flow in the core is single phase and consequently there is a very large margin to thermal limits. This type of oscillation is termed Type 1 instability in the literature.

Figure 4D-5 is a schematic of a generalized stability map in the plane of Subcooling Number vs. Zuber Number. (The figure does not represent a quantitative stability map specifically for the ESBWR and is used primarily for illustrative purposes.) Two different boundaries are shown for core-wide (in-phase) and regional (out-of-phase) oscillations that have been covered earlier in this report. These are driven by density wave oscillations and are known as Type 2 oscillations. The region above the lower (out-of-phase) stability boundary curve is unstable; the region under the curve is stable. The Type 1 oscillations appear at the onset of voiding and occupy a narrow region next to the line that demarcates the single-phase region from the two-phase region. At normal conditions the ESBWR is very stable as shown in the figure, with significant margin to the stability boundary. During startup, the Type 1 instability region is reached to obtain rated pressure and power. It is best to cross the Type 1 instability region at low power before boiling starts in the core to maintain a large margin to thermal limits. Once steady voiding is established in the separators and chimney, the core power can be raised along a trajectory to full power.

The parameters that control Type 1 instability are the Zuber Number and Subcooling Number. The Froude Number is a parameter that is relevant in determining the relationship between the riser buoyancy and the circulation flow. This is important in establishing a scaling basis for tests facility design, but not for loop stability once the scaled flow characteristics are known. Another group that is important for tall columns of liquid at low system pressure is the Flashing Number. These dimensionless numbers are defined below:

$$N_{Zu} = \frac{\rho_l}{\rho_{gsd}} \frac{Q}{W_c h_{fg}}$$

$$N_{sub} = \frac{\rho_l}{\rho_{gsd}} \frac{(h_{fsd} - h_{in})}{h_{fg}} \qquad (4D.1)$$

$$N_{Fr} = \frac{V_c^2}{gH_{dc}}$$

$$N_{fl} = \frac{\rho_l}{\rho_{gsd}} \frac{(h_{fin} - h_{fsd})}{h_{fg}}$$

where

ρ =density (kg/m3)

V_c = core average inlet velocity (m/s)

Q =core thermal power (kW)

W_c =core flow (kg/s)

h = enthalpy (kJ/kg)

h_f = saturated liquid enthalpy (kJ/kg)

h_{fg} =latent heat of evaporation at steam dome pressure (kJ/kg)

H_{dc} = downcomer height (m)

sd denotes properties at the steam dome pressure and in denotes properties at the inlet to the core.

The significance of these quantities is discussed below with the aid of Figure 4D-8.

The Zuber Number is a measure of the enthalpy increase in the core. As there is no increase in the enthalpy in the chimney, the Zuber number is also a measure of the total enthalpy increase in the core and chimney regions. The Flashing Number has special relevance for tall columns of liquid at low pressure. It is a measure of the enthalpy margin to flashing at the core exit (see Figure 4D-8) when the flow just reaches saturation at the top of the chimney. The Subcooling Number is a measure of the enthalpy margin to saturation at the core inlet. At low system pressures, the definition of the Subcooling Number must be considered carefully because of the difference in pressure at different elevations. In Equation 4D.1, it is defined with respect to the saturated enthalpy at the steam dome pressure.

With the above definitions, when saturated conditions are reached at the top of the riser (Path A in Figure 4D-8), an energy balance leads to:

$$N_{Zu} = N_{sub} \qquad (4D.2)$$

For Type 1 oscillations that occur when voiding begins at the top of the riser, Nsub is the relevant parameter to be used in the stability map of Figure 4D-5.

For a rapid heatup rate corresponding to Path C in Figure 4D-8, saturated conditions may be reached at the top of the core (i.e. at a pressure close to core inlet pressure) with a subcooled chimney. In the extreme case when the entire chimney is still subcooled:

$$N_{Zu} = N_{sub} + N_{fl} \qquad (4D.3)$$

These heatup rates can lead to condensation-induced oscillations. A large flashing number requires a correspondingly higher Zuber number (enthalpy increase in the core) to trigger such oscillations and thus provides a buffer to the occurrence of this phenomenon.

At intermediate conditions, as the void initiation location moves down into the chimney,

$$N_{sub} < N_{Zu} < (N_{sub} + N_{fl})$$

This corresponds to Path B in Figure 4D-8.

For the ESBWR at 0.2 MPa, the Zuber Number is of the order of 22, the subcooling number is 22 and the flashing number is 25 and the trajectory corresponding to Path A is followed during the heatup.

4D.2.2 TRACG Analysis of Typical Startup Trajectories

4D.2.2.1 ESBWR Plant Startup

Detailed startup procedures for the ESBWR are developed at a later stage. The startup process is expected to generally follow the established procedure from the Dodewaard plant. The Dodewaard plant started up for 22 cycles of operation without any problems related to flow or power oscillations.

Figure 4D-9 shows the stages of the startup process. In the De-aeration Period, the reactor coolant is de-aerated by drawing a vacuum on the main condenser and reactor vessel using mechanical vacuum pumps with the steam drain lines open. The reactor coolant is heated up to between 80 and 90˚C with the Reactor Water Cleanup/Shutdown Cooling System (RWCU/SDC) auxiliary heater and decay heat. The reactor pressure is reduced to about 50 to 60 kPa.

Following de-aeration, the Main Steam Isolation Valves (MSIVs) are closed to initiate the Startup Period. Control rods are withdrawn to criticality. Fission power is used to heat the reactor water, while maintaining the water level close to the top of the separators but well below the steam lines. Steaming at the free surface starts to pressurize the reactor vessel. The core region remains subcooled due to the large static head in the chimney and separators.

As the reactor heats up and pressurizes, the RWCU/SDC system heat exchangers are used to control the downcomer temperature, enhance coolant flow and reduce lower plenum stratification. The MSIVs are reopened at the end of the Startup Period, when the pressure reaches 6.3 MPa. Subsequently, the turbine bypass valves are used to control pressure. The RPV power is increased and preparations made to roll the turbine.

In the actual plant startup, the reactor vessel will likely be pressurized during the Startup Period with the MSIVs open, and the turbine bypass and control valves closed, similar to the operating BWR plants. The character of the startup transient is not expected to change from what is presented here; however, it is possible that the heatup rate could be lower and the startup time could be longer.

4D.2.2.2 TRACG calculations for Simulated Startup Scenarios

The startup transient for the ESBWR was simulated with TRACG. These TRACG calculations were performed with imposed core power, without activating the kinetics model. This is valid as long as there are no feedbacks from oscillations in the core void fraction during the startup transient. This assumption is validated as part of the calculation. The calculation was initiated at the end of the de-aeration period with the steam dome pressure at 0.52 bar and RPV water at 82˚C. The water level was maintained near the top of the separators. The MSIVs were closed to isolate the RPV. To simplify comparisons, the power level was maintained constant until the pressure reached 6.3MPa. Subsequently, the MSIVs were opened and the power level was increased in steps to achieve rated pressure at 300 MW (6.67% of rated power).

Three heatup rates were considered. The lowest power level of 50 MW corresponds to a heatup rate of 30˚C/hour and is likely to be close to the actual value for startup. The median power level of 85 MW yields a heatup rate of 55˚C/hour, which is the highest allowable to comply with reactor vessel thermal stress requirements. The highest power level of 125 MW heats up the reactor vessel water at 82˚C/hour which is above allowable limits, and is only included as a sensitivity study. The three power trajectories are shown in Figure 4D-10.

Figure 4D-11 shows the pressure response for the three cases. The circulating water heats up because of the core power. The heat exchangers in the RWCU/SDC system are enabled to remove a part of the energy and control the core inlet subcooling. Steam generation begins at the water surface and starts to pressurize the vessel.

Figure 4D-12 shows the variation in core inlet subcooling as a function of time. The local inlet subcooling drops from an initial value around 40 K to less than 10 K as the system pressurizes to 6.3MPa. The core flow transient response is shown in Figure 4D-13. For the lowest heatup rate, the flow trace shows a minor oscillation (noise) between 3000 to 5500 s. The cause of this noise can be traced to the beginning of voiding at the top of the separators (Figure 4D-14). The flow noise is terminated when a steady void fraction is established at the top of the separators. This is the symptom of a Type 1 oscillation at the onset of voiding in the riser. At a power level of 85

MW, the noise is spread over two periods: early on there is some void initiation in the separators (500 to 3000 s) followed by a more sustained period of void generation beginning around 9000 s (Figure 4D-15). At the highest heatup rate (125 MW), the flow becomes noisier. The highest oscillation amplitude occurs between 500 to 1500 s and again between 3500 to 5000 s. The void fractions in the separator are shown in Figure 4D-16.

Further insight into the core flow response is obtained by examining the core void fractions, specifically in the highest power bundles. Figure 4D-17 shows the void fractions for the 50 MW case in the high power bundle at the exit and at cell 30, which is close to the top of the bundle. Voids are not produced even in the high power bundles until 13000 s, well after the noisy flow period is over and the system has pressurized to above 15 bar. Figure 4D-18 shows that for the 85 MW case, vapor generation begins at the top of the high power bundles at 5000s, after the initial flow noise has subsided. At this time the pressure is about 8 bar. Voids propagate to cell 30 at about 8000 s, by which time the system pressure is above 25 bar. The high power level (125 MW) leads to extreme conditions during the heatup. Vapor generation in the core begins early. Figure 4D-19 shows that the high power bundle has an exit void fraction of 15% at 4000 s. Rapid heating of the core leads to conditions that favor condensation-induced oscillations because vapor is generated in the core while the chimney is not yet at saturated conditions. These are the extreme conditions examined in the tests by Aritomi [4D-12] and Kuran, et al [4D-14]. The situation is further illustrated by looking at the flows in individual bundles. The exit flows in the high power and the low power peripheral bundles were examined. Figure 4D-20 depicts the exit flows in the high power bundle for the three cases. These traces follow the core average flow response shown in Figure 4D-13. The exit flows in the peripheral bundles (Figure 4D-21) show a more dramatic distribution. In the two lower power cases, the peripheral bundles are in upflow throughout the transient, despite the noise imposed on the average flow rate. However, at 125 MW, large condensation induced oscillations lead to flow reversals between 3500 to 4000 s.

Margins to thermal limits (CPR) were calculated for the three startup scenarios. The thermal margin for the high power bundles is shown in Figure 4D-22. Large margins are maintained throughout. Figure 4D-23 is the corresponding plot for the peripheral bundles. Again, large margins are maintained throughout the transient. This is true even for the extreme case with 125 MW. Despite the flow reversals, the heat fluxes are low enough that critical heat flux conditions are not approached.

Subsequent to this analysis, a coupled nuclear-thermal hydraulic analysis of the ESBWR startup has been performed [4D-18]. The results are shown in the next subsection.

4D.2.2.3 TRACG Calculation of ESBWR Startup with Neutronic Feedback

A TRACG simulation of ESBWR startup with the neutronic feedback was performed using the limiting heat up rate. This is an example of a startup transient. Results of this simulation have demonstrated that at the limiting heat up rate, no difficulties and no large power oscillations were encountered during the startup transient. COL applicant will analyze a representative startup transient with MSIVs open.

This TRACG calculation was performed activating the 3D kinetics model. The calculation was initiated at the end of the de-aeration period, similar to the calculations in the previous section.

The water level was maintained near the top of the separators. The MSIVs were closed to isolate the RPV. Initially, all control rods are in fully inserted position.

The 269 control rods in ESBWR are divided into 10 groups and the rod group positions are shown in Figure 4D-24. Rod Group # 10 represents the control rods for the 25 control cells. The grouping of control rods and the withdrawal sequence during the startup are similar to those used for operating plants. The withdrawal speeds for each of these groups during the transient are specified as TRACG input to simulate the operator actions to maintain the reactor at power during the startup transient. These rod groups are slowly withdrawn to maintain the total reactivity close to 0.0 and the total power level is maintained at around 85 MW until the reactor is pressurized to the desired value. Subsequently, the MSIVs are opened and the power level is increased in steps (by means of additional rod withdrawals) to achieve rated pressure.

Figure 4D-25 shows the withdrawal fraction for all control rods. After Groups 1, 2 and 3 are fully withdrawn, the control rod withdrawal fraction is 0.37, i.e., 63% of all rods are in fully inserted position. At this time, the reactor is critical. Groups 4 and the next several groups are withdrawn with slower speed to avoid rapid change in total reactivity and reactor power.

Figure 4D-26 shows the total reactor power. For the first 1500 seconds, the total reactor power consists mainly of decay heat. After the core becomes critical, there is a step increase in total reactor power. From this time on, the rod groups are slowly withdrawn to maintain the total reactor power at around 85 MW. The total power is maintained around 85 MW by the continuous withdrawal of the control rods. No significant core void is calculated until the MSIVs are opened, when the temperature and pressure are near the operating conditions. The heatup rate for this case is slightly below the maximum allowed rate considering thermal stress of 55ºC/hour.

Figure 4D-27 shows the steam dome pressure response for this case. The RPV pressurizes to 6.3 MPa in 3.6 hours and the MSIVs are opened. With the MSIV open the power is limited by BOP systems not by heatup rate. The control rods are withdrawn further to step up the power and to reach the rated pressure at 4.4 hours. At this time, Rod Groups 1 to 7 are fully withdrawn and Group 8 is 50% withdrawn. Groups 9 and 10 (25 control cell rods) are in fully inserted position.

Figure 4D-28 shows the core inlet subcooling as a function of time. The local inlet subcooling drops as the system pressurizes to 6.3 MPa. The core flow transient response is shown in Figure 4D-29. There are two periods with small flow noise: around 2000 seconds corresponding to the step increase in power (Figure 4D-26) and around 4500 seconds corresponding to some void initiation at the top of separators. Steady void fraction is established at the top of the separators after 9000 seconds. There are no fluctuations in the neutron flux during these periods. The flow result is similar to the case with no reactor kinetics modeled.

Figure 4D-30 shows core void in the highest power bundles. Vapor generation begins at the top of the high power bundles at pressure of about 5 bar. Voids propagate about a quarter of the height into the bundle at 11000 s, by which time the system pressure is above 30 bar. The high power bundle flow follows the core average flow response. The peripheral bundles are in upflow throughout the transient.

Margins to thermal limits (CPR) were calculated for this startup case. Large margins are maintained for all bundles throughout the transient.

4D.3 COL UNIT-SPECIFIC INFORMATION

The COL applicant shall verify that the stability of the final core design meets the requirements specified in 4D.1.4.4.

The COL applicant shall confirm that an NRC approved detect and suppress stability solution is implemented that will scram or reduce power if an instability occurs. The cycle-dependent Oscillation Power Range Monitor (OPRM) setpoints will be documented in the Core Operating Limits Report (COLR).

The COL applicant startup calculation shown in Section 4D.2.2 will be repeated for the initial core design and a representative rod pull sequence, and will be used to define the heatup rate and core power limits to be used for plant startup.

The COL applicant startup procedures shall be verified to limit core and bundle power to the values used in the 4D.2 analysis.

4D.4 REFERENCES

4D-1 GE Nuclear Energy, J. S. Post and A. K. Chung, "ODYSY Application for Stability Licensing Calculations," NEDC-32992P-A, July 2001.

4D-2 GE Nuclear Energy, "BWR Owners' Group Long-Term Stability Solutions Licensing Methodology," NEDO-31960-A, November 1995.

4D-3 GE Nuclear Energy, B. S. Shiralkar and Y. K. Cheung, "TRACG Application to ESBWR," NEDC-33083P-A, March 2005.

4D-4 GE Nuclear Energy, J. G. M. Andersen, et al., "TRACG Application for Anticipated Operational Occurrences Transient Analysis," NEDE-32906P-A, Revision 1, April 2003.

4D-5 GE Nuclear Energy, F. T. Bolger and M. A. Holmes, "TRACG Application for ATWS Overpressure Transient Analysis," NEDE-32906P, Supplement 1-A, November 2003.

4D-6 GE Nuclear Energy, J. G. M. Andersen, et al., "TRACG Model Description," NEDE-32176P, Revision 2, December 1999.

4D-7 GE Nuclear Energy, J. G. M. Andersen, et al., "TRACG Qualification," NEDE-32177P, Revision 2, January 2000.

4D-8 GE Nuclear Energy, J. R. Fitch, et al., "TRACG Qualification for SBWR," NEDC-32725P, Revision 1, Vol.1 and 2, August 2002.

4D-9 GE Nuclear Energy, J. R. Fitch, et al., "TRACG Qualification for ESBWR," NEDC-33080P, Revision 1, May 2005.

4D-10 USNRC, "Quantifying Reactor Safety Margins: Application of Code Scaling, Applicability, and Uncertainty Evaluation Methodology to a Large-Break, Loss-of-Coolant Accident," NUREG/CR-5249, December 1989.

4D-11 GE Nuclear Energy, B.S.Shiralkar, et al, "TRACG Application for ESBWR Stability Analysis," NEDE-33083P, Supplement 1, December 2004.

4D-12 M. Aritomi, J. H. Chiang. M. Mori, "Fundamental Studies on Safety-Related Thermal-Hydraulics of Natural Circulation Boiling Parallel Channel Flow System under Startup

Conditions (Mechanism of Geysering in Parallel Channels)," Nuclear Safety, Vol. 33, No.2, pp. 170-182, 1992.

4D-13 F. Inada, Y. Yasuo, "The Boiling Flow Instability of a Natural Circulation BWR with a Chimney at Low Pressure Startup," Proc. International Conference on the Design and Safety of Advanced Nuclear Power Plants (ANP '92), Tokyo, Japan, Paper 25.3, October 25-29, 1992.

4D-14 S. Kuran, M. Ishii, X. Sun, L. Cheng, Y. Xu, H. Yoon, S.T. Revankar, "Nuclear Coupled Flow Instability Study for Natural Circulation BWR Startup Transient," Paper N6P002, 6th International Conference on Nuclear Thermal Hydraulics, Operation and Safety (NUTHOS-6), Nara, Japan, October 2004.

4D-15 D.D.B. van Bragt and T.H.J.J. van der Hagen, "Stability Of Natural Circulation Boiling Water Reactors: Part II - Parametric Study Of Coupled Neutronic-Thermohydraulic Stability," Nuclear Technology 121 (1998), 52-62.

4D-16 T.H.J.J. van der Hagen, F.J. van der Kaa, J. Karuza, W.H.M. Nissen, A.J.C. Stekelenburg, J.A.A. Wouters, "Startup of the Dodewaard Natural Circulation Boiling Water Reactor," GKN Report 92-017/FY/R, 1992.

4D-17 A. Manera and T.H.J.J. van der Hagen, "Stability Of Natural-Circulation-Cooled Boiling Water Reactors During Start-Up: Experimental Results," Nuclear Technology, 143 (2003), 77-88.

4D-18 Letter from K. Sedney, GE to A. Cubbage, USNRC, "GE Responses to NRC RAIs on NEDE-33083P, Supplement 1, TRACG Application for ESBWR Stability Analysis," MFN 05-52, June 2, 2005.

Table 4D-1

Initial Conditions for Channel and Core Stability Analysis

Parameter	Value		
	BOC	MOC	EOC
Core Thermal Power (MW)	4500	4500	4500
Core Flow (kg/s)*	9,925	10,003	10,153
Feedwater temperature (K)	488	488	488
Narrow range water level (m)	21.0	21.0	21.0
Feedwater flow (kg/s)*	2421	2421	2421
Core inlet subcooling* (K)	16.6	16.3	16.2
Steam dome pressure (MPa)	7.05	7.05	7.05
ICPR*	1.40	1.46	1.38
Hot Bundle Power (MW)*	5.10	4.94	5.09
Hot Bundle flow (kg/s)*	8.6	8.7	8.8

*Calculated parameter

Table 4D-2

Baseline Stability Analysis Results

Mode	BOC		MOC		EOC	
	Decay Ratio	Frequency (Hz)	Decay Ratio	Frequency (Hz)	Decay Ratio	Frequency (Hz)
Channel	0.23	0.80	0.09	~0.75	0.05	~0.7
Superbundle	0.14	0.74				
Core	0.26	0.74	0.33	0.74	0.29	0.66
Regional	0.40	0.82				

Table 4D-3

Statistical Stability Analysis Results

	Decay Ratio – One Sided Upper Tolerance Limit (95/95)	**Decay Ratio - Design Criteria**
Core	0.50	0.8
Channel	0.36	0.8
Regional	0.57	0.8

Table 4D-4

Limiting AOO Event Results

AOO	Power (% of Rated)	Flow (% of Rated)	Core Decay Ratio	Hot Channel Decay Ratio
LOFWH	116	101	0.47	0.18
LOFW	100	96.6	0.36	0.14

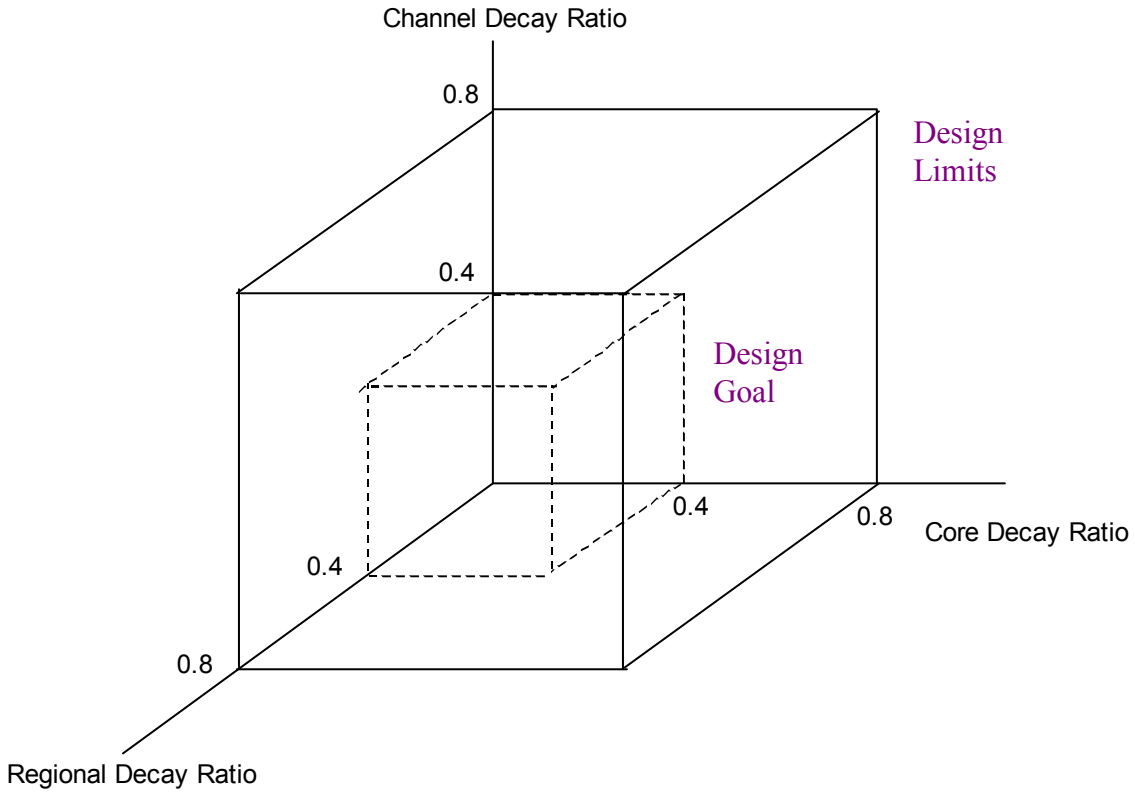

Figure 4D-1. Proposed Stability Map for ESBWR

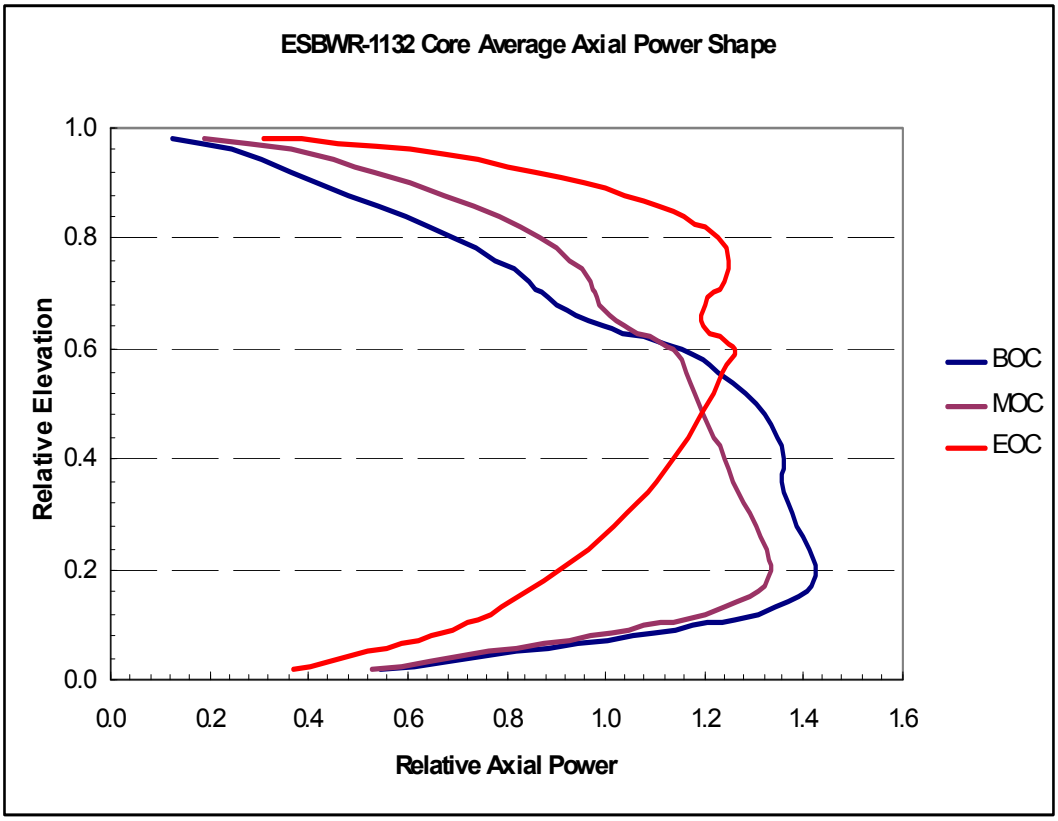

Figure 4D-2. Core Average Axial Power Shape at Different Exposures

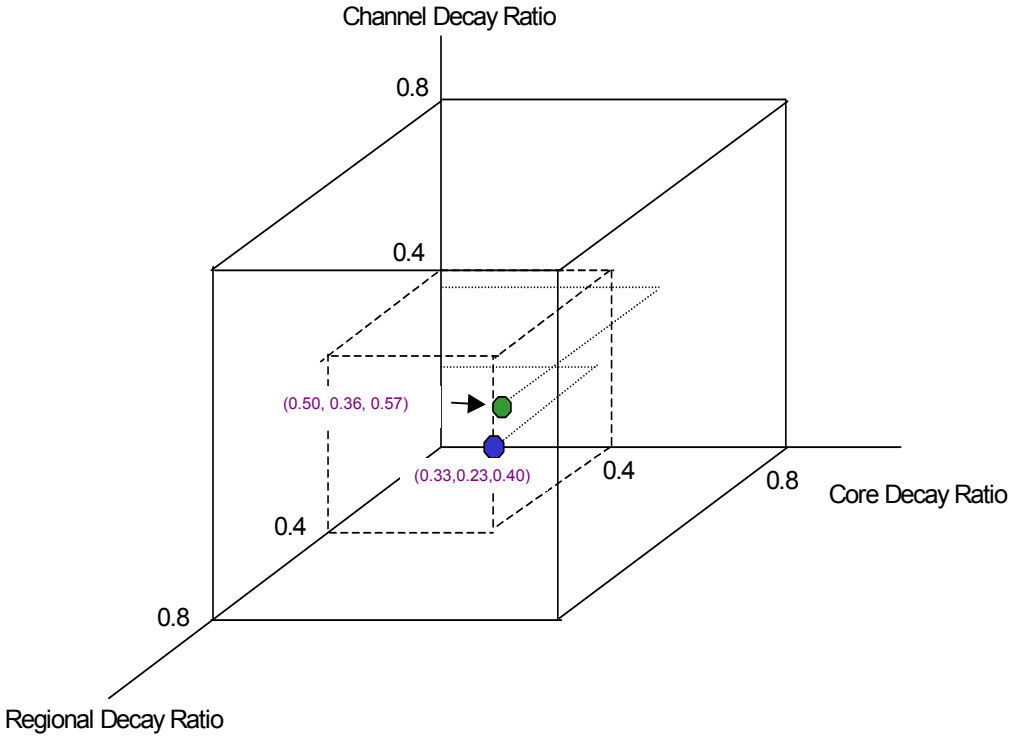

Figure 4D-3. Decay Ratio Results Compared to Design Criteria

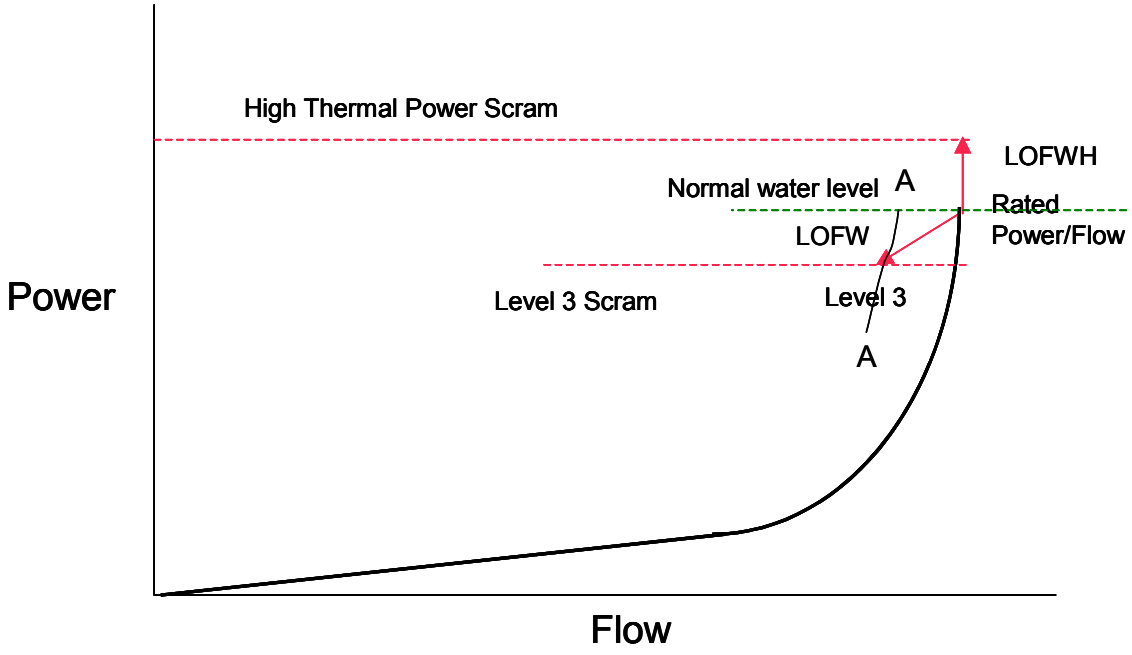

Figure 4D-4. Stability in Expanded Operating Map

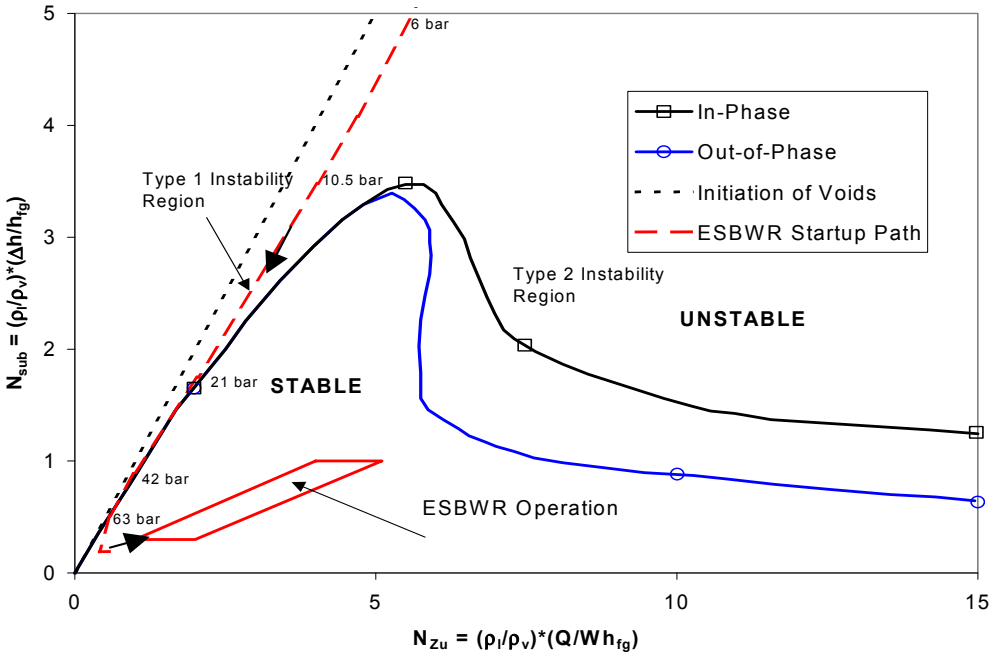

Figure 4D-5. Generalized Stability Map showing Type 1 and Type 2 Instability

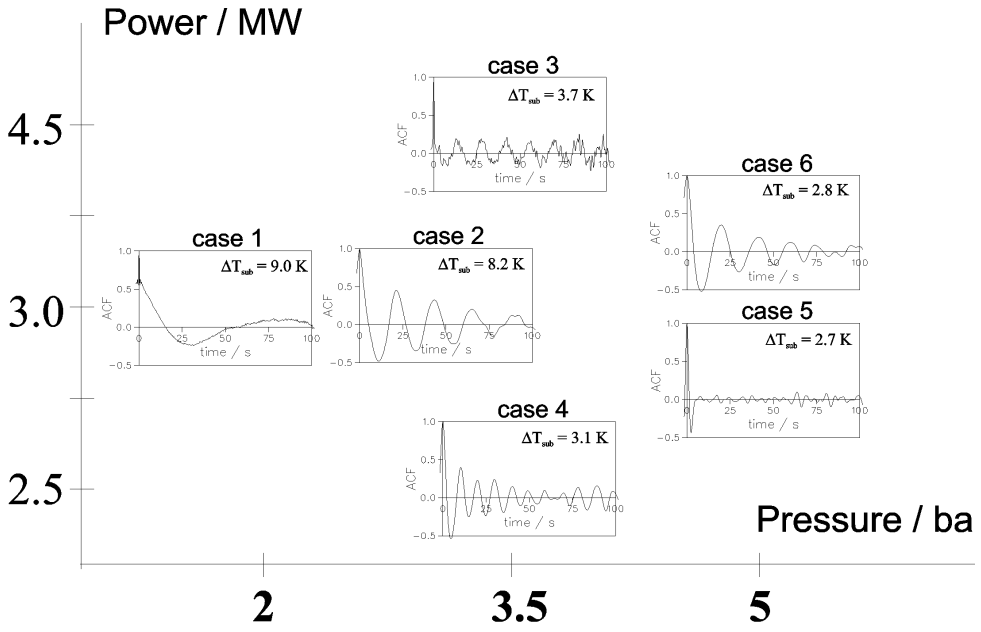

Figure 4D-6. Indications of Periodic Behavior During Dodewaard Startup

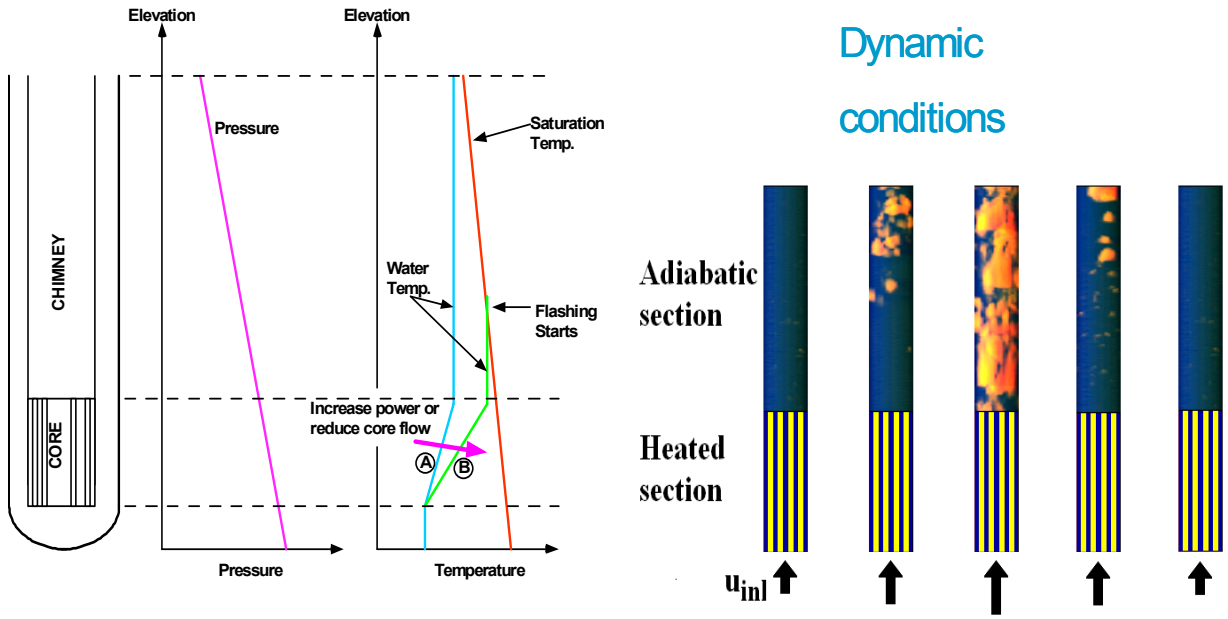

Figure 4D-7. Thermal – Hydraulic Conditions during Startup [4D-17]

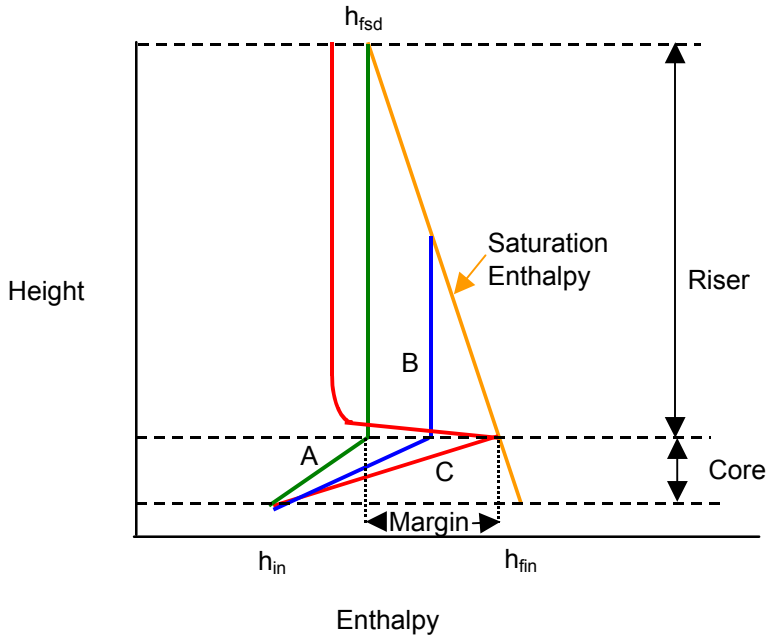

Figure 4D-8. Enthalpy Profiles for Different Heatup Rates

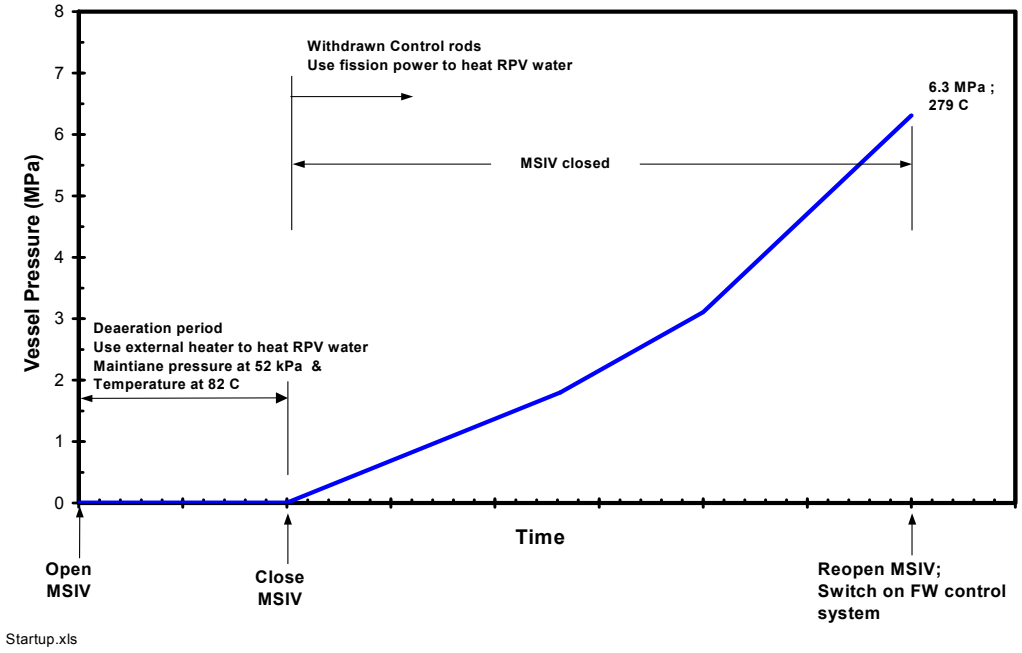

Figure 4D-9. ESBWR Startup Trajectory

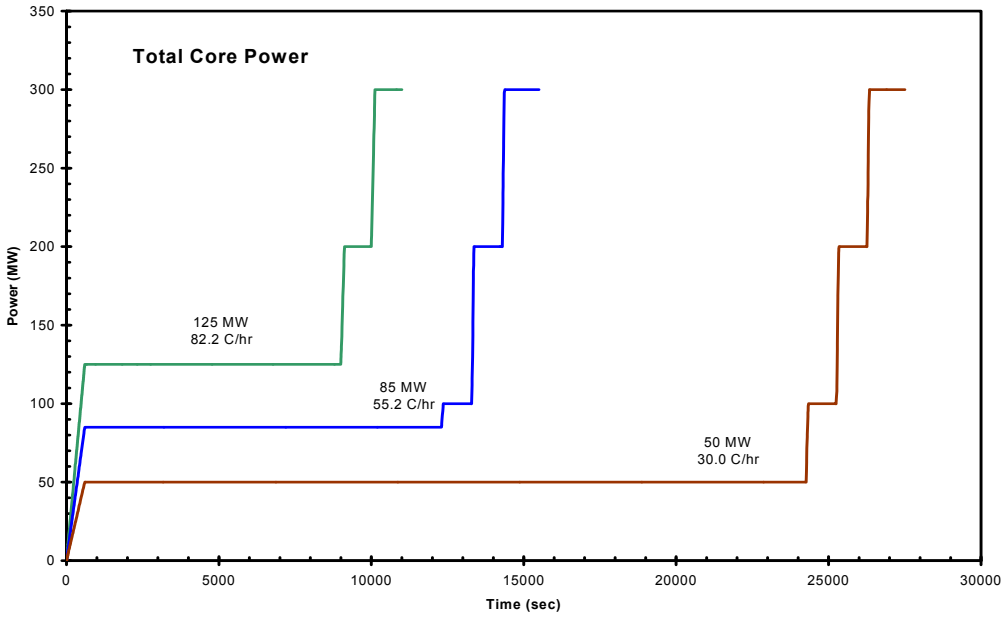

Figure 4D-10. TRACG Startup Simulation: Reactor Power Trajectories

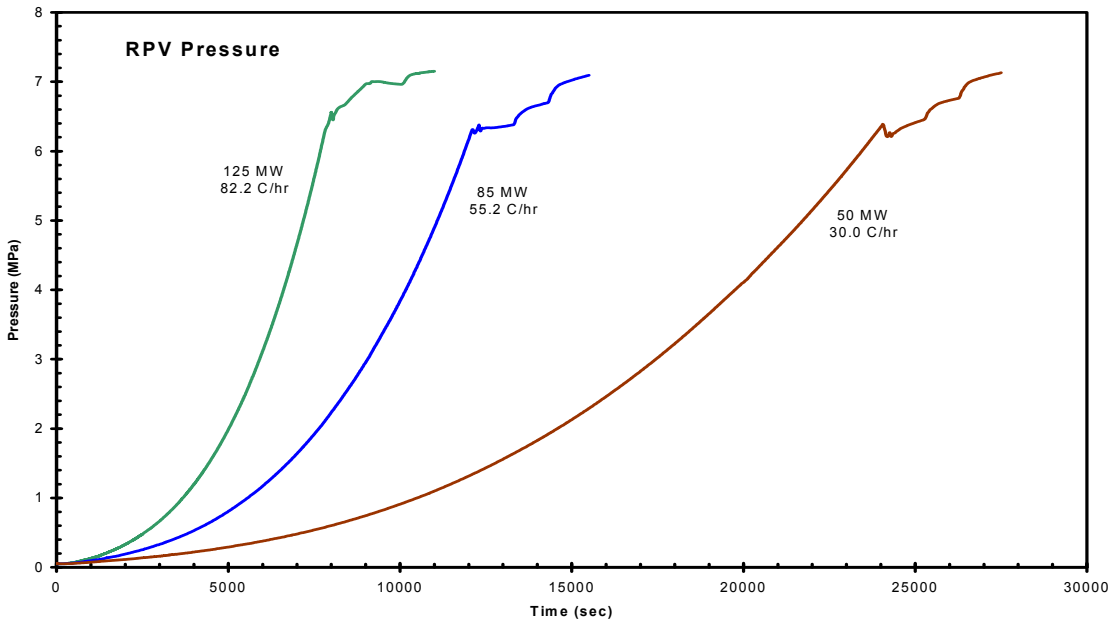

Figure 4D-11. TRACG Startup Simulation: Pressure Response

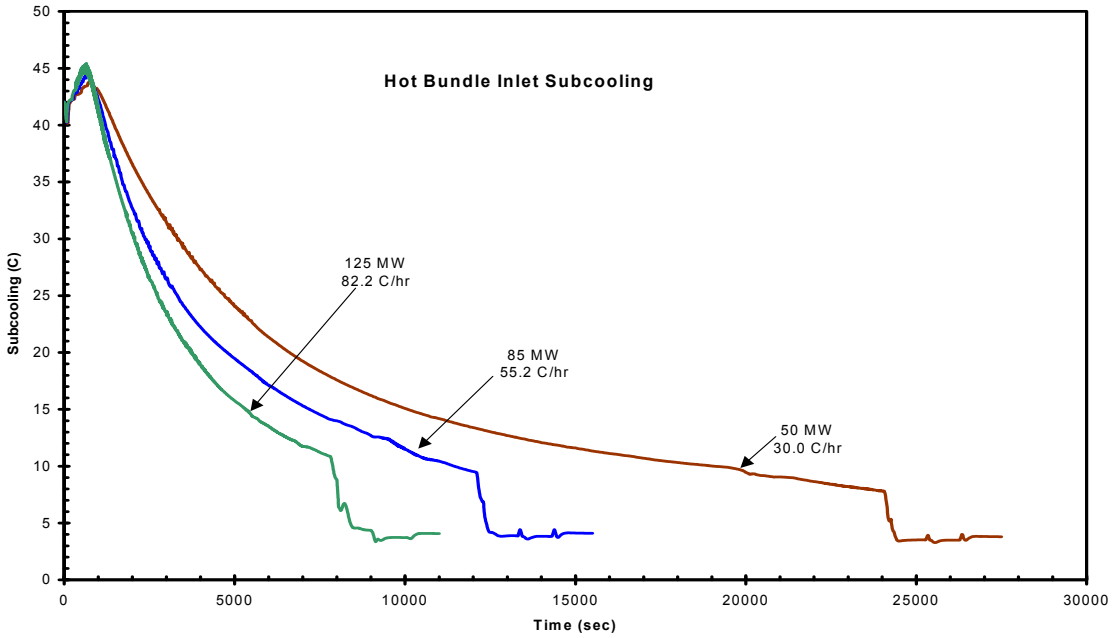

Figure 4D-12. TRACG Startup Simulation – Core Inlet Subcooling

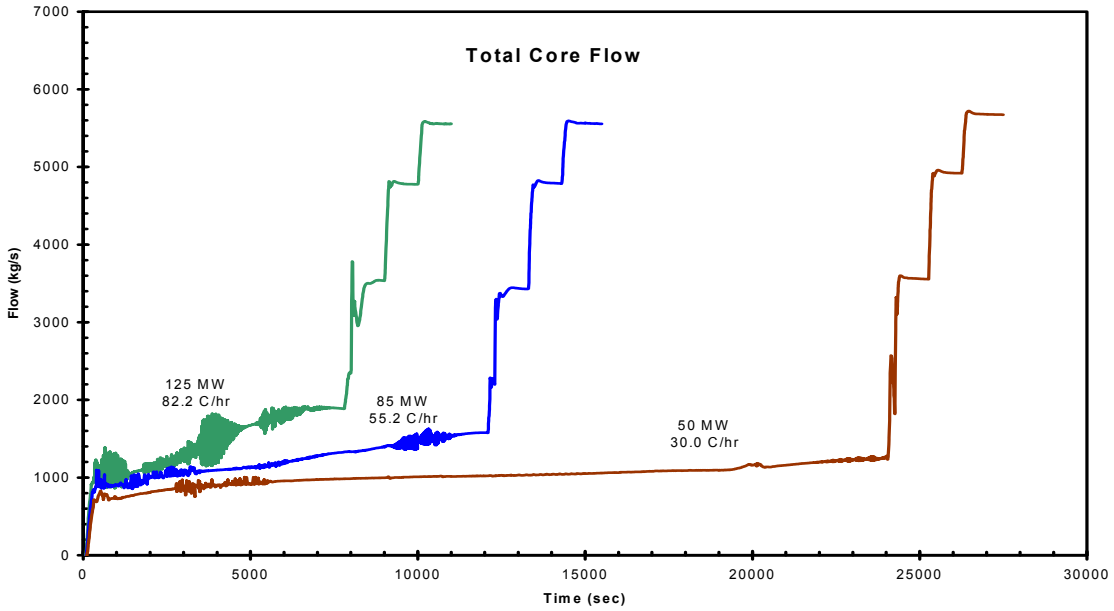

Figure 4D-13. TRACG Startup Simulation – Core Inlet Flow

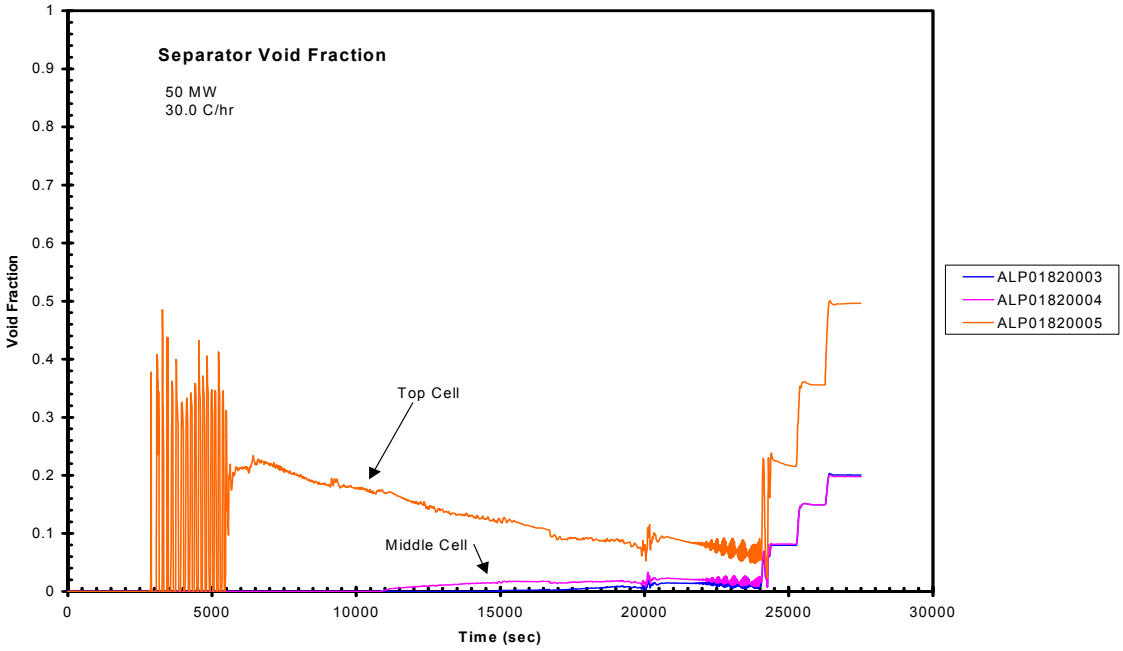

Figure 4D-14. Separator Void Fraction (50 MW heatup)

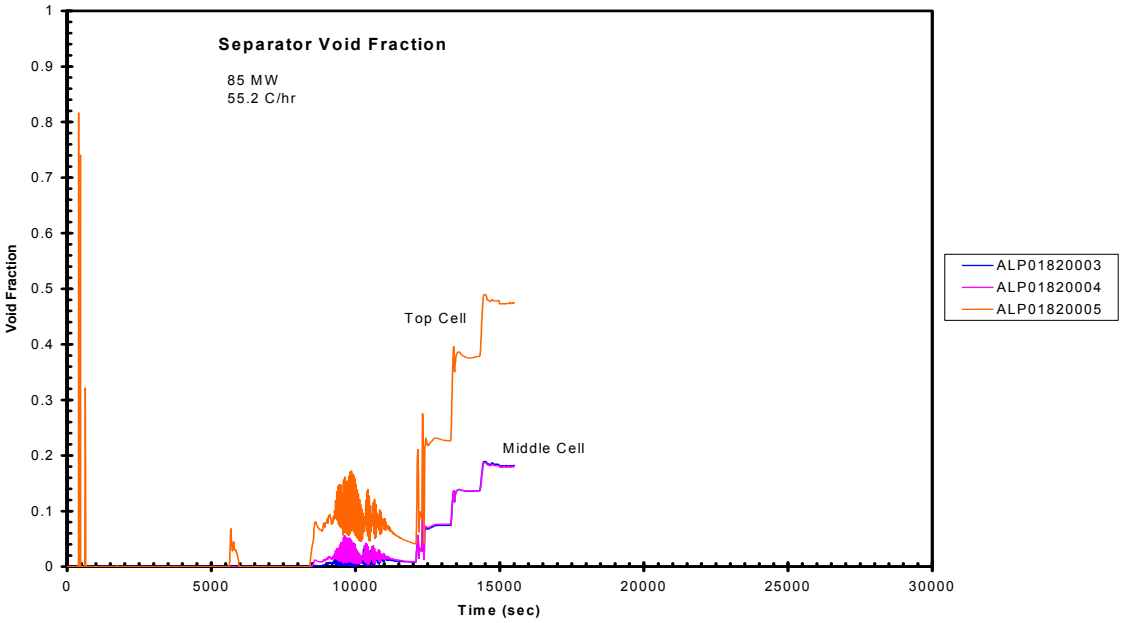

Figure 4D-15. Separator Void Fraction (85MW heatup)

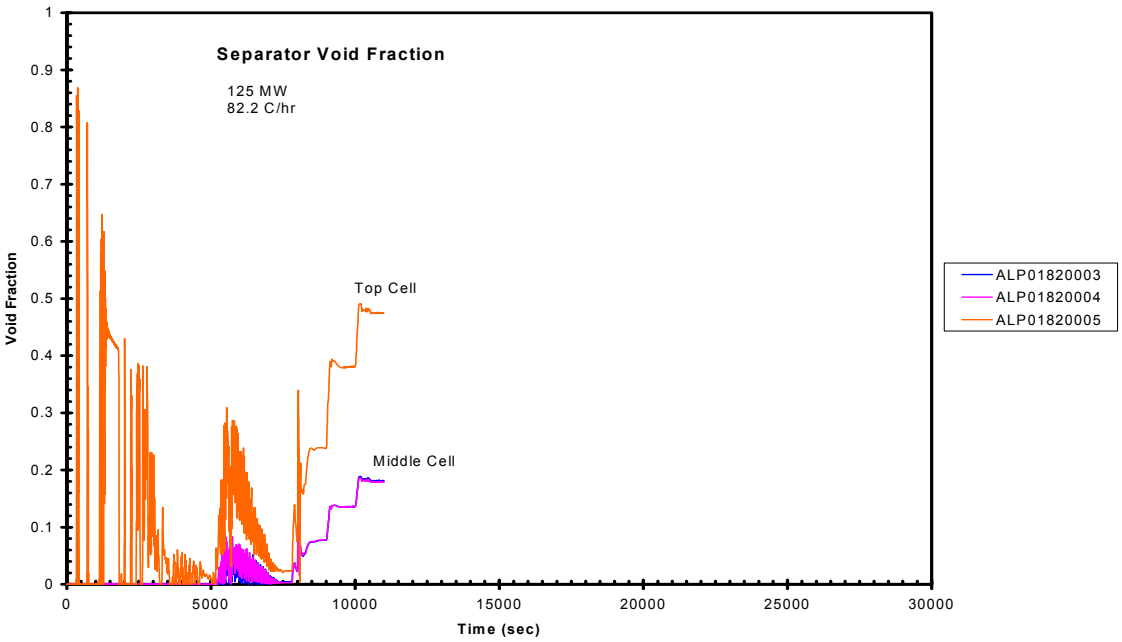

Figure 4D-16. Separator Void Fraction (125 MW heatup)

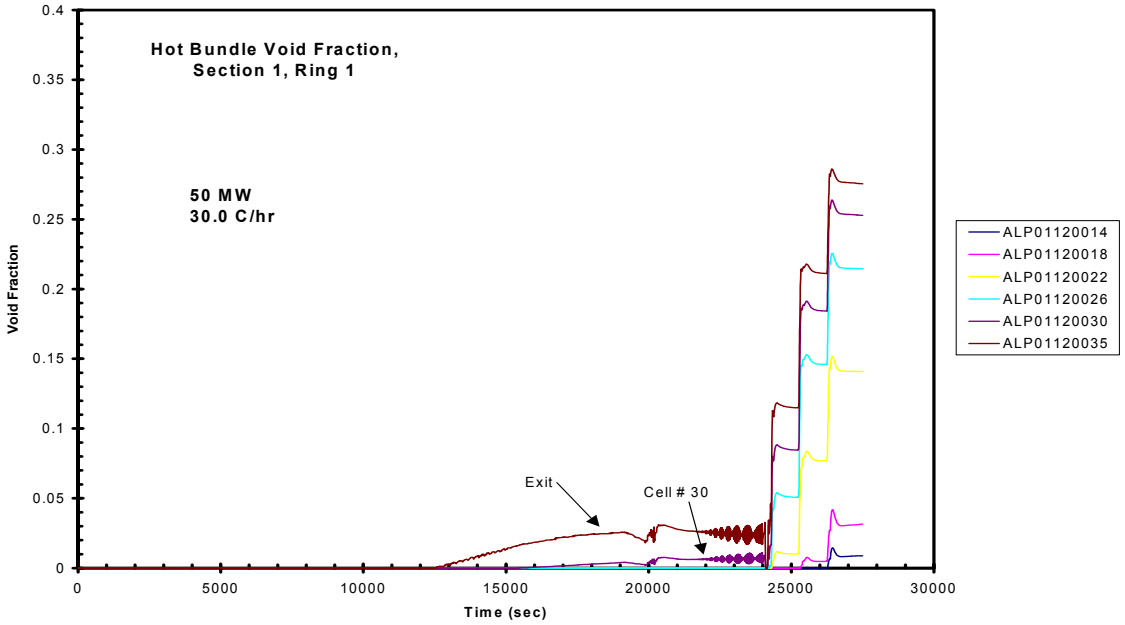

Figure 4D-17. Hot Bundle Void Fraction (50 MW heatup)

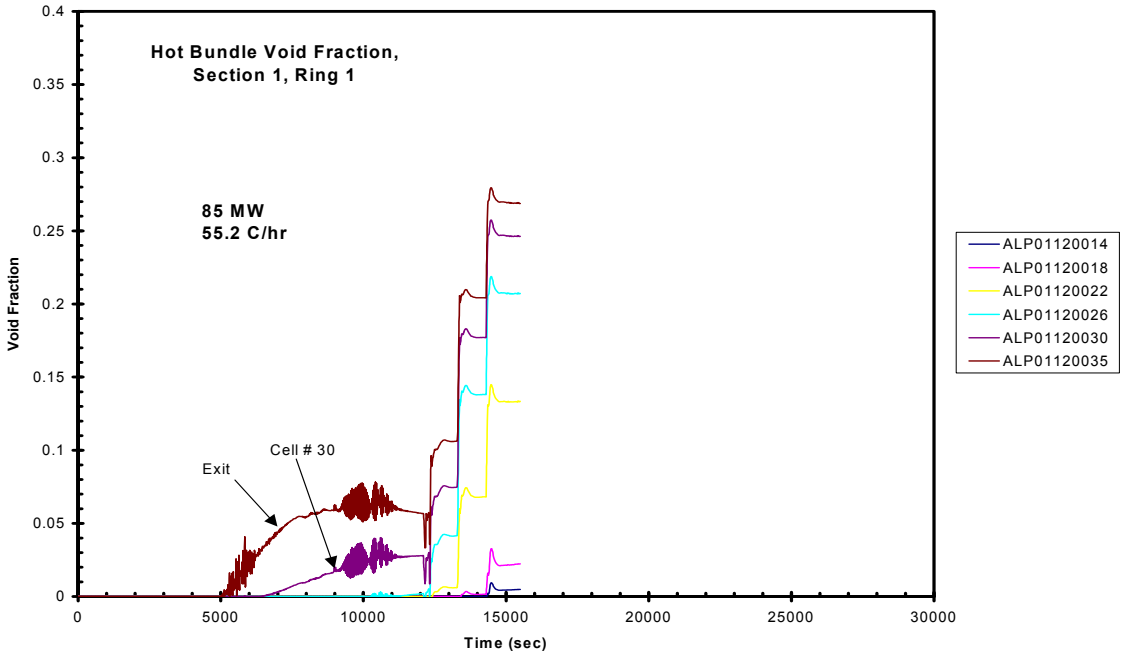

Figure 4D-18. Hot Bundle Void Fraction (85 MW heatup)

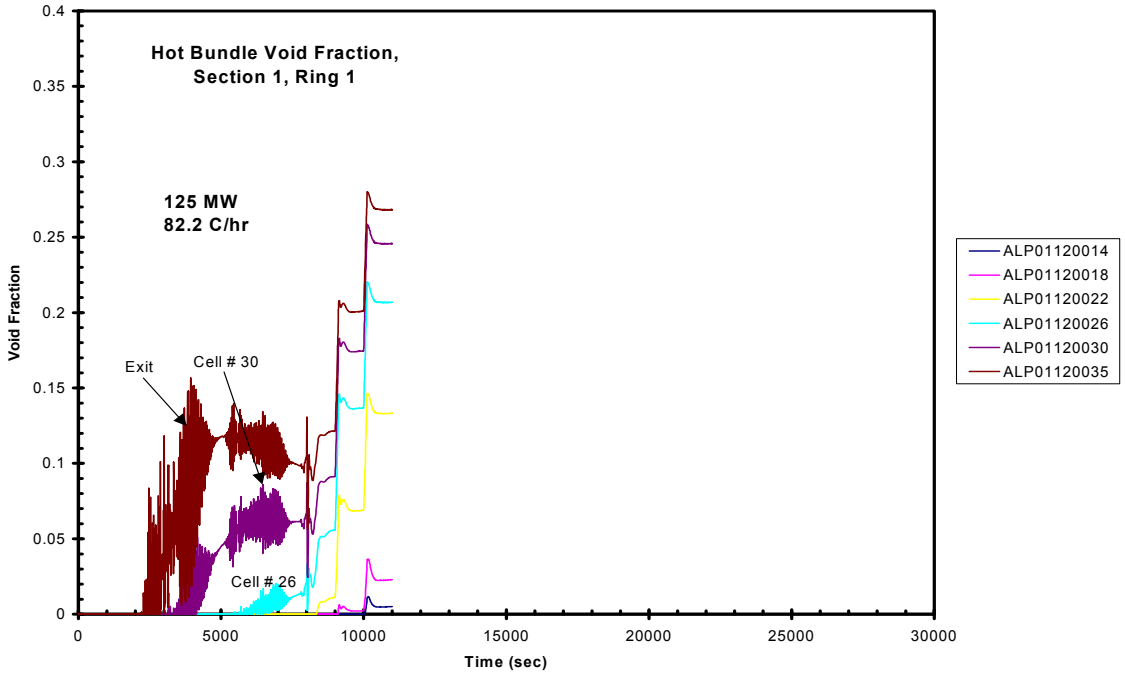

Figure 4D-19. Hot Bundle Void Fraction (125 MW heatup)

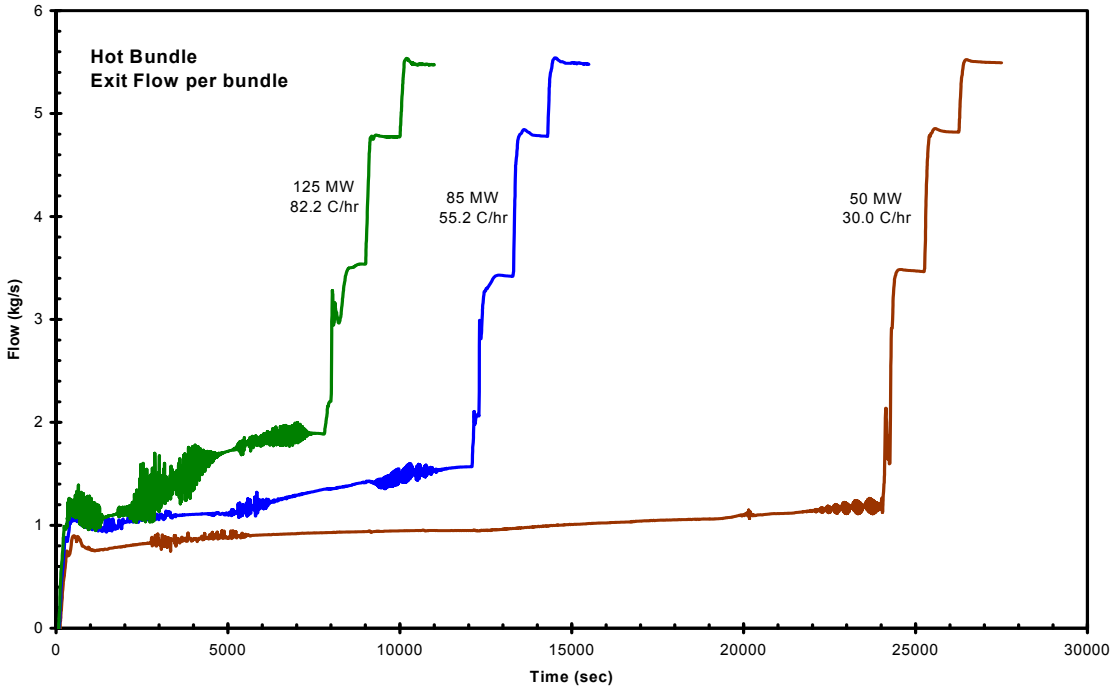

Figure 4D-20. Hot Bundle Exit Flow

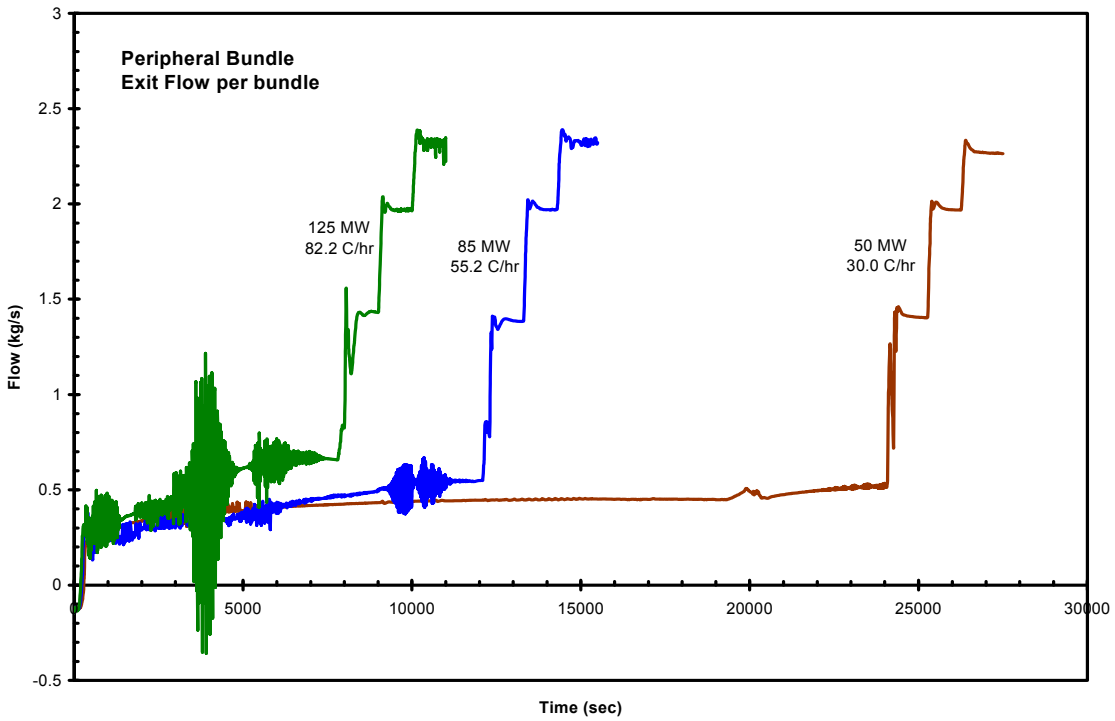

Figure 4D-21. Peripheral Bundle Exit Flow

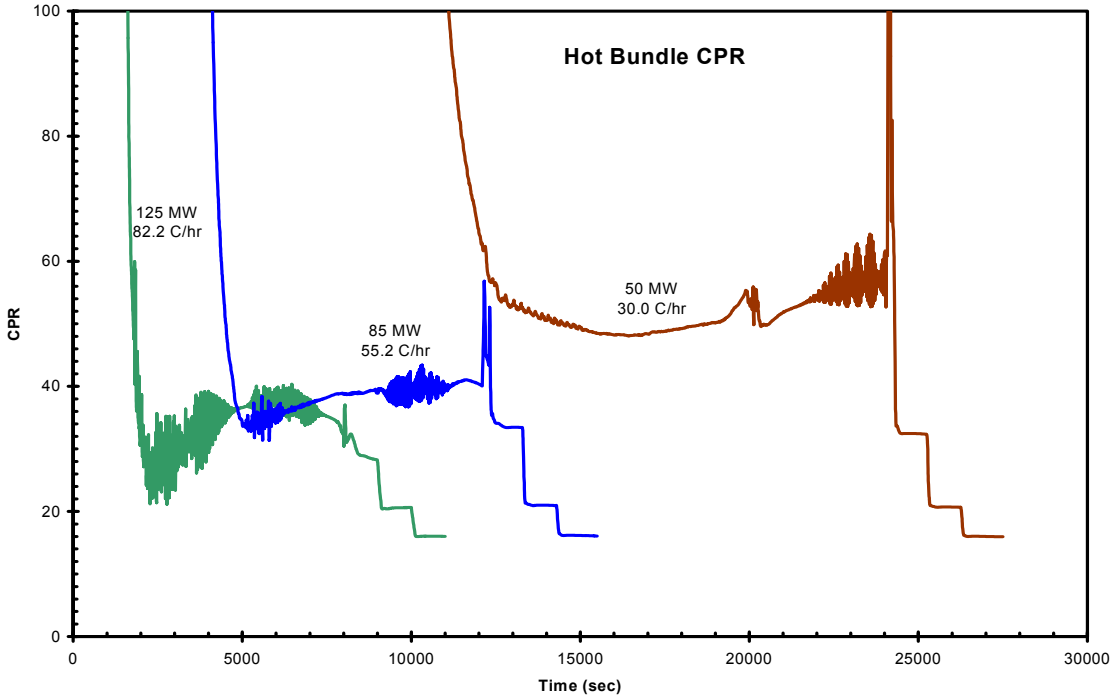

Figure 4D-22. Hot Bundle CPR

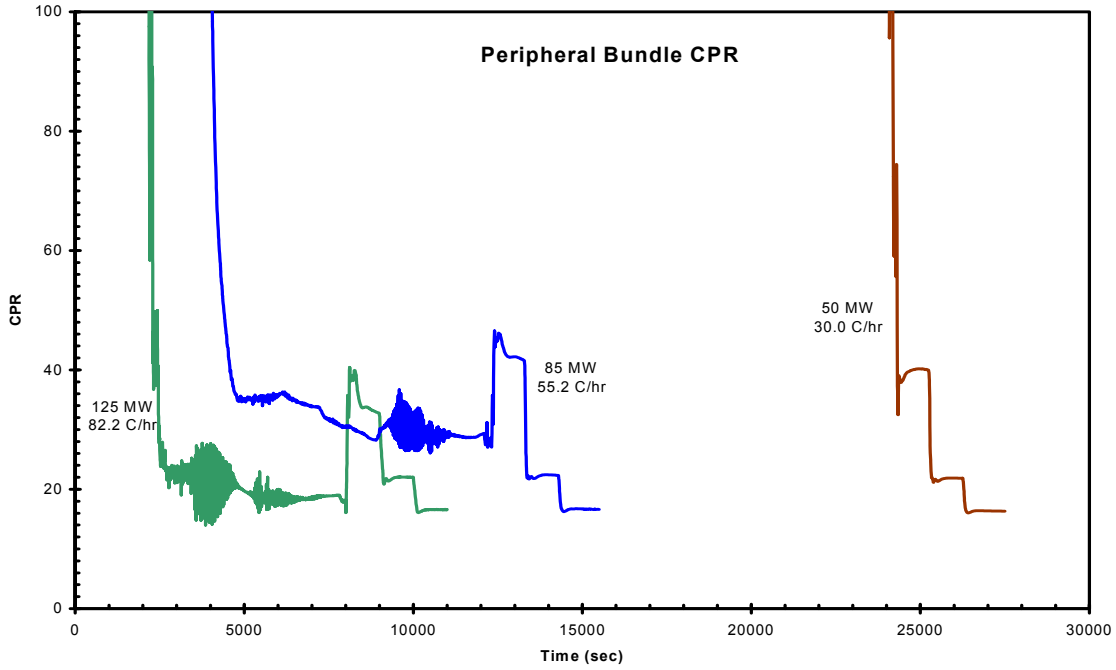

Figure 4D-23. Peripheral Bundle CPR

Row & Column #	1	3	5	7	9	11	13	15	17	19	21	23	25	27	29	31	33	35	37
1								4	5	3	5	4							
3						5	2	9	1	10E	2	9	1	5					
5					6	4	8	3	8	4	8	3	8	4	6				
7				5	2	9	1	10E	2	9C	1	10E	2	9	1	5			
9			6	4	7	3	8	4	7	3	7	4	8	3	7	4	6		
11		5	2	9	1	10D	2	9B	1	10C	2	9B	1	10D	2	9	1	5	
13		4	8	3	8	4	7	3	8	4	8	3	7	4	8	3	8	4	
15	2	9	1	10E	2	9B	1	10B	2	9A	1	10B	2	9B	1	10E	2	9	1
17	5	3	8	4	7	3	8	4	7	3	7	4	8	3	7	4	8	3	5
19	1	10E	2	9C	1	10C	2	9A	1	10A	2	9A	1	10C	2	9C	1	10E	2
21	5	4	8	3	7	4	8	3	7	4	7	3	8	4	7	3	8	4	5
23	2	9	1	10E	2	9B	1	10B	2	9A	1	10B	2	9B	1	10E	2	9	1
25		3	8	4	8	3	7	4	8	3	8	4	7	3	8	4	8	3	
27		5	2	9	1	10D	2	9B	1	10C	2	9B	1	10D	2	9	1	5	
29			6	3	7	4	8	3	7	4	7	3	8	4	7	3	6		
31				5	2	9	1	10E	2	9C	1	10E	2	9	1	5			
33					6	3	8	4	8	3	8	4	8	3	6				
35						5	2	9	1	10E	2	9	1	5					
37								3	5	4	5	3							

Figure 4D-24. ESBWR Control Rod Groups for Startup Simulation

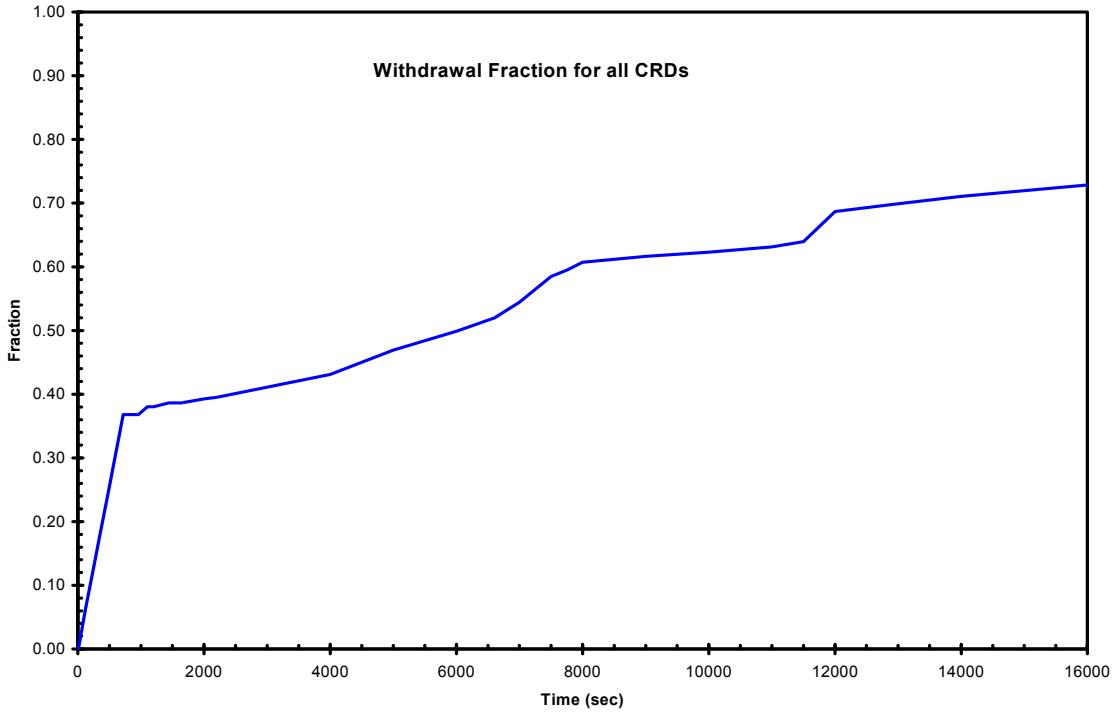

Figure 4D-25. Withdrawal Fraction for all Control Rods

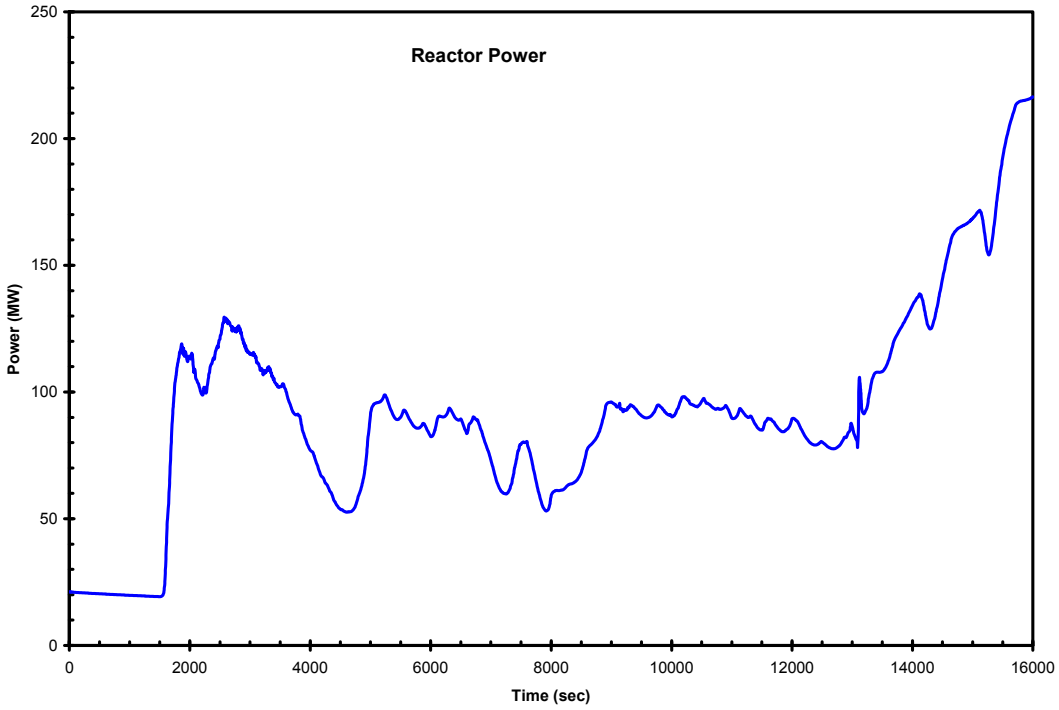

Figure 4D-26. Reactor Power

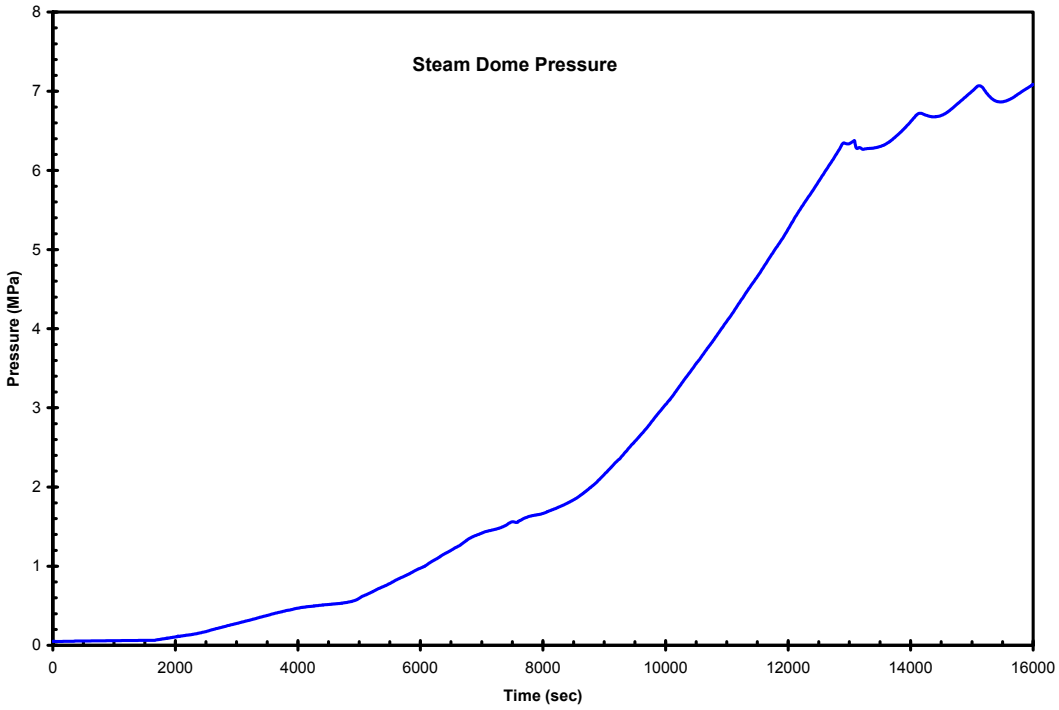

Figure 4D-27. Steam Dome Pressure

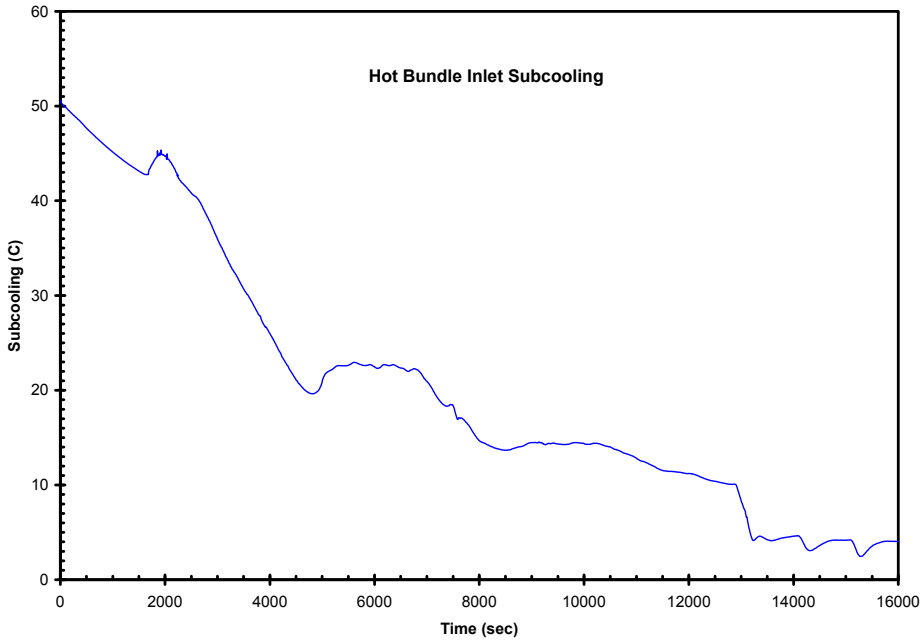

Figure 4D-28. Core Inlet Subcooling

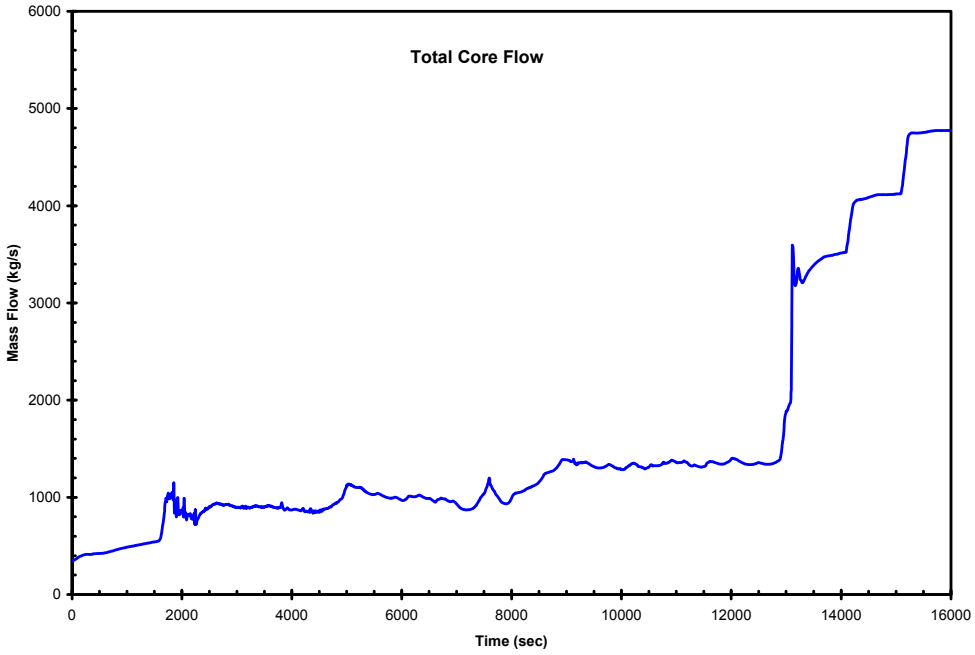

Figure 4D-29. Core Inlet Flow

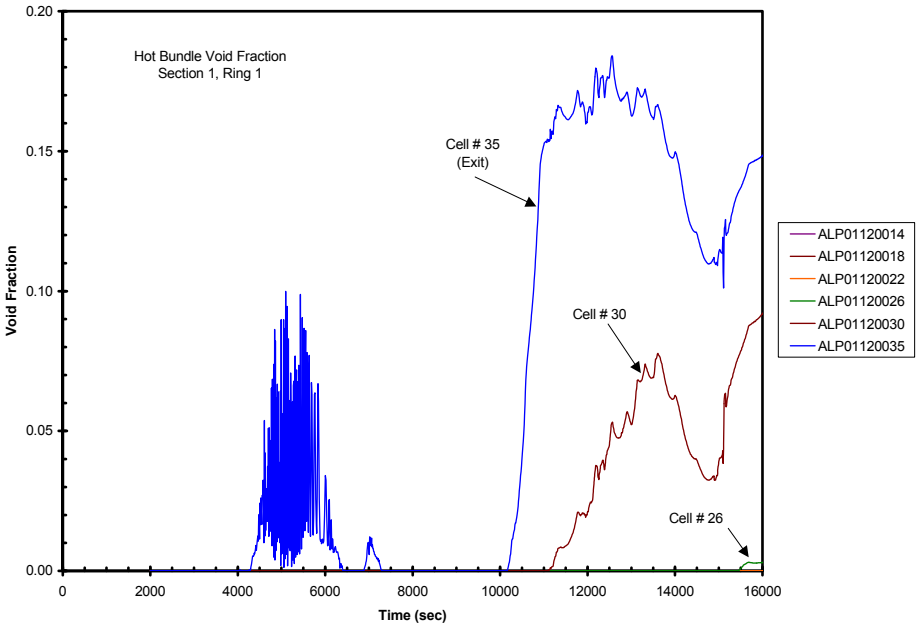

Figure 4D-30. Hot Bundle Void Fraction